Climate Variability in Southwest France During the Last 2000 Years : Proxy Calibration and Reconstruction of Drought Periods Based on Stable Isotope Records from Speleothems and Tree Rings

Inga Labuhn

UNIVERSITÉ PARIS-SUD

ÉCOLE DOCTORALE 534 *Modélisation et Instrumentation en Physique, Energies, Géosciences et Environnement*

Laboratoire des Sciences du Climat et de l'Environnement (LSCE)

DISCIPLINE *Sciences de la Terre*

THÈSE DE DOCTORAT

soutenue le 14/05/2014

par

Inga LABUHN

Climate Variability in Southwest France During the Last 2000 Years

Proxy Calibration and Reconstruction of Drought Periods Based on Stable Isotope Records from Speleothems and Tree Rings

Directeurs de thèse :	Valérie DAUX	Maître de conférences, HDR (LSCE)
	Dominique GENTY	Directeur de recherche (LSCE)
Composition du jury :		
Président du jury :	Christelle MARLIN	Professeur (Université Paris-Sud)
Rapporteurs :	Gerhard HELLE	Senior Scientist (German Research Centre for GeoSciences)
	Christoph SPÖTL	Professeur (University of Innsbruck)
Examinateurs :	Valérie MASSON-DELMOTTE	Directeur de recherche (LSCE)
	Hubert VONHOF	Associate professor (VU University Amsterdam)

Contents

List of Figures

List of Tables

1 Introduction

Since the beginning of the industrial era, the global average temperature has been increasing. Temperature reconstructions show that the recent decades have been the warmest in the last 1400 years (PAGES 2k Network 2013; Figure 1.1). At the same time, our ever increasing energy demand has led to a rise in the concentrations of atmospheric greenhouse gases such as carbon dioxide, methane, or nitrous oxide. The recently published Fifth Assessment Report of the Intergovernmental Panel on Climate Change (IPCC) has confirmed that global warming is unequivocal and will continue, and that it is "extremely likely that human influence has been the dominant cause of the observed warming since the mid-20$^{\text{th}}$ century" (IPCC 2013).

Natural disasters and extreme weather events such as heat waves, floods, severe storms, as well as sea level rise, have raised the discussion whether there is an increased risk of the occurrence of such events with climate change, and an increased vulnerability of societies (van Aalst 2006). In Europe, the heat wave of 2003 or the floods of 2013 are just two examples where people suffered from the impacts of extreme weather on agriculture, economic activity, and infrastructure. Climate change is increasingly recognized as one of the most important challenges for our society, as well as for future generations. Its consequences for ecosystems and socio-economic systems makes the issue of climate change not merely a scientific research topic, but a question of great political relevance.

The only way to make predictions for the future is to use climate models. Models allow to anticipate climate change by exploring different scenarios, e.g. changes in greenhouse gas concentrations, and to evaluate the associated risks. This has implications for public policy on climate change mitigation and adaptation, such as the reduction of greenhouse gas emissions, building resilience, and developing new technologies. However, while climate models agree on the fact that the warming trend will continue during the 21$^{\text{st}}$ century, the rate and magnitude of the global temperature increase remain uncertain (IPCC 2013).

Palaeoclimatology makes two important contributions in this context: first, the detection and attribution of climate change; and second, the evaluation of climate models. In order to investigate causes and effects of climate change, and especially the human influence, we need to understand natural climate variability and its driving forces, putting the currently observed warming in a long-term perspective (Snyder 2010; Edwards et al. 2007; Dearing 2006). The climate models, which have been developed and calibrated using climate observations from the last decades, need to be tested outside this limited range (Braconnot et al. 2012). Reconstructions of past climate changes from palaeoclimate archives can provide a means to test if the models adequately represent the climate variability which is evidenced in the palaeo-records. Such tests of the model performance can help improve the projections of future climate change (Schmidt et al. 2013).

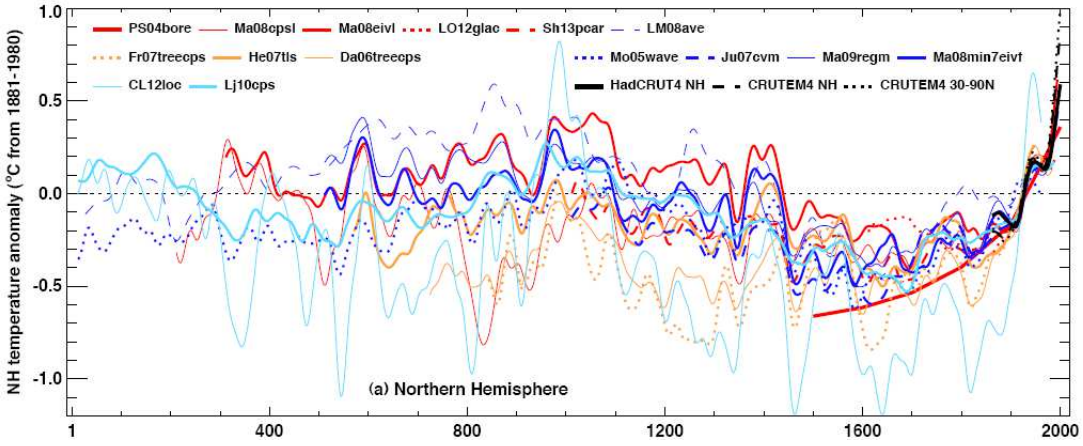

Figure 1.1: Reconstructed Northern Hemisphere temperature during the last 2000 years with different spatial representations (red: land only, all latitudes; orange: land only, extra-tropical latitudes; dark blue: land and sea, all latitudes; light blue: land and sea, extra-tropical latitudes). All temperatures represent anomalies (°C) from the 1881 to 1980 mean (IPCC 2013). Please refer to Table 5.A.6 in IPCC (2013) for information on the individual reconstructions.

1.1 Climate Variability and Climate Reconstruction

The principal control on climate variability is the Earth's radiation balance, which is influenced by various external and internal forcings. The Earth receives its energy in form of shortwave radiation from the Sun. The incoming solar radiation changes with the cyclic variations of the Earth's orbit and its axial tilt (Berger and Loutre 1991; Hays et al. 1976), and with variations in solar activity (Bard et al. 2000). A part of the incoming solar radiation is absorbed, and the rest is reflected back into space by the atmosphere or the Earth surface, which is known as the planetary albedo (Donohoe and Battisti 2011). Finally, back radiation by atmospheric gases of the longwave radiation emitted from the Earth raises the global surface temperature, which is referred to as the greenhouse effect (Mitchell 1989). The orbital parameters lead to variations on diurnal and seasonal time scales with the rotation of the Earth and its orbit around the Sun, as well as on time scales of tens of thousands of years through changes in the eccentricity, obliquity and precession. On top of these cyclic variations, the global climate system is governed by complex processes, interactions and feedback mechanisms between the atmosphere, hydrosphere, cryosphere, biosphere, and land surfaces (Figure 1.2), which act on different spatial and temporal scales.

Climate change studies involve an understanding of these processes, the reconstructions of past climate from natural archives, and climate modelling. Instrumental measurements of temperature and precipitation are of limited spatial and temporal coverage. Only a few series from a small number of locations in the world extend further back than the 20th century. Natural archives can give a long-term perspective on climate change, beyond the instrumental period. They can therefore help identify and quantify the variability of climate conditions in the past, and the Earth system response to climate forcings. These archives include ice cores, marine sediments, speleothems, peat bogs, lake sediments, and trees. They can be dated and thus related to a specific period in the past, but they differ in temporal and spatial resolution, dating accuracy, the continuity of records, and in their potential to provide well-quantified proxies.

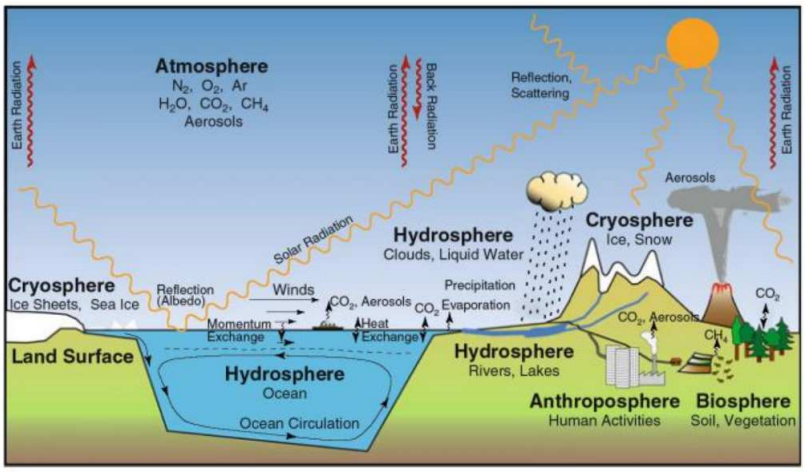

Figure 1.2: Components of the climate system and associated processes (Stocker 2011).

A proxy is an indirect indicator of climate which has been recorded in an archive and allows to infer the climatic and environmental conditions at the time of its formation. The proxy sensitivity denotes how and to what extent the proxy is climate dependent. To be able to extract such information from a proxy record, the proxy needs to be calibrated, i.e. the relationship between the proxy and the influencing climate variable needs to be established (Jones and Mann 2004). Calibration requires an understanding of the archive formation processes and of the control mechanisms which link the proxy to the climatic and environmental factors. For the calibration of proxies, it is often assumed that modern relationships were also valid in the past; this is known as the principle of uniformitarianism. However, the climate-proxy relationship may change over time (Alley and Cuffey 2001). Furthermore, the proxy's climate response always depends on the specific context. If a relationship between the proxy and a climate variable can be established, it is possible to reconstruct the climate parameter of interest.

Proxy records from ice cores and marine sediment cores form the basis of our understanding of climate variability on long time scales, as they reflect the glacial–interglacial cycles (Lang and Wolff 2011). The impact of climate change on human societies, however, depends less on global long-term trends, but rather on short term-variability on the local and regional scale during the different seasons, as well as on the occurrence of extreme events and their magnitude and duration (Easterling 2000; Katz and Brown 1992). Speleothems and tree rings have the potential to provide high-resolution proxy records from the low- and mid-latitude continents, which represent climate variability on annual to centennial time scales in places where human activities are influenced.

There has been an effort to synthesise the proxy-based hemispheric temperature reconstructions for the last two millennia, but the hydrological variability in the past (droughts, floods, extreme precipitation events), which probably has the larger impact on humans, is less well constrained. While most of the reconstructions identify the 20$^{\text{th}}$ century as the warmest (Figure 1.1), there is a discrepancy between them concerning the magnitude and durations of past warm and cold periods like the Medieval Climate Anomaly (about 950–1250 AD) and the Little Ice Age (about 1450–1850 AD). Model simulations agree with the temperature reconstructions of the last 2000 years within their respective uncertainties (IPCC 2013), and indicate that both external climate forcings and internal climate variability are responsible

for this variability (Fernández-Donado et al. 2013; Schurer et al. 2013; Goosse et al. 2012). However, despite the great number of existing proxy records, there is still a need for increased spatial coverage and replication of proxy data (Jones et al. 2009). An improved understanding of the climatic and non-climatic processes which affect the proxies will contribute to a better evaluation of their limitations and uncertainties (Edwards et al. 2007). Lastly, all proxies are limited to certain aspects of climate variability. A combination of proxies gives a broader perspective on past climate change, and may help constrain the causes of variability (Li et al. 2010; Mann 2002).

1.2 Motivation and Objectives

The southwest of France is an agricultural region characterized by recurrent drought periods which might prove to be particularly vulnerable to the consequences of global warming. An increase in the frequency of heat waves has been observed recently, and the predicted temperature rise and precipitation decrease could augment the drought frequency and severity in the future (Mérian et al. 2011; Levrault et al. 2010). The impact of drought depends not only on meteorological conditions, i.e. a precipitation deficiency in combination with high temperature, but also on water resources and water demand. Despite the oceanic climate and the low irrigation demand at present day, agriculture in the southwest of France is vulnerable to an increase in droughts because it is a region which is lacking important water resources (Itier 2008). Droughts impact the local economy, forest productivity and the sustainability of the current agricultural system, and it increases the pressure on water resources (Lemaire et al. 2010; Levrault et al. 2010; Itier 2008). Identifying the patterns of moisture variability in the past may help evaluate the possible future extent of droughts in a changing climate. Until now, low altitude temperate areas are under-represented in European climate reconstructions, and very few high-resolution proxy records of the recent past exist for France (e.g. Yiou et al. 2012; Etien et al. 2008; Masson-Delmotte et al. 2005).

The aim of this thesis is to reconstruct climate variability in the southwest of France during the last two millennia based on multiple proxies from two continental archives, speleothems and tree rings. There are two principal objectives: first, to gain a better understanding of the climatic and non-climatic influences on each proxy in its local context; and second, to reconstruct drought periods in the past.

Speleothems and tree rings constitute complementary climate archives which are adapted to address this issue. Both provide multiple proxies, which differ in their resolution, seasonality, and climate sensitivity (Figure 1.3). The advantage of tree rings lies in their annual resolution and the precise dating. Tree ring proxies can be well quantified, but they can be biased towards climate conditions during the growing season, and they are limited for reconstructing low-frequency climate variability. Speleothems records, on the other hand, have a lower resolution and are less well dated, but preserve a low frequency signal and allow climate reconstructions further back in time.

Both archives have in common that we can measure oxygen isotope ratios ($\delta^{18}O$) in their components: in cellulose from the wood of tree rings, and in water which is incorporated in speleothem calcite, the so-called fluid inclusions. The source of this oxygen in both archives is precipitation. The $\delta^{18}O$ of precipitation bears information about the local climate, and can serve as a tracer of the atmospheric circulation. In order to use $\delta^{18}O$ as a proxy, we need to understand its link with climate, and its fate from precipitation to the proxy record. If

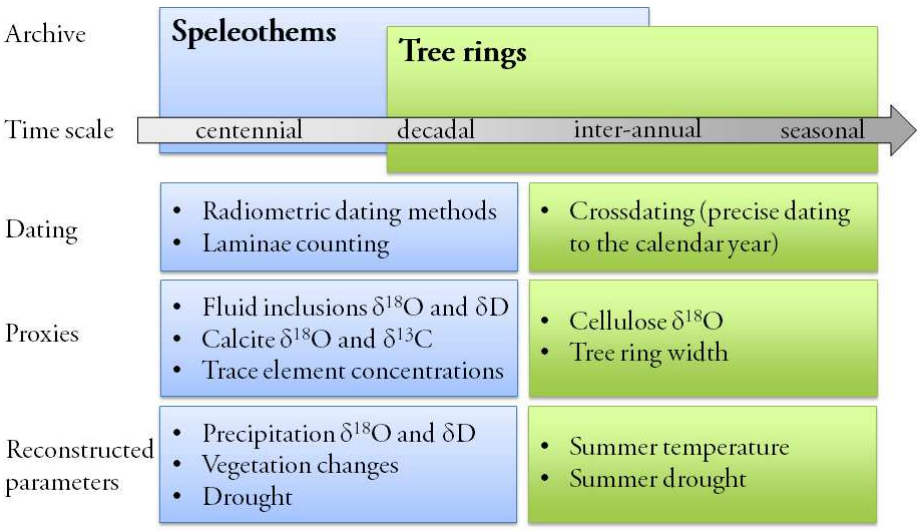

Figure 1.3: Temporal resolution of the speleothem and tree ring climate archives, the proxies which are used in this thesis, and the climate parameters which can potentially be reconstructed from these proxies.

the oxygen isotopic composition of precipitation is preserved in the proxies, it is possible to reconstruct the δ^{18}O of precipitation. Speleothem fluid inclusions have the potential to provide a relatively direct record of palaeo-precipitation δ^{18}O. In trees, physiological processes modify the isotopic composition of oxygen in cellulose relative to the source water, but these processes are also controlled by climate conditions.

This thesis integrates meteorological data, monitoring data of stable isotopes in precipitation and infiltrating water (cave drip water), modern proxy records for calibration, and high resolution measurements of oxygen isotope ratios in speleothem fluid inclusions (covering 2300 years) and tree ring cellulose (covering 650 years) from closely located sites. The principal research questions are:

- What is the link between climate and the δ^{18}O of precipitation in the study area?
- What is the relationship between the δ^{18}O of precipitation and cave drip water? Does the isotopic signal persist from precipitation to the source water of the archives, on the pathway of the water through the soil to plant roots and to the cave?
- Do speleothem fluid inclusions preserve the isotopic composition of the infiltrating water?
- Which climatic and non-climatic factors influence the isotopic composition of tree ring cellulose? How is the source water isotopic composition modified through transpiration?

The results will give a better understanding of the underlying processes, i.e. how the precipitation isotope signal is modified in the biosphere and in subsurface processes before it becomes recorded in the proxies. Based on these calibrations, the local proxy records will be used to reconstruct:

- The δ^{18}O of precipitation based on speleothem fluid inclusions;
- Summer droughts based on cellulose δ^{18}O.

Lastly, the thesis explores the potential of a multi-proxy approach, combining the stable isotope

records from speleothems and tree rings to characterize drought periods and to provide a comprehensive view on past climate variability in southwest France.

1.3 Structure of this Thesis

Part I provides the background on speleothem and tree ring isotope proxies in palaeoclimatology. A general introduction on isotopes (Chapter 2) is followed by a presentation of water isotopes in the hydrological cycle and their link with climate (Chapter 3). The subsequent chapters are dedicated to the two climate archives, speleothems (Chapter 4) and tree rings (Chapter 5); including their formation, dating, the studied proxies and their links with climate. Part II introduces the study area in southwest France (Chapter 6), and presents the methods used to obtain isotope proxy records from speleothems (Chapter 7) and tree rings (Chapter 8). The results are presented and discussed in Part III. Finally, Part IV concludes with a synthesis of the results and an outlook on future research perspectives.

Part I

BACKGROUND

2 Stable Isotope Theory and Notation

Isotopes of an element often behave differently in physical, chemical, and biological processes. The isotopic composition in climate proxies can therefore bear a climatic or environmental signal. An uneven distribution of isotopes between compounds reveals information about the fractionation processes during proxy formation. This chapter provides the background on stable isotopes which is necessary for understanding the behaviour of water isotopes in the environment, including the notation to express isotope ratios, and how isotope ratios are measured.

Isotopes of an element are atoms which contain the same number of protons and electrons, but a different number of neutrons. The consequential mass difference results in so-called *isotope effects*, which are differences in the physical and chemical properties of the isotopes of an element. Isotope effects are strongest for light elements, where mass differences between two isotopes are large relative to the mass of the element, and can lead to a considerable separation of isotopes during phase changes or chemical reactions (Hoefs 2009). The reason for isotope effects lies in the molecular vibrations. The vibrational frequency of a molecule depends inversely on the masses of its atoms. Molecules with the same chemical formula containing different isotopic species have different vibrational frequencies. The molecule with the heavier isotope has a lower vibrational frequency, and therefore a lower zero-point energy, which is the energy a vibrating molecule possesses at a temperature of absolute zero (Bigeleisen 1965). In reactions, the heavy isotope goes preferentially to the chemical compound in which it is bound most strongly. As the bonds formed by the light isotope are weaker, i.e. they have a lower binding energy, molecules containing the light isotopic species react slightly more readily than those with the heavy isotope. Furthermore, lighter molecules have a higher average molecular velocity, which leads to a higher diffusion velocity and a higher frequency of collision with other molecules. With increasing temperature, isotope effects become smaller because the energy of a vibrating molecule becomes independent of mass and bond strength (Mook 2000).

The partial separation of isotopic species during physical or chemical processes is called *isotopic fractionation*. Fractionation leads to different abundances of the isotopes between two phases or substances. Fractionation is expressed by the fractionation factor α, defined as the ratio R of the heavy isotope over the light isotope in compound A divided by the corresponding ratio in compound B:

$$\alpha_{A-B} = \frac{R_A}{R_B} \tag{2.1}$$

The factor α represents either the theoretical isotopic equilibrium between two phases or substances, or represents the measured difference between phases or substances to quantify non-equilibrium conditions (Criss and Farquhar 2008).

Many elements have several stable isotopes. For light elements, one isotope is generally predominant, while the others occur only in trace amounts (Table 2.1). Since isotope abundances can be very small, and absolute ratios are difficult to measure accurately, isotopic composi-

Table 2.1: Stable isotopes of hydrogen, oxygen and carbon and their abundances (Criss and Farquhar 2008).

Element	Isotope	Abundance [%]
Hydrogen	^{1}H	99.985
	^{2}H	0.015
Oxygen	^{16}O	99.76
	^{17}O	0.04
	^{18}O	0.2
Carbon	^{12}C	98.9
	^{13}C	1.1

tion is expressed in terms of δ-*values*, as first presented by McKinney et al. (1950). A mass spectrometer measures the difference between the isotope ratios of two substances much more precisely than the absolute ratio of two individual substances, so the isotope ratio R_X of a sample is reported as the per mil (‰) deviation from the ratio R_{std} of a defined standard (Criss and Farquhar 2008):

$$\delta_X = 10^3 * \frac{R_X - R_{std}}{R_{std}} \tag{2.2}$$

The fractionation factor can be expressed in terms of δ-values:

$$\alpha_{A-B} = 10^3 * \frac{1000 + \delta_A}{1000 + \delta_B} \tag{2.3}$$

Since α is typically close to unity, the difference between δ-values can be used to approximate the fractionation factor:

$$10^3 \ln \alpha_{A-B} \approx \delta_A - \delta_B \tag{2.4}$$

In order to compare isotope data from different laboratories, internationally accepted *standards* recommended by the Commission on Atomic Weights and Isotopic Abundances are used (Coplen 1994). Oxygen and hydrogen isotope values for water are given relative to VSMOW (Vienna Standard Mean Ocean Water), which has an isotopic composition similar to the average composition of the ocean. For carbon, the standard is VPDB (Vienna PeeDee Belemnite), obtained from a fossil belemnite of the Cretaceous PeeDee Formation in South Carolina.

Equilibrium fractionation results from isotope exchange between substances or phases until their distribution obtains a state of minimum free energy. As in chemical equilibrium, there is no net reaction: as many isotopes pass from one phase to the other as vice versa in a reversible chemical reaction or phase change. The equilibrium fractionation factor is temperature dependent, which is an important property for palaeoclimate studies using stable isotopes. Equilibrium fractionation occurs e.g. between liquid water and water vapour in a closed volume, with the heavier molecule enriched in the liquid phase.

Kinetic fractionation occurs during unidirectional, irreversible chemical reactions and physical processes where no equilibrium isotope distribution can establish. In a chemical reaction, lighter molecules react more readily and become enriched in the reaction product. Diffusion also causes kinetic isotope fractionation, because light isotopes are more mobile. An example

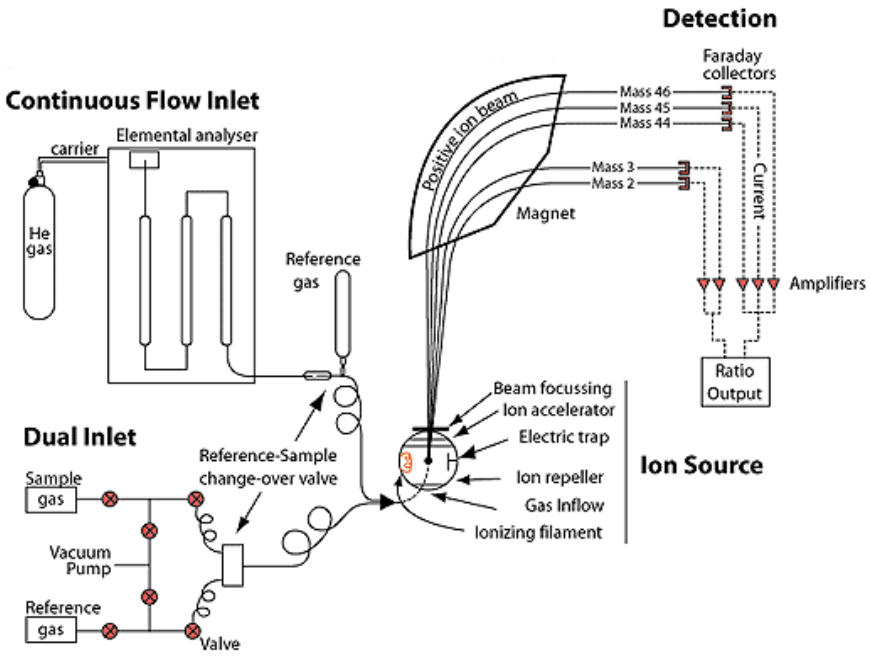

Figure 2.1: Schematic representation of an isotope ratio mass spectrometer (Clark and Fritz 1997).

of kinetic fractionation is the evaporation of water in an open system, where the vapour is removed from the evaporating surface. Fractionation in biologically mediated reactions like photosynthesis is also caused by kinetic effects, with the lighter isotope enriched in the reaction product. Fractionation effects are strongest when the material used in the reaction is small compared to the size of the reservoir (Hoefs 2009).

2.1 Mass Spectrometry

Isotope ratios are usually measured by mass spectrometry, which uses the fact that atoms and molecules of different masses can be separated based on their motion in a magnetic field. The basic principles of isotope ratio mass spectrometry (IRMS) are outlined here (based on Hoefs 2009). The main components of a mass spectrometer are the inlet system, the ion source, the mass analyser and the ion detectors (Figure 2.1). Online techniques use an elemental analyser with a gas chromatographic (GC) column to separate chemical species which is directly coupled to the mass spectrometer.

The inlet system brings the GC separated sample gas to the mass spectrometer by continuous flow of a carrier gas (Helium). The ion source consists of a heated filament which emits a beam of electrons. Molecules of the gas sample are ionised by the electron bombardment. The ions are accelerated and focused into a narrow beam. In the mass analyser, the ion beam passes through a magnetic field, which deflects the ions onto circular paths. The deflection is proportional to the mass/charge ratio of the ions. Thus, the ions are separated into different beams according to their mass. Finally, ion detectors collect the separated ions and convert the input into an electrical impulse, which is then amplified. Multiple detectors are used simultaneously to measure the masses corresponding to different isotopes of an element. The detected peak areas of a sample are compared to a standard gas reference.

Thermal ionization mass spectrometry (TIMS) uses a solid source to generate a beam of charged molecules by thermal ionization. TIMS is used for heavy molecules which are not easily converted to gas, like uranium. Accelerator mass spectrometry (AMS) is employed for high-precision measurements of very low isotope ratios, e.g. $^{14}C/^{12}C$ (Clark and Fritz 1997).

3 Stable Isotopes in the Hydrological Cycle

The palaeoclimate reconstructions presented in this thesis are based on stable isotope proxies in two natural archives, tree rings and speleothems. Their source of oxygen is water, originating from local precipitation. The isotopic composition of precipitation is related to climate, and this climatic influence can be recorded in the proxy. Proxy isotope ratios are further modified by fractionation processes during formation of the archive, which can also bear a climate imprint (see Chapters 5 and 4).

Isotopic fractionation of water molecules occurs during different processes in the hydrological cycle (Figure 3.1). Consequently, isotopic ratios of oxygen and hydrogen measured in different compartments can reveal information about these processes. In order to be able to interpret the climate proxies, it is necessary to understand the fate of water isotopes in the hydrological cycle and the climate controls on the variability of present-day precipitation $\delta^{18}O$ at seasonal and interannual time scales, i.e. the transfer of the isotopic signal from the site of evaporation, through intermediate environments (atmosphere, soil) to the proxy.

This chapter focuses on two compartments of the hydrological cycle: Section 3.1 is concerned with stable isotopes in precipitation, since the water used by the studied proxies originates from precipitation at the site, and Section 3.2 deals with soil water. Trees take their water from the soil, and water percolates through the soil and bedrock before it enters a cave as drip water. The soil water isotopic composition can differ from that of local precipitation by processes of evaporation, transpiration, transport and mixing in the unsaturated zone.

3.1 Precipitation

In evaporation and condensation processes, differences in the vapour pressure of the isotopic species of water lead to a significant isotope fractionation. Water evaporated over the ocean is enriched in the light isotopes compared to ocean water because the lighter molecular species have a higher vapour pressure. On the contrary, during condensation and rainout, water molecules containing the heavy isotopes condensate preferentially from the water vapour and the resulting precipitation has higher δ-values than the vapour (Figure 3.2). The average isotopic composition of ocean water is 0‰ VSMOW, but it can differ in zones of freshwater discharge or high evaporation. Evaporation from the ocean is a kinetic process. The isotopic composition of the evaporated vapour is determined by the isotopic composition of ocean water at the site of evaporation, and by the processes controlling evaporation, i.e. the temperature of water at the ocean surface, relative humidity of the atmosphere and the wind regime (Darling et al. 2006). When the temperature of an air mass decreases during convection, orographic uplift, or frontal cooling, condensation occurs. As an air parcel moves poleward or over a continent, the residual water vapour becomes progressively lighter with each successive rainfall event, and consequently precipitation from the remaining vapour becomes lighter.

The progressive condensation of water vapour on a global scale can be represented as a continuous *Rayleigh distillation* process of cooling of an air mass: a slow process where the condensate

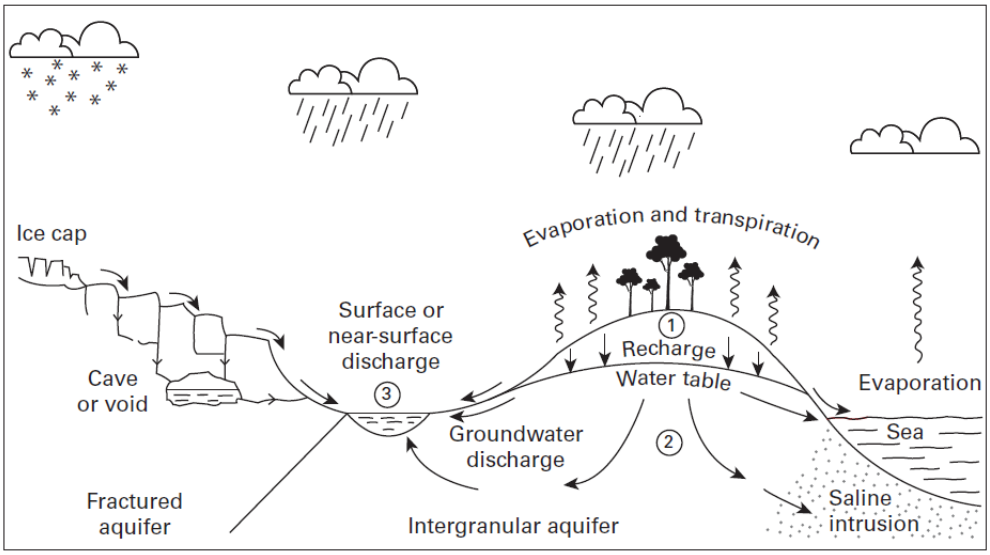

Figure 3.1: Schematic representation of the global hydrological cycle. (1) Soil and unsaturated zone moisture; (2) groundwater; (3) surface waters (Darling et al. 2006).

forms in liquid-vapour equilibrium and is immediately removed from the vapour remaining in the system (Gat 1996). Dansgaard (1964) used the Rayleigh model to evaluate the effects of temperature, latitude, and altitude on the degree of depletion of a vapour mass, and found good agreement with empirical relationships. However, even if the Rayleigh model provides a basic explanation for observed global patterns of isotopes in precipitation, it cannot account for actual air circulation patterns, which are not gradual from the equatorial source regions towards the poles, nor for the contribution of moisture from evaporation at higher latitudes and on continents.

Isotope ratios in precipitation are correlated with local air temperature (*temperature effect*) because condensation in the cloud and the formation of precipitation are controlled by temperature. More specifically, there is a temperature-dependent isotope exchange between condensate and water vapour at the cloud base (Gat 1996). The cloud base temperature is more closely related to surface temperature than to cloud temperature, and the exchange at the cloud base is therefore the main reason why local surface temperature and δ^{18}O of precipitation are correlated. Furthermore, falling raindrops equilibrate isotopically with the surrounding water vapour, the degree of re-equilibration being controlled by relative humidity, the size of raindrops, and the height of the cloud base (Darling et al. 2006).

The isotopic composition of precipitation depends also on the precipitation amount (*amount effect*), both on a seasonal and on an event scale. There are two reasons for this. First, the more it rains, the more the remaining water vapour is depleted in heavy isotopes, and rainfall will become isotopically lighter. Second, water evaporates from falling raindrops, an effect which is stronger for light rain, whereas heavy rain becomes less enriched (Dansgaard 1964).

Since both hydrogen and oxygen isotopes fractionate in a similar way, there is a linear relationship between the δD and δ^{18}O of meteoric waters on a global scale (Craig 1961):

$$\delta D = 8 * \delta^{18}O + 10 \tag{3.1}$$

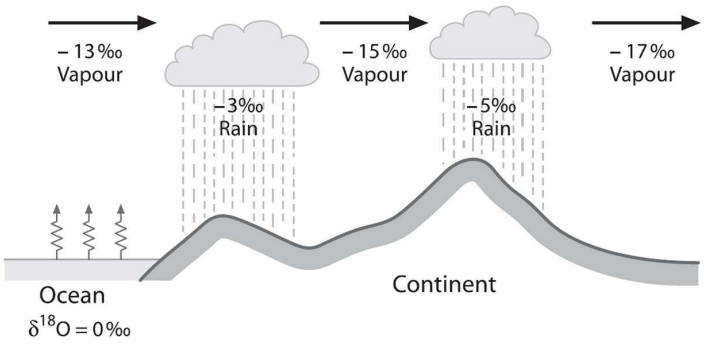

Figure 3.2: Fractionation of oxygen isotopes in atmospheric water (Hoefs 2009).

This equation describes the *Global Meteoric Water Line* (GMWL). In a given place, a Local Meteoric Water Line (LMWL) can have a different slope and intercept depending on locally different moisture sources, precipitation and evaporation. The LMWL thus provides information about local climatic processes. The intercept is called *deuterium excess d*:

$$d = \delta D - 8 * \delta^{18}O \tag{3.2}$$

d is determined by kinetic effects during evaporation of ocean water and can provide information about relative humidity and sea surface temperature in the vapour source region (Merlivat and Jouzel 1979), as well as about continental water recycling (Koster et al. 1993). With increasing humidity, d decreases .

3.1.1 Spatial Variability of Isotopes in Precipitation

The isotopic composition of precipitation depends on the vapour source and the precipitation history of the air mass. The dominant moisture source of the atmosphere is evaporation from low-latitude oceans, but there can be additional sources on the trajectory of an air mass, e.g. through evapotranspiration from the continents (Gat 2000). As a consequence of the temperature and amount effects, δD and δ^{18}O become progressively lower with increasing latitude, altitude and distance from the ocean (Figure 3.3). The amount effect is most pronounced in tropical regions. For surface temperature, the best correlations are obtained in continental regions of mid- and high latitudes. The temperature-dependent gradients of precipitation δ^{18}O (based on mean annual surface air temperature) differ spatially: 0.59‰ per °C for Europe, 0.90‰ per °C for the Antarctic Peninsula, zero for the tropics (Rozanski et al. 1992). Altitudinal δ^{18}O gradients are between –0.15 and –0.50‰ per 100 m (Darling et al. 2006). The continental isotope gradient over Europe is –2‰ per 1000 km (Rozanski et al. 1982).

3.1.2 Temporal Variability of Isotopes in Precipitation

The isotopic composition of precipitation at a given place also varies on different time scales. δD and δ^{18}O vary within a rainfall event (Celle-Jeanton et al. 2001) and between individual rainfall events (Treble et al. 2005). They vary seasonally with seasonal variations in temperature and precipitation amount, and with the dominant circulation patterns which determine the moisture source regions. The seasonal gradient in Europe is 0.32‰ per °C (Rozanski et al.

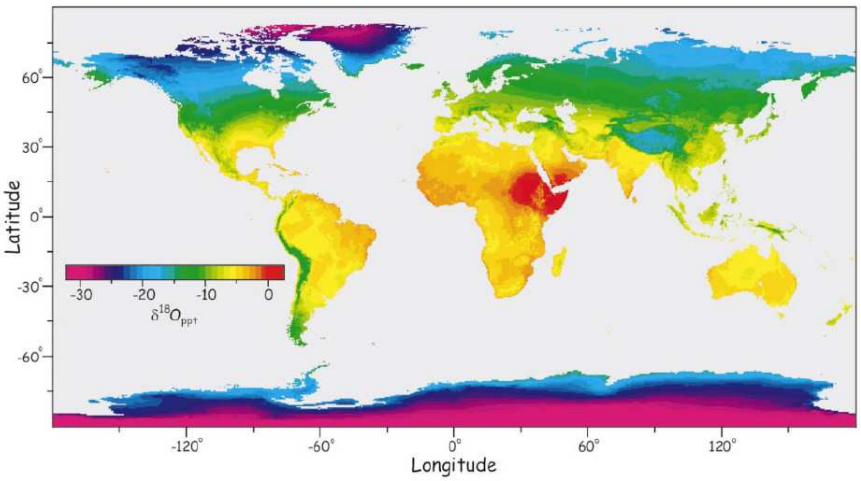

Figure 3.3: Global distribution pattern of δ^{18}O in precipitation (Bowen and Wilkinson 2002).

1982). On longer time scales, atmospheric circulation patterns can change the moisture source regions and air mass trajectories (Jouzel et al. 2013, 1997). The seasonality of precipitation also influences the average annual δD and δ^{18}O. When considering geological time scales, the isotopic composition of the ocean has to be taken into account as well. During glacial periods, the isotopic composition of ocean water changes as a consequence of an increase the polar ice cap and glacier volumes. Light water molecules accumulate in the ice, whereas the ocean water is enriched in heavy isotopes.

3.2 Soil Water

Although their water source is precipitation, the climate proxies measured in this thesis do not directly reflect the δ^{18}O of precipitation. Trees take their water from the soil, and stalagmites are fed by the infiltration water which arrives at the dripping stalactites. Before water is taken up by a plant or enters a cave, it can be modified compared to the original composition of precipitation. Measurements of the soil water isotopic composition are seldom available, so isotope proxies are generally calibrated based on measurements of precipitation. For the interpretation of speleothem and tree ring proxies, however, it is important to understand the surface and subsurface processes which influence the soil water isotopic composition relative to precipitation: interception by the vegetation; the frequency, intensity and duration of precipitation events; mixing with previous soil moisture, which depends on water residence time and flow paths; and a modification of the soil water δ^{18}O by evapotranspiration.

Some of the precipitation water never reaches the soil due to *interception* by the vegetation cover. Water evaporates from plants, and the remaining enriched water is washed down by a subsequent rainfall event. This can change the isotopic composition of the throughfall compared to precipitation, the observed changes in δ^{18}O being at most 0.3 to 0.5‰ (Pichon et al. 1996; Dewalle and Swistock 1994; Saxena 1986). The influence of interception depends on the type of vegetation (Dewalle and Swistock 1994), and is stronger in the summer when trees have leaves and there is less rain. Most evaporative enrichment occurs during less intensive rainfall events. Evaporation therefore does not concern major precipitation events which contribute most to the recharge (Gat 1996).

The water which reaches the soil is called *infiltration* water. The isotopic composition of soil water generally varies less than that of precipitation, because it is a mixing of precipitation events over a certain time period. While holdup and transport of water in the soil do not in themselves affect its isotopic composition, the *residence time* and the type of water flow in the soil column will determine the amount of mixing. The soil water residence time can be several months (Gazis and Feng 2004; Hesterberg and Siegenthaler 1991). *Water flow* can be described by two end member scenarios, piston flow and preferential flow. In homogenous soils, a piston type water flow dominates, where water from a precipitation event pushes older soil water downward. This results in an isotopic front in the soil after rainfall events which differ isotopically from the soil water. In heterogeneous soils, on the contrary, water follows preferential flow paths through fractures and large pore spaces, which leads to a mixing of percolating water from a precipitation event with the water that was present in the soil matrix before the event (Gazis and Feng 2004).

Evaporation from top soil layers modifies the soil water isotopic composition. Enriched soil water can then be flushed down by following rainfall events. The amount of enrichment is poorly constrained, as many soil water evaporation studies focus on evaporation after rainfall events in arid environments, where there is no previous soil moisture and no or little vegetation (Allison 1998; Barnes and Allison 1988). Isotopic enrichment due to evaporation can be very large for a bare soil (Melayah et al. 1996). However, in more humid environments, direct evaporation from a bare soil surface is not important and the system is complicated by antecedent soil moisture, the vegetation cover, and frequent precipitation events. Under a vegetation cover, soil water is lost predominantly from transpiration. The vegetation decouples the free atmosphere from the soil surface and decrease the sunlight absorption by the soil, thus reducing the energy and diffusion gradients necessary for soil evaporation (Polissar and Freeman 2010). This has been shown for temperate deciduous (Harwood et al. 1999) and tropical (Moreira et al. 1997) forests. On a global scale, water flux from the land surface to the atmosphere is also dominated by transpiration, which makes up 80–90% (Jasechko et al. 2013).

There is no isotope fractionation when plant roots take up water (Bariac et al. 1991; White et al. 1985), therefore *transpiration* leaves the isotopic composition of the soil water unchanged. However, there can be a seasonal bias in the soil water when transpiring plants only take up water during the growing season. The remaining soil water that can infiltrate and contribute to groundwater recharge or enter a cave will then be more influenced by the non-growing season precipitation (Darling 2004). This seasonal selection does not have a strong effect on the soil water isotopic composition if most of the precipitation falls in winter, or if the plants' water reservoir is well mixed water from different seasons.

Examples of *soil water isotopic profiles* are given in Figure 3.4. Near the surface, the isotopic composition of soil water is variable, due to the effects of evaporation or new water from precipitation events with a different isotopic signature. The variability of the soil water isotopic composition decreases downward and approaches constant values. The depth at which seasonal variations in the soil water isotopic composition are visible depends on the soil texture and heterogeneity, but it is generally less than 50 cm (Gazis and Feng 2004; Tang and Feng 2001; Hsieh et al. 1998).

When field capacity of the soil is exceeded and the water reaches an aquifer, *recharge* occurs. The isotopic composition of groundwater is generally close to that of the average local precipitation (Gehrels and Peeters 1998; Clark and Fritz 1997). Although the surface processes

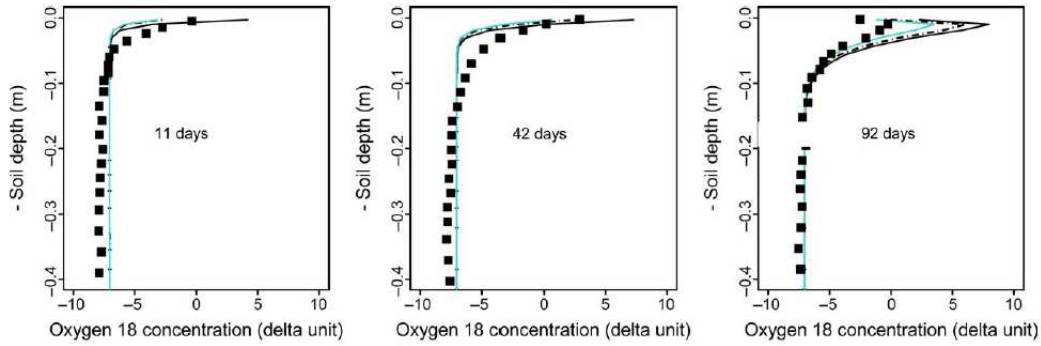

Figure 3.4: Example of soil water isotope profiles; comparison of data (squares) and models (lines) (Braud et al. 2005).

described above generally modify the average δ^{18}O of precipitation by less than 1‰ before it becomes groundwater (Gat 1996), a change of this order of magnitude in a proxy record can be interpreted as a significant temperature change (Darling et al. 2006).

3.3 Applications to Palaeoclimatology

Stable isotopes (δD and δ^{18}O) find widespread applications in palaeoclimatology because there is a link between the isotopic composition of precipitation and climate parameters like local air temperature or precipitation amount, as seen in the previous sections. It is therefore possible to deduce climate information from natural archives which preserve the isotopic composition of precipitation. Furthermore, fractionation processes in the archive depend on environmental parameters, providing further information about the conditions during archive formation.

Reliable estimates of palaeoclimate from stable isotope proxies require a comprehension of how the proxy is related to precipitation (Figure 3.5). This includes the various climatic and hydrological influences on the δ^{18}O of precipitation on different time scales now and in the past, the potential modification of precipitation before turning into the water used by the proxy, and lastly the fractionation processes when water isotopes are incorporated in the proxy.

The link between the isotopic composition of precipitation and climate is not straightforward. Even if the relationships with temperature or precipitation amount are generally valid on a global scale, they are not linear, they depend on the specific site and context and can vary with time. Kern et al. (2013), for example, show that the rule of linear decrease of δ^{18}O with altitude is not valid above a certain altitude in the Alps. Treble et al. (2005) demonstrated that individual rainfall events in Tasmania display an amount effect, whereas on a monthly basis there is a correlation with temperature. Moreover, it is important to consider the time scale which is relevant to the proxy. A linear relationship between monthly temperature and δ^{18}O reflects the seasonal cycle in both. The proxy resolution, however, is often much lower and e.g. decadal scale variations in δ^{18}O recovered from a proxy record are not necessarily linked with temperature in the same way as monthly variations. Thus long-term relationships between temperature and δ^{18}O need to be investigated.

The influences on precipitation δ^{18}O are complex. While early studies attempted to use stable isotopes in precipitation as a proxy to reconstruct temperature or precipitation amount based on a calibration using modern correlations, the focus is increasingly on the δ^{18}O of precipitation itself. The δ^{18}O can be considered as an independent variable, which depends on the

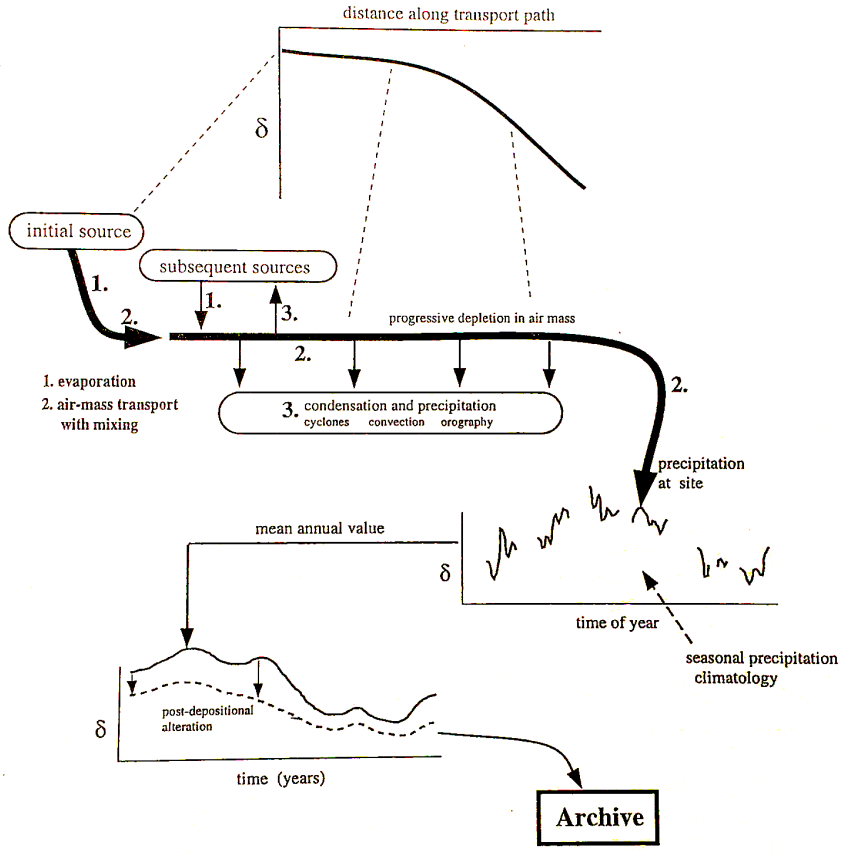

Figure 3.5: Schematic representation of the processes which contribute to the isotopic composition (δ) of water in a palaeoclimate archive (Alley and Cuffey 2001).

integrated effect of several climate variables on a regional scale, rather than on local temperature (Langebroek et al. 2011). Stable isotopes characterize the activity of the climate system, and provide a tracer for large scale changes in atmospheric circulation or in the water cycle. There is a strong influence of the sea level pressure fields which determine the atmospheric circulation, e.g. the North Atlantic Oscillation (NAO), on the δ^{18}O of precipitation in Europe (Field 2010; Baldini et al. 2008). The δ^{18}O is also related to moisture residence time in the atmosphere (Aggarwal et al. 2012). Another great benefit of precipitation δ^{18}O measurements is to test the representation of atmospheric circulation patterns and the hydrological cycle in climate models which include water isotopes (Schmidt et al. 2007; Hoffmann et al. 2005).

In order to interpret isotope proxy records, the links between climate, precipitation δ^{18}O, the proxy source water, and the isotopic composition of the proxy material needs to be established. A calibration period based on measurements of δ^{18}O in precipitation is inevitably short considering the lengths of available instrumental series (IAEA/WMO 2006) and the resolution of proxy records. Modern data can help identify locations where the δ^{18}O of precipitation is sensitive to either temperature or precipitation amount (Lawrence and White 1991). However, present day spatial and temporal relationships cannot necessarily be used to interpret records of the past δ^{18}O variability (Fricke and O'Neil 1999). The annual temperature–precipitation δ^{18}O relation can be impacted by changes in the seasonal distribution of precipitation, which could lead to a misinterpretation of temperature changes of 1 to 3 °C (Vachon et al. 2007). A proxy which depends on the δ^{18}O of precipitation will be biased towards climatic conditions

associated with precipitation events, i.e. the season which receives most precipitation (Lachniet 2009).

When studying proxies from natural archives to reconstruct the $\delta^{18}O$ of precipitation, it is important to keep in mind that there can be modifications between the original isotopic composition of precipitation and the isotopic composition of the water which is used by the proxy (see Section 3.2). In some cases (e.g. in ice cores or in speleothem fluid inclusions) the proxy material is the water itself. In other cases, oxygen from the water is incorporated in the proxy but further fractionation occurs during proxy growth. These fractionation processes can be dependent on environmental parameters at the time of proxy formation. The palaeoclimate information in a proxy is thus linked to the $\delta^{18}O$ of precipitation and/or the modification during proxy growth, which may be controlled by climate parameters other than precipitation $\delta^{18}O$, e.g. temperature. The specific modifications which are relevant for tree rings and speleothems will be explained in Chapters 4 and 5.

4 Speleothems as Palaeoclimate Archives

Speleothems are continental archives which can provide multiple proxies of past climate change. As caves environments are often protected from processes like erosion, speleothems are preserved for a long time after their formation. The parameters that are measured in speleothems to obtain palaeoclimatic and -environmental information include changes in growth rate, thickness of annual laminae, stable isotopes in calcite and fluid inclusions, trace element ratios, or trapped pollen grains, which might be interpreted as indicators for variability in temperature, precipitation, vegetation, or atmospheric circulation (McDermott 2004). They can reflect local and regional processes, but also global shifts in the climate system. Speleothems have provided evidence for major long-term changes like glacial–interglacial transitions (e.g. Affek et al. 2008; Wang et al. 2008; Spötl et al. 2002), as well as high-resolution reconstructions of seasonal climate variability (e.g. Fairchild et al. 2010; Mattey et al. 2008; Treble et al. 2003).

The climatic or environmental signals in a speleothem are generated and modified in the atmosphere, the vegetation, the soil and epikarst, the cave, during calcite precipitation, and possibly through diagenetic alteration (Fairchild and Baker 2012). In order to evaluate whether the speleothem geochemistry reflects climatic conditions at the time of deposition, the processes associated with each of these systems, which link the proxy with the surface environment, have to be understood: the origin of the climatic signal, its evolution in the percolating water, and the conditions during dissolution of calcite and at the time of deposition. The original climatic signal might be lagged, attenuated, or even overprinted progressively through these factors, e.g. the seasonal variability of $\delta^{18}O$ in precipitation is smoothed in the soil reservoir (cf. Section 3.2). The proxy interpretation can be further complicated if its relationship with the surface climate is not stable in time.

This chapter explains how speleothems form, how they are dated, and how they are influenced by climate. The focus is on the proxies used in this study – stable isotopes in fluid inclusion water (oxygen and hydrogen) and calcite (oxygen and carbon) – as well as on the processes relevant for the interpretation of the proxies, which link the proxies to the outside environment and the cave environment.

4.1 The Cave Environment

The meaning of palaeoclimatic or palaeoenvironmental proxy records from speleothems is not unambiguous and depends on the specific climatological and geological context. It is therefore crucial for their interpretation to understand the cave environment and the functioning of the present day cave system. Fairchild et al. (2006a) introduced the term *speleophysiology* to describe the "behaviour of cave environments as functioning systems on an environmental scale". Instead of focusing only on the cave itself – e.g. its temperature and drip water chemistry – one should consider, like for an organism, its water, gas and energy exchanges with the exterior. These factors determine in how far speleothems capture the external environmental signals which are transferred, modified or preserved in the karst system.

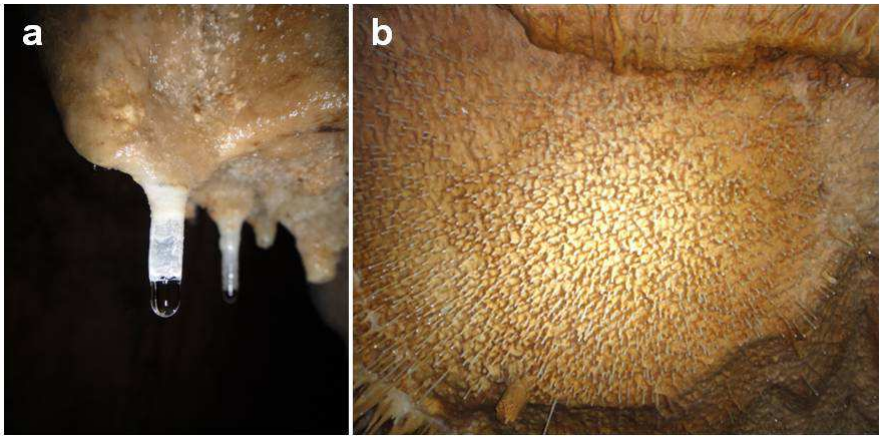

Figure 4.1: a) Water drop forming on the tip of a stalactite. b) Soda straw stalactites on a cave ceiling, indicating matrix flow conditions (Cussac cave, France).

Ideally, a palaeoclimatic study on speleothems is accompanied by a detailed *cave monitoring* (e.g. Genty 2008; Hu et al. 2008; Spötl et al. 2005), in order to calibrate speleothem records based on modern conditions, and to characterize the following parameters which can influence proxy variability. Cave temperature is generally close to the mean annual outside temperature, but shallow caves can show some lagged seasonal variation. The sources of heat are the heat transferred by conduction form the surface to the cave, and the geothermal heat flux, which can influence the temperature in deep caves. When the cave temperature remains relatively constant throughout the year, there will be no seasonal noise in speleothem temperature records.

Cave air CO_2 concentration depends mostly on CO_2 production in the soil and the ventilation of the cave. The partial pressure of carbon dioxide (pCO_2) in the soil air is greater than the atmospheric pCO_2 because of root and microbial respiration and organic matter decay. The soil CO_2 production generally increases with temperature and is limited by soil moisture. Typical cave air pCO_2 values range from from several hundred to several thousand ppm. There is often a seasonal variation in pCO_2, due to the vegetation activity which produces CO_2 in the soil, and due to the exchange of cave air with outside air. This exchange depends on the difference between the often constant cave temperature and the seasonally varying outside temperature.

Humidity in caves is high, typically 95 to 100%. This minimizes the effects of evaporation on the isotopic composition of cave water. The isotopic composition of the cave drip water depends on the water flow pathway, residence time, and the seasonality of recharge. It can be biased towards the season which receives most precipitation.

4.2 The Formation of Speleothems

Speleothems are defined as mineral cave deposits (Moore 1952) of calcium carbonate ($CaCO_3$), composed of the minerals calcite and/or aragonite. They develop in karstic carbonate rocks, under the condition of available liquid water. Karst landscapes with their specific hydrogeology result from water circulation and dissolution of a bedrock like limestone or dolomite. Prerequisites for karstification are a soluble, porous rock, and elevated CO_2 concentration in percolating water from interaction with the soil zone. The epikarst is the part of the bedrock below the soil zone, a highly fractured zone of enhanced dissolution.

Figure 4.2: Stalagmites and stalactites in Cussac cave, France.

Water transit times in the heterogeneous and permeable subsurface of karstic aquifers are highly variable and depend on water flow pathways through three types of porosity: primary (inter-granular pore space), secondary (fractures and joints), and tertiary (conduits which are enhanced by dissolution) (Ford and Williams 2007). The discharge (drip rates and their variability) and hence stalagmite growth depend on the water flow pathways of the individual speleothem (Bradley et al. 2010). A large number of small stalactites with slow and constant drip rates indicate matrix flow (Figure 4.1), whereas fracture flow can lead to faster and more variable drip rates.

There are three main *types of speleothems*: stalactites and stalagmites (Figure 4.2), which both grow from dripping water, and flowstones, which are deposited from water sheets on cave walls and floors. Stalagmites are most commonly used in palaeoclimate studies because of their simple growth structure and relatively high growth rates. Stalactites are often small soda straws with a complex stratigraphy, as water can run along an interior channel as well as along the outside, making it difficult to establish a chronology of deposit. The advantage of flowstones is their lateral extension, so that samples can be replicated by coring.

Stalagmite growth occurs when percolating water, having taken up CO_2 in the soil zone, dissolves calcium carbonate, which is subsequently precipitated in the cave as CO_2 degasses from the solution (Figure 4.3). The most commonly formed mineral is calcite, but aragonite can form in caves with dolomitic host rocks. Aragonite is metastable at Earth surface conditions and susceptible to diagenetic alteration to calcite. Stalagmite growth rates are mainly determined by the Ca concentration of the drip water, the drip rate, and the pCO_2 of the cave atmosphere (Genty et al. 2001b; Dreybrodt 1988).

Percolating water dissolves CO_2 in the soil zone until it is in equilibrium with soil air pCO_2. Dissolution of CO_2 in soil water forms carbonic acid:

$$CO_2 + H_2O \longleftrightarrow H_2CO_3 \tag{4.1}$$

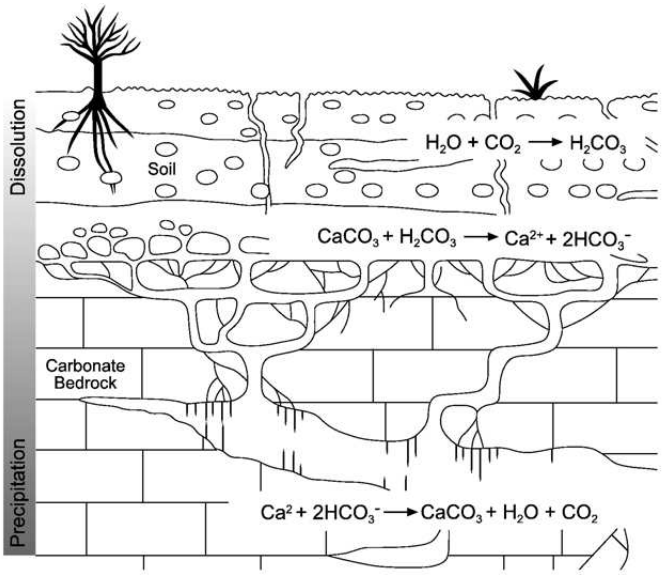

Figure 4.3: Dissolution and precipitation of calcium carbonate ($CaCO_3$) in the karst system (Fairchild et al. 2006b).

which dissociates in two steps:

$$H_2CO_3 \longleftrightarrow HCO_3^- + H^+ \tag{4.2}$$

$$HCO_3^- \longleftrightarrow CO_3^{2-} + H^+ \tag{4.3}$$

The species concentrations depend on the pH of the solution, HCO_3^- being the dominant species at pH values close to neutral.

Then, calcium carbonate is dissolved in the soil and epikarst:

$$CaCO_3 + H_2CO_3 \longrightarrow Ca^{2+} + 2\,HCO_3^- \tag{4.4}$$

Its solubility depends mostly on the pCO_2, but also on temperature (Sigg and Stumm 2011). Normally percolating waters approach saturation for calcite when they arrive in the cave (Fairchild and Baker 2012), but the saturation state of the drip water can be variable.

As the saturated solution enters the cave, calcite precipitates:

$$Ca^{2+} + 2\,HCO_3^- \longrightarrow CaCO_3 + H_2O + CO_2 \tag{4.5}$$

Dreybrodt (2011) and Dreybrodt and Scholz (2011) outline the chemical evolution of the solution during calcite precipitation under typical cave conditions. There are three processes involved: (1) degassing of CO_2; (2) equilibration to the lower pCO_2; and (3) precipitation of calcium carbonate (Figure 4.4). Because their time scales differ in magnitude, these processes can be regarded as three consecutive steps, e.g. the pH stays constant during degassing. The water entering the cave is in chemical equilibrium with respect to calcite. The pH of the solution depends on temperature and [Ca]. When the water enters the cave atmosphere, as the pCO_2

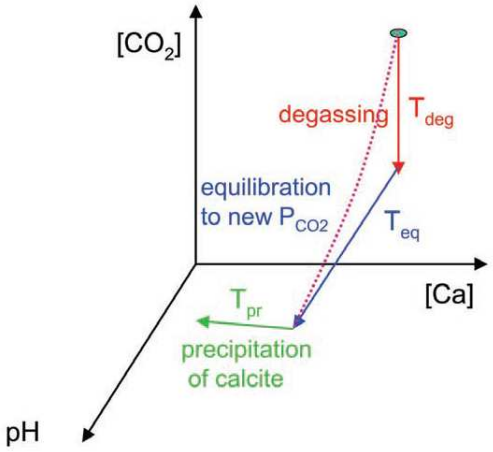

Figure 4.4: Reaction pathways from dripwater to the precipitation of calcite and the associated changes in CO_2 and Ca concentrations and pH of the solution. At 10 °C, the time needed for the degassing of CO_2 from a thin water film (T_{deg}) is 3.5 s, the time to establish a chemical equilibrium (T_{eq}) in the solution with the lower pCO_2 is 321 s, and the time for calcite precipitation (T_{pr}) is 2340 s. The dotted line depicts the case of slow degassing, e.g. due to thick water films, where degassing and equilibration occur simultaneously (Dreybrodt 2011).

in the cave air is lower than in the water, CO_2 degasses until in equilibrium with the lower pCO_2. CO_2 is mostly present as molecular CO_2, degassing thus occurs by molecular diffusion. $CO_{2(aq)}$ is actually 600 times more abundant than H_2CO_3 (Appelo and Postma 2005). The time of degassing is in the order of 10 s. When water flows to the drip site as a thin film, the time depends on the thickness of the water film. Arriving at the dripping point, the degassing of the water is completed. When water is dripping from a soda straw stalactite, the degassing from the drop depends on its drip time (fall height), and the ratio of surface area to volume (Fairchild and Baker 2012). In this case it is slower than from a thin water film, so further degassing occurs on the apex of the stalagmite.

After outgassing of CO_2, the pH, $[HCO_3^-]$ and $[CO_3^{2-}]$ are no longer in equilibrium with respect to the lower pCO_2. Chemical and isotopic equilibrium with the lower pCO_2 is established in the order of 300 s. This causes an increase in pH and a supersaturation with respect to calcite. When supersaturation in attained, calcite begins to precipitate (Figure 4.5), which takes approximately 2000 s. This lowers the [Ca] and pH. For each $CaCO_3$ molecule formed, a CO_2 molecule is released. This is not to be confused with the outgassing in step 1.

Speleothems form only when water is saturated with $CaCO_3$. A *hiatus*, i.e. an interruption of stalagmite growth occurs when drip water is undersaturated or the dripping stops during dry or cold climate conditions. Seasonal changes in the saturation state of the drip water and in cave air pCO_2 may cause a bias in the speleothem proxies towards periods of optimal saturation state in the precipitated calcite (Genty et al. 2001b).

4.3 Dating of Speleothems

A major advantage of speleothems compared to other climate archives is their robust dating. They are not orbitally tuned like marine records but can be absolutely dated by the counting of growth layers or by radiometric methods. Some speleothems display a visible, luminescent

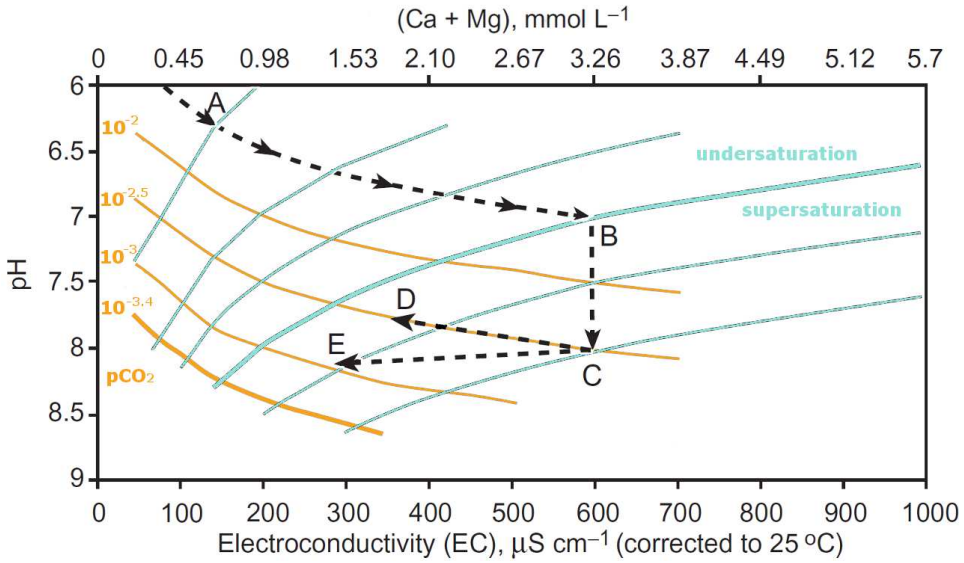

Figure 4.5: Chemical evolution of a typical dripwater in which dissolution occurs (A→B), followed by degassing, which leads to a supersaturated solution (B→C). Then, $CaCO_3$ precipitation occurs: C→D indicates precipitation at a constant pCO_2; C→E represents a situation where degassing continues towards the pCO_2 of the cave, which is lower than the pCO_2 of the solution, at the same time as $CaCO_3$ precipitates. Orange lines depict the pCO_2, light blue lines the saturation state of the solution (modified from Fairchild and Baker 2012).

or chemical lamination. *Annual layer counting* is possible when the growth rate is high and seasonal variability in hydrology, drip water chemistry and cave atmosphere lead to variations in petrography, stable isotopes, trace element concentrations or fluorescent organic matter (e.g. Boch et al. 2011; Baker et al. 2008; Tan et al. 2006). An understanding of the processes in surface climate, hydrology and cave environment is necessary to confirm that the periodicity in these parameters is actually annual (Fairchild and Baker 2012).

Radioactive decay of carbon and uranium incorporated in speleothems is also used for dating purposes. By measuring the abundances of the radioactive isotopes and their decay products, the age can be determined with the known decay constants.

Uranium-thorium dating provides a precise method to date speleothems of up to 500.000 years. The age determination is based on the extent to which the ^{238}U decay series in a speleothem sample have returned to secular equilibrium from an initial state of disequilibrium, which can be expressed as a function of time using the decay constants of the radioactive isotopes (Richards and Dorale 2003). Most speleothems behave as closed systems with respect to uranium and its decay products (McDermott et al. 2006). Uranium (^{238}U and ^{234}U) is transported as a solute in water, and incorporated in the speleothem, where it decays to thorium (^{230}Th) and other products. There is no transport of thorium in water due to its low solubility. From the measurements of the different isotopes, initial concentrations of ^{238}U and ^{234}U can be calculated, and the age of the sample can be determined based on the $^{234}U/^{238}U$ and $^{230}Th/^{234}U$ ratios. Uncertainty arises from detrital ("initial") Th, transported by fine sediment, colloids or organic matter, which leads to an overestimation of the U-Th age. The uranium (^{238}U) content in calcite is typically 0.05 to 10 $\mu g/g$.

In young speleothems or in samples with low U or high detrital Th concentrations, the U-Th

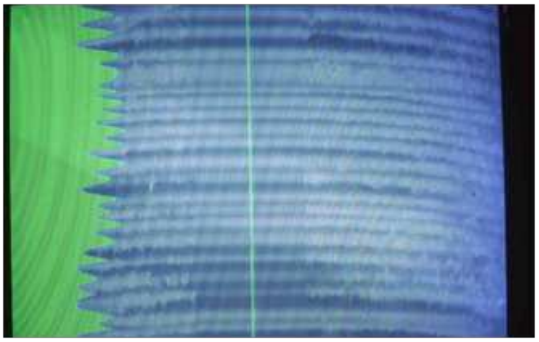

Figure 4.6: Example of annual laminae in a stalagmite from the Godarville Tunnel, Belgium (height 2 cm), where the seasonality of the lamination has been demonstrated. The laminae were counted and measured by digital image processing (Genty 1993).

method is less applicable. In that case, *radiocarbon dating* might be used to date samples which are up to 50.000 years old (Hua et al. 2012). The radioactive isotope of carbon (^{14}C) is produced in the atmosphere from ^{14}N by cosmic rays, and it is taken up by plants and dissolved in rain and surface waters in form of CO_2. It decays with a half-life of 5715 years. The reference level of 100% modern carbon (pMC) is set at the level of 1950, before atmospheric nuclear tests increased the ^{14}C level ("bomb peak") (Hua 2009). The carbon in speleothems originates mainly from soil CO_2, which reflects the ^{14}C of the atmosphere. However, a proportion of carbon is derived from bedrock dissolution, and this so-called dead carbon contains no ^{14}C. The dead carbon percentage (dcp) can be variable (Genty et al. 2001a). This uncertainty limits the use of the ^{14}C dating technique. The bomb peak found in speleothems can be used to confirm modern deposition, and to investigate carbon transfer processes from the surface to the stalagmite, when it is attenuated or lagged compared to the atmospheric peak due to soil carbon dynamics and groundwater residence time (Genty et al. 2001a; Genty and Massault 1999).

Since the spatial resolution of proxies like calcite stable isotopes is much higher than that of the dating points, the age between dating points has to be determined. An *age model* describes the relationship between the distance of the proxy measurement along the stalagmite growth axis and its age (Scholz and Hoffmann 2011). Since stalagmite growth is non-linear, there can be steps and rate changes which increase the uncertainty of the age model.

There is no standard method to interpolate between measured ages, and different age models produce different ages and different age uncertainties (for a comparison of different models see Scholz et al. 2012). The simplest model is a linear interpolation between dating points, but this produces a discontinuous age curve which does not take non-linear growth characteristics into account, and no error quantification is possible. Splines or polynomial functions give smooth curves, but they are not monotonic and the choice of spline of polynomial order is subjective. Bayesian approaches like COPRA (Breitenbach et al. 2012) or StalAge (Scholz and Hoffmann 2011) can take known growth characteristics such as the stratigraphic order into account.

4.4 Fluid Inclusions

Most stalagmites contain microscopic pores filled with water and/or air, called fluid inclusions. The water is incorporated in the calcite at the time of calcite precipitation and thus can be

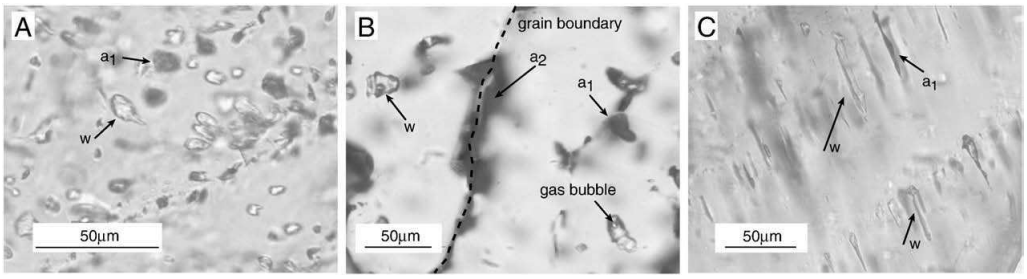

Figure 4.7: Photographs of thin sections from three stalagmites with water (w) and air (a) inclusions (Scheidegger et al. 2010), illustrating different shapes and distributions of fluid inclusions.

stratigraphically related to the time when it was dripping. While kinetic fractionation during calcite deposition can complicate the interpretation of calcite stable isotopes as palaeoclimate records (see section 4.5), the use of fluid inclusions potentially provides a direct record of precipitation δ^{18}O in the past. However, the resolution is considerably lower than the resolution which can be obtained with calcite stable isotope measurements due to the larger sample size which is needed to extract enough water.

The comparison of the isotopic composition of dripwater or fluid inclusions and calcite at a known temperature can give indications about isotopic equilibrium during calcite deposition. Conversely, measurements of δ^{18}O in fluid inclusions and corresponding calcite might allow the calculation of absolute palaeotemperatures, if the calcite was deposited in isotopic equilibrium with the water.

The size of fluid inclusions ranges from nanometres to centimetres, but is typically between 1 and 100 μm in the maximum dimension, the water making up between 0.05 and 0.5 wt. % of the stalagmite. They generally form ellipsoidal or irregular tubes which are oriented parallel to the c axis of the calcite crystal. Fluid inclusions are not distributed regularly throughout a stalagmite (Figure 4.7). Often zones of clear and compact calcite fabric contain few fluid inclusions, whereas zones of opaque, milky calcite contain more water, the inhomogeneities and pores in the calcite causing its milky appearance. These zones likely correspond to periods of rapidly changing, irregular growth rates, where water-filled pores are sealed off instead of being filled with calcite (Vogel et al. 2013; McDermott et al. 2006).

In order to interpret the fluid inclusion record, it is important to evaluate whether fluid inclusions preserve the isotopic signal of the drip water. It has been suggested that isotopes might exchange between trapped water and surrounding calcite (Schwarcz et al. 1976). However, the isotopic exchange is probably negligible on Quaternary time scales at Earth surface temperatures, and there is no petrographic evidence that the shape of fluid inclusions is modified by dissolution or precipitation of calcite (McDermott et al. 2006). The δD values would be unaffected by these processes because there are no hydrogen atoms in the calcite to exchange with. The δD–δ^{18}O relationship can therefore give a hint on possible exchanges of oxygen atoms between water and calcite. Another possible modification of the isotopic composition of fluid inclusions compared to the original drip water is evaporation of the water before cavities close, which depends on the relative humidity of cave air and on cave ventilation.

There are different methods of extracting the fluid inclusions to measure the isotopic composition of the water. Few speleothem samples contain macroscopic fluid inclusions. It is possible to extract this water using a syringe (Genty et al. 2002). In most cases, calcite samples have

to be crushed and/or heated in order to extract the microscopic fluid inclusions (Dublyansky and Spötl 2009; Zhang et al. 2008; Vonhof et al. 2006). Crushed calcite surfaces adsorb a significant amount of water at room temperature, which results in a fractionation, it is therefore important to recover all the water (Dennis et al. 2001).

Besides the isotopic composition of the water, fluid inclusions in stalagmites provide other potential palaeotemperatures proxies, namely noble gas concentrations (Scheidegger et al. 2011; Kluge 2008) and liquid vapour homogenization temperatures (Krüger et al. 2011).

4.5 Stable Isotopes in Calcite

The most widely used proxies in speleothems are stable isotopes of oxygen and carbon. The acquisition of the isotope signals in calcite depends on the isotopic composition of the oxygen and carbon sources, their modification on the way to the cave, and the fractionation during calcite precipitation.

4.5.1 Oxygen

The interpretation of oxygen isotope ratios in calcite is not straightforward as the processes which determine the $\delta^{18}O$ of calcite are numerous and complex, and they differ depending on the geographic location. The two principal influences are the $\delta^{18}O$ of the drip water, and the fractionation of oxygen isotopes between calcite and water during calcite precipitation. The isotopic composition of calcite might therefore contain information about large-scale oceanic and atmospheric processes, as well as site-specific processes like local hydrology and cave microclimate (Figure 4.8).

Early speleothem studies have attempted to interpret calcite $\delta^{18}O$ in terms of palaeotemperature. This interpretation, however, is often too simplified because (1) calcite might not be precipitated in isotopic equilibrium with drip water; and (2) it depends also on precipitation $\delta^{18}O$, which is controlled by many factors besides temperature, notably changes in the atmospheric circulation, and the temperature-dependence of precipitation $\delta^{18}O$ is variable in space and time. Absolute cave temperature can only be derived if calcite is precipitated in isotopic equilibrium and the water isotopic composition can be determined independently, e.g. by the analysis of fluid inclusions. Due to the uncertainties of the "palaeothermometer", the $\delta^{18}O$ of precipitation is often reconstructed instead of local temperature. This measure serves as an atmospheric circulation tracer and can provide estimates of the timing and durations of major climatic events which are characterized by shifts in oxygen isotope values (e.g. Wang et al. 2008; Spötl and Mangini 2002).

The isotopic composition of the drip water has the largest influence, as the amplitude of variation in $\delta^{18}O$ in the hydrological cycle is larger in magnitude than the variation due to the temperature-dependent equilibrium fractionation during calcite precipitation (Lachniet 2009). However, kinetic fractionation may mask the original $\delta^{18}O$ signal of the drip water. The drip water isotopic composition is generally considered to be a mean of precipitation, and is therefore linked with the processes in the hydrological cycle (Chapter 3). The water which participates in the precipitation of calcite is called the isotopically effective recharge, which can be different from the mean annual precipitation (Lachniet 2009). Processes like evaporation, mixing in the soil zone and epikarst, and the type of water flow (seepage flow vs. fracture flow)

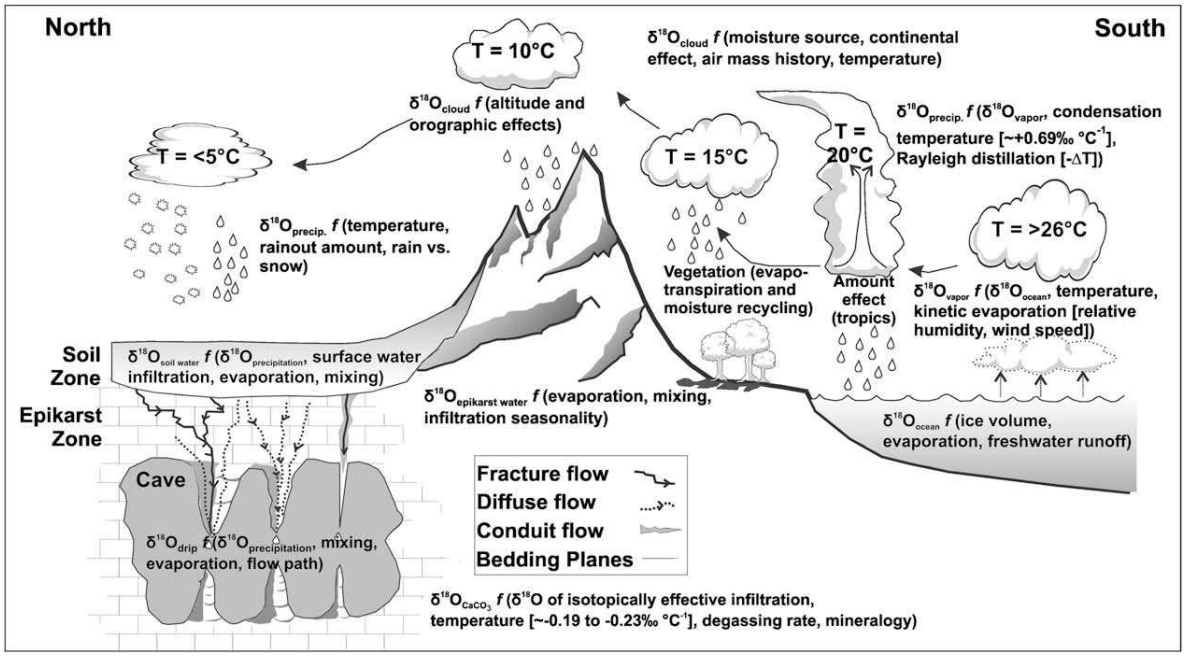

Figure 4.8: Processes in the ocean, atmosphere, soil, epikarst, and the cave which influence the $\delta^{18}O$ of speleothem calcite (Lachniet 2009).

will control the isotopic composition of drip water compared to precipitation, as well as its seasonal variability.

Oxygen originating from bedrock dissolution has a different $\delta^{18}O$, but oxygen in the carbonate species will equilibrate isotopically with the water. The number of oxygen atoms is 10^4 times larger in the water than in the dissolved carbonate species. The dissolved inorganic carbon (DIC) therefore carries the isotopic signature of the water and its imprinted climate signal. The equilibration time is temperature dependent, but progresses fast (in the order of one day) compared to the travel time of water from the site of dissolution to the cave (Dreybrodt and Scholz 2011; Dreybrodt 2008).

The isotopic fractionation between water and calcite during calcite precipitation is temperature dependent (Figure 4.9). Fractionation occurs due to different rate constants for the heavy and light isotopes, the heavy isotope being preferentially incorporated in the calcite (Dreybrodt and Scholz 2011). If the calcite is in isotopic equilibrium with the water, the $\delta^{18}O$ of calcite reflects the $\delta^{18}O$ of drip water and the temperature during calcite deposition. The fractionation between water and calcite decreases with increasing temperature (–0.24‰ °C^{-1}). Note that this counteracts the temperature dependence of the precipitation $\delta^{18}O$, which shows a positive correlation with temperature. Although it has often been assumed that calcite is precipitated in isotopic equilibrium with the drip water, an increasing number of studies questions this assumption (see Section 4.5.3).

4.5.2 Carbon

The carbon isotopic composition of speleothems depends on the sources of carbon and its transfer processes (Figure 4.10). The two main carbon sources are the soil CO_2 production and the dissolution of carbonate bedrock. Carbon in soil CO_2 is isotopically lighter than carbon derived from bedrock dissolution, which is typically around 1‰. Their respective proportions

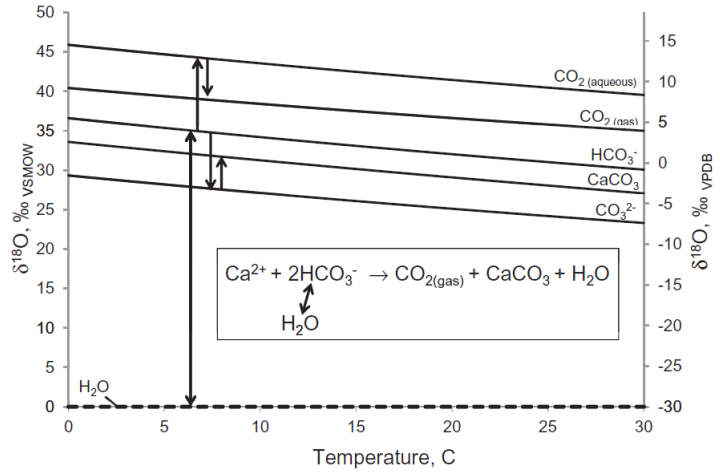

Figure 4.9: Oxygen isotope fractionations and the composition of phases with respect to a H_2O $\delta^{18}O$ value of zero. Temperature variations result in significant effects on the $\delta^{18}O$ of the precipitated calcite under equilibrium conditions, because the oxygen isotope composition of all phases is buffered by the large reservoir of H_2O molecules. The fractionation between heavy calcite and light water decreases at higher temperatures (Fairchild and Baker 2012).

are variable, but in most temperate sites, the soil CO_2 represents about 90% of the carbon in $CaCO_2$, which has been quantified using the bomb peak ^{14}C signal (Genty and Massault 1999, 1997; Genty et al. 1998).

The $\delta^{13}C$ of soil CO_2 is partly determined by the type of vegetation. The CO_2 respired from plants carries a characteristic $\delta^{13}C$ signature depending on their photosynthetic pathway. Soil CO_2 derived from a C3 vegetation has a $\delta^{13}C$ of about –26‰, the CO_2 derived from a C4 vegetation has a $\delta^{13}C$ of about –13‰. Exchange with the atmosphere raises the $\delta^{13}C$ of soil air CO_2, because the $\delta^{13}C$ of atmospheric CO_2 is –8‰ (Keeling et al. 2005). As there is no natural C4 vegetation (drought tolerant grasses) in a temperate climate, changes in the dominant vegetation type are not relevant in the European context.

The density of vegetation also has an impact on the $\delta^{13}C$ of speleothems. A dense vegetation cover leads to an increased soil CO_2 production through plant respiration and microbial activity. This raises the proportion of ^{12}C in the dissolution zone, and consequently lowers the $\delta^{13}C$ in the speleothem (Baldini et al. 2005). An increased biogenic CO_2 production is generally associated with warm and wet conditions. A lowering of the $\delta^{13}C$ of soil CO_2 due to increased vegetation activity can also be seen on a seasonal scale, as the soil respiration rate (soil pCO_2) is higher in the summer than in the winter (Frisia et al. 2011).

An alteration of the vegetation- and soil-derived $\delta^{13}C$ signal can occur during bedrock dissolution in the epikarst, depending on the dissolution conditions. When bedrock is dissolved, heavier carbon enters the solution. Under open system conditions, the water is in contact with the soil air, which means that there is an unlimited reservoir of CO_2. The DIC is in isotopic equilibrium with the CO_2 and thus carries the isotopic signature of the CO_2. In a closed system, the water is not in contact with the soil air. Therefore, the $\delta^{13}C$ of the DIC depends on the isotopic composition of both the soil air CO_2 and the bedrock carbonate (Fohlmeister et al. 2011). In nature, an intermediate state between open and closed system conditions is likely, and with more closed system conditions the $\delta^{13}C$ of speleothems tends to increase (Genty et al. 2001a; Genty and Massault 1999).

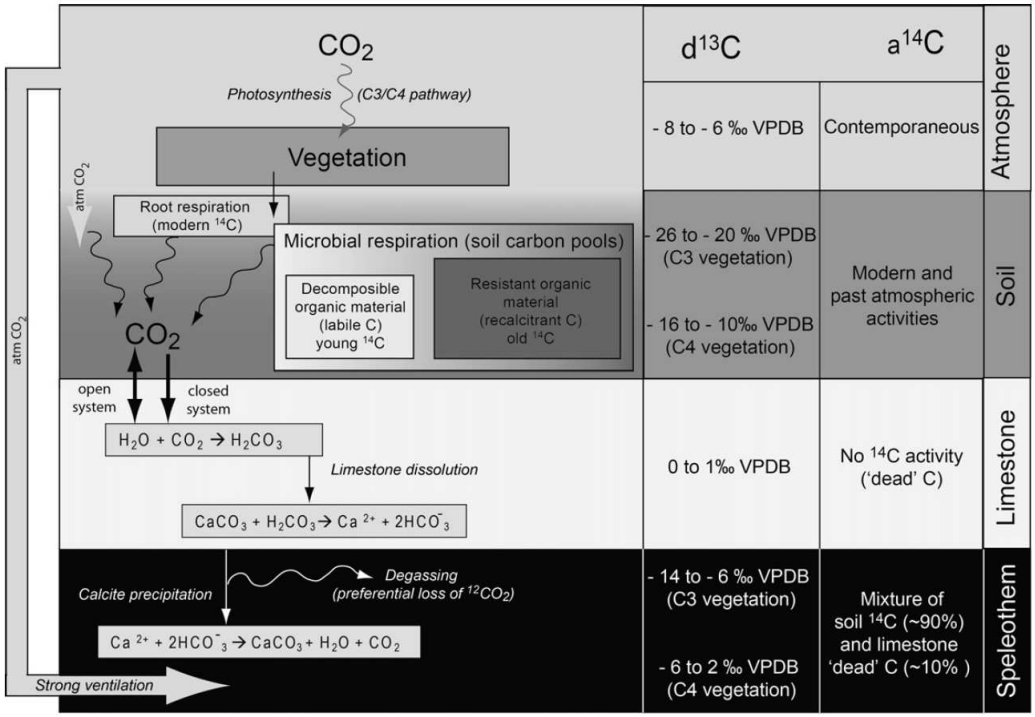

Figure 4.10: Speleothem carbon sources and transfer processes (Rudzka et al. 2011).

Finally, processes of degassing and calcite precipitation in the cave can further modify the isotopic composition of DIC in the drip water which contributes to speleothem growth. The degassing of CO_2 from the drip water causes fractionation due to different coefficients of molecular diffusion for the heavy and light isotopes of carbon, which results in an increase of $\delta^{13}C$ of the DIC (Dreybrodt and Scholz 2011). The $\delta^{13}C$ of the CO_2 is about 10‰ lower than the $\delta^{13}C$ of the dissolved carbon species. Kinetic effects during fast degassing are counteracted by a slower isotopic re-equilibration between drip water and cave air, which lowers the $\delta^{13}C$ of the DIC when drip rates are slow. This equilibration takes about 1 h (Dreybrodt and Scholz 2011). The rate of degassing is controlled by the pCO_2 difference between water and cave atmosphere. The amount of re-equilibration is determined by drip rate and calcite precipitation rate. A low cave air pCO_2 in a well-ventilated cave enhances rapid degassing (i.e. high $\delta^{13}C$ of the DIC, and also high calcite precipitation rates), while a higher pCO_2 promotes equilibration (i.e. low $\delta^{13}C$ of the DIC). Likewise, slow drip rates and slow calcite precipitation rates leave time for isotope exchange and equilibration with cave air, leading to lower $\delta^{13}C$ of the DIC and the precipitated calcite.

The fractionation between HCO_3^- and $CaCO_3$ during calcite precipitation is small and leads to a slight enrichment of ^{13}C in the solid phase (Figure 4.11). It is dependent on temperature, but unlike for oxygen isotopes, the temperature-dependent fractionation during precipitation plays only a minor role compared to the changes in $\delta^{13}C$ of DIC in the percolating water due to degassing.

Prior calcite precipitation (PCP) can happen above the site of deposition of the studied speleothem, when CO_2 degasses into air-filled pores during dry conditions (Fairchild et al. 2000). PCP changes the composition of the percolating water, leading to lower Ca concentrations and a higher $\delta^{13}C$ of the remaining DIC.

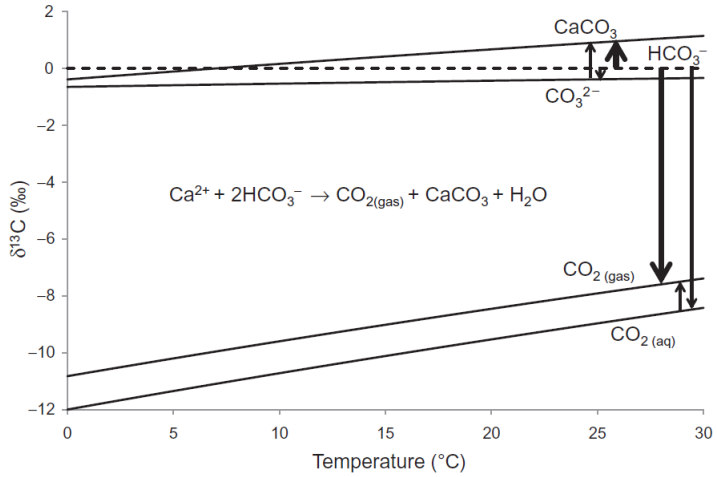

Figure 4.11: The isotopic composition of carbon species with reference to a HCO_3^- $\delta^{13}C$ value of zero. The most important fractionation during calcite precipitation is the degassing of ^{13}C-depleted CO_2, which results in an increase in the $\delta^{13}C$ value of the solution. The fractionation between the HCO_3^- and $CaCO_3$ is much smaller, and the temperature effect is small compared to variations in the solution $\delta^{13}C$ during progressive precipitation (Fairchild and Baker 2012).

Several of the above mentioned processes can lead to a seasonal variation in the $\delta^{13}C$ of speleothem calcite. The isotopic composition of carbonate species varies throughout the year depending on the seasonal vegetation activity, PCP (seasonal dryness) and flushing events, as well as seasonal changes in degassing due to enhanced cave ventilation and changing pCO_2 of the cave atmosphere in winter.

In summary, there is little carbon fractionation during calcite precipitation. $\delta^{13}C$ variations in speleothems can be interpreted as vegetation density and soil activity changes, which can be climate driven, but also anthropogenic, e.g. due to deforestation (Zhang et al. 2004). On the other hand, the vegetation signal imprinted in the soil CO_2 can be changed deeper into the karst by PCP and degassing, processes which might be linked to cave ventilation or dry weather conditions.

4.5.3 Isotopic Equilibrium and "Hendy Test"

In order to interpret speleothem isotopic records, it is crucial to evaluate whether the calcite was deposited in isotopic equilibrium. Kinetic fractionation significantly affects the isotopic composition of speleothem calcite and can obscure the original environmental signals imprinted in e.g. the $\delta^{18}O$ of precipitation or the $\delta^{13}C$ of soil CO_2. Equilibrium conditions are likely when there is sufficient time for isotopes to exchange. Kinetic fractionation occurs in rapid or incomplete reactions, such as fast CO_2 degassing from the drip water, fast calcite precipitation, or the evaporation of drip water (Mickler et al. 2004).

A simple and widespread method to recognize equilibrium conditions is the "Hendy test" (Hendy 1971). The criteria for isotopic equilibrium according to this test are (1) the $\delta^{18}O$ remains constant along a growth layer (i.e. it stays in equilibrium with the water), while $\delta^{13}C$ varies irregularly; and (2) there is no correlation between $\delta^{18}O$ and $\delta^{13}C$ along a growth layer or along the central axis of the stalagmite. Kinetic fractionation is thus recognized by covarying $\delta^{13}C$ and $\delta^{18}O$, which both increase from the centre towards the flanks of the stalagmite: A

rapid loss of CO_2 leads to kinetic fractionation between HCO_3^- and CO_2, and a simultaneous enrichment of ^{13}C and ^{18}O in the solution, which progresses as the water moves over the stalagmite surface away from the apex (Hendy 1971).

However, even if the Hendy test can give an indication of kinetic effects, it is not a sufficient criterion to determine equilibrium precipitation (Dorale and Liu 2009). Equilibrium can occur at the central axis, but not on the flanks of a stalagmite (Romanov et al. 2008; Spötl et al. 2002). Furthermore, there are environmental conditions which can lead to covarying $\delta^{18}O$ and $\delta^{13}C$ in a stalagmite over time. A vegetation change, which has an impact on the $\delta^{13}C$ can be linked with a change in climate or hydrology which influences the $\delta^{18}O$. Instead, Dorale and Liu (2009) propose a replication of records to test the robustness of the signal (see e.g. Fohlmeister et al. 2012). Another possibility to test for isotopic equilibrium is to measure the $\delta^{18}O$ of drip water and contemporaneous calcite, and to then compare the measured cave temperature to the temperature calculated using theoretical equilibrium fractionation factors between water and calcite, but this is only applicable to modern samples with available monitoring data.

Laboratory experiments and field studies often point to a lack of isotopic equilibrium during the precipitation of speleothem calcite (Wiedner et al. 2008; Watkins et al. 2013). However, speleothems can be suitable for palaeoclimate reconstructions even if isotopic equilibrium between the dissolved carbonate species and the precipitated calcite is not given, and equations describing the temperature-dependent equilibrium fractionation to calculate palaeotemperatures (e.g. Kim and O'Neil 1997) cannot be applied. The interpretation of speleothem records requires the calibration of cave environmental conditions including kinetic isotope effects (Mickler et al. 2006), as it has been done in empirical approaches (Tremaine et al. 2011; Coplen 2007) based on observed modern cave temperatures along with drip water and calcite isotopic compositions. Furthermore, kinetic isotope effects are driven by physical processes in the cave which are related to climate (Mattey et al. 2008).

4.6 Other Proxies from Speleothems

A number of other proxies measured in speleothems provide information on different environmental parameters which may help interpret the fluid inclusion and calcite isotope records.

4.6.1 Morphology and Growth Rate

Stalagmite growth rates determine the temporal resolution of the proxies, and they can also serve as a proxy themselves. Typical growth rates are between 0.01 and 1 mm per year. They are principally controlled by the saturation state of the drip water (Ca concentration), drip rate, temperature, and the pCO_2 of the cave atmosphere (Genty et al. 2001b; Baker et al. 1998). Growth rates can therefore be an indicator of a number of environmental parameters: the amount of precipitation (drip rate), vegetation activity (soil CO_2 production, bedrock dissolution, Ca concentration), and cave air circulation (pCO_2). On long time scales, phases of slow growth are related to cold or dry climate conditions, which can reduce the water flow. In annually laminated stalagmites, it is possible to reconstruct the influencing parameters on an inter-annual scale (e.g. Proctor et al. 2002). The same parameters and transfer processes also influence the shape of a stalagmite. A reduced drip rate or reduced saturation, for example, leads to less calcite precipitation along the flanks and thus a thinner stalagmite (Fairchild and Baker 2012).

4.6.2 Trace Elements

Speleothems do not consist of pure calcite but incorporate impurities, ions which are substituted in the crystal structure, like Mg, Na, Sr, Ba, P or U. Sources of trace elements are the atmosphere, the soil, and the bedrock (Fairchild and Treble 2009). For the elements originating from bedrock dissolution, the important controlling factors are weathering rate and water residence time. Trace elements are transported as particles, colloids or in solution. Their concentrations are further controlled by the calcite precipitation process. Prior calcite precipitation leads to increased Mg/Ca and Sr/Ca ratios in a stalagmite, associated with a higher $\delta^{13}C$ (Fairchild et al. 2000). Trace element concentrations vary seasonally, and high-resolution measurements enable the identification of annual layers based on these concentrations (Treble et al. 2003).

4.6.3 Clumped Isotopes

The clumped isotope proxy is based on measurements of $\Delta 47$, which is the per mil deviation in the abundance of CO_2 with mass 47 ($^{13}C^{16}O^{18}O$) from random distribution (the CO_2 is derived from phosphoric acid digestion of calcite for mass spectrometric analysis). The combination of two heavy isotopes in a molecule results in a slight energy gain. This "clumping" is energetically relevant at low temperatures, like when calcite forms at Earth surface temperatures. At high temperatures, isotopes are distributed randomly. When calcite is precipitated in isotopic equilibrium, $\Delta 47$ depends only on temperature and is independent of the $\delta^{18}O$ and $\delta^{13}C$ of carbonate species in the drip water. If there is no isotope equilibrium, the combined measurements of $\Delta 47$ and $\delta^{18}O$ allows an identification and quantification of kinetic fractionation when either the cave temperature or the $\delta^{18}O$ of the drip water, e.g. obtained from fluid inclusion measurements, is known (Kluge et al. 2013; Kluge and Affek 2012; Daëron et al. 2011; Wainer et al. 2011).

5 Tree Rings as Palaeoclimate Archives

Tree rings have significantly contributed to our knowledge of late Holocene climate variability on annual to centennial time scales (Briffa 2000). They provide information about the amplitude, timing and geographical extent of climate change (Kromer et al. 2001). The great advantage of tree rings lies in their annual resolution, the precise dating, and the possibility to compare them directly to meteorological data from the same year. Tree growth responds to annual and long-term variations in the environmental conditions, such as temperature or water availability and other environment. The physiological response of the tree to this variability is recorded in their annual rings and can be deduced from tree ring proxies. The parameters which can be reconstructed depend on the site and species, and on the specific climate response of the tree.

Tree rings proxies are employed to reconstruct different climate variables such as temperature and precipitation amount (e.g. Grudd 2008; Loader et al. 2008), the isotopic composition of precipitation (Danis et al. 2006; Robertson et al. 2001; Saurer et al. 1997b), as well as derived climate variables like drought or atmospheric circulation indices (e.g. Kress et al. 2014; Heinrich et al. 2009). Furthermore, they offer the possibility to study geomorphological processes, river flow (e.g. Singh and Yadav 2013), and the history of ecological disturbances like forest fires (e.g. Flatley et al. 2013; Poulos et al. 2013) or insect outbreaks (e.g. Paritsis and Veblen 2011; Larson et al. 2009). The most widely used proxy from tree rings is tree ring width. It is also the basis of dating, and therefore its measurement is essential for the study of other tree ring proxies. Many parameters can be measured in tree rings and provide complementary information about past environmental changes. These include maximum latewood density (e.g. Björklund et al. 2012; Briffa et al. 1998), stable isotopes of carbon, oxygen and hydrogen in wood or cellulose (e.g. Daux et al. 2011; Etien et al. 2009), as well as wood anatomical features (e.g. Eckstein 2013; Olano et al. 2013; DeSoto et al. 2011).

This chapter gives an introduction to tree rings as palaeoclimate archives: the background on tree growth and the formation of tree rings (Section 5.1), the dating of tree rings (Section 5.2), as well as the different tree ring proxies and their link with climate (Section 5.3).

5.1 Tree Growth and Ring Formation

Many tree species growing in regions with seasonal changes in temperature and precipitation form annual rings. In order to interpret tree rings as a result of the influence of their environment, it is important to understand the physiological processes which link environment and ring formation (Speer 2012). The statistical models used to reconstruct climate from tree rings can only be successful when they adequately represent the biological effect of climate on tree growth (Fritts and Guiot 1990).

Trees take water and nutrients from the soil via their root network and exchange gases with the atmosphere through the leaves. The gas exchange of the leaves is controlled by the opening

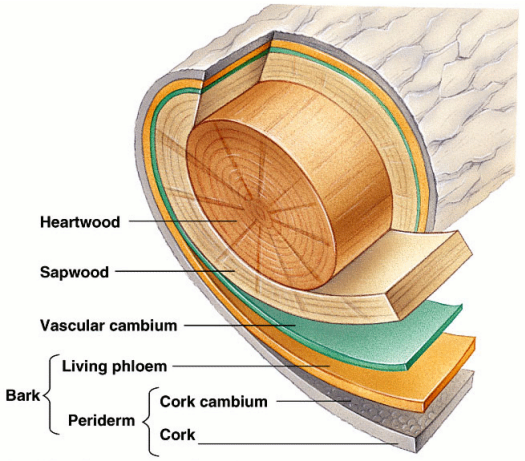

Figure 5.1: Cross-section of a tree stem (Reece et al. 2011). The vascular cambium is located between the wood and the bark.

and closing of the stomata. Trees are autotrophic organisms capable of fixing CO_2 during photosynthesis to form carbohydrates from CO_2 and water using solar energy. In the stem, the photosynthesis products are transported downward to where the tree rings are formed. The stem is also responsible for upward transport of water and nutrients. The water flow is driven by transpiration, water potential differences and capillary forces. The stomata aperture regulates water loss, which is therefore linked with the rate of CO_2 uptake. The wood synthesized in the stem is the result of these processes. It thus records conditions at the root–soil and the leaf–atmosphere interface, which are subject to diurnal and annual cycles, as well as to variations on interannual and longer time scales.

Tree growth comprises the elongation and the increase in diameter of the stem, branches and roots of a tree, resulting from meristematic tissue, i.e. cells capable of dividing and producing new cells (Parham and Gray 1984). The apical meristem is located at the tip of stem, branches and roots and is responsible for longitudinal growth. The lateral meristem, also called the vascular cambium, is a thin layer of meristematic tissue between the wood and the bark which is responsible for circumferential growth and thus produces the tree rings (Figure 5.1). Xylem cells are produced on the inside of the cambium, and differentiate into fibres, vessels, and other cell types which make up the wood structure of the tree. The function of the xylem is the conduction of water from the roots to the leaves, as well as mechanical support. Phloem cells are produced on the outside of the cambium and become the bark. The function of the phloem is the downward conduction of photosynthates from the leaves (Parham and Gray 1984).

Wood formation includes cell division, cell enlargement, cell wall thickening, and lastly lignification of the cellulose cell walls, which makes them more rigid. The wood formation process is influenced by genetic predisposition, day length (the photoperiod), as well as climate and soil conditions. While during the winter cambium cells are dormant, they start to form new cells at the beginning of the growing season in spring. As a tree grows, each year new layers of xylem and phloem are produced. A cross-section of a tree exposes these growth layers as concentric rings. The ring boundaries can be defined anatomically based on the different cell structures within a ring. At the beginning of the growing season, new cells are formed rapidly. The inner part of a tree ring, called earlywood, thus consists of large cells with thin cell walls. Towards

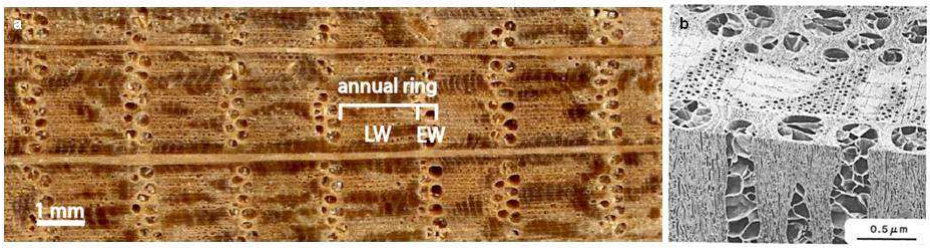

Figure 5.2: a) Transversal cross-section of the stem of an oak tree, exposing the annual rings with porous earlywood (EW) and denser latewood (LW). The growth direction is from right to left. b) Transversal and tangential cross-sections showing the vessels (Parham and Gray 1984).

the end of the growing season, tree growth slows down. Cells become gradually smaller and cell walls thicker; these cells form the latewood. Between two rings there is a sharp boundary with an abrupt increase in cell size (Fritts 1976).

The wood structure of gymnosperms (conifers) is mostly made up of fibres, the wood of angiosperms (deciduous trees) is composed of fibres and larger vessels, which are capillary-like cells for efficient water transport. For most angiosperms, there is no significant change in fibre cells from earlywood to latewood. Ring boundaries are rather distinguished by changes in distribution of vessels, which are seen as pores in the transversal cross-section (Figure 5.2). In ring-porous species like oak, vessels occur at the beginning of a growth ring. They are formed early in the growing season before leaves develop using stored photosynthates from the previous growing season to be able to transport water to the canopy, as old vessels are blocked in autumn (Speer 2012).

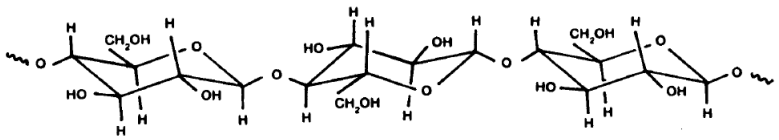

Figure 5.3: Molecular structure of cellulose (Pettersen 1984).

Wood consists mainly of cellulose (40–50%), hemicellulose (25–35%), and lignin (18–35%), with a smaller proportion of organic extractives and inorganic minerals (4–10%) (Pettersen 1984). Cellulose is a polysaccharide made of long glucose chains and has the molecular formula $(C_6H_{10}O_5)_n$ (Klemm et al. 2005; Figure 5.3).

5.2 Crossdating and Standardization

Trees growing in the same area respond to external environmental factors in a similar way. This results in patterns of wide and narrow rings, which can be identified among different trees. *Crossdating* denotes the matching of ring width patterns among radii within a tree and among different trees. Strong common patterns of year-to-year variability enable good crossdating. When using living and dead trees, a chronology can be extended far back in time, as long as the individual series overlap (Figure 5.4). When a chronology extends to a known date, a calendar year can be assigned to each ring. Some of the longest chronologies date back to about 12,500 BP (Friedrich et al. 2004).

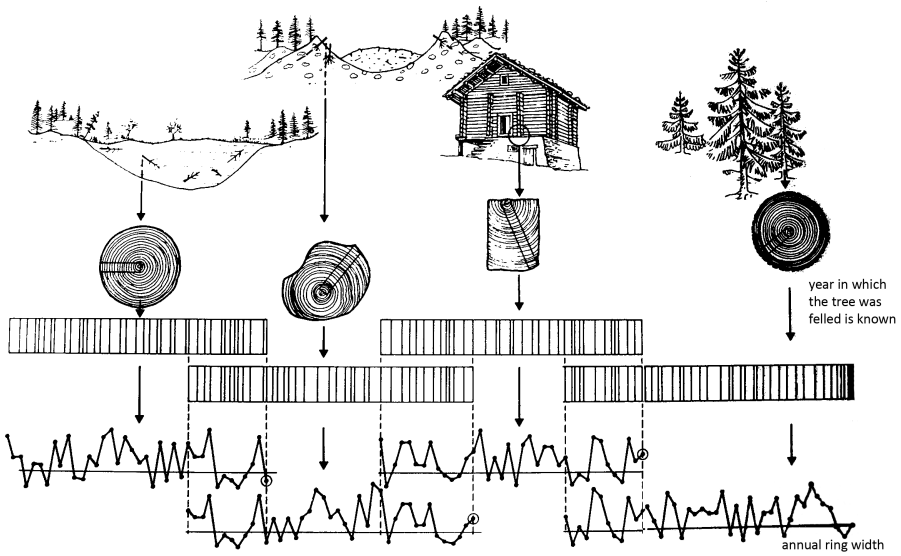

Figure 5.4: Schematic illustration of crossdating. Samples from different sources can be crossdated when the time spans they cover overlap and similar patterns of ring width variation are identified. By using living and dead trees, logs from buildings, and subfossil wood, a chronology can be extended far back in time (modified from Schweingruber 1988).

There is a systematic decline in ring width with increasing age of the tree, because as the circumference of the stem increases, a larger volume of wood tissue needs to be produced to form a new annual ring (Fritts 1976), and because photosynthetic rates and growth slow down with increasing tree age (Peñuelas 2005; Bond 2000; Yoder et al. 1994). The age-related biological trend and other non-climatic trends are considered as noise and need to be distinguished from climatic signal. This signal is considered to be the variability that is in common between all tree ring series at a site. In order to enhance the climate signal and remove the noise, tree ring width series are usually standardized by fitting a smooth growth curve through the data, using a deterministic or stochastic function (Cook and Kairiukstis 1990). The choice of the *standardization* methods depends on the scientific question and the specific growth patterns of the trees. For crossdating purposes, long-term trends are removed and the inter-annual variability is enhanced. In order to build a tree ring width chronology for climate reconstruction, it might be of interest to preserve the lower frequency variability. However, some of the low-frequency climate variability will be inevitably be lost in the standardization process when age trends are removed. The maximum wavelength of climate information which can be recovered from tree ring width is further limited by the lengths of individual series, typically about 100–400 years (Cook et al. 1995).

5.3 Tree Ring Proxies and their Links with Climate

Tree growth is influenced by a variety of climatic and non-climatic factors (Schweingruber 1996). These include temperature, precipitation, insolation, soil properties such as available nutrients and water holding capacity, wind, the CO_2 concentration of the atmosphere, the effects of competition with other plants for light, root space and water, as well as mechanical damage, e.g. caused by insects or fire. Changes in these environmental factors influence plant physiological processes, resulting in certain structural and chemical characteristics of tree rings.

These influences are therefore recorded as variations in the tree-ring proxies, which, in turn, can be used to reconstruct the variable of interest.

5.3.1 Tree Ring Width and Density

The strongest climate signal in tree ring width, and thus the most reliable climatic information, can be expected from trees growing at their climatic distribution limit, where growth processes strongly depend on climate. A strong growth limitation results in high sensitivity, i.e. a large year-to-year variation in ring width (Travis and Meentemeyer 1990). If there is only one main limiting factor to growth, it will cause similar ring width variations in many trees and there will be a strong correlation between ring width and this factor.

Favourable growth conditions lead to large tree ring widths, whereas under less favourable conditions, smaller rings are formed. Ring width can be significantly correlated with precipitation at arid sites, where low precipitation leads to drought stress and the formation of smaller rings (e.g. Stahle et al. 2007). Temperature is a strongly limiting factor at high-elevation or high-latitude tree line sites, and trees will have a high sensitivity to temperature (e.g. Coppola et al. 2013; Jacoby and D'Arrigo 1989). But also trees found in regions with generally favourable conditions can provide sensitive proxies if they are selected in order to maximise their response to a certain factor, e.g. by choosing trees from a dry site for precipitation reconstruction (Jönsson and Nilsson 2009).

Maximum latewood density is significantly correlated with temperature in cold and humid sites at high latitudes and altitudes (e.g. Grudd 2008; Briffa et al. 2001). High summer temperature prolongs the growing season, resulting in the formation of more dense latewood. However, the applicability of this proxy is restricted to certain conifer species; it is less suitable when increasing temperature is associated with an increase in drought stress (Helle and Schleser 2004b).

In a temperate climate like in the study area in southwest France, environmental conditions are often close to an optimum for plant growth. There is no single limiting factor for tree growth and the sensitivity of proxies like tree ring width and maximum latewood density is weak. In this case, stable isotopes in tree ring cellulose might show a stronger climate response (Young et al. 2012; Loader et al. 2008) and potentially provide powerful climate proxies, because fractionation mechanisms that affect the isotopic ratios of water and carbon dioxide are controlled by environmental conditions.

5.3.2 Oxygen Isotopes in Cellulose

Oxygen in organic matter has two sources, CO_2 and water. However, as the CO_2 is in isotopic equilibrium with the water, the $\delta^{18}O$ of the organic matter is principally determined by the $\delta^{18}O$ of the water (DeNiro and Epstein 1979). This water, which is also the source hydrogen in tree ring cellulose, is taken from the soil by the roots. Oxygen and hydrogen isotope ratios in cellulose are very different from those of their source water. The fractionation has biological causes, and there is a certain degree of fractionation which is dependent on the tree's response to environmental conditions.

Oxygen and hydrogen isotope ratios in cellulose have essentially the same control mechanisms, although different fractionation factors apply. Hydrogen has the largest variations in stable isotope ratios because it has the largest mass difference in isotopes relative to the mass of the

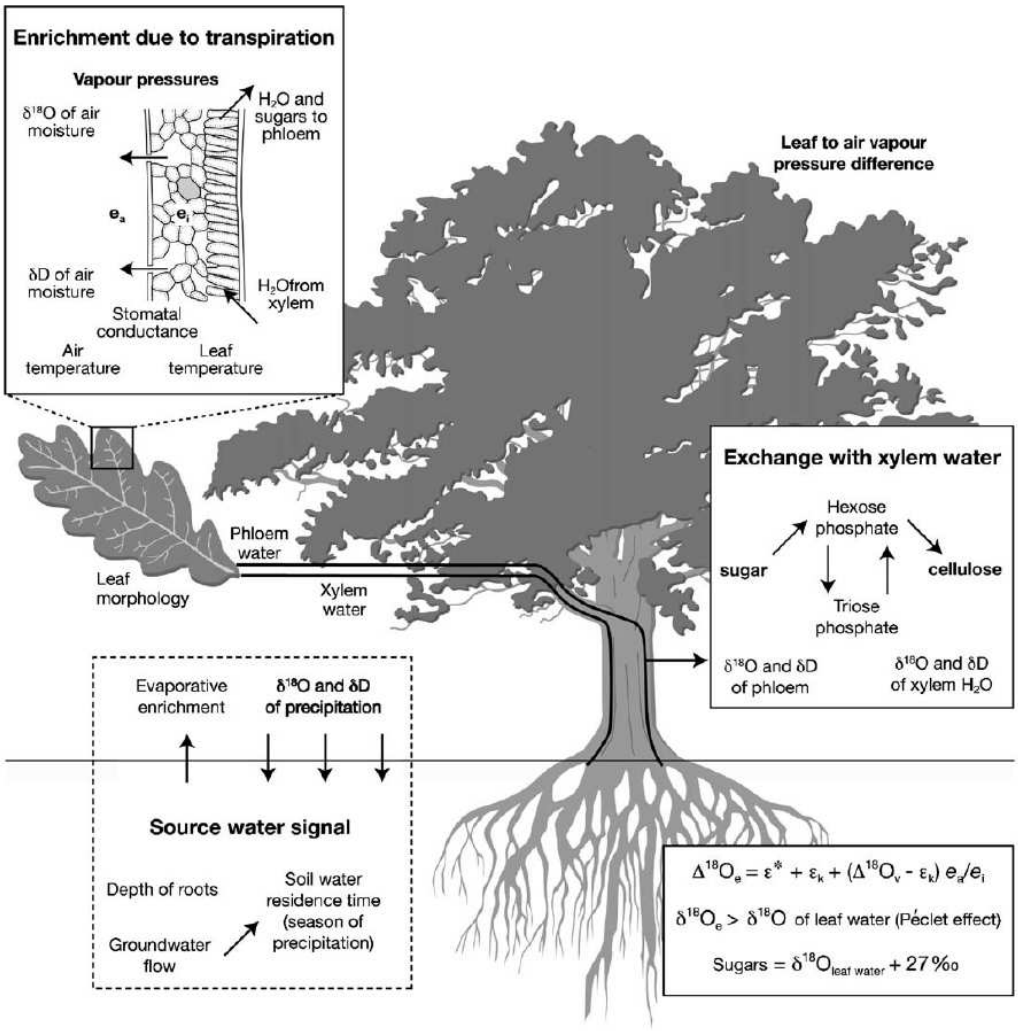

Figure 5.5: Main controls on the fractionation of oxygen isotopes in cellulose and the influencing environmental factors. The variables and equations are explained in the text (McCarroll and Loader 2004).

element (cf. Chapter 2). But sample preparation for δD analysis is much more complicated, as the hydrogen in hydroxyl groups of cellulose can exchange with atmospheric moisture. To prevent this, cellulose has to be nitrated or equilibrated with water of known isotopic composition (McCarroll and Loader 2004). This section explains the mechanisms with the example of oxygen isotopes, which are the focus of this thesis and of most other studies.

Acquisition of the Oxygen Isotope Signal in Cellulose

There are four main controlling factors on the isotopic composition of cellulose: (1) the isotopic composition of the source water; (2) the evaporative enrichment in the leaves during transpiration; (3) the biochemical fractionation during photosynthesis; and (4) the isotopic exchange during cellulose formation in the tree ring between ascending xylem water (i.e. source water) and photosynthates which are transported down in the phloem (Figure 5.5).

The isotopic composition of the *source water* depends primarily on the isotopic composition of precipitation at the site. However, the δ^{18}O signal of precipitation can be modified before

being taken up by the tree roots through evaporation from the soil, and through the mixing of water from different seasons in the soil zone (cf. Section 3.2). The rooting depth of the tree is also important for the source water. Trees can take water from different depths. This depth is species dependent and can change with tree age and with the availability of water (Phillips and Ehleringer 1995; Ehleringer and Dawson 1992). The isotopic composition of shallow soil water can be similar to that of precipitation, or at least contain a seasonal signal, whereas deeper soil water has a longer residence time and its isotopic composition may represent a long-term mean of precipitation. There is no fractionation during water uptake by roots and during transport of water from the roots to the leaves (Bariac et al. 1991; White et al. 1985).

During transpiration, water evaporates from the leaves and isotopic fractionation occurs as the lighter molecules evaporate faster than heavy molecules (cf. Chapter 3). The remaining leaf water is isotopically enriched by as much as 20‰ (Saurer et al. 1998). The *enrichment of leaf water* above the original source water ($\Delta^{18}O_e$) is given by the equation

$$\Delta^{18}O_e = \varepsilon^* + \varepsilon_k + (\Delta^{18}O_v - \varepsilon_k) * e_a/e_i \tag{5.1}$$

where ε_k is the kinetic fractionation during diffusion through the stomata, ε^* is the liquid-water equilibrium fractionation associated with the depletion of water vapour in $H_2{}^{18}O$, $\Delta^{18}O_v$ is the oxygen isotope composition of atmospheric water vapour relative to source water, and e_a/e_i is the ratio of ambient to intercellular vapour pressure (Barbour et al. 2005; Dongman et al. 1974; Craig 1965). This means that the leaf water $\delta^{18}O$ depends on the relative air humidity, as well as on the isotopic composition of the source water and of the water vapour of the surrounding air. When stomatal conductance, i.e. the rate of water vapour going out of the leaves, increases, the evaporative enrichment decreases. The $\delta^{18}O$ of leaf water is actually less enriched than predicted by Equation 5.1, because the backward diffusion of $H_2{}^{18}O$ is opposed by the transpirational flow of non-enriched source water to the sites of evaporation. This is known as the *Péclet effect* (Barbour et al. 2004; Farquhar and Lloyd 1993).

A *biochemical fractionation* occurs during photosynthesis. The sugars which are produced have $\delta^{18}O$ values 27‰ higher than the leaf water (Sternberg et al. 1986; Yakir and DeNiro 1990; Cernusak et al. 2003). This fractionation is constant. There is no alteration of the $\delta^{18}O$ of photosynthetic sugars when they are transported in the phloem from the leaf to the stem. Another fractionation process occurs during cellulose synthesis in the tree ring, where oxygen isotopes of the transported sugars *exchange with xylem water* ascending in the stem. When cellulose is formed, the sucrose molecules cleave to form hexose phosphates, whereby 20% of the oxygen atoms can exchange with the water (Barbour and Farquhar 2000). Furthermore, a proportion of the hexose phosphate goes through a futile cycle to triose phosphates before forming cellulose, which allows further exchange (Hill et al. 1995). The proportion of oxygen atoms which exchange with the xylem water determine to what extent cellulose $\delta^{18}O$ represents the source water signal and the evaporative enrichment respectively. Cernusak et al. (2005) reviewed studies which estimate this proportion for a variety of plants and found an average value of 42%. The same value was found by Roden et al. (2000) in a controlled experiment on tree rings. However, the proportion seems to be variable throughout the growing season (Offermann et al. 2011) and its controls are poorly constrained (McCarroll and Loader 2004).

Taking into account the biochemical fractionation and isotope exchange between sucrose and xylem water, the isotopic composition of cellulose ($\delta^{18}O_{cell}$) can be related to the isotopic composition of the leaf water ($\delta^{18}O_{lw}$) and the source water ($\delta^{18}O_{sw}$) (Yakir and DeNiro

1990; Sternberg et al. 1986):

$$\delta^{18}O_{cell} = 0.42 * \delta^{18}O_{sw} + 0.58 * \delta^{18}O_{lw} + 27‰ \quad (5.2)$$

Climate and Environmental Signals

It can be concluded from the previous section that the environmental signals recorded in the oxygen isotope composition of cellulose are those determining the source water isotopic composition, and those controlling leaf water enrichment, i.e. principally the δ^{18}O of precipitation and relative humidity. The relative strength of these two signals, however, can be variable (McCarroll and Loader 2004).

Often a strong link between δ^{18}O of cellulose and temperature can be established (e.g. Etien et al. 2008). Although temperature has little direct influence on the δ^{18}O of cellulose, temperature is highly correlated with relative humidity, which is the dominant control on leaf water enrichment. As relative humidity decreases, stomatal conductance decreases and the enrichment of leaf water increases, resulting in a higher δ^{18}O of the assimilated sugars. Furthermore, depending on the site, temperature can have an influence on the δ^{18}O of precipitation. These two effects influence δ^{18}O of cellulose in the same direction: A higher temperature is associated with a higher δ^{18}O of precipitation and a stronger evaporative enrichment of the leaf water.

The oxygen isotopic composition of cellulose can provide a measure of drought conditions (e.g. Haupt et al. 2011; Treydte et al. 2007; Raffalli-Delerce et al. 2004), because several drought-related parameters influence the tree at the root-soil and leaf-atmosphere interface, all leading to an increase in the δ^{18}O of cellulose. Both soil dryness and low relative humidity of the ambient air reduce stomatal conductance. High temperatures and low humidity also increase evaporation from the soil, which increases the δ^{18}O of the source water, and from the leaves, which increases the δ^{18}O of the leaf water. Drought indices such as the PDSI (Wells et al. 2004; Palmer 1965) are often employed in dendroclimatic reconstructions as they represent the combined temperature and precipitation/humidity influence on trees.

Oxygen isotope ratios in cellulose enable also the reconstruction of the δ^{18}O of precipitation, which determines the isotopic composition of the source water (Brienen et al. 2012; Danis et al. 2006; Robertson et al. 2001; Saurer et al. 1997b). It is important to select an appropriate site for the purpose of the study. To reconstruct relative humidity or temperature, it is advisable to choose a site where trees get their water supply from ground water, where the source water signal is rather constant and the cellulose isotopic composition will be dominated by the leaf water enrichment. In order to reconstruct the δ^{18}O of precipitation, one should use a well-drained site and species with shallow roots which are influenced by changes is the isotopic composition of the soil water (Helle and Schleser 2004b).

Age Trend in Cellulose δ^{18}O Series

Both tree ring width and maximum density series are usually standardized in order to remove trends linked to tree age and other non-climatic factors (Section 5.2). It is a well-known problem of palaeoclimatic studies using these proxies that standardization also eliminates long-term climatic trends in the series (Cook et al. 1995; Briffa et al. 1992). An often stated advantage of stable isotope proxies compared to tree ring width is that the time series do not need to be standardized, and a possible low-frequency climate signal can be preserved (Young

et al. 2011; Gagen et al. 2007). Indeed, a clear age trend as for ring width is not observed in oxygen isotope series. However, there is still a debate about whether age related effects on the oxygen isotopic composition of cellulose exist, and in many studies possible trends are masked by pooling. Several authors give indications on juvenile effects or age trends, most of them focusing on coniferous trees, but they do not provide a coherent picture.

Decreasing δ^{18}O trends over several centuries have been described in pine trees from the Pyrenees (Esper et al. 2010) and in junipers from Pakistan (Treydte et al. 2006). In *Pinus nigra* from Corsica, on the contrary, no long-term age trend was observed, but a significant decrease in δ^{18}O in the juvenile phase of tree growth (Szymczak et al. 2012). Marshall and Monserud (2006) compared cellulose δ^{18}O trends in different species and found a decreasing trend in Douglas fir over a period of 100 years, whereas ponderosa pine and western white pine from the same site showed no trend. Spruce trees from the Tibetan Plateau (pooled records from two groups of trees with a mean age difference of 140 years) showed no significant difference in δ^{18}O (Shi et al. 2011). Raffalli-Delerce et al. (2004) found no effect of tree age on δ^{18}O in oak trees from Brittany, north-west France. Lastly, Young et al. (2011) investigated carbon and oxygen isotopes in pine trees from Norway, leaving out the first 50 years of each tree, and found no significant age trend.

A study to test systematically whether an age trend in the oxygen isotopic composition of cellulose exists would need well-replicated samples, which are not pooled, and long enough to observe the supposed trend. If juvenile effects of age trends in cellulose δ^{18}O should be confirmed, it would be necessary to correct the series before they can be used in climate reconstructions. Furthermore, it is important to consider whether the climate response of the proxy changes with tree age (Dorado Liñán et al. 2011a; Voelker 2011).

5.3.3 Carbon Isotopes in Cellulose

The δ^{13}C of cellulose depends on the isotopic composition of the carbon source (i.e. atmospheric CO_2), the leaf carbon budget, and the fractionation associated with photosynthesis (Hayes 2001). The present day δ^{13}C of atmospheric CO_2 is –8‰ (Keeling et al. 2005). Carbon isotope ratios measured in cellulose must be corrected for the atmospheric δ^{13}C trend because the anthropogenic increase in carbon dioxide concentrations since the beginning of the industrial era has lowered the δ^{13}C of atmospheric CO_2 by 1.5‰. As fossil fuels are of organic origin, they are depleted in ^{13}C (Friedli et al. 1986).

Typical δ^{13}C values of cellulose are lower compared to atmospheric CO_2, between –20‰ and –30‰ (McCarroll and Loader 2004). The opening and closing of stomata regulates transpiration, and so the uptake of carbon dioxide. CO_2 moves through the stomata, is dissolved in leaf water and then used in the photosynthetic reactions. In times of water stress, stomatal conductance is reduced in order to reduce the moisture loss. The first fractionation step occurs during the diffusion of air through the stomata. The CO_2 molecules containing the lighter ^{12}C diffuse more easily than those containing ^{13}C. This fractionation due to diffusion leads to a depletion of the heavy isotope in leaf air compared to ambient air of –4.4‰ when stomatal conductance is small (Farquhar et al. 1989). The second fractionation step occurs during carboxylation through the CO_2 fixing enzyme RuBisCO, where the light isotope is used preferentially, leading to a fractionation of about –27‰.

Figure 5.6 illustrates these processes. The resulting δ^{13}C value of assimilated carbohydrates is controlled by the ratio of the leaf internal (c_i) and ambient air (c_a) CO_2 concentrations, and

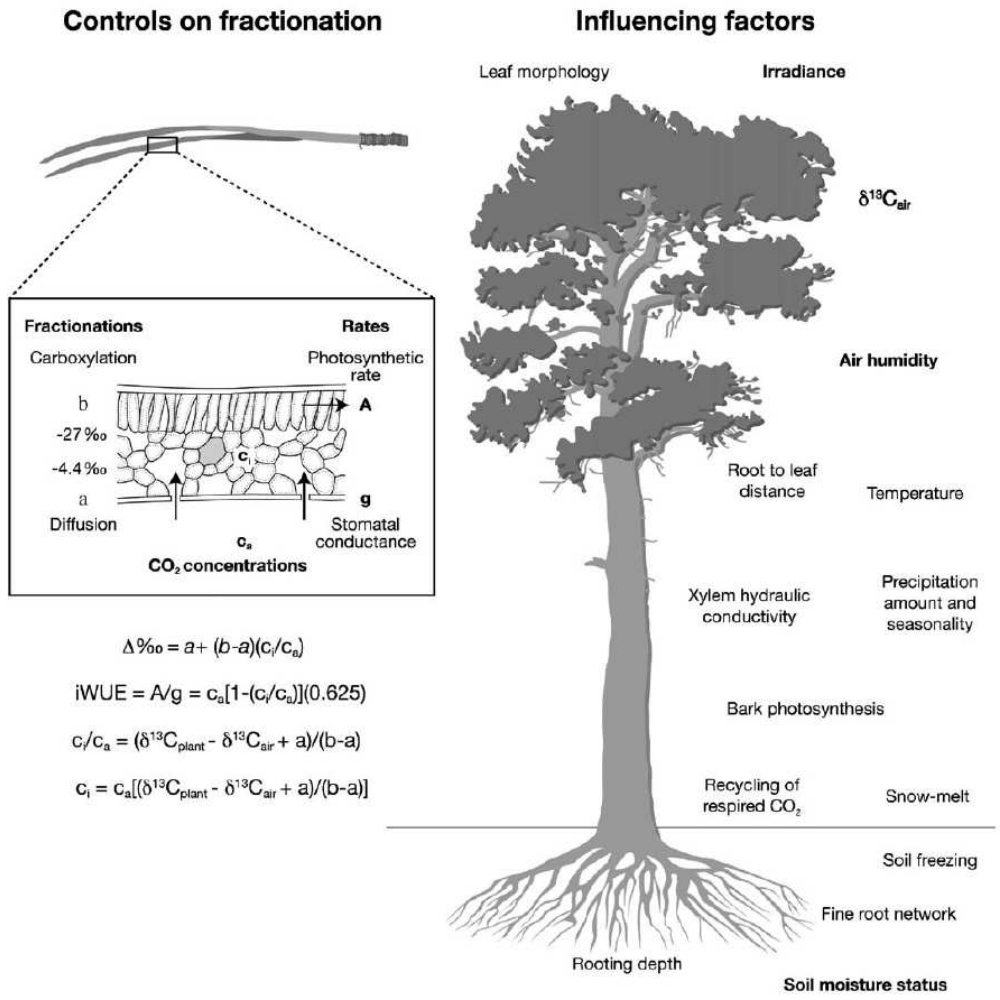

Figure 5.6: Main controls on the fractionation of carbon isotopes in cellulose (left), and the influencing environmental factors (right). $\Delta‰$ is the discrimination against ^{13}C, a is the discrimination of $^{13}CO_2$ during diffusion through the stomata, b is the discrimination during carboxylation, c_i and c_a are the leaf internal and ambient air CO_2 concentrations. Water use efficiency (WUE) is defined as the ratio of photosynthetic rate (A) and stomatal conductance (g) (McCarroll and Loader 2004).

the rate of photosynthesis. If stomata are open and c_i is high, the carboxylation fractionation step determines the $\delta^{13}C$ of the assimilates, leading to low $\delta^{13}C$ values. If stomata are closed and c_i is low, most of the carbon is used in photosynthesis, so there is little carboxylation discrimination of ^{13}C and the resulting $\delta^{13}C$ is higher (Helle and Schleser 2004b).

Climate and Environmental Signals

The $\delta^{13}C$ of cellulose is a measure of the balance between stomatal conductance and photosynthetic rate. The environmental parameters which can be reconstructed from cellulose $\delta^{13}C$ are those which control the rate of stomatal conductance and the rate of photosynthesis. At a humid site, the photosynthetic rate, which depends on temperature and irradiance, is the dominant control. On the contrary, for moisture-stressed trees the stomatal conductance is the principal control; it depends on environmental parameters related to air humidity and soil moisture (McCarroll and Loader 2004).

A combination of carbon and oxygen isotope ratios in cellulose can help distinguish the different influences on each individual proxy (Danis et al. 2006). Only the oxygen isotopic composition depends on the $\delta^{18}O$ of the source water, and only the carbon isotopic composition is controlled by photosynthetic rate. Both isotopes, however, are affected by changes in stomatal conductance and can therefore reflect moisture conditions (Saurer et al. 1997a). The variability they have in common should be linked to this factor.

Box 5.1 What is Relevant for Analytical Procedures?

Some of the characteristics of oxygen isotope ratios on the rings of oak trees, the species studies in this thesis, which are relevant for the following analytical procedures are outlined here.

Why Use Only Latewood?

In ring-porous tree species like oak, all earlywood vessels are embolized by frost events in the winter. The tree has to produce new earlywood vessels to restore its hydraulic conductivity before leaf expansion in the spring (Barbaroux and Bréda 2002). 30 to 40% of the annual growth increment is achieved before new leaves develop and CO_2 assimilation starts (Michelot et al. 2012; Bréda and Granier 1996). This means that the earlywood is formed using carbohydrates which were accumulated during the previous growing season. Furthermore, residual stem water which is used in the synthesis of earlywood can be isotopically enriched by evaporation during the winter (Phillips and Ehleringer 1995). Consequently, the earlywood of oak trees does not contain the climate signal of the year of its formation, and only the latewood is used in isotope analysis. The dependence of ring formation on the material which is stored from the previous year's growing season leads to an autocorrelation in tree ring width series. Since only the latewood is analysed in isotope studies, autocorrelation is weaker in isotope series.

Why Homogenize the Sample?

The oxygen and carbon isotopic composition of cellulose varies within a tree ring, and within the latewood, which has been shown for oak (Helle and Schleser 2004a,b) and other species (Ogée et al. 2009; Roden et al. 2009; Barbour et al. 2002). This gives the possibility to reconstruct intra-annual climate variability from tree rings (Loader et al. 1995), but a measured value cannot precisely be linked to a certain time of the year. The intra-annual $\delta^{18}O$ variability of cellulose is in the same order of magnitude as the inter-annual variability. In order to obtain a signal representative of the whole growing season (or rather, season of latewood formation), a complete homogenization of the sample before isotope measurement is necessary (Laumer et al. 2009), especially since the quantity of a cellulose sample analysed by mass spectrometry is small compared to the total amount of cellulose extracted from a ring.

Why Analyse Cellulose Instead of Whole Wood?

In most tree ring isotope studies, the measurements are not conducted on the whole wood but on cellulose, one of the dominant wood components. There are several reasons for this. The different wood components like cellulose and lignin differ isotopically (Wilson and Grinsted 1977). Whole wood and cellulose display very similar interannual isotope variations, although with an offset (Cullen and Grierson 2006; Harlow et al. 2006). The problem is that the proportion of cellulose and lignin varies between rings and between trees (Gindl 2001). Furthermore, cellulose decays faster than lignin (Spiker and Hatcher 1987). Although the isotopic composition of cellulose does not change during decay, differential decay changes the cellulose to lignin ratio (Loader et al. 2003). Cellulose can easily be extracted from the wood and shows a long-term stability (Savard et al. 2012). Although isotope exchange is rapid between organically bound oxygen of carbonyl and carboxyl functional groups and water, the oxygen of cellulose is only very slowly exchangeable (Epstein et al. 1977).

Part II

STUDY AREA AND METHODS

6 Sites and Samples

The study area is located in the southwest of France (Figure 6.1). The speleothems, the old trees, as well as the timber wood from historic buildings collected here provide the material for a multi-proxy climate reconstruction. The selection of the sampling sites was based partly on the potential to create new proxy records, and partly on available data from previous studies, which help to put the newly acquired results in context and facilitate their interpretation. An overview of the data is presented at the end of this chapter (Table 6.2). All sites lie in a similar climatic and geological setting, between 100 and 180 km from the Atlantic coast, at relatively low altitudes of 100 to 175 m a.s.l. The area can be considered as homogeneous with respect to meteorology and the isotopic composition of precipitation, as there is no important relief separating the closely located sites. The bedrock in the region is a Jurassic limestone, in which karstification has led to the development of caves during the Tertiary and the beginning of the Quaternary.

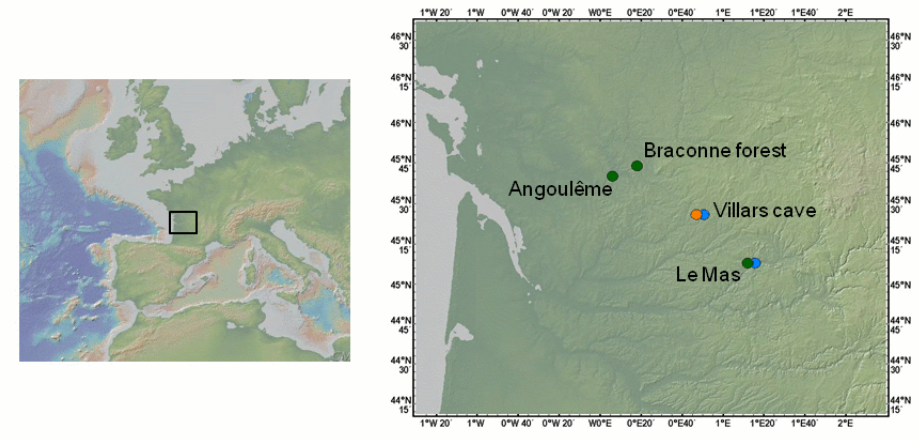

Figure 6.1: Location of the study sites in southwest France. Precipitation isotope monitoring data are available from Le Mas and Villars (blue dots). Speleothem samples originate from Villars cave (orange dot). Living trees were sampled at Braconne forest and Le Mas, and timber wood was sampled in historic buildings near the city of Angoulême (green dots) (maps from www.geomapapp.org).

6.1 The Climate of Southwest France

6.1.1 Present-Day Climate

The present-day climate in southwest France is temperate and characterized by a strong Atlantic influence with dominant westerly winds. The average annual temperature in the region is 11.8 °C, with relatively mild winters (average DJF temperature 5.2 °C) and warm summers (average JJA temperature 18.8 °C). Average annual precipitation is 817 mm, 18% of precip-

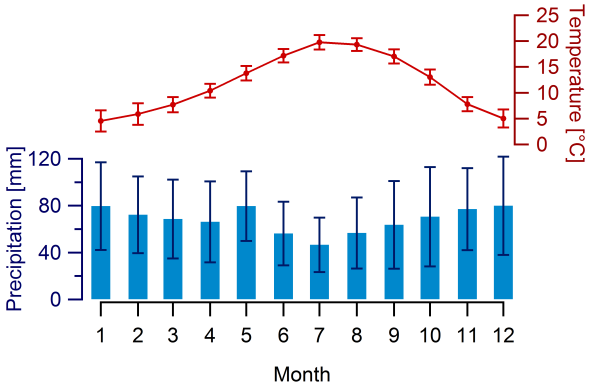

Figure 6.2: Annual cycle of temperature and precipitation in the study area for the period 1961–1990. Error bars indicate the standard deviation.

itation fall during the summer months (Figure 6.2).[1] Precipitation is mostly associated with fronts and depressions, with a contribution of convective rainfall events in summer. As no important relief separates the sites from the ocean in this zone of dominant westerly winds, the local proxies could be well representative of the general circulation in the north Atlantic, which influences the large-scale climate in western Europe.

6.1.2 Climate Trends in the Twentieth Century

The mean annual temperature of the study area shows a warming trend throughout the 20th century. From 1901 to 1979, this trend is about 0.01 °C/year. There is a marked increase in the warming trend from 1980 onwards to 0.05 °C/year (Figure 6.3). The positive temperature trend is significantly greater in France than on the global scale, and the strongest temperature increase in France is seen in the southwest region (Moisselin et al. 2002).

Tree ring proxies are often biased towards climate conditions during the growing season. It is therefore important to consider how representative summer temperatures are of the mean annual temperature, although it must be kept in mind that the relationship between average climatic conditions during the summer and during the whole year can change over time (Jones et al. 2003). The trends are similar in the average summer temperature and the average annual temperature, but with a more pronounced shift to higher summer temperatures between 1920 and 1940 (Figure 6.3).

Annual precipitation sums do not show a unidirectional trend as temperature does. There is an increase in the beginning of the 20th century, followed by a period of low precipitation from 1940 to 1960. Precipitation sums of recent decades are comparable to those at the beginning of the century. Summer precipitation sums are less variable than the annual sums and do not show the same multi-decadal trends. On the country scale, there is a slight increase in annual precipitation amounts, but it is spatially less coherent than the temperature increase. In many regions of France, there is a significant increase in winter precipitation, and a less significant decrease in summer precipitation, together leading to an increase in the seasonal contrast (Moisselin et al. 2002). However, this trend is not well marked in the study area.

[1] The meteorological data presented in this section were obtained from CRUts3.1 (Harris et al. 2013), a gridded data set of monthly climate data with a spatial resolution of 0.5°. The time series and the seasonal and annual means represent averages over the grid cells containing the study sites.

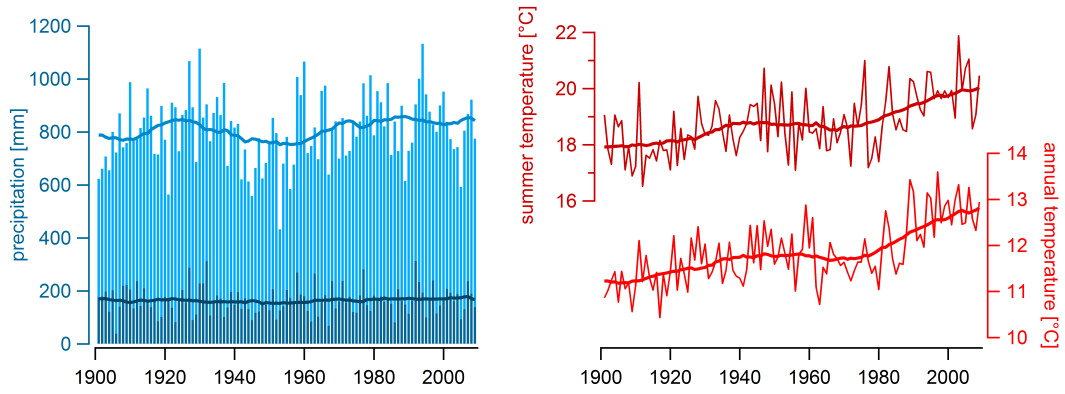

Figure 6.3: Temperature and precipitation trends in the study area for the 20th century. The dark red curve shows the mean summer (JJA) temperature, the light red curve the mean annual temperature. Dark blue bars indicate summer precipitation sums, and light blue bars annual precipitation sums. The thick lines are 30-year running means.

Droughts are a recurrent feature of the climate in southwest France. Even the relatively humid, oceanic regions of France can be impacted by summer droughts, despite an increase in winter rainfall (Dubreuil 1997; Dubreuil et al. 1997). While the drought of 1976 was recognized as an extreme event (Brochet 1977), the repeated droughts in 2003, 2004 and 2005 were perceived as a possible consequence of climate change, the occurrence of drought periods having increased in France since the 1970s (Itier 2008).

Future climate change might therefore have severe impacts on southwest France, and the study of past climate variability is important to understand possible causes and impacts, as well as the magnitude of these changes. Different climate change scenarios predict a temperature increase for Europe, especially in the summer months, together with an increase in the frequency, intensity and duration of heat waves (Clark et al. 2010; Tebaldi et al. 2006). Changes in precipitation, however, which are more relevant for local agriculture and water supply, are much more uncertain in the model predictions for France, as France is on the limit between a predicted increase in precipitation amounts for northern Europe and a predicted decrease for the Mediterranean region (Christensen et al. 2007). Levrault et al. (2010) predict an increased risk of drought for southern France through the combined effects of temperature increase, a reduction in total annual precipitation amounts and a significant increase in potential evapotranspiration.

6.1.3 The Isotopic Composition of Precipitation

If the $\delta^{18}O$ of precipitation at a site is to be used as a palaeoclimate indicator, its relationship with temperature, precipitation amount and atmospheric circulation must be determined at a time scale which is relevant for the proxy isotope record. Interannual changes and long-term trends are more appropriate for the proxy interpretation than e.g. monthly temperature–precipitation $\delta^{18}O$ correlations, which are linked to their seasonal cycles. European precipitation $\delta^{18}O$ is generally characterized by a seasonal temperature effect, and spatial comparisons demonstrate a continental effect. Rozanski et al. (1992) have also observed that long-term trends in the $\delta^{18}O$ of precipitation over mid and high latitudes follow closely the long-term changes in surface air temperature. However, local isotope ratios are primarily con-

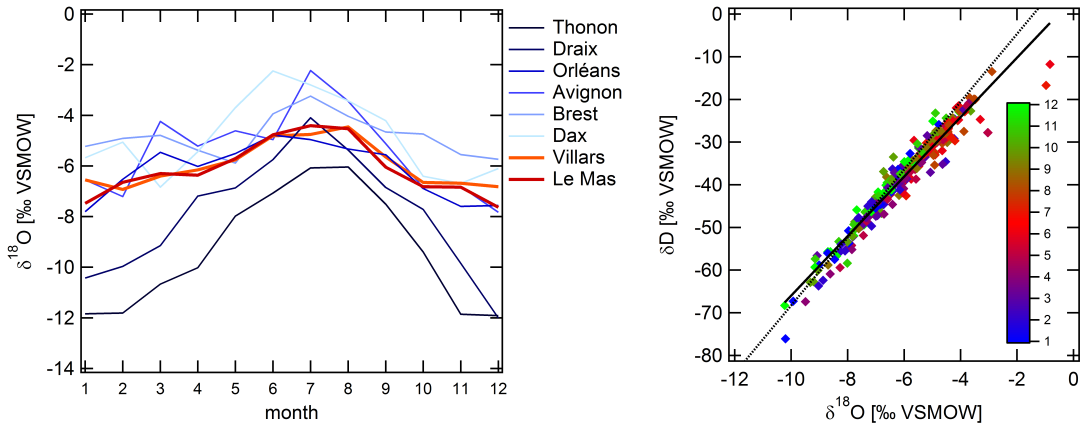

Figure 6.4: Mean annual cycle of δ^{18}O in precipitation for two sites in the study area, Le Mas and Villars (1997–2012), compared to the French GNIP stations which have more than five years of observations (IAEA/WMO 2006). Right: δD–δ^{18}O plot of Le Mas and Villars precipitation isotope data. The solid line is the local meteoric water line (LMWL), the dotted line is the global meteoric water line (GMWL). The colour scale indicates the months from January (1) to December (12).

trolled by regional scale atmospheric processes such as the trajectories and the precipitation-evapotranspiration history of the air masses. Local temperature and precipitation amount modify the isotopic composition of precipitation only slightly (Rozanski et al. 1982). Several studies have highlighted the important influence of the North Atlantic Oscillation (NAO) on the isotopic composition of precipitation in Europe (Langebroek et al. 2011; Field 2010; Baldini et al. 2008).

The isotopic composition of precipitation has been monitored at two sites in the study area, Villars and Le Mas, since 1997 (Genty 2008; see also Chapter 9 for an update to 2012). The annual cycle of precipitation δ^{18}O displays a seasonal variability which is similar to the temperature variation, with low values in the winter and high values in the summer (Figure 6.4). δ^{18}O increases steadily to a maximum in August, followed by a rather abrupt decrease to lower values in October. This pattern is similar to the patterns observed at the French stations which are included in the Global Network of Isotopes in Precipitation (GNIP). The local meteoric water line (LMWL) for Villars and Le Mas has a slope of 7.3, close to the global meteoric water line (GMWL). This indicates that there is no significant influence of water recycling from the continent (Koster et al. 1993). Due to the proximity to the coast and the prevailing westerly winds, the water vapour is dominantly coming from the Atlantic Ocean.

While precipitation δ^{18}O is correlated with temperature on a monthly scale, no significant correlations are observed at the seasonal or annual time scale, possibly due to a limited number of observations. The time series is too short to determine whether long-term (e.g. decadal) temperature trends are represented in the isotopic composition of precipitation. The link between temperature and the isotopic composition of precipitation in the study area will be further discussed in Chapter 9.

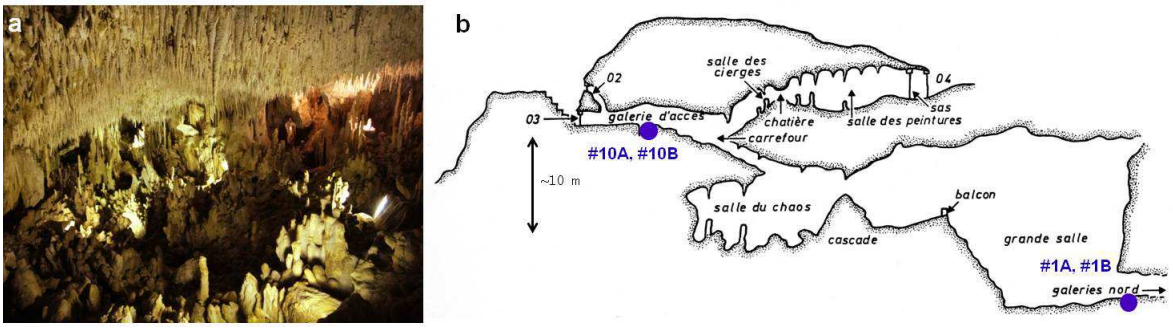

Figure 6.5: a) Photograph of Villars cave, which is very rich in speleothem deposits ("salle des peintures"). b) Vertical cross-section of Villars cave (Delluc and Delluc 1974). The blue circles indicate the drip water sampling stations.

6.2 Villars Cave

All speleothems which have been analysed in this thesis originate from Villars cave (for a detailed description see Genty 2008). The cave is located at 45°26'N, 0°47'E, at an altitude of 175 m a.s.l. and 150 km from the coast. The bedrock is a Middle Jurassic oolithic limestone formation from the Bajocian and Bathonian stages, which is 25 to 45 m thick and covered by a thin calcareous brown soil layer of about 20 cm. Villars cave was discovered in 1953 and is now developed as a tourist cave. It is very rich in speleothem deposits and also contains some prehistoric paintings. The cave has a gallery network of about 10 km, with two levels of galleries separated by 10 to 20 m of rock (Figure 6.5). The vegetation above the cave today consists mainly of oak and hornbeam forest; the southern part of the cave where the stalagmite vil-stm1 was sampled is covered by grassland.

The present day cave conditions have been monitored since 1997 (Genty 2008; see also Chapter 9 for an update to 2012). Monitoring stations have been set up at four dripping stalactites, two in the upper and two in the lower galleries of the cave (#1A, #1B, #10A, #10B; Figure 6.5). They are equipped with automatic drip counters. At one to two month intervals, water samples are taken at the four drip sites to determine their isotopic composition, and the cave temperature is measured. Together with the measurements of stable isotopes in precipitation at Villars, this long-term monitoring provides a unique data set for a calibration study on speleothem fluid inclusions. The present day cave conditions and the isotopic relationships can help interpret the proxy records.

Cave temperature in the upper gallery is close to the mean annual external temperature, in the lower gallery it is 1 °C lower. While the lower gallery temperature shows no seasonal variation, the upper gallery temperature varies by up to 1 °C, the seasonal cycle being lagged compared to the outside temperature by about 3 months. Throughout the monitoring period, cave temperature has increased by about 0.04 °C yr^{-1} (Genty 2008). Cave air CO_2 concentrations vary between 1500–3000 ppm (upper galleries) and 4000–8000 ppm (lower galleries).

Average drip rates vary between the four monitored stalactites from 0.73 to 2.69 ml min^{-1}, which highlights the influence of the individual water pathways through the bedrock that feed each stalactite. At all monitoring stations, the drip rates show a well-marked seasonal variation. A comparison with the above ground water excess (precipitation minus potential evapotranspiration) shows that there is a lag of one to two months between the start of a period with positive water excess in autumn and the increase in drip rates (Genty 2008). Despite the

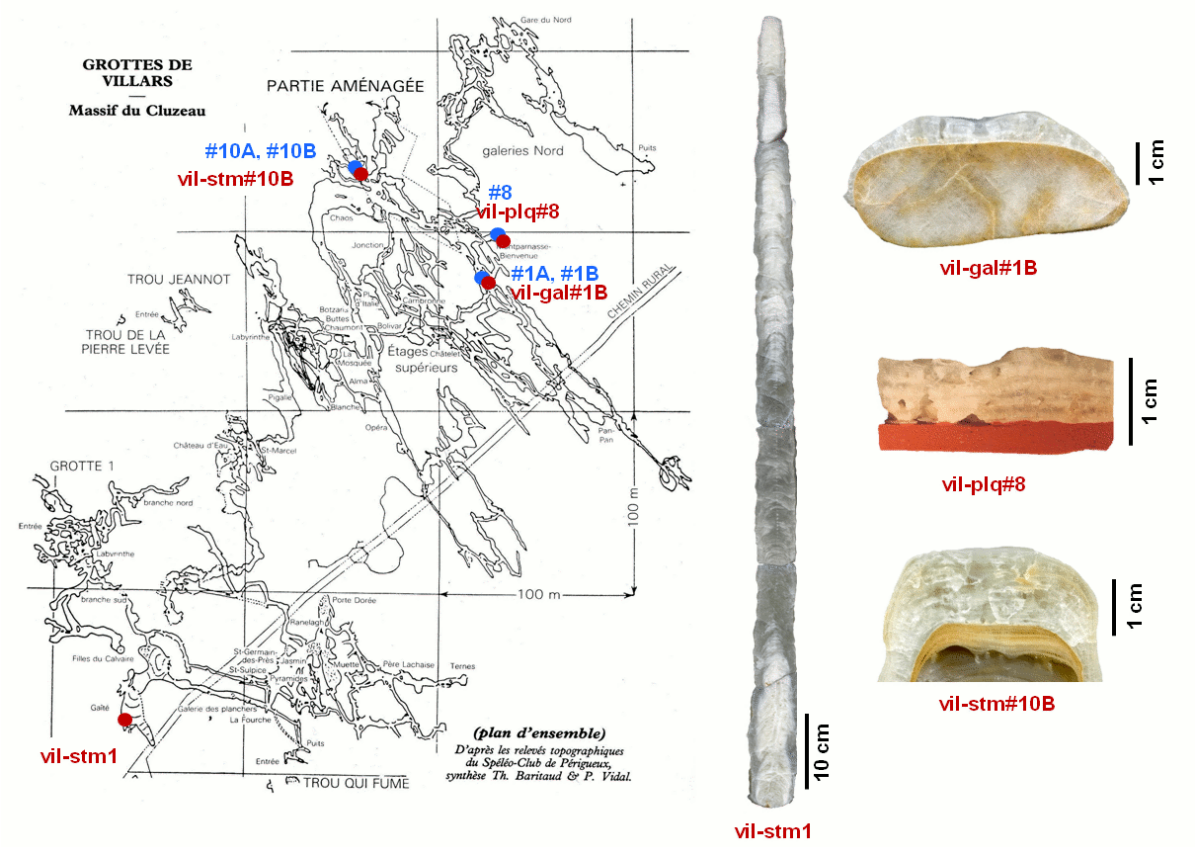

Figure 6.6: Left: Map of Villars cave (from Vidal and Baritaud, Spéléo Club de Périgueux) indicating the locations of drip water sampling stations (blue) and speleothem samples (red). Right: Speleothem samples from Villars cave which have been analysed in this study.

seasonality of the discharge, the isotopic composition of the drip water has been relatively constant throughout the monitoring period, pointing to a well-mixed infiltration water.

6.2.1 Speleothem Samples from Villars Cave

The speleothem samples obtained from Villars and their locations in the cave are shown in Figure 6.6. The main sample is the *stalagmite vil-stm1*, a 3000-year old, fast-growing stalagmite, which has the potential to provide high resolution proxy records comparable to the tree-ring chronologies from the region. Vil-stm1 was sampled in 1993, at a depth of 8 m below the surface, in a part of the cave inaccessible to the public ("Trou qui fume"). It was located in a dead end about 130 m from one of the cave entrances and could be reached only through several narrow passages. The stalagmite is 109.5 cm high, with a diameter of 6 cm at the bottom and 4 cm at the top. It was active at the time of sampling, and the top of the stalagmite was 30 cm from the cave ceiling. The sample was cut in half with a diamond bladed saw along the central growth axis, and the surfaces were polished to make their structure more visible. There is no evident hiatus in vil-stm1, and no offset in the growth axis. The stalagmite is composed of columnar calcite fabrics with well-marked laminae in the top half and at the base of the stalagmite, i.e. alternating layers of white porous calcite and dark compact calcite. For this study, only the top 68 cm of the stalagmite, which cover approximately the last two millennia, were analysed.

For calibration purposes, three *modern calcite samples* deposited at the drip water monitoring stations were also analysed: the top of an active stalagmite (vil-stm#10B), as well as calcite deposits which precipitated on objects placed under dripping stalactites (vil-gal#1B and vil-plq#8). These samples allow a comparison of the fluid inclusion isotopic composition with contemporaneous drip water.

6.3 Braconne Forest and Le Mas

The living tree samples which were analysed in this study originate from Braconne forest (45°44'N, 0°18'E) and Le Mas (45°08'N, 1°12'E). They are complemented by timber samples from historic buildings around the nearby city of Angoulême. Despite the exploitation of wood from Braconne over several centuries, trees up to 400 years of age are still found in this forest. The timbers provide wood samples dating back to the 14th century.

Like Villars cave, Braconne forest is located on Jurassic limestone bedrock. Karstic features such as dolines, caves, and surface collapses characterize the landscape. The topography is hilly, with altitudes between 70 and 160 m a.s.l. Braconne was a Royal forest from the 14th century to the French revolution in 1789. In the 17th century, Colbert, King Louis XIV's Minister of Finances, found the French forests in poor condition and took a set of measures to enhance their economic value. The Knight Froidour, an Adviser Lieutenant General of Water and Forests, ordered a reforestation and implemented standardized coppice practices, which were still in use in the 19th century in some stands of the forest (Office National des Forêts, ONF, *pers. comm.*). Braconne forest consists of 74% deciduous trees, dominated by sessile oak (*Quercus petraea* (Matt.) Liebl.) and pedunculate oak (*Quercus robur* L.) (INPN 2013). Today, the forest is comprised in the Natura 2000 protected area "Forêt de Braconne et Bois Blanc", which covers an area of 46 km^2.

The site of Le Mas, 100 km to the southeast of Braconne, is a small patch of forest on a slope with a thin soil layer and karstic limestone bedrock. At this site, precipitation isotope monitoring data since 1997 are available (Section 6.1.3).

6.3.1 Living Tree and Timber Samples

At Braconne forest, living trees were sampled in three stands representing two different age groups: 6 "young" trees from two adjacent stands (samples named B for "Braconne"), about 145 years old, and 13 "old" trees (samples named GR for "Gros Roc"), between 310 and 405 years old, from a stand 1 km away. Some of the old trees were not cored to the pith, so the given ages are minimum ages. As karstic terrains are rather heterogeneous (White 2002), the sites of old and young trees may have different hydrological characteristics, despite their proximity. The old trees grow on a thin soil less than 30 cm deep, while the young trees grow on a thicker soil of at least 60 cm depth. We could not obtain samples from old and young trees in the same stand, as trees on the same forest parcel are generally homogeneous in age. At Le Mas (LM), four living trees were sampled, which were about 70 years old.

A total of 70 timber beams was sampled in six historic buildings in and around the city of Angoulême (Table 6.1; Figure 6.7). These samples were combined in a composite timber chronology named AT (for "Angoulême Timber"). The provenance of the timbers is not documented. However, the possibility to crossdate these samples with the living trees and among buildings points to a local origin of the wood.

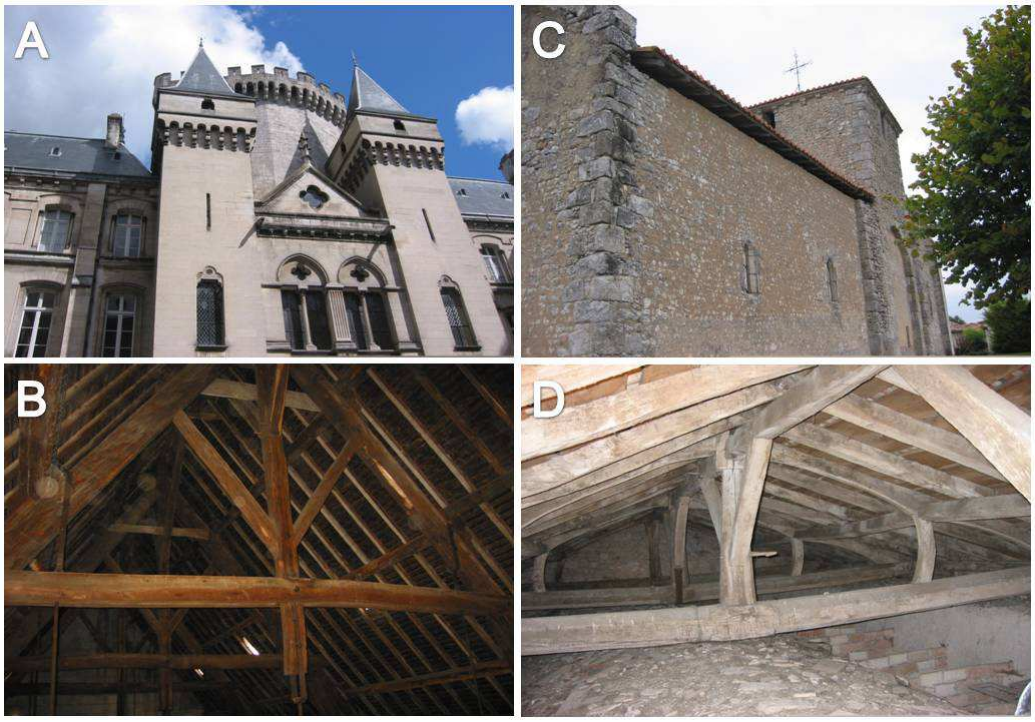

Figure 6.7: Examples of historic buildings and roof beams where wood samples were taken: La Rochefoucauld Castle (A, B) and the church of Poullignac (C, D). Photographs M. Stievenard.

Sampling of Trees

The living trees were sampled using an increment borer with a diameter of 5 mm to extract cylinders of wood from the stem. Three cores were taken from each tree at an angle of 120°, 1.3 m above ground. The trees of site B had been felled. Discs were cut from the stems at 2 m height, and 3 radii were cut from the discs at an angle of 120°. Timbers were sampled using an electric drill with a 10 mm diameter, and only one core per timber beam was taken. According to the length,shape and diameter of the beams, one sampled beam corresponds to one tree, i.e. trees were not cut to provide several beams. This is important because we do not artificially increase the coherence between samples by taking two samples from the same tree.

Species Determination

All trees analysed in this study are of the genus *Quercus* (oak). Le Mas trees were recognized as sessile oak (*Quercus petraea* (Matt.) Liebl.) based on the morphology of leaves and acorns. The oak species of the B and GR sites at Braconne forest had not been determined in the field during the sampling campaign in 2004. For the timber samples, the only possibility is to determine the species based on wood anatomy. Different characteristics of the wood can hint at a certain species (for a review see Feuillat et al. 1997), but Schoch et al. (2004) state that the oak species *Q. robur*, *Q. petraea*, and *Q. pubescens* cannot be differentiated on the basis of their wood anatomy.

To date, no study exists which demonstrates a difference in the oxygen isotopic composition of cellulose in different oak species. However, the species have different site preferences (Lévy et al. 1992), and the local soil hydrology can influence the $\delta^{18}O$ of the source water. This site

Table 6.1: Overview of the tree samples. The living tree samples consist of 3 cores per tree; for the timber samples, one core per timber beam was taken. A subset of samples was selected for oxygen isotope analysis (numbers in parentheses; see Section 8.2.1)

Site/building	**Abbreviation**	**Type of samples**	**Number of trees (δ^{18}O analysis)**
Le Mas	LM	living trees	4 (4)
Braconne young trees	B	living trees	6 (6)
Braconne old trees	GR	living trees	13 (4)
Angoulême Hôtel de Ville	AHDV	timber	16 (0)
Angoulême Musée	AMUS	timber	13 (0)
Angoulême Maison du Comte	AMDC	timber	12 (4)
Poullignac Église	POUL	timber	10 (3)
Château de l'Oisellerie	OISEL	timber	5 (0)
Château de la Rochefoucauld	LRF	timber	14 (7)

effect is not only species dependent, but also affects trees within a species. We did not attempt to determine the oak species for this study, as we assume the site effect to be more important than a possible species effect, and the species determination is not unambiguous.

Table 6.2: Overview of the available data.

Data	**Site**	**Time span**	**Source**	**Objectives**
Precipitation δD and δ^{18}O	Villars, Le Mas	1996–2012	Genty (2008), Genty et al. (2014)	Characterization of precipitation isotope variability and its link with climate
Cave drip water δD and δ^{18}O	Villars	1999–2012	Genty (2008), Genty et al. (2014)	Trace the isotopic composition of water from precipitation to cave drip water, which feeds stalagmites in the cave and which might also correspond to the water taken by trees
δD and δ^{18}O of fluid inclusions in modern calcite deposits	Villars	1990–2007	This study	Calibration of the fluid inclusion record
δD and δ^{18}O of fluid inclusions in stalagmite vil-stm1	Villars	2300 years	This study	Reconstruction of drip water δ^{18}O variability in the past
Other proxies from stalagmite vil-stm1 (calcite stable isotopes, trace elements)	Villars	2300 years	Bourdin (2012), D. Genty, D. Blamart	Constrain the causes of fluid inclusion variability
Cellulose δ^{18}O and TRW in living trees	Angoulême, Le Mas	1860–2010	This study*	Calibration with instrumental meteorological data and precipitation δ^{18}O to define which climate variables can be reconstructed
Cellulose δ^{18}O and TRW in living trees and timber wood	Angoulême	1330–2004	This study*	Reconstruction of summer droughts in the past

*measurements were accomplished with the help of A. Feron, O. Girardclos, M. Pierre, and M. Stievenard

7 Speleothem Data and Methods

During this thesis, 50 fluid inclusion samples were prepared and measured from modern calcite deposits and a late Holocene speleothem, for which previous measurements of stable isotopes in calcite and trace element concentrations, as well as an age model were available (Table 6.2). The precision of the chronology required for a comparison with tree ring proxy records necessitated laminae counting and new U-Th measurements to create a new age model, as analytical methods have progressed since the previous analysis.

7.1 Dating and Age Models

The modern calcite samples vil-gal#1B and vil-plq#8 grew on artificial supports placed under dripping stalactites during known time periods, so their exact age is known. The regular lamination visible on these samples indicates that the lamination observed in several stalagmites from Villars cave is very likely also annual (Genty 2008). The age of the third modern sample, the top of stalagmite vil-stm#10B, was determined by counting visible growth layers.

The age of the stalagmite vil-stm1 was determined by laminae counting and by two radiometric dating methods, U-Th and ^{14}C. Laminae were counted in the upper 486 mm, where the lamination is almost continuous. The stalagmite was scanned on a flatbed scanner at a resolution of 4800 dpi. The contrast was enhanced using the image processing software GIMP (www.gimp.org) to make the lamination more visible. Laminae were counted on the scans using the programme CooRecorder (www.cybis.se). The counting was repeated four times. Interruptions of the lamination around 80 mm and 180 mm from top, obliged to interpolations in the growth rate for 35 mm of the total counted height.

Thirteen calcite samples were taken for U-Th dating. Since the uranium content in the stalagmite is low (0.13 μg/g calcite) and the sample is young, about 500 mg of calcite were needed for the U-Th dating to give reliable results. Previous U-Th measurements for this stalagmite had been carried out by thermal ionization mass spectrometry (TIMS) at the Open University, Milton Keynes, United Kingdom (Genty et al. 1999). They were complemented in 2013 by new measurements using multicollector inductively coupled plasma mass spectrometers (MC-ICP-MS) at Xi'an Jiaotong University, China, and at LSCE, Gif-sur-Yvette, France. See Cheng et al. (2013) and Fontugne et al. (2013) for details on the analytical procedure. For radiocarbon (^{14}C) measurements, eleven calcite samples of 10–20 mg were taken with a 0.5 mm microdrill. Carbon atoms were counted by accelerator mass spectrometry at ARTEMIS, UMS 2572, Saclay, France.

The age model for vil-stm1 was calculated with the programme StalAge (Scholz and Hoffmann 2011). StalAge is an algorithm which constructs speleothem age models based on measured ages and their associated uncertainty as well as stratigraphic information, i.e. the condition that the first point is younger than the second etc. As no manual selection of potentially inaccurate dates is necessary, StalAge provides an objective, reproducible and comparable age

model. The algorithm identifies major and minor outliers and age inversions. Straight lines are fitted through subsets of the data to calculate the age model and the corresponding 95% confidence interval through a Monte Carlo simulation.

7.2 Fluid Inclusion Measurements

Fluid inclusions were measured at VU Amsterdam University using the "Amsterdam Device", a continuous-flow preparation device for online δD and δ^{18}O analysis of speleothem fluid inclusions (Vonhof et al. 2007, 2006). Small blocks of calcite were cut from the speleothem samples with a diamond bladed saw. Samples of approximately 0.3 g of calcite were needed in order to extract a sufficient quantity of water (about 0.2 μl) for the analysis. For each modern calcite sample, the fluid inclusion measurement was repeated on two adjacent blocks. The vil-gal#1B and vil-plq#8 samples were taken over the entire height of the calcite deposit. The vil-stm#10B samples represent the upper 3 mm of the stalagmite. From the stalagmite vil-stm1, 34 blocks of 4 mm height were cut out along the central axis.

The fluid inclusion analysis includes the water extraction from the speleothem samples by crushing and heating, and the mass spectrometric measurement of the released water. The Amsterdam Device consists of a crusher and a cold trap unit, which is connected to the carrier gas inlet of a Thermo-Finnigan TC-EA pyrolysis furnace. The TC-EA allows a combined δD and δ^{18}O analysis. Calcite samples are crushed and heated to 120 °C under a continuous flow of helium carrier gas. The released water carried in the helium flow is retained in the cold trap unit during 4 min to leave time for all the water to evaporate from the sample. The cold trap consists of a coiled capillary plunged into an ethanol slush which has been cooled to -90 °C using liquid nitrogen. After 4 min the frozen sample is flash heated by an electrical current and transferred to the TC-EA, which is connected to a Finnigan mass spectrometer.

0.2 μl of a standard water (laboratory standard NTW3) with an isotopic composition close to the fluid inclusion water are measured at least twice before each calcite crush. This is to ensure the stability of the mass spectrometer and to minimize memory effects. The water is injected in the crushing chamber with a micro-syringe and undergoes the same procedure heating and cold trap as the calcite samples. After measuring the calcite sample, two more standard water injections are made, with a quantity of water corresponding to the amount of water extracted from the calcite sample. This amount is approximated from the size of the CO peak of the mass spectrometric analysis relative to the average peak size of the 0.2 μl standard water injection. The water content of the calcite sample in μl g^{-1} calcite is also calculated. The analytical error of the fluid inclusion measurements is 0.3‰ for δ^{18}O and 1.5‰ for δD.

7.3 Other Proxies from Speleothems

Calcite stable isotopes (δ^{18}O and δ^{13}C) have been measured previously in the modern samples at different resolutions (D. Genty, unpublished data). In this study we use only an average calcite δ^{18}O value for each sample to compare to the corresponding fluid inclusions measurement.

Several other proxies were available from former studies on the stalagmite vil-stm1. These can help interpret the fluid inclusion record and constrain the possible influences on fluid inclusion variability. Calcite samples for δ^{18}O and δ^{13}C measurements were taken at a resolution of 1.5 mm in the upper 507 mm, and at a resolution of 5 mm from 507 to 670 mm from the

top (D. Genty, unpublished data). Trace element concentrations (Na, Mg, Sr, Ba, U, Y) in the calcite have also been measured previously for vil-stm1 (Bourdin 2012). These samples were taken at a resolution of 4 to 8 mm. See Chapter 10 for details about the other proxy measurements.

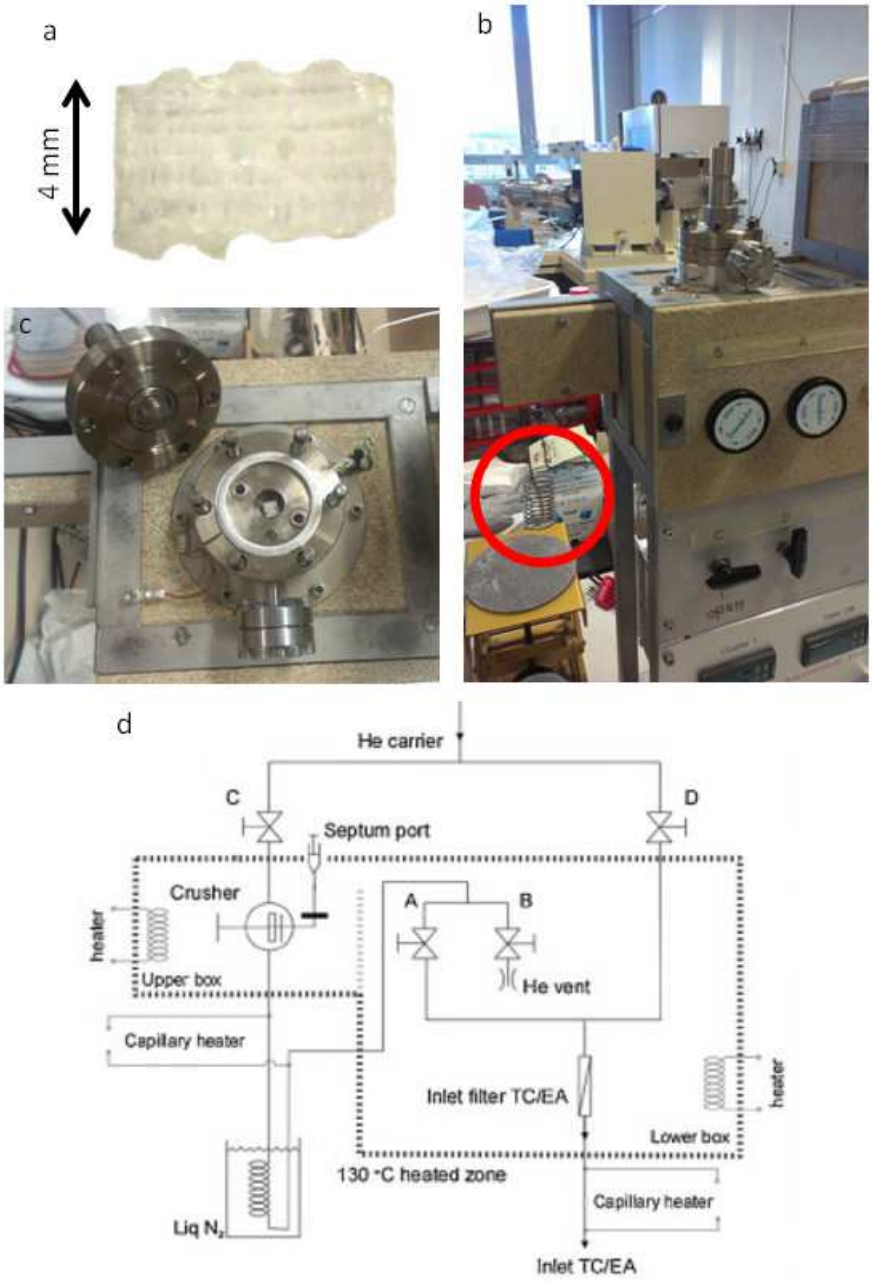

Figure 7.1: a) Example of a fluid inclusion sample from stalagmite vil-stm1. There are seven annual growth layers; it therefore represents seven years of drip water. b) Photograph of the Amsterdam Device with crusher on top and cold trap (red circle). c) Photograph of the open crusher with a calcite samples inside. d) Schematic of the Amsterdam Device (Vonhof et al. 2006). The dotted line represents the part of the device that can be heated.

8 Tree Ring Data and Methods

For this study, 139 cores (with a total of 23 000 rings) were crossdated. 56 of these cores (8 400 rings) were cut for stable isotope measurements. Pooling of rings from several cores left 1 500 wood samples for individual milling, cellulose extraction, and mass spectrometric analysis.

8.1 Ring Width Measurement, Crossdating, and Standardization

For tree ring width (TRW) measurements a flat surface perpendicular to the fibres was cut using a razor blade to make ring boundaries and cell structure visible. The Le Mas samples were measured and crossdated at LSCE from high-resolution scans using the CooRecorder and CDendro software (www.cybis.se). All other samples were measured at Université de Franche-Comté by O. Girardclos. For the living trees, the year of coring or felling, i.e. the year of the last ring, was known. The timbers were dated by comparing patterns of interannual ring width variability with both the living trees from this site and other reference chronologies. Periods of overlap with living trees where the samples show similar variations enable the dating of the timbers. The crossdating was verified by visual comparison of plots and statistically checked for errors using the programme COFECHA (Grissino-Mayer 2001; Holmes 1983). COFECHA correlates segments of ring width series and checks whether higher correlations exist in alternative positions when shifting the series in year-by-year steps. An overview of the crossdated tree ring width series is given in Figure 8.1. The three cores from each living tree are averaged to form a single tree series.

The crossdated TRW series were standardized with the programme ARSTAN (Cook and Krusic 2005; Cook 1985) in order to eliminate non-climatic trends. TRW in many of the samples shows suppression and release patterns, which are due to competition between trees (Figure 8.2). In order to eliminate these increasing and decreasing trends, which are not climatic, a flexible, data-adaptive standardization method was chosen: a cubic smoothing spline filter with a 50% variance cutoff, where 50% of the variance was removed at a period of 30 years.

A biweight robust estimate of the mean (Cook et al. 1990b) was used to calculate the mean chronology index value for each year from the individual standardised series. This estimation is less sensitive to the influence of outliers compared to the arithmetic mean.

8.2 Oxygen Isotope Ratios in Cellulose

8.2.1 Selection of Samples for Stable Isotope Analysis

Sample preparation and measurement of stable isotopes in cellulose are time consuming and costly, so the analysis is generally limited to a few samples, which have to be chosen wisely. 28 trees were selected for isotope analysis in order to obtain an adequate sample depth and overlap between sites (Figure 8.3). A sample depth of at least 4 is often considered sufficient

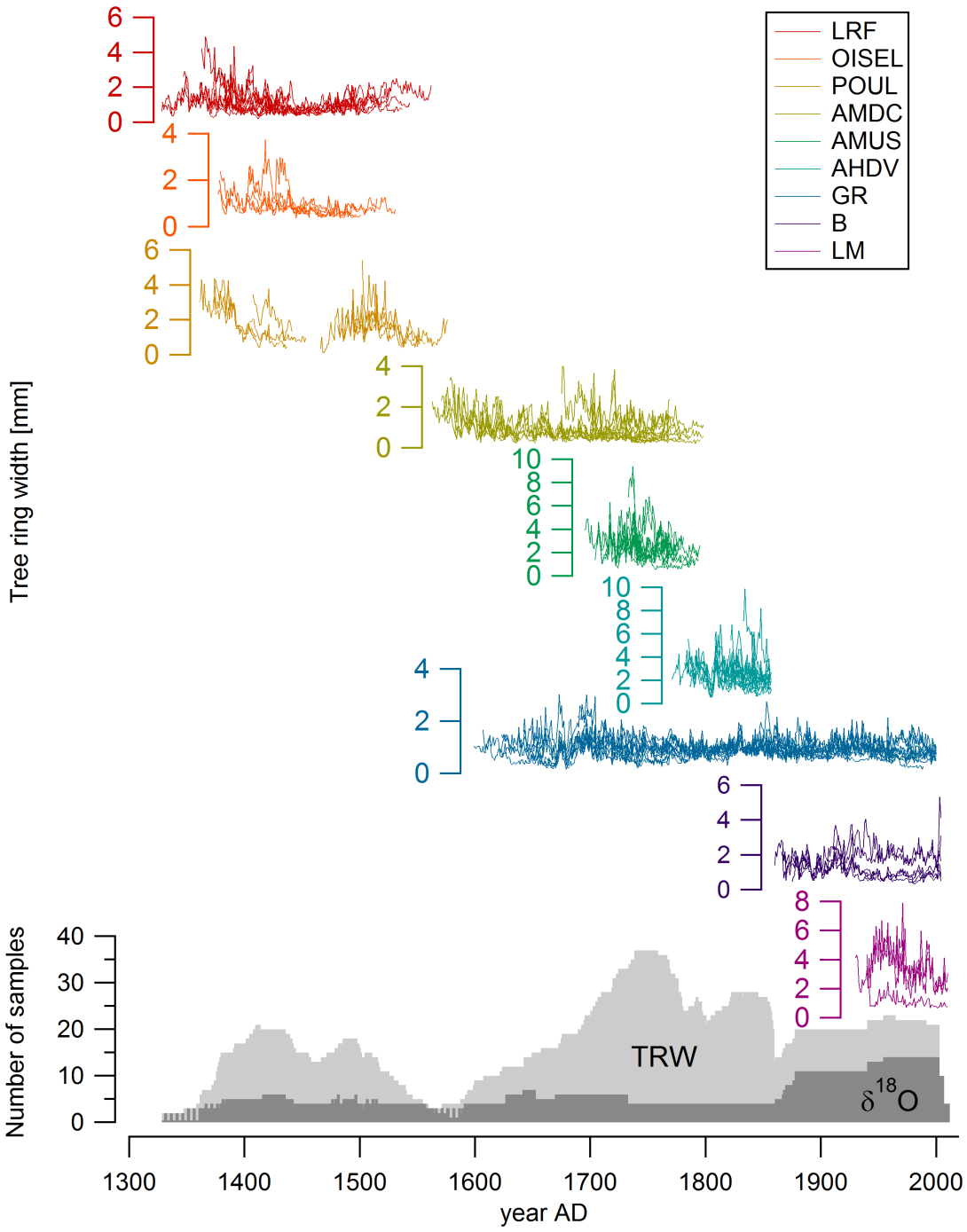

Figure 8.1: Overview of all tree samples used in this study. Plotted are the tree ring width curves, each colour representing a site or a building. Ring width is given in mm. The bottom panel indicates the number of samples for the tree ring width (TRW) and oxygen isotope (δ^{18}O) chronologies.

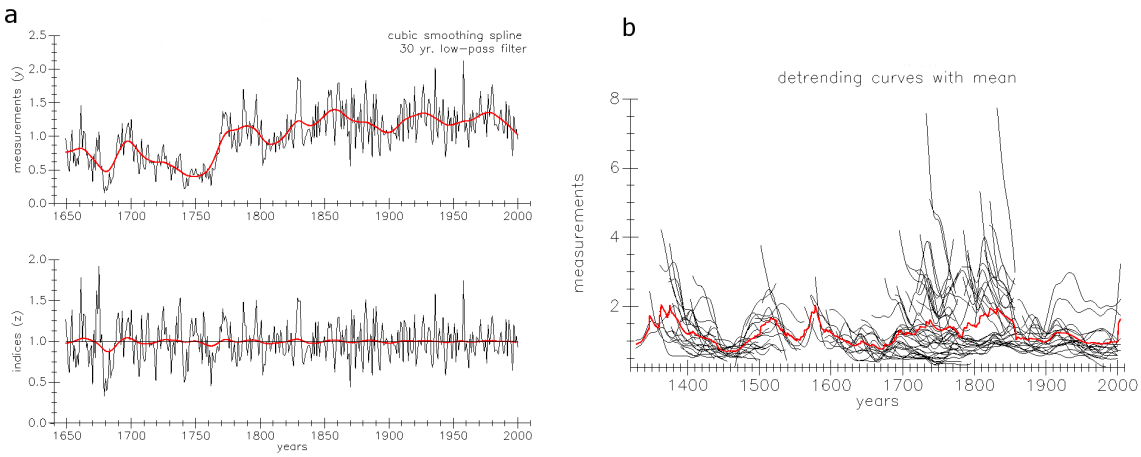

Figure 8.2: a) Example for the standardization of a TRW series. The top panel shows the ring width measurements in mm; the red curve is a 30-year smoothing spline fitted to the data. The bottom panel shows the standardized series. The tree ring index is calculated by dividing the measured value by the corresponding value of the spline curve. b) Standardization curves for all ANG samples using a 30-year smoothing spline.

to obtain a representative isotope signal (Leavitt 2010). For some samples, only a part of the core was selected because the outermost rings were too small to separate them properly with a scalpel.

8.2.2 Pooling of Trees

Crossdated cores were cut ring by ring under a microscope using a scalpel. Earlywood and latewood were separated, and only the latewood was used for isotope analysis, because the earlywood is formed with carbohydrates from the previous growing season (cf. Box 5.1). For the living trees, the corresponding rings from the three cores of each tree were pooled and further processed together.

The goal of this analysis was to obtain an average time-series of cellulose $\delta^{18}O$ from several trees which is representative of local climatic conditions. The question arose whether or not to pool the rings of several trees prior to cellulose extraction. The advantage of pooling is that it significantly reduces analysis time and costs. Pooled isotope values are often similar to the mean of individually analysed trees (Szymczak et al. 2012; Dorado Liñán et al. 2011b; Shi et al. 2011; Treydte et al. 2001). However, pooling makes it impossible to identify outliers and to estimate the error by calculating a confidence interval around the mean, or to characterize the isotope variability between trees. We decided to test the site-specific inter-tree variability on shorter time periods. The following analysis steps were first applied to individual tree series for selected sub-periods. Then, for the remaining time spans, rings of the same year from all trees from a site were pooled together before subsequent analysis. An overview of the pooled vs. individually analysed time spans for each site is given in Figure 8.3.

8.2.3 Sample Preparation

The wood was milled in order to obtain a homogeneous sample, as the $\delta^{18}O$ of cellulose may vary between pooled trees, but also within one ring (cf. Box 5.1). Isotopic homogeneity of the

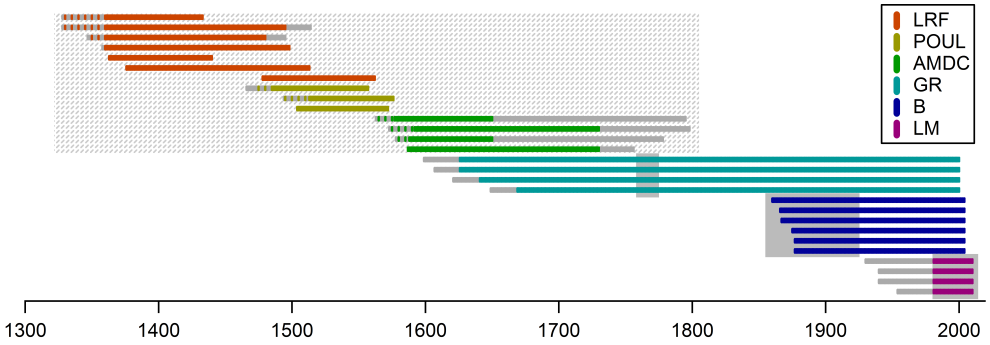

Figure 8.3: Tree cores selected for stable isotope analysis. The total length of the cores is shown in grey, the time spans for which $\delta^{18}O$ was measured are shown in colour. For the living trees (LM, B and GR), the solid grey boxes indicate the time spans for which the trees were analysed individually. For the remaining time spans the analysis was performed on pooled samples, which were grouped by site. The shaded grey box indicates the timber samples (LRF, POUL and AMDC), which were analysed individually every 5^{th} year, and pooled together for the remaining years.

sample is crucial since the small amount of cellulose which is measured must be representative of the whole sample (Rinne et al. 2005; Borella et al. 1998). Samples were homogenized using a centrifugal mill with a 0.08 mm sieve. As the loss of material is about 25%, a ball mill was used for very small samples.

The samples were chemically treated to extract α-cellulose from the wood powder. The extraction method was developed by Green (1963) and modified by Leavitt and Danzer (1993). Each milled sample (maximum about 50 mg) was put in a small pouch formed from a Teflon filter with 10 μm pores and closed with a Teflon thread. A tag with the sample number was attached to each pouch. Batches of 25 to 30 samples were processed together. In a first step, extractives such as resins and waxes were removed with a 2:1 toluene–ethanol mixture heated at 70 °C in a Soxhlet extractor for 10 h. This step was then repeated with only ethanol. Secondly, water-soluble constituents like inorganic salts and polysaccharides of low molecular weight were eliminated by boiling the samples in de-ionized water for 6 h. The third step was the elimination of lignin by oxidation in a solution of acidified sodium chlorite to yield holocellulose. The samples were heated overnight to 70 °C in 700 ml of de-ionized water with 7 g of sodium chlorite ($NaClO_2$) and 1 ml of glacial acetic acid (CH_3COOH). The following day, three successive additions of sodium chlorite and acid were made at an interval of 2 h. In a fourth step, samples were put in a 17.5% solution of sodium hydroxide (NaOH) for 1 h to remove hemicellulose, and finally in a 10% solution of acetic acid (CH_3COOH) for 10 min to neutralize. Lastly, samples were dried in an oven at 70 °C over night.

8.2.4 Mass Spectrometric Analysis of Cellulose

The $\delta^{18}O$ of cellulose was determined by isotope ratio mass spectrometry (IRMS) using a continuous flow on-line method (Saurer et al. 1998a; Farquhar et al. 1997; Koziet 1997; Werner et al. 1996). We used a high temperature conversion elemental analyser (TC-EA, Thermo Scientific) coupled with a Finnigan MAT252 mass spectrometer at LSCE, Gif-sur-Yvette, France. Measurement settings and precision of the mass spectrometer are described in detail by Etien (2008). Cellulose samples of 0.20 mg were weighed into silver foil capsules with a precision

balance. 100 samples and standards can be put in an autosampler which is purged with helium, and the samples are automatically dropped into the TC-EA one by one. Oxygen isotopes ratios are measured as CO gas produced from pyrolysis of cellulose under a continuous flow of helium carrier gas. The pyrolysis in a tube with vitrified carbon at 1350 °C converts cellulose to simple compounds (mainly CO and H_2, but also H_2O and CO_2). The pyrolysis products are passed through a CO_2 trap and a water trap and are separated in a gas chromatographic column (heated to 60 °C) containing a molecular sieve of 5 Å. CO gas is carried from the elemental analyser via an open split interface directly into the ion source of the mass spectrometer, where it is ionized. The ion beams are accelerated and deflected in a magnetic field (cf. Section 2.1). The masses 28, 29 and 30 are measured, and the ratio 30/28 ($^{12}C^{18}O/^{12}C^{16}O$) is determined from the time integrals of the peak areas of the ion intensities (Saurer et al. 1998). The peak areas of a sample are compared to a standard reference CO gas. The measurements are calibrated using a cellulose reference of known isotopic composition (Whatman CC31, $\delta^{18}O$ of 31.85‰), which had been measured in an inter-laboratory comparison for the ISONET project (Boettger et al. 2007). All oxygen isotope ratios in cellulose are reported with reference to VSMOW (Coplen 1994).

A sequence of 10 CC31 cellulose standards was measured before each sample run to ensure the stability of the mass spectrometer. The standard deviation of the CC13 was typically 0.20‰. Additional standards were measured after every third sample. Each sample was measured twice. If the difference between the two samples was > 0.20‰, the measurements were repeated up to four times, and the final value was calculated as the mean of these replicates. Outlier measurements were rejected. For the pooled sequences, a high analytical accuracy with rigorous criteria is crucial because no error can be calculated based on the inter-tree variability. The duplicated measurements generally correspond very well. The analytical uncertainty was 0.20‰ based on the maximum accepted standard deviation. These results demonstrate the quality of the analysis as they show that the extracted cellulose is homogeneous and the reproducibility of the mass spectrometer is good.

8.3 Results with Implications for Further Analysis Strategy

The results on the analysis of the tree ring proxies will be presented in Part III. Some of the results which had implications for the further analysis strategy are detailed here.

8.3.1 Replicate Measurements

In this study, all measurements of pooled and individual tree samples were replicated, according to the established laboratory protocol at LSCE. However, double measurements might not be necessary in future inter-tree studies. The reproducibility of the mass spectrometric measurements was generally good, and an inter-tree comparison provides a control on the measurement and the possibility to calculate an error around the mean.

8.3.2 The Effect of Tree Age on Cellulose $\delta^{18}O$

The $\delta^{18}O$ in individually analysed trees from site B showed and increasing trend of +2‰ during the juvenile growth phase (see results in Chapter 11). In order to avoid a juvenile bias, the first 20 years of the remaining samples were therefore omitted from the isotopic analysis. For samples which were not cored to the pith and the tree age was unknown, the 20 innermost

Table 8.1: Comparison of mean δ^{18}O values for individually analysed trees at the four sites, weighted by ring width and unweighted. AT samples were measured individually every 5th year. The correlation is Pearson's product-moment correlation coefficient. SD is the standard deviation.

Site (time span)	**LM (1981-2010)**	**B (1877-1924)**	**GR (1758-1772)**	**AT (1330-1730)**
Number of trees	4	6	4	13
Unweighted mean (M) of the whole time span ±SD [‰]	32.32 ±0.67	31.04 ±0.94	30.27 ±0.65	30.95 ±0.80
Weighted mean (M_w) of the whole time span ±SD [‰]	32.37 ±0.69	31.04 ±0.94	30.29 ±0.65	30.97 ±0.82
Correlation between weighted and unweighted series	0.9945	0.9987	0.998	0.9935
Maximum range of values for a single year [‰]	0.23	0.13	0.09	0.26

rings were omitted as a precaution. In the calculation of the mean δ^{18}O chronology, the juvenile years of the B trees were also omitted.

8.3.3 Inter-Tree and Inter-Site Variability: Implications for Pooling

The trees from the closely located B and GR sites showed an average offset in δ^{18}O values of 0.76‰, despite their proximity. Such offsets are not observed between trees within a site (see results in Chapter 11). The difference between sites is likely attributed to differences in their pedological and hydrological characteristics. For the timbers samples, the site where they grew is unknown. An assessment of the inter-tree variability was therefore considered necessary before pooling these samples, as it allows to detect trees which have significantly different isotopic values compared to the others. This is important especially since the sample depth is quite low and one outlier would have a large influence on the mean. If one of the trees grew next to a river for example, it could react differently to changes in drought conditions than a tree on a dry site. Since there is no common overlap period between all timber cores, the samples were analysed separately every 5th year to evaluate the inter-tree variability in δ^{18}O values (as proposed e.g. by Tardif et al. 2008; Raffalli-Delerce et al. 2004).

8.3.4 Should Samples Be Weighed Before Pooling?

When rings from several trees are pooled together, a different mass contribution from the trees can introduce a bias in the measured δ^{18}O value towards the value of the largest ring (Leavitt 2008). This is especially important for trees which show large differences in δ^{18}O and ring width. In order to measure a value that corresponds to the mean of individually analysed trees, which is not strongly influenced by possible individual effects of trees with large rings, an equal mass of wood should be weighed from each ring before pooling. To test whether this is necessary, the arithmetic mean (M) δ^{18}O value of all individually analysed trees was compared to a mean weighted by ring width (M_w):

$$M = \frac{\sum_{i=1}^{n} \delta^{18}O_i}{n} \tag{8.1}$$

$$M_w = \frac{\sum_{i=1}^{n} \delta^{18}O_i * TRW_i}{\sum_{i=1}^{n} TRW_i} \tag{8.2}$$

Equation 8.1 represents the value one would measure from pooled samples of equal mass (same influence of every tree); Equation 8.2 represents the value one would measure if samples are pooled without weighing, where a tree with larger rings would have a stronger influence on the measured isotopic ratio of the pooled sample (Leavitt 2010). As the rings had not been weighed before isotopic analysis, tree ring width (TRW) was used as an approximation of the mass of the ring, although it must be kept in mind that the wood density varies between rings.

The difference between the weighted mean and the unweighted mean at each site is negligible (Table 8.1). This confirms previous results (for $\delta^{13}C$ see Leavitt 2008; Borella et al. 1998) that weighing is not necessary and the bias introduced by different wood masses in pooled rings is negligible compared to other analytical errors. Besides, further uncertainty might be introduced if the mass of wood, which is constrained by the narrowest ring, is very small and it is difficult to cut a piece of wood representative of the whole latewood. Therefore, rings were pooled without weighing.

Part III

RECORDS OF CLIMATE VARIABILITY IN SOUTHWEST FRANCE

The data obtained during this thesis, presented in the previous chapters, form the basis for the calibration of proxies and the reconstruction of climate variability in south-western France during the last two millennia. In response to the research objectives stated in the introduction, these data allow to characterize the isotopic composition of precipitation in the study area, its link with climate, and its relationship with cave drip water $\delta^{18}O$ (Chapter 9); to verify if speleothem fluid inclusions preserve the isotopic composition of the feeding drip water and therefore enable the reconstruction of the variability of drip water $\delta^{18}O$ in the past (Chapter 10); to determine the influence of source water $\delta^{18}O$ as well as other climatic and non-climatic factors on the isotopic composition of tree ring cellulose (Chapter 11); and to reconstruct summer droughts using cellulose isotope chronologies constructed from living trees and timber wood (Chapter 12).

These results are presented in form of articles, which have been published or will be submitted in the framework of this thesis. A short introduction is given to each article, which highlights its most relevant findings, as well as the implications for subsequent analysis strategy and for the interpretation of results.

Lastly, a synthesis of the two archives is presented, which discusses to what extent the speleothem and tree ring proxies are comparable and can provide complementary records of climate change (Chapter 13).

9 The Relationship Between Precipitation and Cave Drip Water

The source of oxygen in tree ring cellulose and in speleothem fluid inclusions is precipitation, which infiltrates in the soil, and is taken up by tree roots or arrives in the cave. In this context, it is important to understand the climate imprint on precipitation $\delta^{18}O$, as well as the relationship between precipitation and the proxy source water. The isotopic composition of soil water can differ from precipitation because of evaporation, seasonal plant transpiration, and the mixing of different rainfall events, which depends on water residence time. The contribution of enriched soil water to drip water and speleothem $\delta^{18}O$ is poorly constrained with few monitoring studies (see e.g. in Fairchild and Baker 2012), and depends on the local climate conditions. Likewise, the necessary data to compare oxygen isotope ratios in cellulose and in the source water of the trees are not available in most palaeoclimate studies.

This article presents the relationship of stable isotopes in precipitation and cave drip water in the south of France. The exceptionally long monitoring time series from Le Mas (precipitation) and Villars (precipitation and cave drip water) constitute a unique data set for a local proxy calibration. For this purpose, the available data from 1996 to 2012 were compiled. The water sampling had been made at an irregular time interval of 1–2 months and necessitated the calculation of monthly values to make them comparable to meteorological data, and calculate amount-weighted seasonal averages.

The results show that the $\delta^{18}O$ of present-day drip water in Villars cave corresponds to a weighted mean $\delta^{18}O$ of pluri-annual precipitation, and that there is no seasonal bias caused by a transpiring vegetation. Despite a non-linear recharge, i.e. seasonal differences in precipitation and evapotranspiration, which lead to varying drip rates, the $\delta^{18}O$ of drip water has been remarkably constant throughout the monitoring period.

This has implications for the interpretation of our proxy records in speleothems from Villars cave, and in tree rings from Angoulême (50 km from Villars), a site in a similar climatic and geological setting, if we suppose similar conditions in the past: (1) we can define the isotopically effective recharge (Lachniet 2009), which should be represented in the fluid inclusion of older stalagmite samples; (2) the absence of a seasonal bias in the drip water indicates that the dominant water supply of the vegetation above the cave is a mixed source water with a rather constant isotopic composition and not only the growing season precipitation.

Supplementary data associated with this article can be found in the online version at http://dx.doi.org/10.1016/j.gca.2014.01.043.

Rainfall and Cave Water Isotopic Relationships in Two South-France Sites

Dominique Genty[1], Inga Labuhn[1], Georg Hoffmann[1,2,3], Pierre-Alain Danis[4], Olivier Mestre[5], François Bourges[6], Karine Wainer[7], Marc Massault[8], Sandra Van Exter[8,9], Edouard Régnier[1], Philippe Orengo[1], Sonia Falourd[1], Bénédicte Minster[1]

[1]*Laboratoire des Sciences du Climat et de l'Environnement (LSCE/IPSL), laboratoire CEA/CNRS/UVSQ, CE Saclay, Orme des Merisiers, 91191 Gif-sur-Yvette, France*
[2]*Institute for Marine and Atmospheric Research Utrecht (IMAU), Utrecht University, Princetonplein 5, 3584 CC Utrecht, the Netherlands*
[3]*Estación Biológica de Donñada CSIC, c/ Americo Vespucio, s/n Isla de la Cartuja, 41092 Sevilla, Spain*
[4]*Pôle d'Etudes et Recherches Hydro-écologie des plans d'eau, IRSTEA, Unité Hydrobiologie HYAX, 3275 route Cézanne, CS 40061, 13182 Aix-en-Provence cedex 5, France*
[5]*Météo-France, Direction de la Climatologie, 42 av. Gaspard-Coriolis, 31057 Toulouse cedex, France*
[6]*Géologie-Environnement-Conseil, 30, rue de la République, 09200 Saint-Girons, France*
[7]*Dept. of Earth Sciences, Oxford University, South Parks Road, Oxford OX13AN, United Kingdom*
[8]*IDES, Université Paris-Sud, bât. 504, 91400 Orsay cedex, France*
[9]*UMR HydroSciences Montpellier, Maison des Sciences de l'Eau de Montpellier, UM2, 34095 Montpellier cedex 5, France*

9.1 Introduction

The isotopic composition (δ^{18}O and δD) of precipitation is a key parameter used to better understand the present-day atmospheric circulation of and, when dealing with fossil waters, of past periods (Sturm et al. 2005). Precipitation δ^{18}O is often the controlling factor for the isotopic composition of paleo-archives used to reconstruct the climate of the past: for example, precipitation δ^{18}O controls a large part of the isotopic composition of speleothem calcite (McDermott 2004; McDermott et al. 2011; Wang et al. 2001), lake ostracod calcite (von Grafenstein et al. 1996), tree-ring cellulose (McCarroll and Loader 2004; Treydte et al. 2007), soil secondary calcite (Marlin et al. 1993), human teeth (Daux et al. 2005), landsnails (Lécolle 1985), beetles (Hardenbroek et al. 2012), and other archives where the water molecule is involved. Besides, direct records of past precipitation δ^{18}O can be obtained from ice cores from Greenland, Antarctica and continental glaciers, as well as from fossil waters found in aquifers (Corcho Alvarado et al. 2011) or in fluid inclusions trapped in speleothems (Vonhof et al. 2006), which are composed of fossil precipitation water.

Long precipitation δ^{18}O time series allow the comparison of the isotopic signal with meteorological measurements and the calibration of proxy records (Anderson et al. 2002). Cave drip water isotopic composition can be used to reconstruct past temperatures with the help of speleothem calcite δ^{18}O and clumped-isotope Δ47 measurements (Daëron et al. 2011). Consequently, measurements of precipitation δ^{18}O open the possibility of calculating past con-

tinental climate parameters such as temperature, humidity or precipitation $\delta^{18}O$, which are closely linked to air circulation patterns.

Since long local measurement series are not always available, model simulations can be used instead to investigate the link between precipitation and the isotopic proxy. However such an approach needs careful evaluation of the respective proxy forward model. Atmospheric circulation, cloud physics, in particular the role of convective precipitation, and atmosphere-surface interactions have a strong influence on water isotope composition and need to be validated in order to extend the modelled relationships between the water isotopes and various climate parameters to the distant climatic past. A large number of general circulation models are equipped with water isotope modules, allowing the computation of $\delta^{18}O$ and δD patterns of all water reservoirs represented by the respective model (Schmidt et al. 2007; Hoffmann et al. 2000; Joussaume et al. 1984). More recently, high-resolution mesoscale models (potentially with a spatial resolution of 15 km) were fitted with such isotope modules as well (Sjolte et al. 2011; Sturm et al. 2007). Long time series of $\delta^{18}O$ are of primary importance to verify and test the models' capacity to represent crucial features of the hydrological cycle on seasonal, interannual and decadal time scales.

Although it is well known that cave drip water $\delta^{18}O$ is controlled by precipitation $\delta^{18}O$, the temporal relationship between them is still not well constrained because long monitoring series of both drip waters and local rainfall are rare. The main questions are: which months contribute to the underground recharge that feeds stalactites? What is the average residence time of the mixing reservoir in the soil and bedrock before the water reaches the cave? Several recharge models involving diffuse and fracture flows linked to the great variety of porosity in karst formation hosting the cave have been proposed (Fairchild and Baker 2012). These models were developed based on (1) geochemical data of drip water (e.g. Mg/Ca; Fairchild et al. 2006b; Tooth and Fairchild 2003); (2) fluorescent dye experiments, which are rare because of the complexity of the fracture network (Bottrell and Atkinson 1992); and (3) the study of water isotopes ($\delta^{18}O$, δD and tritium).

Isotope time series of both rainfall and cave drip water at the same place during several months or years have been investigated in only a few studies. Most of these have revealed that isotope ratios in the cave drip water are very stable compared to the well-marked seasonal changes of the rain water, as in Carlsbad Cavern, New Mexico (Chapman et al. 1992), Waitomo Cave, New Zealand (Williams and Fowler 2002), in Bunker Cave, Germany (Kluge et al. 2010), and Nerja cave, Spain (Caballero et al. 1996). In some specific caves, a significant seasonal $\delta^{18}O$ variation is detected in the dripwater because of evaporation processes in the soil and epikarst, like in Soreq Cave, Israel (Bar-Matthews et al. 1996) or mid-western USA caves (Denniston et al. 1999). Strong rainfall events and a rapid connection through the epikarst zone, as is the case with Santana Cave, Brazil (Cruz et al. 2005) or on Socotra Island, Yemen (Van Rampelbergh et al. 2013) can also cause seasonal variability. The conclusion of most studies is that cave drip water $\delta^{18}O$ is close to the weighted mean precipitation $\delta^{18}O$ of the year (Williams and Fowler 2002; Yonge et al. 1985); however, since most time series are short (i.e. from a few months to 2–4 years of monitoring), no modelling has been attempted to closely link rain and cave $\delta^{18}O$ values and to give an average residence time of the water in the karstic zone above the cave.

This article presents the results of stable oxygen and hydrogen isotope monitoring in precipitation at three sites in the south of France: Le Mas, Villars and Orgnac (Figure 9.1). Close to these sites, the drip water from several stalactites was monitored in two caves which are known

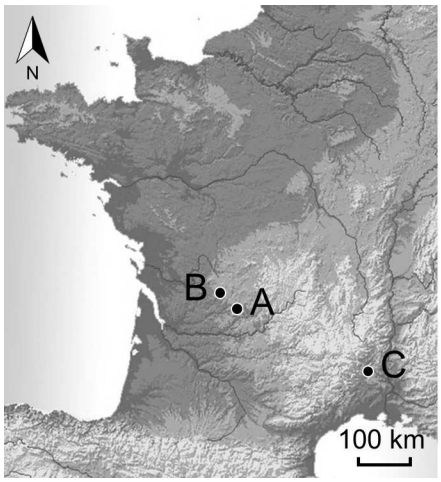

Figure 9.1: Locations of the precipitation sampling stations and the corresponding cave sites. (A) Le Mas; (B) Villars/Villars cave; (C) Orgnac/Chauvet cave.

Table 9.1: The three studied sites as referred to in the text. The rainfall isotope stations are given with the respective meteorological stations and caves and their corresponding distances from the isotope stations (in km).

Site	**Rainfall isotope station**	**Meteorological station**	**Cave**
Le Mas	Le Mas	Montignac/Brive (7.9/27)	Villars (50)
Villars	Villars-Doggy	Nontron (13.5)	Villars (0.4)
Orgnac	Orgnac (Museum)	Orgnac (Bruguier) (3.0)	Chauvet (7.3)

for their prehistoric remains and for their speleothem-based paleoclimatic reconstructions: Villars Cave and Chauvet Cave. A better knowledge of the relationship between rainfall $\delta^{18}O$ and drip water $\delta^{18}O$ is of primary importance for the understanding of $\delta^{18}O$ variations found in speleothems and isotope-based climate reconstructions, especially those involving fossil water trapped in speleothem fluid inclusions (de Cisneros et al. 2011; Wainer et al. 2011; Dublyansky and Spötl 2009; van Breukelen et al. 2008; Zhang et al. 2008; Matthews et al. 2000). The age of the drip water feeding stalagmites determines the time representativeness of fluid inclusions and helps in the interpretation of calcite $\delta^{18}O$ records. The data sets presented here from rainfall stations and nearby caves cover more than a decade and provide a unique opportunity to clarify the link between rainfall and cave drip water $\delta^{18}O$.

9.2 Study Sites

The three rainfall monitoring stations have been chosen to be as close as possible to the caves where seepage water monitoring and speleothem studies are conducted (Figure 9.1; Table 9.1). Meteorological data were obtained from the closest meteorological stations which give daily temperature and precipitation data that can be reasonably interpolated to the rainfall stations. In order to simplify the text, the main sites are as follows: Le Mas, Villars and Orgnac, keeping in mind that there are a few kilometres between meteorological, rainfall isotope monitoring and cave stations (Table 9.1).

The sites of Le Mas and Villars, located about 150 km from the Atlantic ocean in south-west France, are under a typical maritime climate with mild winters (an average temperature of

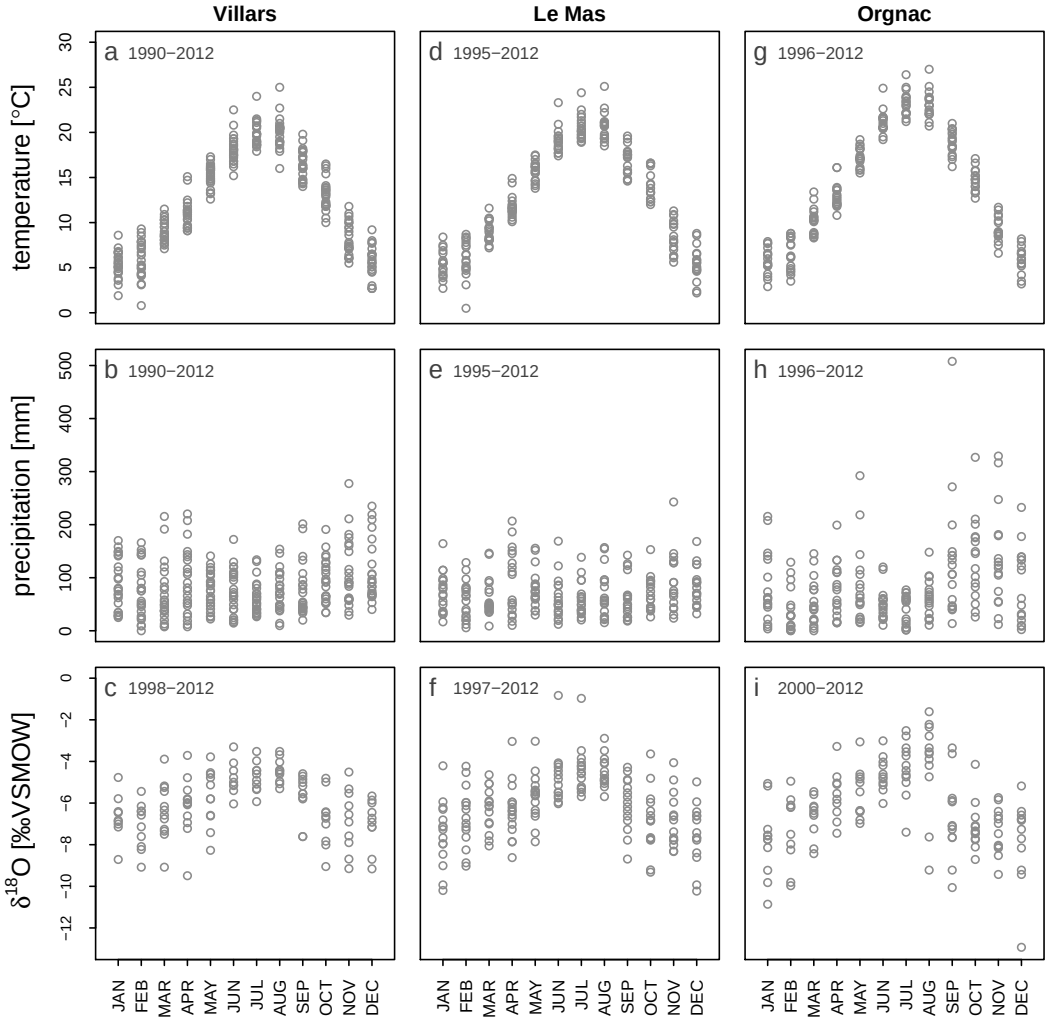

Figure 9.2: Variability of mean monthly temperature, monthly precipitation sums and monthly precipitation $\delta^{18}O$ at the studied sites: Villars, Le Mas and Orgnac.

5.6 °C and 274 mm of precipitation during December, January and February for Villars) and relatively humid summers (an average temperature of 19.3 °C during June, July and August and 212 mm of precipitation for Villars) (Figure 9.2a). Note that, despite their proximity, Villars is slightly colder (0.8°C during June, July and August) than Le Mas because it is closer to the higher plateau of the crystalline terrains of the Limousin (near the Massif Central). Much closer to the Mediterranean Sea, the Orgnac site experiences drier and warmer summers (22.5 °C and 153 mm during June, July and August) (Figure 9.2g) and intense precipitation events (e.g. 400 mm on 9–10 September 2002). This site is also characterized by higher precipitation variability (Figure 9.2h).

Villars and Chauvet (close to Orgnac) cave sites have already been described in previous studies (Genty, 2008; Genty et al., 2001; Genty et al., 2006). Villars Cave has developed in Bajocian limestone (middle Jurassic), while the Chauvet Cave has developed in hard and compact Barremian limestone (lower Cretaceous). In Villars Cave, drip stations are from small soda-straw stalactites (3–5 cm) that are directly connected to the gallery vault. Microfissures, not visible, likely feed these stalactites but a diffuse flow through the oolithic matrix of the

Table 9.2: Coordinates, geology, vegetation and external meteorological characteristics of the studied caves.

Cave	Cave latitude, longitude, altitude (average depth)	Precipitation [mm/year]	Annual temperature [°C] (DJF/ JJA)	Geology	Vegetation
Villars	45°26'N, 0°47'E 175 m (12–25m)	1005	12.4 (5.6/19.3)	oolithic limestone Bajocian (Jurassic)	temperate vegetation, (oaks, hornbeams)
Chauvet	44°23'N, 4°24'E 205 m (40–60m)	977	14.1 (6.1/22.5)	compact limestone Baremian (Cretaceaous)	mediterranean vegetation (bushes, green oaks)

Table 9.3: Overview of French GNIP stations (IAEA/WMO 2006) with monthly δD and δ^{18}O measurements, completed with the three new stations presented in this study.

Station name	GNIP Code	Latitude	Longitude	Altitude [m]	Start	End	Number of Years	Number of samples δ^{18}O	Number of samples δD
BREST PLOUZANE	711001	48°21'36"	-4°34' 12"	80	1996	2002	6	79	79
ORLEANS-LA-SOURCE	724901	47°54'0"	1°54' 0"	109	1996	2005	9	111	111
THONON-LES-BAINS	748501	46°22'20"	6°28' 15"	385	1963	2002	39	465	124
CESTAS-PIERROTON	753001	44°44'17"	-0°46' 29"	59	2007	2009	2	33	33
DRAIX	758801	44°8'0"	6°20' 0"	851	2004	2009	5	58	58
DAX	760301	43°41'0"	-1°4' 00"	9	1999	2005	6	67	67
CAMPISTROUS	762101	43°7'12"	0°22' 48"	600	1997	1998	1	15	15
MONTPELLIER	764301	43°34'12"	3°57' 00"	45	1997	1998	1	20	20
AVIGNON	764501	43°57'00"	4°49' 12"	30	1997	2009	12	130	129
CARPENTRAS	764601	44°57'00"	5°46' 48"	99	1997	1998	1	23	23
GARDANNE	765301	43°27'00"	5°27' 00"	215	1997	1998	1	19	19
MALAUSSENE	768801	43°55'12"	7°7' 48"	359	1997	1998	1	13	13
PONTE LECCIA	778701	42°28'48"	9°12' 0"	200	1997	1998	1	12	12
Le Mas	—	45°7'45"	1°11'31"	191	1997	2012	**16**	**111**	**109**
Villars-Doggy	—	45°26'18"	0°47'2"	175	1998	2012	**15**	**86**	**83**
Orgnac	—	44°19'8"	4°24'47"	305	2000	2012	**12**	**84**	**83**

limestone is possible too. In Chauvet Cave, the compact aspect of the limestone likely favour a more direct water flow through the fissures. Both caves are relatively shallow caves: Chauvet is about 50 m from the surface, and Villars is 10–30 m deep. It is important to know the recharge altitude of each cave and to check that it is similar to the altitude of the related meteorological station in order to avoid a bias due to the altitude effect on rainfall stable isotopes, which is generally close to –0.3‰/100 m but can be very variable (Clark and Fritz 1997). On all studied sites the distance and altitude differences between the cave recharge area and the rainfall station are negligible: Villars Cave's recharge area is between 10 and 20 m higher than the rainfall station (175 m a.s.l.); the Orgnac rainfall station is at 305 m a.s.l. while the Chauvet Cave recharge area is between 240–250 m a.s.l (Table 9.2).

9.3 Methods

The collected data constitute a unique set of isotope values, which is useful for atmospheric and hydrological studies. The precipitation isotope measurements from Le Mas, starting in 1997, represent the second longest published series in France in terms of the time span covered, and the third most extensive in terms of the number of samples. The other two stations, Villars and Orgnac, are also among the longest in France (15 and 12 years, Table 9.3). The drip water isotope monitoring in Villars Cave since 1997 is likely the longest in the world. Monitoring continues at all sites.

9.3.1 Precipitation and Cave Water Sampling

Rainfall water was collected using a similar procedure as recommended by the IAEA for the Global Network of Isotope in Precipitation (GNIP) stations (IAEA 1997): the water is collected in a funnel at a height of 2 m, which is connected to a 5 l tank with a plastic tube.

The tank is buried so that temperature variations are dampened; a film of paraffin oil is used to prevent evaporation. A sample is taken from the tank in a 15 ml brown glass bottle with a conic top specifically designed for stable isotopes. Every time the water is collected, the amount of water in the container is measured. Thus, for each isotope value the corresponding amount of precipitation for the water collection period is known. Some of these values of precipitation amount are missing. In order to fill the gaps of missing measurements and to check the amount of water measured in the container, sums are calculated for each sampling period from daily precipitation data from the corresponding meteorological stations. Despite the sometimes irregular sampling interval (see supplementary material for the sampling dates), samples are taken continuously, so that each sample consists of all precipitation since the preceding sampling date, and the whole year's precipitation is collected. This is important because it allows the calculation of weighted seasonal or annual averages. Drip water in Villars Cave was sampled on the same dates as precipitation. The sampling interval in Chauvet was larger due to limited access to the cave (see Table 9.6 for the number of samples and Figure 9.9 and 9.10 for sampling dates in each cave). The water was collected in a 15 ml brown glass bottle at the tip of each stalactite. The time to fill the bottles varies from few minutes to few hours depending on the sampling station and the season. As no significant variability in the drip water isotopic composition is observed here, "instantaneous" samples are representative of the seepage water composition between each sampling. Moreover, it is not necessary to weight the drip water δ^{18}O by the drip rate as we do for the rainwater; we did the calculation for the most variable drip station (Villars #10A), and the weighted δ^{18}O is in the error margin of the unweighted one (see Table 9.6).

9.3.2 Calculation of Monthly δ^{18}O Values to Create a Time Series with Regular Time Steps

It was not possible to take precipitation samples on a monthly basis. Although the monthly time step for sampling precipitation is arbitrary (i.e. it has no hydrological basis), our irregular sampling interval makes it difficult to compare the measurements directly to monthly meteorological data and to calculate mean values over different months. Therefore, a new time series of monthly rainfall δ^{18}O values was created based on the δ^{18}O measurements and on daily precipitation data from the closest meteorological stations. The δ^{18}O value of a given sampling period is assigned to each day of this period. Then the monthly isotopic composition $\delta^{18}O_m$ is calculated as the mean δ^{18}O of all days of the calendar month, weighted by the amount of precipitation:

$$\delta^{18}O_m = \frac{\sum_{i=1}^{n} P_i * \delta^{18}O_i}{\sum_{i=1}^{n} P_i} \tag{9.1}$$

where P_i is the daily precipitation amount, $\delta^{18}O_i$ is the "daily" δ^{18}O value, 1 is the first and n the last day of the respective month m. $\delta^{18}O_m$ is only calculated for those months where at least 70% of the monthly precipitation is available, which excludes some points near the periods where the sampling was interrupted. The time series of recalculated monthly δ^{18}O and δD values are very similar to the original time series for all three stations (see example in Figure 9.3).

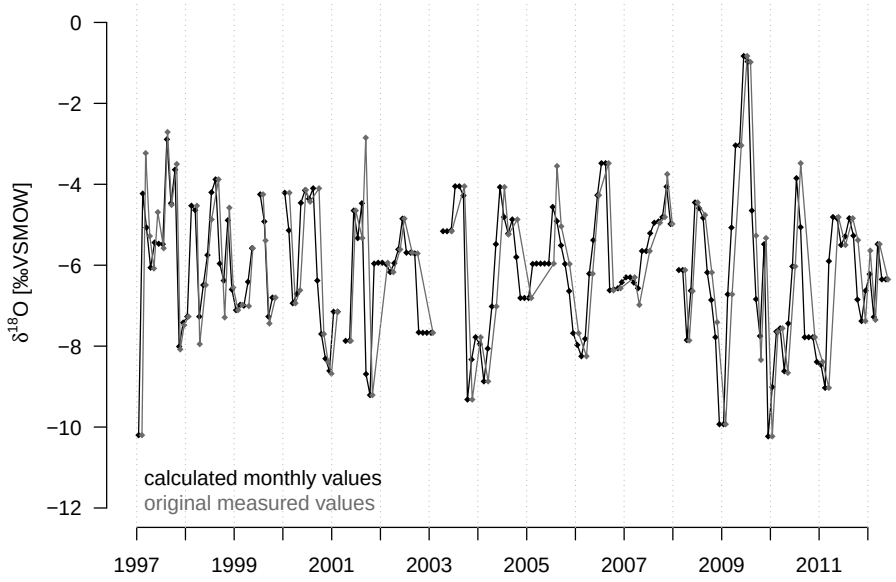

Figure 9.3: Comparison between calculated monthly δ^{18}O values (in black) and the original measured values (in grey) using the example of Le Mas. The slight shift between the two curves appears because the date assigned to each monthly value is the 15th of that month, whereas the date for the original values is the last day of the sampling period.

9.3.3 Measurements

Hydrogen isotopes (δD) were measured on an ISOPRIME mass spectrometer and a PICARRO laser spectrometer. The 1 sigma error for both methods is ±0.5‰. Oxygen isotopes (δ^{18}O) were measured on a Finnigan MAT 252 by equilibration with CO_2. The 1σ error of the δ^{18}O is ±0.05‰. Early measurements in 1997 and 1998 were performed on a VG SIRA IRMS with an error of ±0.2‰ for the δ^{18}O while δD was measured using the zinc reduction method with an error close to ±2‰.

9.3.4 The Mesoscale Model REMOiso

The REMO (REgional MOdel) model was derived from the European weather forecast model of the Deutscher Wetterdienst (Jacob and Podzun 1997) and then updated with ECHAM-4 physics (Jacob 2001). The model solves the full equations of conservation of mass, energy and momentum on a numerical grid ("primitive equations"). The principal prognostic variables are T (temperature), q (specific humidity), v (three dimensional wind vector). Most physical processes (e.g. cloud formation, soil hydrology, etc.) are solved on a sub-grid scale and are parameterised, that means that the effect of these sub-grid processes on the resolved scale is computed using often empirical relationships between the respective variables and large scale variable (for example the relation between the concentration of aerosols and cloud coverage). In a following step REMO was equipped with a module allowing the computation of the water isotopes in all compartments of the model's hydrological cycle. The respective model version is called REMOiso and discussed in Sturm et al. (2007) and Sturm et al. (2005). The standard spatial resolution of REMOiso, which was also used in this study is 0.5° * 0.5°, with 19 vertical layers and a time step of 5 minutes. The mesoscale model covers typically an area of several thousand square kilometres and obviously needs information on all relevant three-dimensional

climate parameters at the borders of its numerical grid. It is therefore embedded in a global circulation model which is equally equipped with a water isotope module (ECHAM4iso; Hoffmann et al. 1998). Further details about the embedding technique are described in detail in von Storch et al. (2000). It involves in particular the spectral nudging of the mesoscale model's wind fields towards the global model's winds. The ECHAM4 winds are also nudged toward ECMWF re-analysis winds (ERA40; Uppala et al. 2005). This double nudging technique (ERA40 $\rightarrow$ ECHAM4iso $\rightarrow$ REMOiso) is aimed at allowing a dynamically coherent high-resolution simulation close to the real observed synoptic variability. In summary, the REMO model needs the information of the state of the atmosphere (T, q, v) at its boundaries and additionally in its nudged mode the observed wind field within its numerical domain. The entire simulated time period covers the time period from 1958 to 2001. Here, we focus only on the period of overlap between model and our in situ measurements in the 1990s and early 2000s.

9.4 Results and Discussion

The first part of the results describes the rainfall isotopic time series, which are compared to the other available series and characterized by their meteoric water lines. We discuss the temperature–δ^{18}O correlations and the representativeness of REMOiso δ^{18}O simulations, both being important for the calibration of the speleothem δ^{18}O. In a second part, we present the drip water isotopic time series and then discuss the estimation of the time residence of the infiltrated water in the studied sites using the rainfall data.

9.4.1 Rainfall Isotopic Composition Characterization

Seasonal Variations, Local Meteoric Water Lines and Comparison with Other French GNIP Records

The three rainfall isotopic stations Villars, Le Mas and Orgnac display similar seasonal isotopic variations compared to other French GNIP stations (Figure 9.4, supplementary material). Note the particularly similar behaviour between the Orgnac station and Avignon and Draix, with, for example, low δ^{18}O values during winter 2006/07 and 2008/09 or high values during summer 2006. The seasonal amplitude is larger at most of these stations between 2004 and 2010; this is noticeable during the year 2008/2009 where Le Mas and Orgnac stations registered about a 9‰ amplitude change between winter 2008/2009 and summer 2009. Large changes also occurred between 2005 and 2006. After 2010, the seasonal amplitude is reduced again (Figure 9.4).

Figure 9.2 shows annual cycle graphs of monthly δ^{18}O and δD variations for Le Mas, Villars and Orgnac, where all measured values are plotted. This type of representation is very useful for characterizing the local rainfall isotopic composition, displaying both the monthly isotopic variation (i.e. difference between different months) and the interannual variability for a single month. The δ^{18}O variability is much more pronounced during the winter months than during the summer months, especially for Le Mas (without the exceptional values for the summer of 2009) and Villars, the two Atlantic stations. This is in agreement with larger winter variability of most climate parameters in mid- and high latitudes. At Orgnac, the summer variability is as pronounced as that in winter (Figure 9.2i). For all stations, there is an increasing δ^{18}O trend from winter months (December/January) until August. Then, there is a threshold after which the rainfall isotopic composition decreases more or less abruptly until November/December

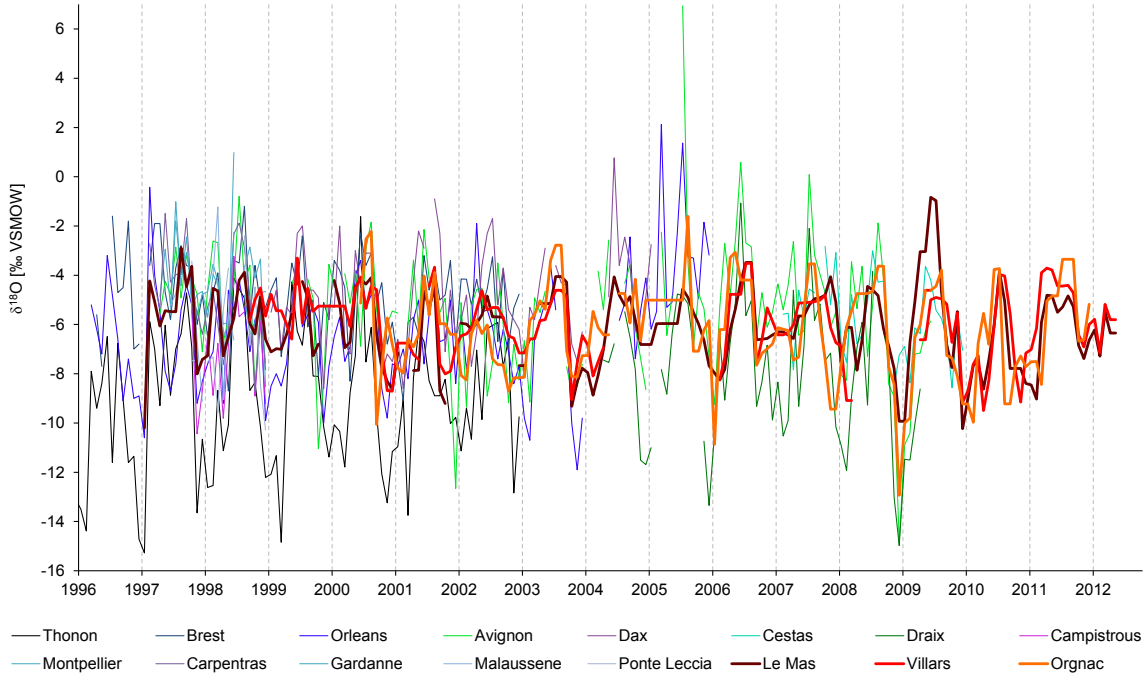

Figure 9.4: Monthly precipitation $\delta^{18}O$ time series for all French GNIP stations (IAEA/WMO 2006) and the new stations presented in this study, Le Mas, Villars and Orgnac.

(Figure 9.2c, f, i). Note that this decrease is much more marked at the Orgnac station, likely due to changes in the precipitation regime and the influence of Mediterranean storm tracks, which start to be more frequent at this period (Celle-Jeanton et al. 2004). Average seasonal differences between July–August and January–February are –3.1‰ at Le Mas, –2.1‰ at Villars and –3.6‰ at Orgnac.

Most of the isotopic values from the three stations lie on the global meteoric water line (GMWL), but all the slopes are lower than the global average slope of 8 (Figure 9.5). Le Mas and Villars local meteoric water lines (LMWL) are parallel with a similar slope of 7.3 when removing the two points of summer 2009, which show abnormally high values (Figure 9.5, supplementary material). If these two points are integrated, then the Le Mas LMWL slope would be slightly lower (6.9). It should be noted that such high monthly $\delta^{18}O$ values are often visible on GNIP data sets and are likely due to evaporation during the rainfall in a dry air column (see Figure 2.18 in Clark and Fritz 1997). Orgnac rainfall data show larger variations and the slope is slightly lower (7.0), but overall the data set is very similar to the two other stations, which are mainly controlled by the Atlantic climate regime.

Correlations Between Temperature and Rainfall $\delta^{18}O$

In the middle- and high latitudes, $\delta^{18}O$ is strongly affected by temperature through its control on the rainout of air masses ($\delta^{18}O$ depletion due to evacuation of a condensed phase –

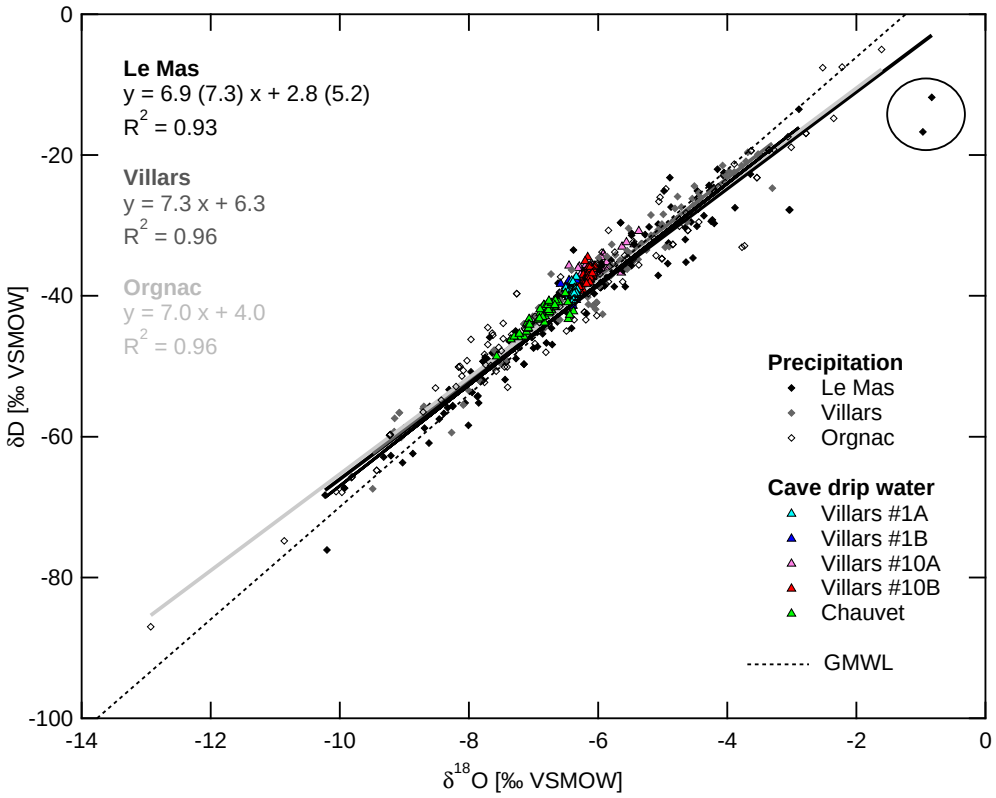

Figure 9.5: Scatter plot of δD vs. δ^{18}O in cave drip water and precipitation, and local meteoric water lines for Le Mas, Villars and Orgnac. For Le Mas, one line is plotted for all the data (slope 6.9) and another line (slope 7.3) without the two data points of summer 2009 (encircled points in the upper right corner). See text for explanation of these outliers. The dotted line is the global meteoric water line (GMWL).

the rain – from the cloud vapour; Clark and Fritz 1997). The temperature influence on the rainout process is the basis for using the water isotopes in paleoclimate archives like speleothems, tree rings or ostracods for temperature reconstructions. Consequently, it is of first importance to constrain the causes of δ^{18}O variation at a specific location by studying correlations with temperature. However, while the correlation between rainfall isotopic composition and surface temperature on a global scale is certain, it is less obvious to quantify it at a specific site because in-cloud temperatures rather than surface temperatures control condensation and isotope fractionation. Surface temperature from meteorological stations is often the only available data, but it disregards all the processes that occur outside the clouds, like air mass mixing or evaporation. Furthermore, it is preferable to consider the temperature when it rains and not the averaged air temperature. As done by Kohn and Welker (2005), we investigated the correlations between mean monthly temperature (MMT) and rainfall δ^{18}O, and between the mean monthly temperature weighted by the daily amount of precipitation (MMPT) and rainfall δ^{18}O (Table 9.4 and 9.5). MMT and MMPT are generally very similar for the three stations with the following small differences:

- For Le Mas and Villars stations, the MMPT is slightly higher than the MMT (+0.6°C and +0.2°C on average respectively);
- For Orgnac, the MMPT is generally lower than the MMT (–0.6°C on average); this occurs more often during the winter months.

Table 9.4: Correlations between temperature and precipitation δ^{18}O on the monthly, seasonal and annual time scale. MMT is the mean monthly temperature, MMPT is the mean monthly temperature weighted by the amount of precipitation. The first number is the slope of the linear regression line in ‰/°C, the number in parentheses is the linear correlation coefficient R^2. The asterisks indicate the significance level: * $p < 0.01$, ** $p < 0.001$.

Site	Monthly		Summer (JJA)	Winter (DJF)	Annual
	$\Delta\delta^{18}O/\Delta$ MMT (R^2)	$\Delta\delta^{18}O/\Delta$ MMPT (R^2)	$\Delta\delta^{18}O/\Delta T$ (R^2)	$\Delta\delta^{18}O/\Delta T$ (R^2)	$\Delta\delta^{18}O/\Delta T$ (R^2)
Le Mas	0.16 (0.35**)	0.18 (0.37**)	0.24 (0.12)	0.51 (0.14)	0.47 (0.14)
Villars	0.14 (0.33**)	0.16 (0.35**)	0.17 (0.10)	–0.11 (0.02)	0.56 (0.35)
Orgnac	0.18 (0.37**)	0.18 (0.37**)	0.33 (0.10)	0.95 (0.42*)	0.05 (0.00)

Table 9.5: Weighted mean annual precipitation δ^{18}O and mean annual temperature at the study sites.

Year	Le Mas		Villars		Orgnac	
	Weighted mean annual $\delta^{18}O$[‰]	Mean annual temperature [°C]	Weighted mean annual $\delta^{18}O$[‰]	Mean annual temperature [°C]	Weighted mean annual $\delta^{18}O$[‰]	Mean annual temperature [°C]
1997	–5.59	13.3		13.0		14.5
1998	–6.22	12.4		12.1		13.8
1999	–6.33	12.8	–5.40	12.5		14.1
2000	–6.32	13.0	–6.42	12.9		14.3
2001	–7.69	12.6	–6.62	12.3	–6.15	14.1
2002	–6.62	13.0	–5.90	12.8	–7.63	14.4
2003	–6.72	13.5	–6.50	13.5	–6.55	14.6
2004	–6.43	12.3		12.2	–5.45	13.7
2005	–6.17	12.4		12.4	–6.30	13.5
2006	–6.44	13.3	–6.13	13.2	–6.04	14.3
2007	–5.66	12.8	–5.78	12.5	–6.96	14.3
2008	–6.82	12.4		11.9	–6.60	13.6
2009	–5.31	12.9	–6.53	12.5	–7.64	14.5
2010	–7.36	11.8	–7.49	11.3	–7.71	13.2
2011	–6.20	13.6	–5.48	13.6	–6.05	15.0

The differences between stations are possibly due to the difference in the precipitation regimes, such as the more pronounced seasonality in the precipitation for the Orgnac station, which is influenced in winter by Mediterranean storms as shown, for example, in data from the nearby station of Avignon (Celle-Jeanton et al. 2001).

Whether MMT or MMPT is considered, the correlations between rainfall δ^{18}O and mean monthly temperature generally have a low significance (R^2 of 0.33 to 0.37; Table 9.4, Figure 9.6). The mean values for each month (triangles in Figure 9.6) plot close to the linear regression line of all measured monthly values. This suggests that the correlation on a monthly time scale is due to the similar seasonal cycle in both temperature and δ^{18}O. The correlation for winter and summer months separately gives even lower R^2 and is not significant. The average slopes between monthly rainfall δ^{18}O and monthly temperatures (MMT or MMPT) are low and very similar between the stations (0.14 to 0.18‰/°C; Table 9.4). Compared with other published data, like those found in North America (0.55‰/°C Kohn and Welker 2005), these values are low. But it is now well known that the T–δ^{18}O relationship is often linked to site specific circulation patterns and that highly significant correlations are rather rare. Since the global study of Dansgaard (1964), which gave an annual $\Delta\delta^{18}$O/ΔT of 0.69, marine and continental data sets have given different slopes, highlighting the importance of local geography (continentality, altitude, latitude etc.). Between continental, marine and polar sites, the annual $\Delta\delta^{18}$O/ΔT varies from 0.17 to 0.9‰/°C (Clark and Fritz 1997).

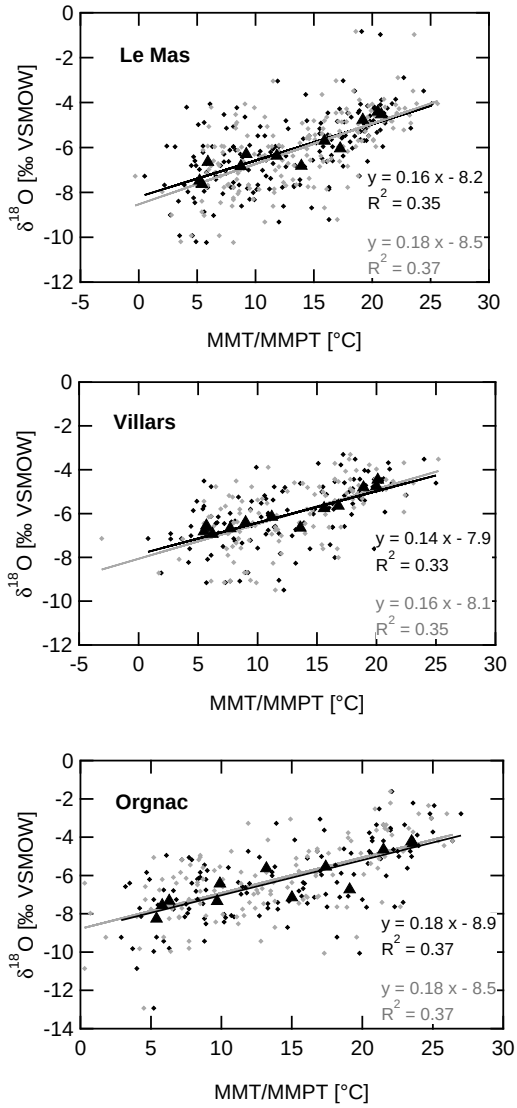

Figure 9.6: Scatter plots between mean monthly temperature (MMT, black points) or mean monthly temperature weighted by the amount of precipitation (MMPT, grey points) and monthly precipitation δ^{18}O for Le Mas, Villars and Orgnac. The triangles represent the mean values for each month (January to December).

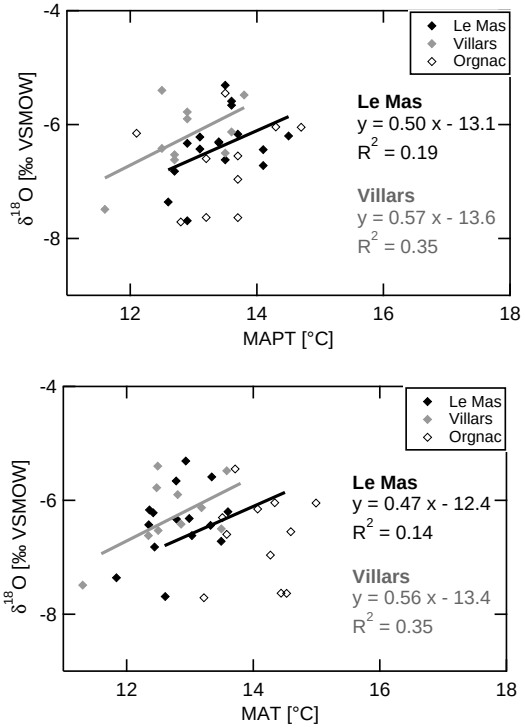

Figure 9.7: Scatter plots between mean annual temperature (MAT, top) or mean annual temperature weighted by the amount of precipitation (MAPT, bottom) and mean annual precipitation δ^{18}O for Le Mas, Villars and Orgnac. The equation of the regression line and R^2 for Orgnac are not given because there is no correlation between annual temperature and precipitation δ^{18}O.

T–δ^{18}O dependency has been extensively studied in the past and a general slope for mid-latitude continental stations has yielded a mean slope of 0.58‰/°C (Rozanski et al., 1993). However, it appears that, depending on the location, the slope is highly variable, i.e. from 0.18 to 0.49 in Canada (see examples and references in Clark and Fritz 1997), and, moreover, T–δ^{18}O correlations are generally weak (Hoffmann et al. 2005) but not always published except rare local studies like the ones near Avignon, relatively close to the Orgnac site (Celle et al. 2000).

Our data lead to similar conclusions: the highest correlation between mean annual temperature (MAT) and mean annual rainfall δ^{18}O occurs at Villars station ($R^2 = 0.35$), then Le Mas station displays a weak correlation ($R^2 = 0.14$), while Orgnac data are not correlated at all (Figure 9.7a). For the two south-western stations, Villars and Le Mas, the T–δ^{18}O slopes are close to the global one: 0.54‰/°C for Villars and 0.47‰/°C for Le Mas, even if for this last station the low R^2 makes this value uncertain (Figure 9.7). As for the mean monthly temperature, correlations with precipitation δ^{18}O were investigated for the mean annual temperature weighted by the amount of precipitation (MAPT, Figure 9.7b). Results are very close to the one obtained using the MAT: a slope of 0.57‰/°C for Le Mas and 0.50‰/°C for Villars. Correlation coefficients are also similar: $R^2 = 0.35$ for Le Mas and slightly higher for Villars ($R^2 = 0.19$), but there no significant correlation for the Orgnac site.

Summarizing the T–δ^{18}O relationships, whether monthly or annual values, weighted or unweighted temperatures are considered, the correlations between rainfall δ^{18}O and air surface temperature are very low. Similar results were found in southern France stations, where different air masses from the Atlantic and the Mediterranean interact. As a consequence, any estimated transfer function between a palaeoclimate proxy based on rainfall δ^{18}O and surface air temperature, is not statistically robust.

Comparison of Data with REMOiso Simulations

REMOiso results were extracted for the respective grid boxes containing the south-west stations Le Mas and Villars, and the Orgnac station in the south-east (see supplementary material). For technical reasons, the simulation ended in 2001, which is why the period of overlap between the model results and the isotope observations is rather short: 58 months for Le Mas, 39 months for Villars and 18 months for Orgnac (Figure 9.8). A comparison between the REMOiso simulation and the rainfall δ^{18}O measurements shows the following:

- At all sites, the phasing of the seasonal cycle is well simulated;
- For Le Mas and Villars, REMOiso δ^{18}O is significantly more enriched than measurements, by 1 to 2‰ during the summer months winter values are quite well simulated;
- The Orgnac station displays a better agreement between modelled and measured values, but summer months are still slightly overestimated by REMOiso;
- An intriguing result of the REMOiso simulation is the good agreement with parts of the observed intra-annual variability, in particular the double peaks in δ^{18}O, which are clearly observed at Le Mas in February–March and July–August, or the secondary winter peak in December at Orgnac.

For the last point, it is interesting to note that the double peak simulations are not linked to any corresponding temperature or rainfall variations because these two parameters do not show

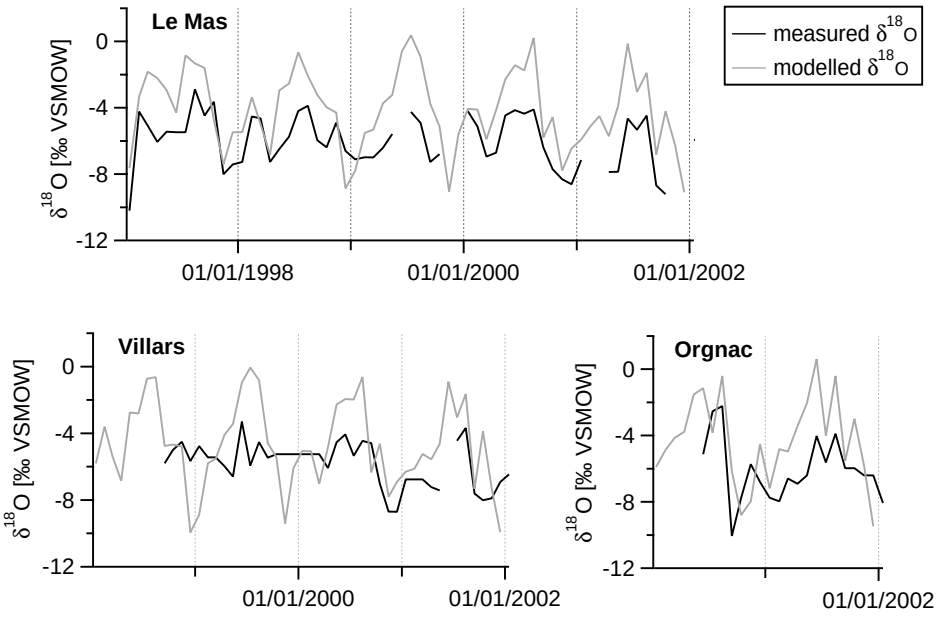

Figure 9.8: Comparison between measured precipitation δ^{18}O (black lines) and REMOiso simulations (grey lines) for Le Mas, Villars, and Orgnac.

such a pattern. It needs additional analysis to (a) confirm the robustness of these peaks in the observation and (b) to investigate the respective causes. Here we only speculate that varying transport lengths and accompanying rainout histories both possibly associated to atmospheric circulation anomalies might have a negligible impact on local temperatures and precipitations but produce a significant change of the isotopic composition of the respective water vapour. It is in any case remarkable that REMOiso is able to reproduce this type of intra-annual variability.

In summary, the double-nudged REMOiso simulation provides a good representation of local rainfall δ^{18}O, although its average level and its seasonal amplitude differ significantly from the observations. The overestimation of the seasonal amplitude, in particular during summer time, points to possible model problems with the representation of convective rain events and their isotopic signatures. It is well known that summer convection is a major challenge for weather forecast models. In particular the exact location, intensity and duration of these events are badly described by GCMs/RCMs in general and insufficiently constraint by the regional wind fields as it was done here in our double nudging approach.

9.4.2 Comparison Between Rainfall δ^{18}O and Drip Water δ^{18}O at Villars and Chauvet Cave – Importance for Cave Water Residence Time and Age Estimation

Water movement in a karstic structure is guided by three types of porosity: inter-granular pore space, joints and fractures, and larger conduits (Ford and Williams 2007). Speleothems are mainly fed by joints and fractures and/or millimetric pore spaces (Fairchild and Baker 2012). Depending on the porosity type of the rock formation above the speleothem, flow time between the surface and the stalactite exit can be highly variable: diffuse flow through micro-

fractures or small pores will show dampened seasonal variations while preferential flow through large fractures or conduits will be more sensitive to rainfall events and seasons (Fairchild and Baker 2012; Genty 2008). It is of primary importance for speleothem and dendro-isotopic paleoclimate studies to know the origin and the average age of the feeding water, especially in a context where paleoclimatic studies focus on annual signals and temperature quantification, both of which require calcite and water $\delta^{18}O$ values (Daëron et al. 2011; van Breukelen et al. 2008). The residence time of cave drip water can be estimated by studying the discharge under stalactites, leading to conceptual models of cave drip water hydrology, but there are few studies dealing with this topic (Wackerbarth et al. 2012; Bradley et al. 2010; Fairchild et al. 2006b; Friedrich and Smart 1981). However, even if until now the average age of the seepage water feeding stalagmites in most caves is not well constrained, the following observations have been made: (1) most stalactite drip waters display seasonal variability, with increasing flow rate in late November/early December for middle latitudes of temperate areas (Genty and Deflandre 1998); (2) the mean residence time of these dripping ground waters is very variable from one site to the other and ranges from a few weeks to one or several years up to decades, as demonstrated by tritium and $\delta^{18}O$ tracers (Chapman et al. 1992; Kaufman et al. 2003; Kluge et al. 2010; Yonge et al. 1985). This large discrepancy is certainly due to the heterogeneity of the karstic terrains.

Recently, a model study focused on the mechanistic understanding of the relationship between rainfall $\delta^{18}O$, cave drip water $\delta^{18}O$ and speleothem calcite $\delta^{18}O$ (Wackerbarth et al. 2012). Nevertheless this relationship has never been empirically quantified before using such a long time series, despite its importance for the interpretation of paleoclimatic proxies. Stable isotopes recovered from speleothem fluid inclusions or tree-ring cellulose, for example, both depend on soil water $\delta^{18}O$ rather than rainfall $\delta^{18}O$, which can differ from precipitation due to evaporation, soil water residence time and mixing (see also Wackerbarth et al. 2012). The comparison of rainfall and cave drip water $\delta^{18}O$ on the long time series of Villars/Le Mas and Chauvet/Orgnac allows the construction of a water mixing model to estimate the origin and the age of the infiltration water at these sites.

Cave Drip Water $\delta^{18}O$ and δD Time Series

Monitoring of drip water in Villars and Chauvet Cave shows that the stable isotope composition has been very constant since the beginning of measurements (Figure 9.9, Figure 9.10, Table 9.6 and supplementary material). The four drip stations of Villars represent two depths inside the cave: #10A and #10B are situated in the upper galleries, about 10 m below the surface, while stations #1A and #1B are situated in the lower galleries at about 25 m depth (Genty 2008). For each gallery level, the $\delta^{18}O$ (like the δD) displays homogeneous values: –6.17‰ ($1\sigma = 0.22$; N = 86)) and –6.17‰ ($1\sigma = 0.07$; N = 67) for the upper gallery and –6.38‰ ($1\sigma = 0.06$; N = 70) and –6.39‰ ($1\sigma = 0.05$; N = 79) for the lower gallery (Table 9.6). In the calculation of mean values, early data measured on the VG mass spectrometer were discarded because of their low accuracy (see section 9.3.3; Table 9.6). Beside the stability of the drip water isotopic signal found in Villars and Chauvet Cave, there is a significant difference of 0.21‰ between the lower and the upper galleries in Villars Cave, the lower gallery having the lowest values (Figure 9.9, Table 9.6). Chauvet Cave consists of only one level, and there is not enough data available to have a long continuous series for each sampling station, which is why all the drip water data were averaged. Only Villars station #10A displays significant $\delta^{18}O$ variations of up to 1.2‰ (Figure 9.9), which is likely due to its more direct connection with the surface, as

suggested by its relatively high drip-rate variability (Genty 2008). The other stations (#10B, #1A, #1B) have very stable values, which means that they represent a mixing of the rainfall input over several months or years, similar to previous studies (Chapman et al. 1992; Williams and Fowler 2002; Yonge et al. 1985). The link between the rainfall δ^{18}O and the cave drip water δ^{18}O is explored in the following sections.

Cave Water Isotopic Composition Modelling and Infiltration Residence Time

The time during which precipitation is integrated in the rock formation above the cave is crucial for estimating the effective age of drip water. At both sites Villars and Orgnac, the weighted annual mean of precipitation δ^{18}O (i.e. 12 months averaging) varies from year to year by up to 3‰ (Figure 9.9b and Figure 9.10). When calculating a weighted mean of the months during which the water excess (precipitation minus potential evapotranspiration; PET) is positive (by using this method we discarded the possibility of infiltration during dry months, which might still be possible for intense rain events), which is between October/November and April/May for this area (Genty 2008), the year-to-year variability is as high as that for the annual mean (not shown). Since the drip water isotopic composition in both caves is constant, the stalagmites must be fed by water which has a residence time in the soil and in the bedrock above the cave greater than one year. This is also the reason why it is not necessary to weight the drip water by the drip rate when comparing to the rainfall data. One way to determine the residence time of the seepage water is to integrate, month by month, the weighted rainfall δ^{18}O since the beginning of measurements and to compare this against the drip water δ^{18}O values. The number of integrated months required to reach the cave water δ^{18}O value should provide a reliable estimate of the minimum duration of rainfall mixing. Our hypothesis is that seasonal rainfall δ^{18}O does not change considerably from one year to the other (i.e. there are no exceptional years that would significantly modify the underground reserve δ^{18}O) and that there is no change in the isotopic signature during infiltration. Furthermore, we use local data which is sampled directly above the respective caves and not modelled or interpolated from nearby stations. Integrated rainfall $\delta^{18}O_{int}$ is then defined as:

$$\delta^{18}O_{int} = \frac{\sum P * \delta^{18}O_i}{\sum P} \tag{9.2}$$

In order to determine which months contribute to the recharge, we first considered that rainfall feeds the karst water reserve when the water excess is positive, as proposed in former studies (e.g. Genty and Deflandre 1998). Then, depending on the results, the number of months that contribute to the recharge was increased, until the integrated δ^{18}O reached the cave δ^{18}O value. If only the months with a positive water excess are considered, when infiltration to the underground should theoretically occur, we obtain integrated rainfall δ^{18}O values which are much lower than the cave drip water values. The best fit is obtained by integrating all months, or by removing only August, the hottest month (Figure 9.9). This implies that the rainfall of the whole year contributes to the recharge, even in summer when the PET exceeds precipitation. A study of soil water δ^{18}O in the Netherlands also demonstrated that the whole year's precipitation contributes to groundwater recharge, despite a soil-moisture deficit in summer and a precipitation surplus during the winter (Gehrels and Peeters 1998). The authors explain this by preferential flow which dominates soil water movement. Certainly, water is lost from the soil to the atmosphere during months with a large PET, but mainly through the vegetation cover and not through direct evaporation from the soil, which would modify the

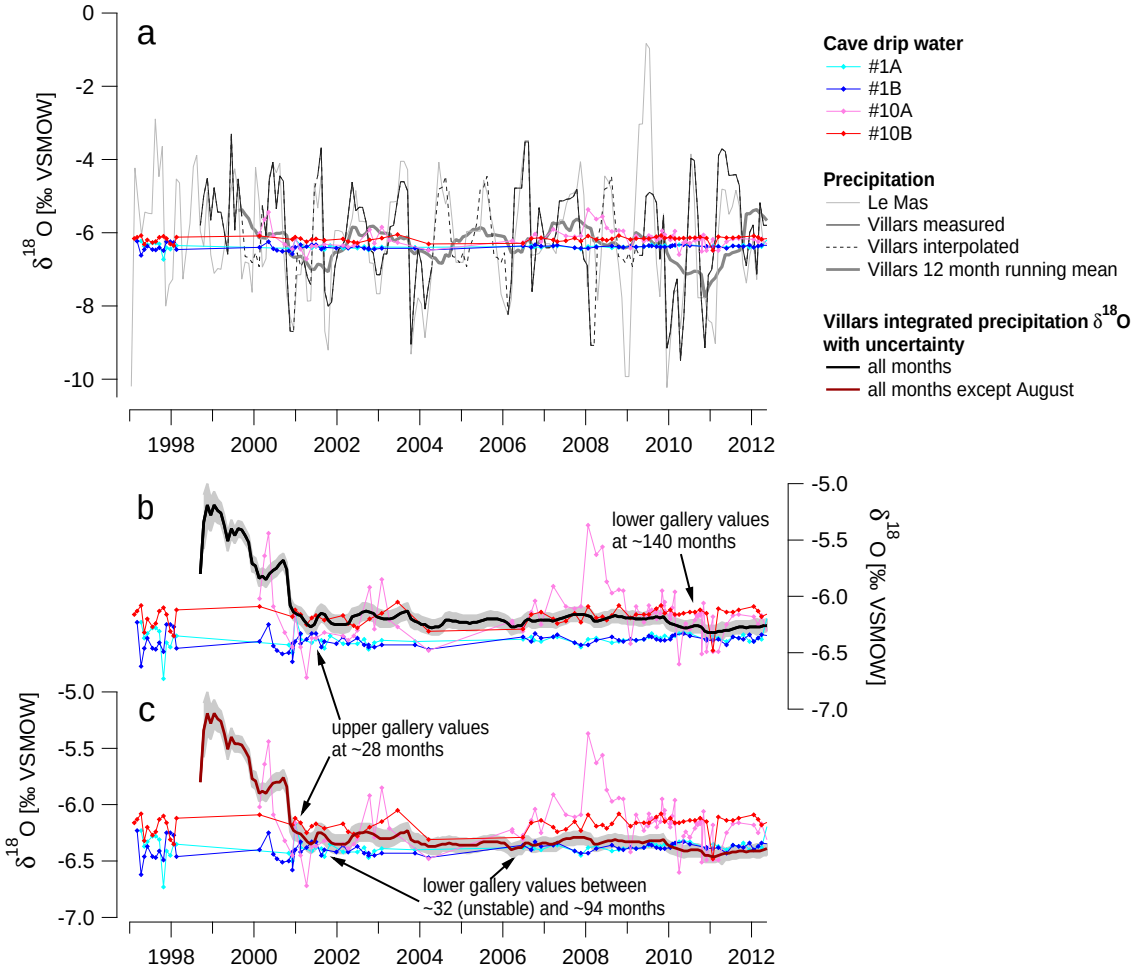

Figure 9.9: (a) Precipitation and drip water δ^{18}O at Villars cave. Light blue and dark blue lines are drip water measurements from the lower gallery (#1A, #1B); pink and red lines are drip water measurements from the upper gallery (#10A, #10B). Grey and black lines are the precipitation δ^{18}O (black: measured data; black dotted: interpolated data with mean monthly values – see methods section; grey: Le Mas data). The thick grey line is a 12 month running mean of precipitation δ^{18}O weighted by the amount of precipitation (it considers all months of the year). (b) Drip water δ^{18}O compared with the integrated precipitation δ^{18}O for all months (black). (c) Drip water δ^{18}O compared with the integrated precipitation δ^{18}O for all months except August (brown). Errors on measurements (±0.05‰ for δ^{18}O, ±0.5 mm for precipitation amount) were added to the variance of the cumulative weighted δ^{18}O mean, resulting in the upper and lower uncertainties close to ±0.06‰ (grey shading).

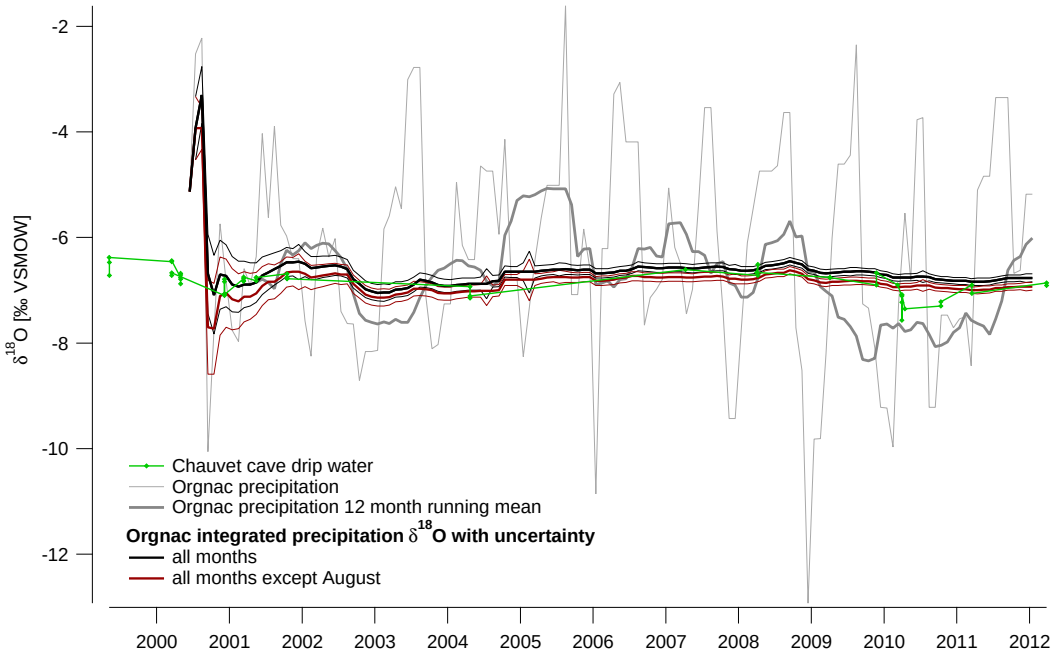

Figure 9.10: Precipitation and drip water δ^{18}O at Chauvet cave. The thin grey line is the Orgnac precipitation δ^{18}O. The green line is the drip water δ^{18}O from different stations in Chauvet cave. It is compared to (1) a 12-month running mean of precipitation δ^{18}O weighted by the amount of precipitation (it considers all months of the year; thick grey line); (2) the integrated precipitation δ^{18}O for all months (black) and for all months except August (brown) with their respective uncertainties.

isotopic composition of the remaining soil water. This is true for the studied sites where there is no bare soil but only forest and grass cover. There is generally no fractionation of isotopes when water is taken up by plant roots (Obrist et al. 2004). Furthermore, at these sites we assume that there is minimal seasonal bias introduced by transpiring plants, which could theoretically only take up water consisting of, for example, the growing season precipitation. Such a process would lead to a cave drip water that is composed to a large part of non-growing season precipitation. Apparently this is not the case, since the cave drip water's isotopic composition corresponds to the weighted mean of all months' precipitation. An important consequence of this finding for the interpretation of tree ring cellulose δ^{18}O is that trees – at least at this site – use mixed water with a certain residence time in the soil, which represents several years' precipitation. Alternatively, the cave drip water δ^{18}O values could be explained by a mixing of: (1) rain water that infiltrates when the water excess is positive (i.e. between October/November and April/May); and (2) summer precipitation which is enriched by evaporation. Since a part of the summer precipitation is lost to the atmosphere in this process, its contribution to the weighted mean δ^{18}O would be smaller, but its higher isotopic value would give the same result. It is not possible to quantify the water loss and isotopic enrichment of the remaining soil water, because direct soil water measurements are not available and would be difficult to perform in karstic terrains where the soil layer is thin and irregular. But, whatever the hypothesis concerning the seasons which contribute to the recharge, the only way to explain the stability of the cave drip water δ^{18}O is to consider mixing of rainwater spanning several years in a reservoir, and, by doing this, the only way to reach the mean drip water values, is to consider either all months of

the year or all months except August (Figures 9.9 and 9.10). Removing more summer months in the calculations leads to too low values.

Figure 9.9 shows that the actual $\delta^{18}O$ value of the lower gallery lies between the two curves: the integrated rainfall $\delta^{18}O$ value among the entire period (∼14 years) for all months (black thick curve, Figure 9.9b) and the integrated rainfall $\delta^{18}O$ for all months except August, the hottest month (brown thick curve). This implies that there is a small deficit of heavier rainfall water due to evaporation during a few days for the entire year. However, given the uncertainties of the measurements, the integration, and the insufficient period of survey (there is still a slight decreasing trend in the integrated rainfall $\delta^{18}O$ curves), we can only conclude that, at Villars, rainfall contributes to underground recharge during the entire year or the entire year minus the month of August. Consequently, it appears that vegetation transpiration does not produce significant seasonal bias in the isotopic signal of the seepage water at this site.

The Chauvet Cave drip water $\delta^{18}O$ time series has much fewer data points, which is why only one time series was constructed using different drip stations. The variability between these locations is relatively low, because the bedrock thickness above them is about the same, although it is still higher than in Villars (Figure 9.10). As for the Villars site, the mean drip water value (–6.89‰ ±0.22) is reached only when considering all months, or all months except August (Figure 9.10). Contrary to Villars, the integrated $\delta^{18}O$ value becomes stable very early, after about half a year. Here too, it appears that rainfall during the whole year contributes to the recharge. The slightly lower drip water values of the year 2010 might signify a lower contribution to the warmest days/months, but a more frequent sampling would be necessary to be more affirmative.

The integration of monthly precipitation $\delta^{18}O$ values at Villars shows that the upper gallery's drip water $\delta^{18}O$ value (–6.17‰) is reached after about 28 months for both tests (integration on all months of the year, or on all months except August), whilst for the lower gallery, 15 m deeper, the $\delta^{18}O$ value (–6.39‰) is reached only after about ∼140 months if we consider all months (Figure 9.9b) and after ∼94 months if we consider all month except August (Figure 9.9c). All other tests with less summer water for the recharge contribution lead to too low $\delta^{18}O$ values and shorter time integration (considering or not all months of the year) lead to too high $\delta^{18}O$ variability. Although infiltration times may be much shorter (i.e. a few weeks in the very well drained karst (10–20 m thick) of Black Chasm Cavern, California (Oster et al. 2012) or a few months in Nerja Cave, south Spain (for 30 m thickness, Carrasco et al. 2006), these surprisingly long durations are coherent with previous studies that investigated the seepage water residence time in caves with stable isotopes and tritium. Vertical travel time in Carlsbad Cavern, New Mexico, was found to be of the order of decades for depth up to 250 m (Chapman et al. 1992); it takes 26 to 36 years for the rain water to reach galleries 10-50 m below the surface in Soreq Cave, Israel (Kaufman et al. 2003); and it takes about 2–4 years to reach galleries at 10–30 m depth in Bunker Cave, Germany (Kluge et al. 2010). Considering the average depth of the galleries, the residence times found in Villars Cave are close to the ones found in Soreq Cave.

Insights into the Villars Cave Drip Water $\delta^{18}O$ and Flow Rate Behaviour

More information can be extracted from Villars Cave, where the drip water was studied at two different levels, and at two stations, close each other (1–4m), at each level. We observe the following (Table 9.6; Figure 9.11):

Figure 9.11: Drip water δ^{18}O (top) and flow rates (bottom) at four monitoring stations in Villars cave. Note the well marked seasonality in the drip rates, while the oxygen isotope composition stays very stable for #1A, #1B and #10B. The higher variability at station #10A is likely due to a more direct fracture network connection of this stalactite with the outside.

Table 9.6: Stable isotope values and drip characteristics of the dripping water at different monitoring stations in Villars and Chauvet cave. N is the number of samples, σ is the standard deviation, L/year is the mean annual quantity of water from a station, $\Delta\delta^{18}$O is the maximum δ^{18}O amplitude between min and max δ^{18}O during the observation period, Δdrip rate is the maximum amplitude between min and max drip rate during the observation period. Mean annual drip water δ^{18}O have been weighted by the drip rate of each station and gave similar results to the unweighted δ^{18}O, only Villars-#10A displays a slight difference which close to the analytical uncertainty, –6.13 being the weighted value.

Station	δ^{18}O	1σ	δD	1σ	N	L/year	$\Delta\ \delta^{18}$O	Δ drip rate
Villars-Vil#1A	–6.38	0.06	–39.52	0.83	73	375	0.37	2.57
Villars-Vil#1B	–6.39	0.05	–39.62	0.63	82	1419	0.25	8.87
Villars-Vil#10A	–6.17/–6.13	0.22	–37.17	1.72	91	1326	1.35	12.84
Villars-Vil#10B	–6.17	0.07	–37.34	0.90	74	334	0.44	2.5
Chauvet-all	–6.89	0.22	–42.76	1.89	53			

- All four stations display a great stability in the drip water δ^{18}O values since the beginning of observations; average drip water δ^{18}O values are similar for each gallery, weighted or not by the drip rate (because of the stability of the δ^{18}O and despite the seasonal changes in the drip rates);
- There is a small (–0.2‰) but significant difference between the upper (#10A, #10B) and lower (#1A, #1B) galleries drip water δ^{18}O, the lower gallery stations δ^{18}O being lower (–6.38‰) compared to the upper gallery ones (–6.17‰);
- The highest δ^{18}O variability is observed in the stations from the upper gallery;
- There is no link between the mean quantity of water that flowed under the stalactites and the depth of the galleries: stations #10A (upper) and station #1B (lower), display the highest flow rates, four times higher than the nearby stations;
- But there is a link between the mean annual drip rate and the variability of the flow: the highest the mean flow rate, the highest the variability, whatever the depth of the gallery;
- The drip rate variations show well marked seasonal variability in all the stations; the amplitude of this seasonality is not linked with the depth of the galleries; since the

beginning of the observation, dripping never stopped in all these stations.

Indeed, these data confirm the great heterogeneity of the karst aquifer: because of the complexity of the micro-fractures network in the karst above caves, it is very likely that different conduits and fractures with different types of flow rates (i.e. diffuse, preferential), contribute to the reservoir that feed the stalactite drips (Fairchild and Baker 2012; Baker et al. 2010; Bradley et al. 2010; Tooth and Fairchild 2003; Bar-Matthews et al. 1996). A good illustration of this is the difference observed in the high resolution drip flow rate measurements between #10A and #10B, only 4 m from each other, and where a significant delay of several weeks in the autumn/winter seasonal flow rate increase was observed coupled with a difference in the flow rate amplitudes (Figure 13 and Table 1 in Genty 2008). The residence times found in our study are thus likely an average time of different hydrological components, fast (hours to days) and slow (days to months to years) at a specific place in the cave, for this reason we can call them "apparent residence times". But stable isotope data bring here new light in the understanding of the origin of the drip water feeding stalagmites. First, it appears that there is no link between the hydrological behaviour (flow rate quantity, variability) and the mean drip water $\delta^{18}O$ in each gallery, weighting or not these measurement do not change anything in the average values; second, the significant difference between the upper and lower galleries drip water $\delta^{18}O$ raises questions about its cause; third, the fact that the lower galleries have the lowest drip water $\delta^{18}O$ and also have the highest stability leading to longest apparent residence times might be connected to the former observation. The independence between the drip rate and the $\delta^{18}O$, combined with the perennial dripping (i.e. no drying), confirms the existence of a mixing reservoir above each gallery that has a piston flow functioning: rainfall recharges a water reserve, more or less large, that feed the stalactites/stalagmite system. The existence of such a reservoir is already known and was describes in several other studies (e.g. see references in Fairchild and Baker 2012; Baker et al. 2010; Ford and Williams 2007; Genty and Deflandre 1998). Already known also is the heterogeneity of the fractures/conduits that leads to different types of flow (slow/fast; diffuse/preferential etc. see above references). But recent hypotheses combining hydrology and water isotopes during infiltration in karst suggest that variations in the hydrological routing might occur and may explain offsets in drip water $\delta^{18}O$ compared to weighted mean $\delta^{18}O$ of precipitation (Bradley et al. 2010). Overflows or bypass flows could be the cause of lower drip water $\delta^{18}O$ when they are activated by high recharge periods (i.e. winter during which the rainfall $\delta^{18}O$ is lower). This would be a tempting hypothesis in order to explain the lower $\delta^{18}O$ of the lower gallery drips in Villars Cave (Figure 9.12): rainfall flows into a first reservoir, with a mean $\delta^{18}O$ of –6.17‰, which feeds the upper gallery stations #10A and #10B; overflows, that are more likely to occur during winter and spring, go into another reservoir through preferential conduits, this reservoir, with a lower mean $\delta^{18}O$ (–6.39‰), feeds the two deepest stations in Villars (#1A and #1B). We suggest that this reservoir is also mainly fed by the upper reservoir with smaller fractures or more diffuse infiltration and that its lower $\delta^{18}O$ value is the result of a mixing of both overflows and regular seepage. Finally, its size, likely larger than the upper reservoir, might explain its longer time residence. Another hypothesis could explain the $\delta^{18}O$ difference between upper and lower galleries in Villars Cave: because the apparent time residence of the lower gallery drip water is longer, we can suggest that the mean rainfall $\delta^{18}O$ was lower during the past decades and its imprint arrives in the present days in the seepage water. This hypothesis is reinforced by the local air temperature records which show a significant lower air temperatures (by about 2–3 °C) during the winter season before the years 1987 (see Figure 17 in Genty 2008).

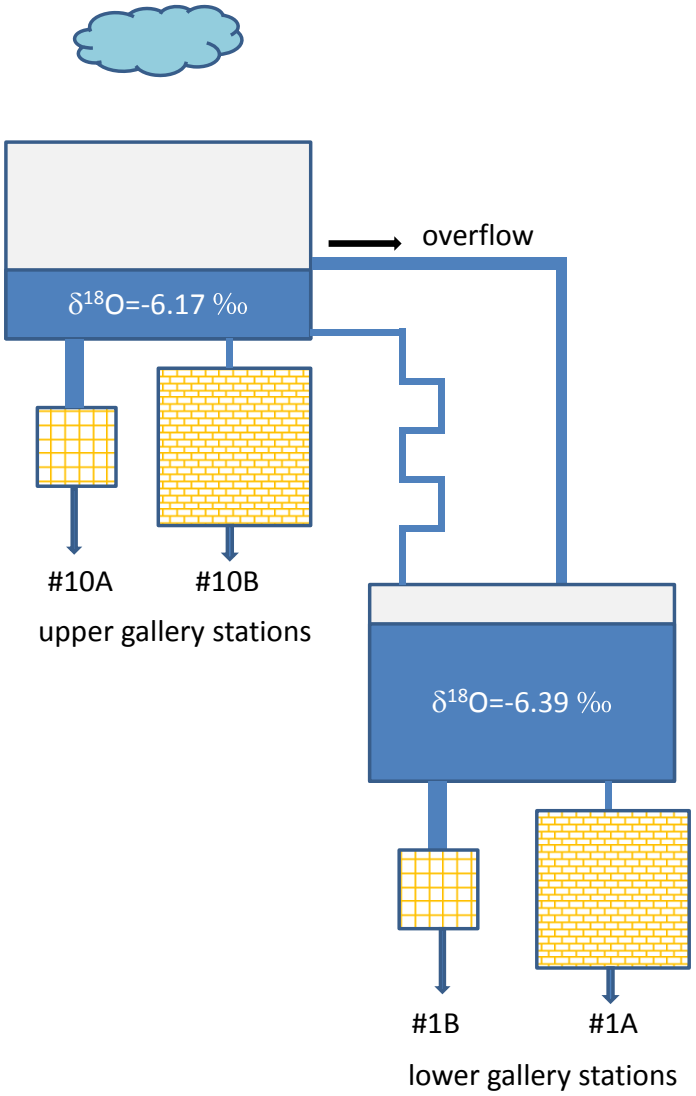

Figure 9.12: Conceptual model of the infiltration in Villars cave. Rainwater fills a first reservoir, where mixing of precipitation during all the year leads to a mean $\delta^{18}O$ of –6.17‰. This reservoir feeds sub-reservoirs of station #10A and #10B. Differences in capacity and fracture size explain the different drip flow behaviour (#10A shows a much higher seasonal amplitude; see Figure 9.11 and Table 9.6) of these two stations which have a similar $\delta^{18}O$. During humid periods (i.e. winter, spring), overflows feed a second larger reservoir, which is also fed by a more regular flow from the first reservoir giving a final value of $\delta^{18}O$ of –6.39‰. This reservoir feeds sub-reservoirs connected to #1A and #1B. Like for the upper level, differences in capacity and fracture size explain the different drip flow behaviour (#1B shows a much higher seasonal amplitude).

Drip Water and LMWL

The local meteoric water lines (LMWL) of Villars, Le Mas and Orgnac show close similarities and are characterized, like most rainfall stations, by large seasonal variations (Figure 9.5). Due to the large number of measurements, and to the good analytical accuracy, we confirm here a second and important characteristic of cave waters: the gravity centre of the cave isotopic clouds are slightly above the LMWL (Figure 9.5). This specific feature was already noted for Villars (Genty 2008), and is confirmed here by the Chauvet data. A possible explanation for such an offset slightly above the meteoric line would be a contribution of condensed water to drip water (Clark and Fritz 1997). Studying moonmilk deposits and cave waters in the Caverne de l'Ours (Canada), Lacelle et al. (2004) found out that the condensed water on the cave walls that feed the deposits was situated above the local meteoric water line. It is well known that there are condensation zones near cave entrances due to the interaction between outside air and cave air (Ford and Williams 2007). It has been observed in many caves that condensed water flows along walls, vaults and external surfaces of stalactites and forms drops at the stalactites tips, similar to regular seepage water. Such phenomena can occur in galleries and conduits that are located in the upper part of the karst, close to the surface, where temperature variations are large. More measurements are needed to confirm this hypothesis, and sampling of condensation water in such zones is in progress.

9.5 Conclusions

The comparison between 12- to 16-year-long rainfall isotope series of and on-site cave waters in two different regions of south France allows a better understanding of the isotope signal of the drip water which feeds stalagmites. Comparison of these isotopic series with meteorological data and numerical model simulations bring information about the controlling factors that constrain the water $\delta^{18}O$ in these areas. The main results are:

1. In the two studied caves, Villars (north SW-France, Atlantic climate influence) and Chauvet (SE-France; Atlantic/Mediterranean climate influences), all the stalactite drip stations, from 10 to 50 m depth from the surface, display a remarkable stability in their isotopic composition since the beginning of measurements (i.e. $>$ 10 years);
2. The average $\delta^{18}O$ values of these cave drips do not correspond to the weighted mean annual value of rain water $\delta^{18}O$, neither when considering all the months, nor with the months during which water excess is theoretically positive;
3. The very stable isotopic signal of cave drip waters can only be explained by considering a mixing of rainwater over several months to several years (up to 32 and to 140 months for the lower galleries of Villars Cave) and an infiltration of rainwater during all months of the year or all months except August. This result is of great importance for the interpretation of speleothem and tree rings isotopic measurements for two main reasons: a) at least at present, there is no seasonal bias in the $\delta^{18}O$ of cave drip water, which means that fluid inclusions recovered from speleothems should represent the mean annual (or pluri-annual) rainfall water composition unless local evaporation changes its composition; b) the vegetation above the cave (trees, grass), despite an important water consumption, does not provoke any seasonal bias as it would be the case if they used only spring/summer waters. On the contrary, they use the water from reserves that are already mixed for several months/years. This has important consequences for the

interpretation of tree ring cellulose $\delta^{18}O$;

4. At Villars Cave, the drip water $\delta^{18}O$ of the lower galleries is significantly lower (–0.2‰) compared to the upper galleries; this could be the consequence of overflows that feed lower reservoirs and/or to older rainwater that reach the lower galleries at present days and which were formed during a colder period as it is shown buy the local air temperature records;
5. The relationship between rainfall $\delta^{18}O$ and surface air temperature shows slopes between 0.14 and 0.18‰/°C at the monthly scale and between 0.47 and 0.57‰/°C at the annual scale; there is a weak correlation between the weighted rainfall $\delta^{18}O$ and the mean air temperature, considering mean air temperature of all days or mean air temperature of rainy days only;
6. Local meteoric water lines (LMWL) have been characterized in three different rainfall stations: Villars and Le Mas (north SW-France) and Orgnac (close to Chauvet Cave; SE-France); they display very similar slopes, close to 7, but show slight differences in the seasonal variability has seen in monthly isotopic graphs: $\delta^{18}O$ variability is much higher in winter than in summer and presents an abrupt isotopic threshold which is observed between August and September. This threshold effect is particularly well marked at the Orgnac station, likely due to its more Mediterranean climate;
7. Comparisons between rainfall $\delta^{18}O$ measurements and REMOiso simulations show a systematic overestimation of the $\delta^{18}O$ by the model. This holds both for the annual mean and for the seasonal amplitude at all stations. However, despite the short-duration period where a direct comparison was possible, REMOiso apparently simulates many features of the observed isotope signals. In particular, the model reproduces some interesting patterns of the observed intra-seasonal variability, such as isotopic double peaks, which appear in winter at all stations and which are not related to surface air temperature or precipitation. However, our finding of common intra-seasonal variability needs to be confirmed on longer time scales both for observations and for model simulation. The model's evaluation here suggests that the modelling technique of nudging a regional model within a global model employed here is sufficiently suitable for obtaining reliable rainfall isotopic times series on much longer time scales, which are needed for a reliable proxy interpretation.

10 Fossil Water in Stalagmites as a Record of Past Drip Water $\delta^{18}O$

The present-day relationship between the $\delta^{18}O$ of precipitation and the $\delta^{18}O$ of drip water in Villars cave is well constrained by the long term monitoring study presented in the previous chapter. In this article, we examine the link between drip water and fluid inclusions in speleothems from the same cave, and investigate whether the fossil water in the stalagmites provides a record of the isotopic composition of precipitation.

Well-replicated fluid inclusion isotope measurements from two modern calcite samples, which had precipitated under the monitored stalactites, are in agreement with the corresponding drip waters. The drip water, in turn, represent the average annual precipitation. This gives strong evidence that the isotopic composition of the infiltrating water, and thus of average precipitation, is preserved in the pores of speleothem calcite.

Furthermore, we measured oxygen isotope ratios in fluid inclusions in the stalagmite vil-stm1, a fast-growing 2300 year old sample with high water content, which allows a high-resolution reconstruction of the drip water isotopic composition covering the last two millennia. The amplitude of fluid inclusion $\delta^{18}O$ variability in vil-stm1 is 2‰.

Other proxies measured in the same stalagmite indicate that the cave environment has undergone substantial changes during this period: Stable isotopes in calcite and trace element concentrations show large variations, with amplitudes that correspond to those found in other Villars speleothems during large climatic shifts such as Dansgaard–Oeschger events or glacial–interglacial transitions. In the context of the last 2000 years, the proxy variability cannot be attributed to climate alone, but is likely influenced by anthropogenic deforestation and the associated changes in carbon dynamics. A decrease in vegetation activity is clearly evidenced by the calcite $\delta^{13}C$. The co-variation of different trace element concentrations indicates prior calcite precipitation, which could be linked to dry conditions or CO_2 degassing from the percolating water.

These changes might also have an influence on the isotope ratios in drip water relative to precipitation, e.g. through an altered evaporation–transpiration ratio. Nevertheless, despite some common trends in all proxy records, the marked shifts in the $\delta^{13}C$ are not seen in the fluid inclusions, which gives strong evidence that the relationship between precipitation and drip water $\delta^{18}O$ in the past was similar to present-day conditions, and not much affected by the anthropogenic impact.

Altogether, the multiple proxies from this stalagmite give insights into the history of local climate and environmental changes. A replication of the fluid inclusion isotope record using stalagmites from the same region will be necessary to determine whether local processes or large-scale temperature and atmospheric circulation dominate the fluid inclusion $\delta^{18}O$ signal, and in how far the fluid inclusions can provide a direct record of precipitation $\delta^{18}O$.

The reconstructed drip water isotope variability might provide an estimate of tree source water

$\delta^{18}O$ in the region and thus enable the calculation of leaf water enrichment and of relative humidity – the principle controlling factor of this enrichment – using the tree ring cellulose $\delta^{18}O$ record from Angoulême (see Chapter 13). Supplementary material to this article can be found in Appendix A.

Article in preparation

A High-Resolution Multi-Proxy Stalagmite Record of Climate and Environmental Changes in Southwest France During the Last 2300 Years

Inga Labuhn[1], Dominique Genty[1], Hubert Vonhof[2], Dominique Blamart[1], Clément Bourdin[1,3], Jiaoyang Ruan[1], Valérie Daux[1], Eric Douville[1], Hai Cheng[4,5], Edwige Pons-Branchu[1], Monique Pierre[1]

[1]*Laboratoire des Sciences du Climat et de l'Environnement (LSCE/IPSL), laboratoire CEA/CNRS/UVSQ, CE Saclay, Orme des Merisiers, Gif-sur-Yvette, France*
[2]*Faculty of Earth and Life Sciences, VU University Amsterdam, the Netherlands*
[3]*School of Geography, Earth and Environmental Sciences, University of Birmingham, UK*
[4]*Institute of Global Environmental Change, Xi'an Jiaotong University, Xi'an, China*
[5]*Department of Geological Sciences, University of Minnesota, Minneapolis, MN, USA*

10.1 Introduction

Speleothems are increasingly contributing to our understanding of past climate and environmental changes. The great potential of stalagmites as palaeoclimate archives lies in their precise dating (Cheng et al. 2013; Hoffmann et al. 2009; Shen et al. 2002), their geographical coverage, as well as the time scales they cover, from seasonal resolution (e.g. Fairchild et al. 2010; Mattey et al. 2008; Treble et al. 2003) to glacial-interglacial time scales (e.g. Affek et al. 2008; Wang et al. 2008; Spötl et al. 2002). The interpretation of proxies and the quantification of influencing climate variables, however, is a challenge because for each speleothem record, the functioning of the cave system in its specific climatologic and geologic setting has to be considered (Fairchild et al. 2006a). This implies that the same measured parameter can have a different climatological meaning depending on the context. Long-term cave monitoring can help identify and quantify the relationships between proxies and climate (Genty et al. 2014; Genty 2008; Hu et al. 2008; Spötl et al. 2005). An advantage of speleothems is that multiple proxies can be measured on the same sample to identify the causes of proxy variability (Asrat et al. 2007; Xia et al. 2001; Hellstrom and McCulloch 2000). Comparisons of a speleothem proxy record with records from other sites or from other climate archives, on the contrary, can be complicated by dating errors in each record.

Speleothem fluid inclusions are a promising proxy because they can potentially provide a relatively direct record of stable isotopes in precipitation (δD and δ^{18}O) at the site. Stable isotopes in calcite can be measured at a higher spatial resolution, but kinetic fractionation effects during calcite precipitation might obscure the climatic signal (Polag et al. 2010; Wiedner et al. 2008; Mickler et al. 2006, 2004). Precipitation isotopes are of great importance for understanding atmospheric circulation patterns, and find widespread application in hydrology and palaeoclimatology (e.g. Aggarwal et al. 2012; Langebroek et al. 2011; Darling 2004; Gat 1996). They can be reconstructed from ice cores from the polar caps and glaciers (Thompson et al. 2003; Johnsen et al. 2001; Grootes et al. 1993; Jouzel et al. 1987), but these archives are of limited geographical extension. Other proxies such as tree ring cellulose (e.g. Danis et al. 2006; Robertson et al. 2001; Saurer et al. 1997b) or ostracod calcite (von Grafenstein et al. 1999) can provide palaeo-records of precipitation δ^{18}O. However, although their isotopic

composition depends on the isotopic composition of their source water (i.e. precipitation), it can be modified by evaporation, biochemical reactions, and other temperature dependent or kinetic fractionation processes.

Fluid inclusions form when microscopic cavities in the calcite which are filled with drip water are sealed off, and can be found in almost all speleothems (McDermott et al. 2006). Cave drip water is incorporated in the calcite at the time of its precipitation and thus can be stratigraphically related to the time when it was dripping. The drip water isotopic composition, in turn, represents the weighted mean of local precipitation (Genty et al. 2014; Cruz et al. 2005; Caballero et al. 1996; Yonge et al. 1985), but can be modified by evaporation in the soil zone under semi-arid climate conditions (Denniston et al. 1999; Bar-Matthews et al. 1996). The fossil drip water can sometimes be extracted from macroscopic pores (Genty et al. 2002), but usually the water is released by crushing and heating the calcite (Dublyansky and Spötl 2009; Zhang et al. 2008; Vonhof et al. 2006). Measurements of the fluid inclusion isotopic composition also offer the possibility to calculate palaeotemperatures in combination with the corresponding calcite $\delta^{18}O$ measurements, because the fractionation of oxygen isotopes between calcite and the water from which it precipitates is temperature dependent, under the condition that the calcite is precipitated in equilibrium with the water (Kim and O'Neil 1997; O'Neil et al. 1969; Craig 1965).

Former studies on speleothem fluid inclusions, which focus mainly on millennial time scales, have contributed to our understanding of rainfall $\delta^{18}O$ variability in the past and helped interpret calcite $\delta^{18}O$ records. Variations in precipitation $\delta^{18}O$ are attributed to temperature and hydrological changes associated with glacial-interglacial transitions (McGarry et al. 2004; Matthews et al. 2000), to changing moisture sources (Fleitmann et al. 2003) or precipitation amount (Griffiths et al. 2010b; van Breukelen et al. 2008).

At Villars cave, southwest France, detailed monitoring has been carried out since 1996 to characterize the present-day cave environment (Genty 2008), including the relationships between the isotopic composition of precipitation and cave drip water (Genty et al. 2014). This site-specific information is crucial to understand the relevant processes and interpret speleothems proxies. Here, we present a high-resolution fluid inclusion record (δD and $\delta^{18}O$) from a 2300-year old stalagmite from Villars cave, as well as stable isotope measurements of fluid inclusions in modern calcite deposits and corresponding drip waters. We hypothesize that 1) the isotopic composition of fluid inclusion water corresponds to the associated drip water (= average rainfall) in modern samples; and 2) high-resolution fluid inclusion measurements in stalagmites can therefore be used to reconstruct the variability of drip water $\delta^{18}O$ in the past. We investigate possible causes of this variability such as changes in temperature or atmospheric circulation, as well as the potential to calculate palaeotemperatures from oxygen isotope ratios in calcite and corresponding fluid inclusions. A multi-proxy approach, which includes records of stable isotopes in calcite and trace element concentrations from the same stalagmite, helps identify the climate and environmental changes which may influence fluid inclusion isotope variability.

10.2 Study Site and Samples

10.2.1 Villars Cave

Villars cave is located in southwest France, 45°26'N, 0°47'E, at an altitude of 175 m a.s.l. and 150 km from the coast (Figure 10.1). The region is characterized by a temperate climate under

Atlantic influence with dominant westerly winds. Average annual precipitation at Villars is 1005 mm and the average annual temperature is 12.5 °C, with mild winters (average December to February temperature 5.6 °C) and warm summers (average June to August temperature 19.3°C; average values 1990–2012). The vegetation above the cave today consists mainly of oak and hornbeam forest, but the part of the cave where the stalagmite was sampled is covered by grassland. The bedrock is an oolithic limestone formation of the Middle Jurassic, which is 25–45 m thick, covered by a thin calcareous brown soil layer of 0–20 cm (Genty 2008). Villars cave consists of 10 km of gallery network, and there are two levels of galleries separated by 10–20 m of rock.

Monitoring was started in Villars cave in 1996 and is still being continued (Genty 2008; Genty et al. 2014). The present day cave air temperature in the upper galleries is close to the mean annual temperature outside the cave, and shows seasonal variations with an amplitude of about 1 °C. While the external temperature maximum occurs in July and August, the cave temperature maximum is delayed by 1–2 months. Temperature in the lower galleries is 11.5 °C and shows no seasonal variation. At both gallery levels, there is a linear warming trend of 0.4 °C over the period 1997–2009, which is consistent with the increase in average annual temperature outside the cave.

The isotopic composition of cave drip water is monitored at four drip sites from two different depths (10 m and 20 m below the surface) at an interval of one to two months. Isotopic values are remarkably constant and correspond to a weighted mean of several years of precipitation. There is no significant evaporative enrichment before the water arrives in the cave, and no seasonal bias from plant transpiration during the growing season. The δD and $\delta^{18}O$ of the drip water at 20 m depth are slightly more negative (2‰ and 0.2‰ respectively) than at 10 m depth (Genty et al. 2014).

10.2.2 Modern Calcite Samples

In order to compare the isotopic composition of present day drip water and contemporaneous fluid inclusions in calcite precipitated under the dripping stalactite, we collected three modern calcite samples (Figure 10.1):

- vil-gal#1B: an 8 mm thick layer of calcite grown on a quartz pebble from September 2000 to November 2007 (under stalactite #1B at 20 m below the surface);
- vil-plq#8: a 7 mm thick layer of calcite grown on a brick tile from August 1996 to September 2000 (fed by three stalactites at 15 m below the surface);
- vil-stm#10B: top of an active stalagmite sampled in 2000 (under the stalactite #10B at 10 m below the surface).

These samples were deposited just before, or during the drip water monitoring period. Since the isotopic composition of drip water has been constant from the beginning of monitoring in 1996 until 2013, we suppose that a comparison between fluid inclusions and drip water which is a few years younger is acceptable, and that their isotopic composition is likely to be very similar.

10.2.3 Stalagmite vil-stm1

Stalagmite vil-stm1 (Figure 10.1), sampled in 1993, at a depth of approximately 8 m below the surface, is 1095 mm high and was active at the time of sampling. It was cut in half along

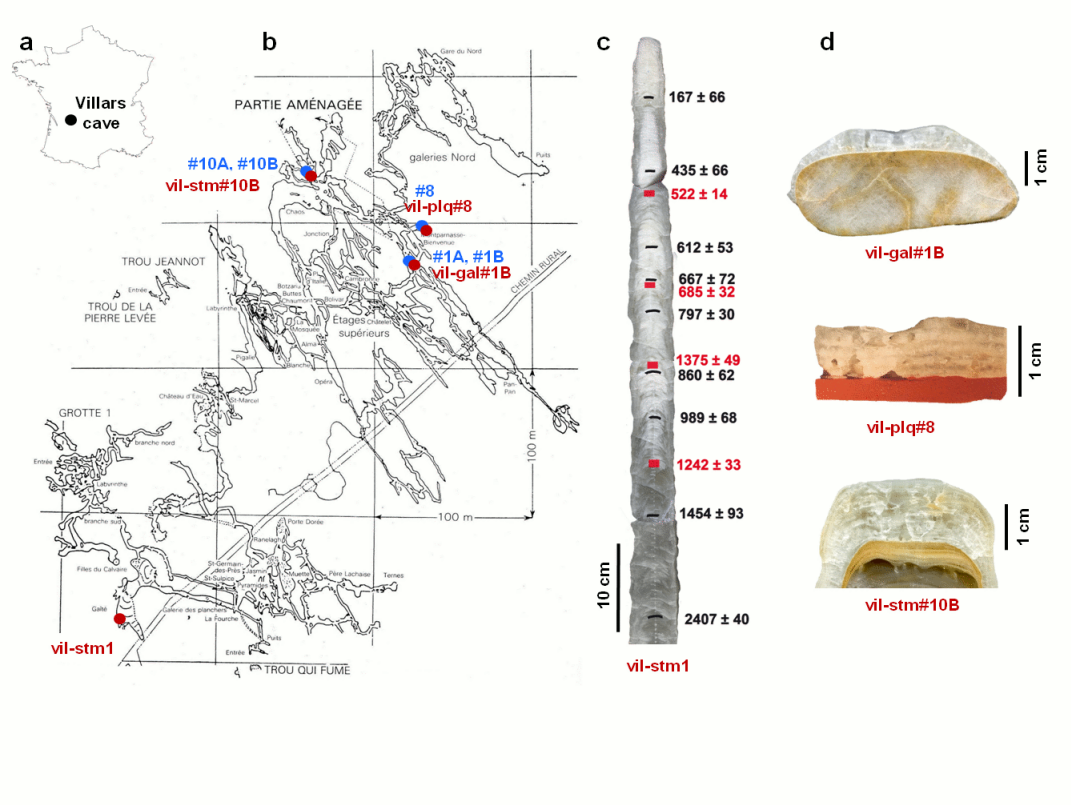

Figure 10.1: (a) Map of France showing the location of Villars cave; (b) map of Villars cave (from Vidal and Baritaud, Spéléo Club de Périgueux), indicating the sample sites (red) and drip water monitoring stations (blue); (c) stalagmite vil-stm1 with U-Th dates; ages are given in years b2k ± error; the dates in red are from Genty et al. (1999), the dates in black were obtained for this study; (d) modern calcite samples.

the central axis and the surface was polished. The stalagmite is composed of columnar calcite fabric, with well-marked laminae (alternating layers of white porous calcite and dark compact calcite) at the top half and at the base, and no visible lamination in the central part. There is no visible hiatus in vil-stm1 and no offset in the growth axis. For this study, the upper 680 mm of the stalagmite were analysed.

10.3 Methods

10.3.1 Dating

The samples vil-gal#1B and vil-plq#8 were deposited on objects placed under dripping stalactites, and their precise time spans are known. The stalagmite vil-stm#10B was active at the time of sampling and the time span covered by the fluid inclusion and calcite samples from the top of this stalagmite was estimated by counting visible growth laminae.

The age of the stalagmite vil-stm1 was determined by laminae counting, and by radiometric dating methods. Laminae were counted in the upper 486 mm, where the lamination is almost continuous. Interruptions of the lamination around 80 mm and 180 mm from top obliged to interpolations of the growth rate for 35 mm of the total counted height. The counting was repeated four times, and the laminae age model was calculated based on the average counting.

Thirteen calcite samples were taken for U-Th dating (Figure 10.1). Previous U-Th measurements for this stalagmite were performed by thermal ionization mass spectrometry (TIMS) (Genty et al. 1999). They were complemented in 2013 by new measurements using multicollector inductively coupled plasma mass spectrometers (MC-ICP-MS) at Xi'an Jiaotong University, China, and at LSCE, Gif-sur-Yvette, France. For details on the analytical procedure see Cheng et al. (2013) and Fontugne et al. (2013). An age model and its 95% confidence limits were calculated for vil-stm1 using the programme StalAge (Scholz and Hoffmann 2011).

For radiocarbon (^{14}C) measurements, eleven calcite samples of 10–20 mg were taken with a 0.5 mm microdrill. Calcite powder samples were reacted with H3PO4 at 60 °C to obtain about 1 mg of carbon as CO_2 gas. The CO_2 was then graphitized on iron with hydrogen at 600 °C. Carbon atoms were counted by accelerator mass spectrometry (ARTEMIS, UMS 2572, Saclay, France). The ^{14}C activity was normalized for a –25‰ $\delta^{13}C$. Conventional radiocarbon ages were calculated according to Mook and van der Plicht (1999). The given uncertainties take into account the statistics, results variability and blank error (0.083 pMC ±0.033). Two corrections must be applied in order to estimate an age from the measured ^{14}C activity (for details see Genty et al. 2011): (1) the radiocarbon calibration, which was made using the Intcal13 curve (Reimer et al. 2013); and (2) the correction for the dead carbon proportion (dcp). Dead carbon incorporated in the calcite originates from limestone dissolution and from the decomposition of old organic matter, and contains no ^{14}C (Genty et al. 2001a). The average dcp has previously been estimated at 9.4% for this stalagmite by U-Th–^{14}C age comparison and by the ^{14}C-bomb peak detection (Genty et al. 1999; Genty and Massault 1999, 1997).

10.3.2 Fluid Inclusions

The isotopic composition of fluid inclusion water ($\delta^{18}O$ and δD) was measured at VU Amsterdam University using the Amsterdam Device according to the procedure described in Vonhof et al. (2007, 2006). Calcite samples were crushed and heated to 120 °C under a continuous flow of helium carrier gas. The water was retained in a cold trap unit during 4 min to leave time for all the water to evaporate. It was then released by heating the cold trap to a Thermo-Finnigan TC-EA pyrolysis furnace connected to a mass spectrometer. Each modern sample measurement was repeated for adjacent calcite blocks. From the stalagmite vil-stm1, blocks of 4 mm height were cut out along the central axis, and a total of 34 samples was measured. In order to extract a sufficient quantity of water for the analysis (about 0.2 μl), approximately 0.3 g of calcite were needed. 0.2 μl of a standard water of known isotopic composition were measured at least twice before each calcite crush. The water was injected in the crushing chamber with a micro-syringe and underwent the same procedure as the fluid inclusion samples. After measuring the sample, two more standard water injections were made, with a quantity of water corresponding to the amount of water extracted from the calcite sample. This amount was approximated from the CO peak size of the mass spectrometric analysis of the fluid inclusion sample in relation to the average peak size of the 0.2 μl standard water injection. The analytical error was 0.3‰ for $\delta^{18}O$ and 1.5‰ for δD. Water isotope ratios are reported with reference to VSMOW.

10.3.3 Calcite Stable Isotopes

In the modern samples, calcite stable isotopes ($\delta^{18}O_{ct}$ and $\delta^{13}C_{ct}$) have been measured previously at different resolutions (unpublished data, D. Genty). Here, we use only an average

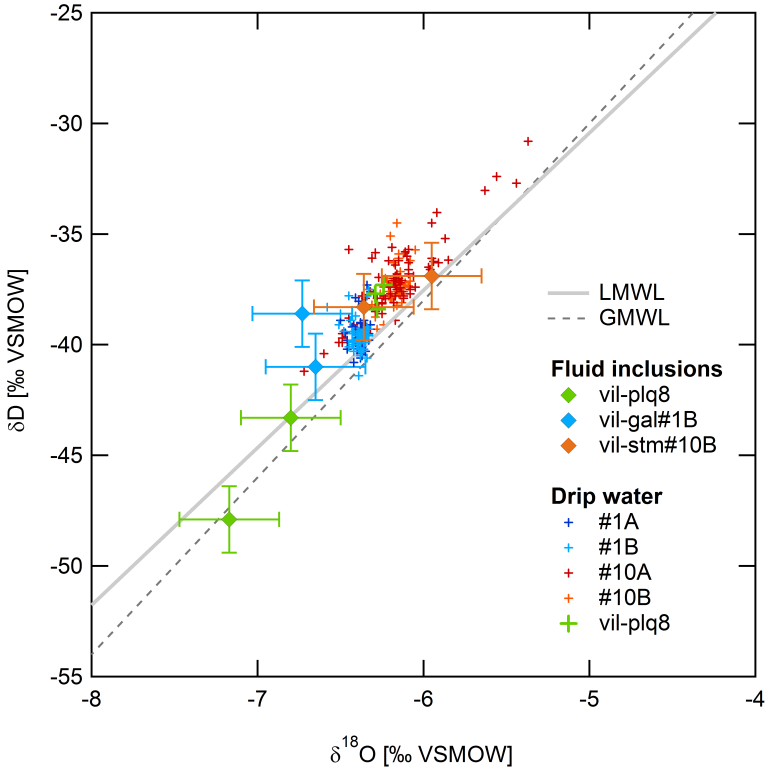

Figure 10.2: δD–δ^{18}O plot of fluid inclusions in modern calcite deposits (diamonds) and present day drip water (crosses). Corresponding fluid inclusions and drip water from the same drip site are plotted in the same colour. The grey line is the local meteoric water line (LMWL), the dashed line is the global meteoric water line (GMWL).

$\delta^{18}O_{ct}$ value for each sample to compare to the corresponding fluid inclusions samples.

Along the central axis of the stalagmite vil-stm1, 342 calcite samples of 100 μg were taken with a 0.4 mm microdrill at a resolution between 1.5 and 5 mm. Additionally, samples were taken along four individual growth layers to perform a "Hendy test" for isotopic equilibrium (Hendy 1971). After CO_2 extraction from calcite powder by reaction with phosphoric acid, isotope ratios were measured on a VG OPTIMA mass spectrometer at LSCE, Gif-sur-Yvette, France. The analytical error is 0.08‰ for $\delta^{18}O_{ct}$ and 0.05‰ for $\delta^{13}C_{ct}$. The calcite isotope ratios are reported with reference to VPDB. A mean $\delta^{18}O_{ct}$ was calculated for each interval which corresponds to a fluid inclusion sample.

10.3.4 Trace Elements

For the measurement of trace element concentrations (Na, Mg, Sr, Ba, U and Y), 107 calcite samples of 5–10 mg were taken with a 0.7 mm microdrill at a resolution between 3.5 and 8 mm. The measurements were performed on a Quadrupole ICP-MS (X series^{II} Thermo), at LSCE, Gif-sur-Yvette, France, following the methods described in Bourdin et al. (2011), which are based on previous works by (Harding et al. 2006; Rosenthal et al. 1999). Typical analytical errors were 2–3% for Na, Mg, Sr and U, and 5% for Y.

10.3.5 Grey Level

The grey level is not a quantitative proxy, but provides a means to illustrate changes in the petrography of the stalagmite (Genty and Massault 1997; Genty and Quinif 1996). On a digitized greyscale image, we defined a window along the central axis which was filtered horizontally. Grey level values are expressed between 0 (black) and 255 (white). This analysis is feasible for the stalagmite vil-stm1, as it consists of pure calcite without any visible detrital material. The grey level value is therefore primarily linked to the porosity of the calcite.

10.4 Results

10.4.1 Modern Fluid Inclusions and Drip Water Isotopic Composition

The isotope ratios in fluid inclusions water from the samples vil-stm#10B and vil-gal#1B are very close to the corresponding drip water, and their replicates are within the error margins (Figure 10.2). The shift in the drip water isotopic composition from higher values in the upper gallery (drip water monitoring stations #10A and #10B) to more negative values in the lower gallery (stations #1A and #1B) is also seen in the respective fluid inclusion samples (Table 10.1; Figure 10.2). Like the drip water, the fluid inclusion values plot slightly above the local meteoric water line in a δD–δ^{18}O plot. The fluid inclusions of vil-plq#8, on the contrary, are offset from the corresponding drip waters to more negative values ($\sim$0.7‰ in δ^{18}O and $\sim$7.8‰ in δD), and the replicates are not within the error of the measurement.

10.4.2 Stalagmite vil-stm1 Proxy Records

Age Models and Growth Rate

The stalagmite was active at the time of sampling in 1993 and the analysed part covers 2300 years (Figure 10.3). The age model based on laminae counting indicates a relatively constant growth rate of about 0.47 mm yr^{-1}. The U-Th dating (Table 10.2) yielded slightly older ages than the laminae age model ($\sim$100 years). However, the slopes of the two age models are very similar, which confirms that the visible lamination is annual. The offset between the two age models is likely due to short growth hiatuses or periods of slow growth where the laminae cannot be distinguished. The laminae counting was included in the final age model only until 30 mm from the top, where the laminae age is confirmed by the ^{14}C bomb peak (Genty and Massault 1997). One U-Th date was defined as an outlier by StalAge and was excluded from the age model (grey point in Figure 10.3). ^{14}C dates are coherent with the U-Th dates, but they are not included in the age model because of their larger measurement error.

The radiometric age model gives an average growth rate of 0.37 mm yr^{-1}, with a period of slower growth ($<$ 0.2 mm yr^{-1}) from 400 BC to 500 AD (and consequently, a lower proxy resolution), followed by an increased growth rate to about 1500 AD (up to 0.6 mm yr^{-1}). After that the growth rate slows down to about 0.3 mm yr^{-1}. During the periods of high growth rates, the stalagmite displays an annual lamination, while slow growth rates result in a compact calcite without annual layers.

Fluid Inclusions

Each sample taken for fluid inclusion analysis represents about 10–20 years of calcite deposition, depending on the growth rate. As the water residence time in the epikarst is estimated

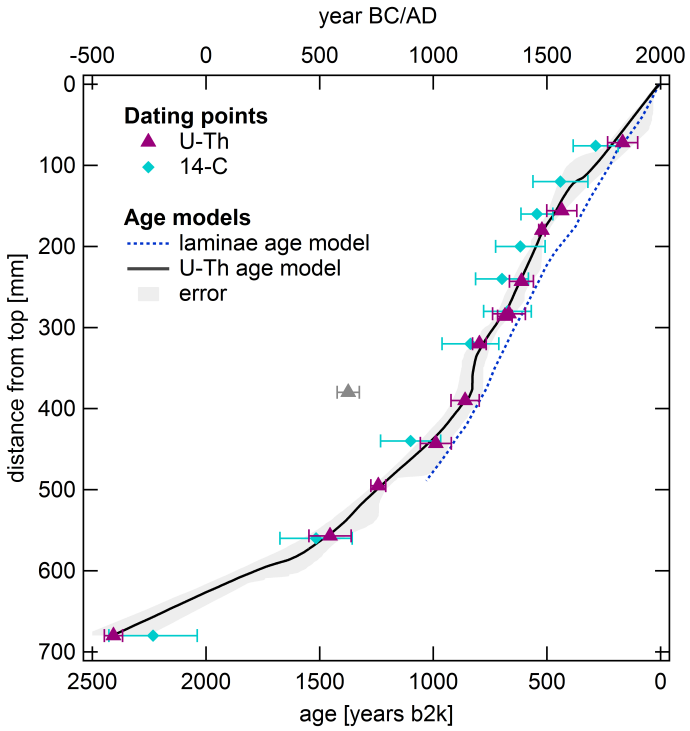

Figure 10.3: Age models for the stalagmite vil-stm1 based on laminae counting (dashed blue line), and based on U-Th dating (black line), calculated with the programme StalAge (Scholz and Hoffmann 2011). The shaded area marks the 95% confidence interval. Radiocarbon (^{14}C) ages are shown for comparison. Ages are given in years before 2000 (b2k), the corresponding calendar years are given on the top axis.

to be in in the order of several years (Genty et al. 2014), approximately 15–25 years of precipitation are represented in a fluid inclusion sample.

Most of the fluid inclusion isotope values plot close to the global meteoric water line (GMWL), but some of the samples deviate from this line (Figure 10.4). We suppose that there are analytical issues with the δD which cause this scatter around the GMWL, and not e.g. a post-depositional modification of the $\delta^{18}O$ through water–rock isotope exchange. Some of the fluid inclusion samples which contained little water gave high δD values, and some samples with high water content gave low δD values (Figure 10.4), suggesting a relationship between water quantity and the measured isotope ratios. For the standard water injections, both very small and very large water quantities yielded below-average δD values. As the δD seems to be potentially influenced by analytical effects, we will focus on $\delta^{18}O$ in our interpretation of the fluid inclusion isotope record.

The amplitude of fluid inclusion $\delta^{18}O$ variability over time is about 2‰ (Figure 10.5). $\delta^{18}O$ shows an increase from 500 to 1400 AD, followed by a sharp decrease until 1700 AD. After that, the $\delta^{18}O$ increases again until present day, with an abrupt peak at 1720 AD. The estimated water content of vil-stm1 varies throughout the stalagmite and ranges from 0.07 to 1.61 $\mu l\ g^{-1}$ calcite, with an average of 0.21 $\mu l\ g^{-1}$. The zones of dark compact calcite generally contain less water than the zones with annual layers of white porous calcite. This is consistent with the grey level profile, which indicates a lower porosity in the compact zones without annual lamination.

Table 10.1: Calcite $\delta^{18}O$ and fluid inclusions $\delta^{18}O$ and δD of modern calcite samples with corresponding drip water values and measured cave temperature at the respective site. The time span corresponding to each measurement is indicated. Calcite $\delta^{18}O$ was measured at different resolutions for the different samples. The given value is a mean over the height which corresponds to the fluid inclusion sample. Each fluid inclusion sample was measured twice, the given value is the average of the two measurements. For drip water isotopes and temperature, the number of measurements (N) and the standard deviation (σ) are given.

Sample name	**Time span covered by the measurement**			**Calcite**	**Fluid inclusions**		**Drip water**		**Temperature**
	Calcite samples	Drip water samples	Temperature	$\delta^{18}O$ [‰]	$\delta^{18}O$ [‰]	δD [‰]	$\delta^{18}O$ [‰]	δD [‰]	[°C]
vil-gal#1B	27.09.2000– 19.11.2007	27.09.2000– 19.11.2007	27.09.2000– 19.11.2007	-4.87	-6.69	-39.8	**-6.41** (σ=0.06, N=32)	**-39.4** (σ=0.7, N=32)	**11.47** (σ=0.12, N=34)
vil-stm#10B	1990– 02.11.2000	04.12.2000– 31.05.2012	03.01.1997– 28.05.2009	-3.13	-6.15	-37.61	**-6.17** (σ=0.07, N=53)	**-37.2** (σ=1.7, N=85)	**12.49** (σ=0.37, N=96)
vil-plq#8	22.08.1996– 29.09.2000	04.12.2000– 24.05.2001	22.08.1996– 26.03.1998	-5.00	-6.98	-45.62	**-6.27** (σ=0.02, N=3)	**-37.8** (σ=0.4, N=3)	**11.38** (σ=0.18, N=9)

Table 10.2: U-Th measurements for vil-stm1. Ages are given in years before present (BP), where "present" is defined as the year 1950 AD. Measurements were performed at Xi'an Jiaotong University, China (X'aJTU), and at LSCE, Gif-sur-Yvette, France. For details on the method, see Cheng et al. (2013).

Sample mm/top	**^{238}U (ppb)**		**^{232}Th (ppt)**		**^{230}Th/^{232}Th (atomic x10-6)**		**δ^{234}U (measured)**		**^{230}Th/^{238}U (activity)**		**^{230}Th Age (yr) (uncorrected)**		**^{230}Th Age (yr) (corrected)**		**$\delta^{234}U_{Initial}$ (corrected)**		**^{230}Th Age (yr BP) (corrected)**		**Lab**
72	152	±0.2	202	±4	24.4	±7	-15.0	±1.7	0.0020	±0.0005	219	±60	179	±66	-15	±2	**117**	**±66**	X'aJTU
156	139.4	±0.2	36	±2	262	±39	-6.8	±1.8	0.0041	±0.0006	455	±65	447	±66	-7	±2	**385**	**±66**	X'aJTU
243	133.4	±0.2	42	±1	297	±26	-11.3	±1.6	0.0057	±0.0005	633	±53	624	±53	-11	±2	**562**	**±53**	X'aJTU
283	105.6	±0.1	64	±2	173	±18	-10.7	±1.5	0.0063	±0.0006	696	±71	679	±72	-11	±2	**617**	**±72**	X'aJTU
320	143.5	±0.04	86	±0.1	38	±0.8	-17.5	±0.7	0.0074	±0.0001	828	±18	808	±27	-18	±1	**746**	**±27**	LSCE
390	128.6	±0.2	107	±2	161	±11	-10.1	±1.7	0.0081	±0.0005	896	±60	872	±62	-10	±2	**810**	**±62**	X'aJTU
443	121.0	±0.1	38	±1	479	±36	-5.8	±1.4	0.0092	±0.0006	1011	±68	1001	±68	-6	±1	**939**	**±68**	X'aJTU
557	95.8	±0.1	81	±2	265	±17	-6.8	±2.4	0.0135	±0.0008	1490	±91	1466	±93	-7	±2	**1404**	**±93**	X'aJTU
680	129.9	±0.03	69	±0.0	126	±1.6	-5.3	±1.1	0.0219	±0.0003	2435	±34	2418	±43	-5	±1	**2356**	**±43**	LSCE

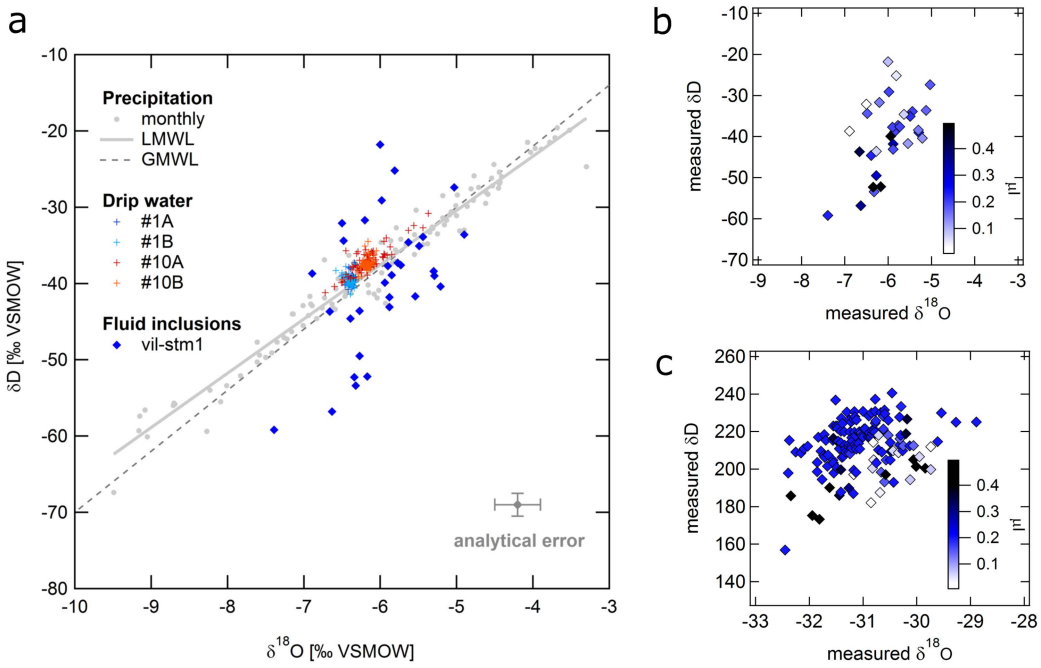

Figure 10.4: (a) δD–$\delta^{18}O$ plot of fluid inclusions in stalagmite vil-stm1 (diamonds) with present-day precipitation above the cave (circles) and cave drip waters from four stalactites (crosses). Precipitation and cave drip water samples were taken at 1–2 month intervals from 1997 to 2013 (Genty et al. 2014). The grey line is the local meteoric water line (LMWL), the dashed line is the global meteoric water line (GMWL). The error bars on the bottom indicate the analytical error for the fluid inclusion measurements. (b) δD–$\delta^{18}O$ plot for vil-stm1 fluid inclusions; (c) δD–$\delta^{18}O$ plot for the standard water injections; the colour scales indicate the amount of water in the calcite sample and the water injection.

Oxygen and Carbon Isotopes in Calcite

The $\delta^{18}O_{ct}$ and $\delta^{13}C_{ct}$ time series of vil-stm1 are highly correlated: r = 0.79; p < 0.001; N = 342 (Table 10.3). $\delta^{18}O_{ct}$ values vary between –3.3 and –5.3‰, $\delta^{13}C_{ct}$ values between –7.2 and –11.9‰. These amplitudes are close to the ones observed in other Villars speleothems during major climate changes, such as Dansgaard–Oeschger events or the glacial termination II (Wainer et al. 2011; Genty et al. 2010, 2003). Shifts in isotopic values are more pronounced in the $\delta^{13}C_{ct}$ record, but both oxygen and carbon isotopes show common patterns (Figure 10.5). The relatively low values in the older part of the stalagmite, which is characterized by slow growth, increase abruptly in $\delta^{13}C_{ct}$, and more gradually in $\delta^{18}O_{ct}$, from 700 AD. Values decrease around 1450 AD, again more gradual in $\delta^{18}O_{ct}$, and increase again in the most recent period from about 1800 AD. The large shift of $\delta^{13}C_{ct}$ to higher values starting around 700 AD coincides with the increase in growth rate and the onset of the annual lamination.

Trace Element Concentrations

All of the measured trace element concentrations are significantly correlated, Y being negatively correlated to the other elements (Table 10.4), and they show similar profiles throughout the stalagmite (inverted for Y, Figure 10.6). From the beginning of the records to about 700 AD, there is a decreasing trend in the concentrations, followed by an increase to 1400 AD.

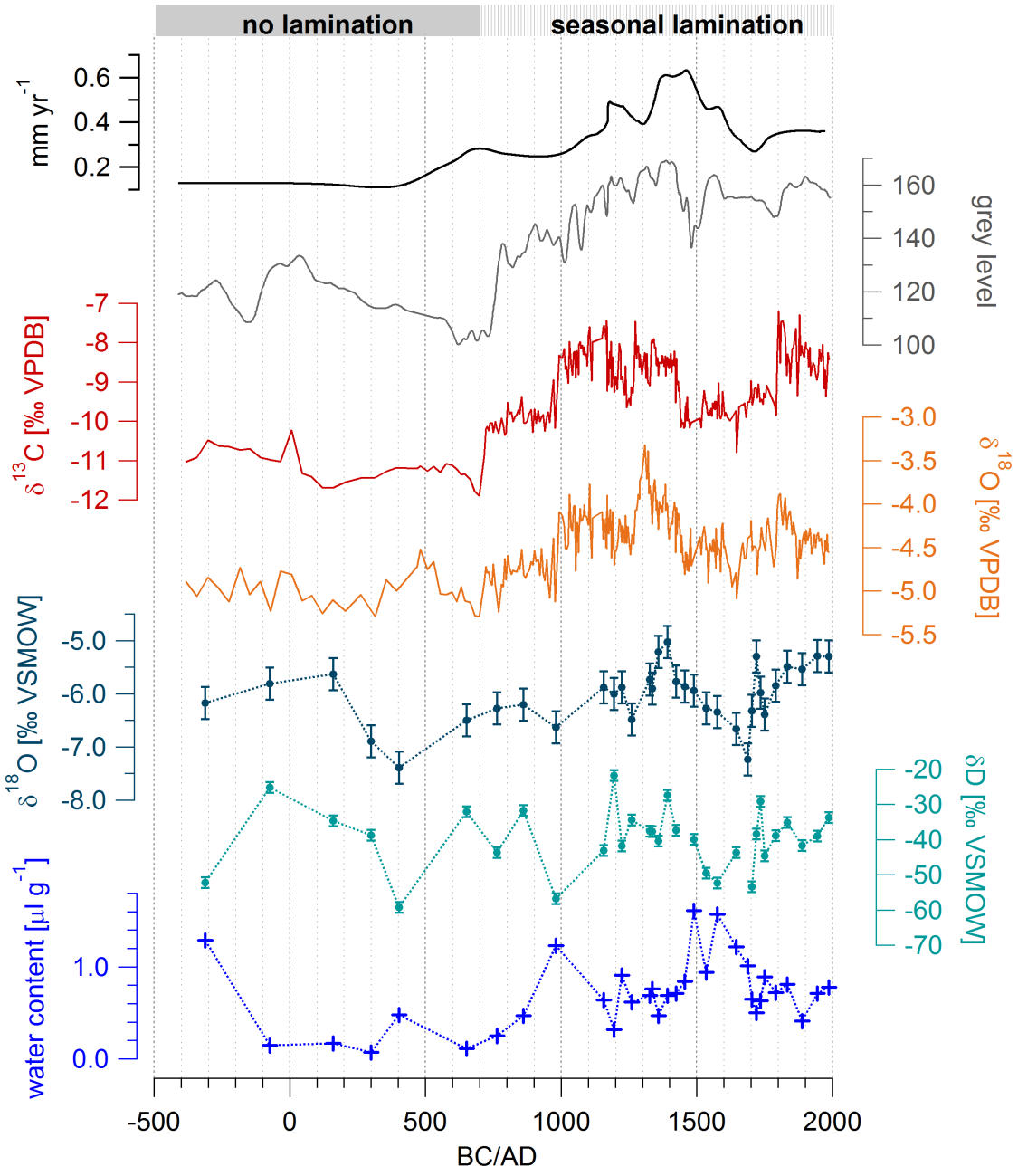

Figure 10.5: Proxy records from stalagmite vil-stm1. From top to bottom: growth rate, grey level, δ^{13}C and δ^{18}O of calcite, δ^{18}O and δD of fluid inclusions, water content of the fluid inclusion samples.

Table 10.3: Correlations between different proxies measured in stalagmite vil-stm1. "Trace elements" denotes a composite trace element time series (average of the z-scores of all single trace element time series; the Y time series was multiplied by –1). Numbers on italic indicate time series which were re-sampled in order to make the different resolutions comparable (see text for detail). The asterisks indicate the significance level: * < 0.05, ** < 0.01, *** < 0.001. The reduced degrees of freedom for re-sampled data are taken into account.

	$\delta^{18}O_{ct}$	$\delta^{13}C_{ct}$	$\delta^{18}O_{fi}$	δD_{fi}	Grey level	Trace elements
$\delta^{18}O_{ct}$	1					
$\delta^{13}C_{ct}$	0.79***	1				
$\delta^{18}O_{fi}$	*0.40****	*0.45**	1			
δD_{fi}	*0.10*	*0.11*	0.50**	1		
Grey level	*0.83****	*0.86****	*0.55***	*0.02*	1	
Trace elements	*0.77****	*0.82****	*0.42**	*-0.04*	*0.79****	1

Table 10.4: Correlations between concentrations of different trace elements measured in stalagmite vil-stm1. The asterisks indicate the significance level: * < 0.05, ** < 0.01, *** < 0.001.

	Na	Mg	Sr	Ba	U	Y
Na	1					
Mg	0.78***	1				
Sr	0.61***	0.59***	1			
Ba	0.50**	0.37*	0.77***	1		
U	0.76***	0.78***	0.65***	0.58***	1	
Y	-0.57***	-0.51**	-0.61***	-0.72***	-0.56***	1

After that, there is a marked decrease in Sr and Ba, which is less pronounced in the other elements, and increase again to present day. Trace element concentrations and variations in vil-stm1 are generally in the same order of magnitude as those measured in other speleothems from Villars cave which grew during the last glacial period (unpublished data).

Correlations Between Re-sampled Proxy Time Series

Some of the proxies were measured at different resolutions. In order to correlate the time series, all series were re-sampled at a time step of 10 years based on linear interpolation of existing data, using the programme AnalySeries (Paillard et al. 1996). It has to be kept in mind that the re-sampling procedure might create spurious correlations, but this way we can attempt to quantify the relationships between the proxies. The trace element series (z-scores of the individual series; the Y time series was multiplied by -1) were first averaged to form a composite trace element time series. We observe several significant correlations between proxies (Table 10.3). All correlations between the composite trace element series, calcite stable isotopes and grey level are high ($r \approx 0.7$ to 0.8) and significant. The correlations between fluid inclusion $\delta^{18}O$ and the other proxies are intermediate ($r \approx 0.4$ to 0.5).

10.4.3 Isotopic Equilibrium and Theoretical Temperature Calculations

The isotopic fractionation between calcite and water from which the calcite is precipitated is temperature dependent, but it is only possible to calculate palaeo-temperatures from the isotopic composition of fluid inclusions and calcite under the condition that the calcite was deposited in isotopic equilibrium with the water. The "Hendy test" for four growth layers of vil-stm1 showed that $\delta^{18}O_{ct}$ and $\delta^{13}C_{ct}$ are correlated, but there is little variation of $\delta^{18}O_{ct}$ and

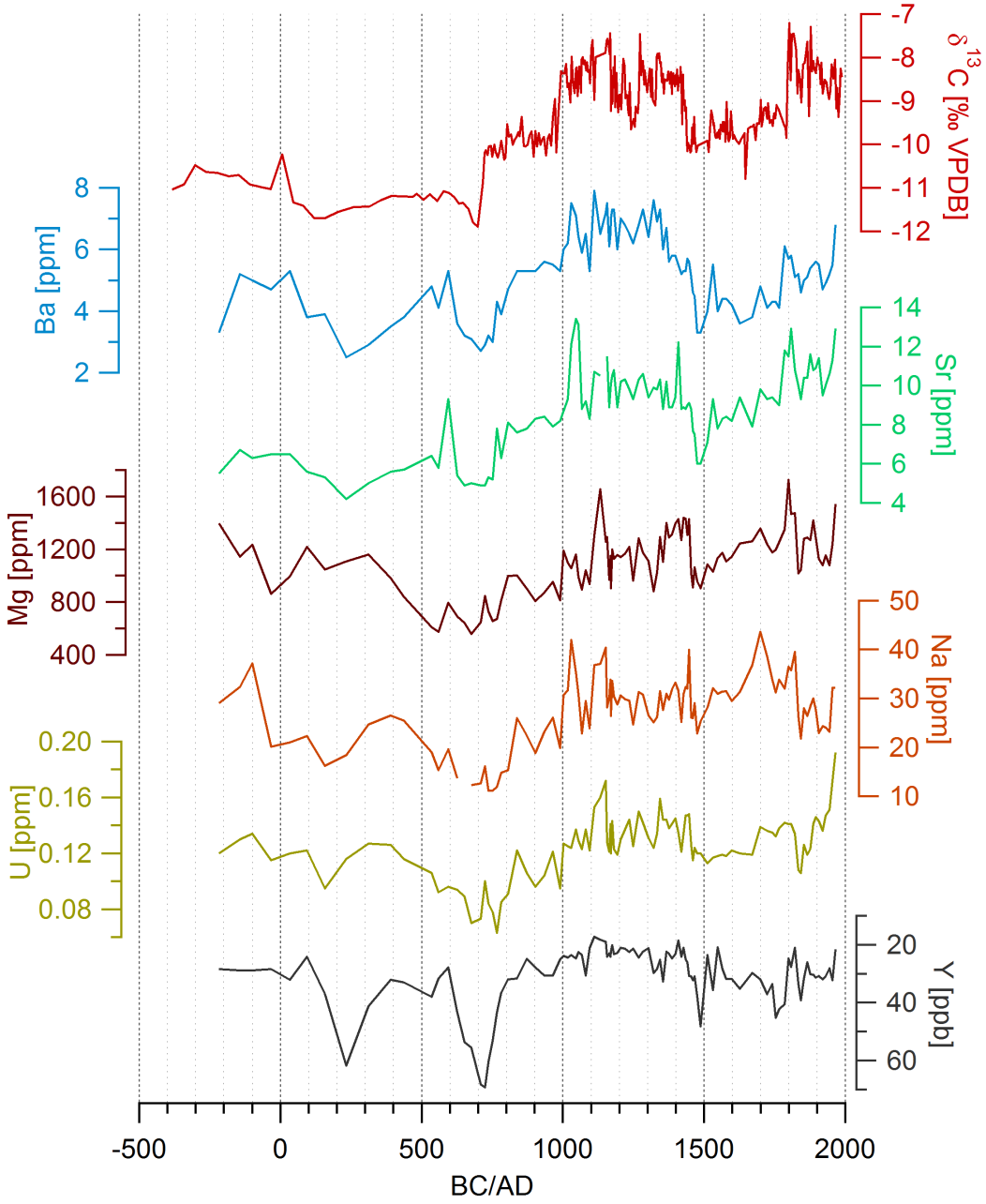

Figure 10.6: Vil-stm1 trace element concentrations. From top to bottom: $\delta^{13}C$ of calcite, concentrations of Ba, Sr, Mg, Na, U, and Y. Note the inverse scale for Y.

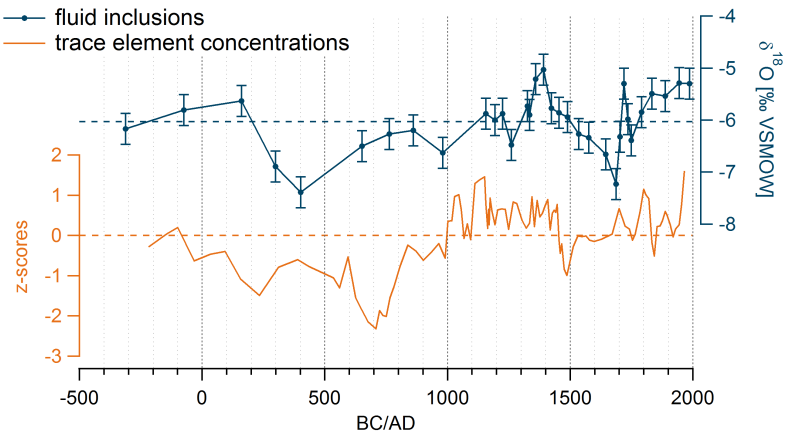

Figure 10.7: Vil-stm1 fluid inclusion $\delta^{18}O$ compared to a composite record of trace element concentrations (the averaged z-scores of individual trace element time series, with Y inversed).

$\delta^{13}C_{ct}$ along a single layer (Figure A.1). The average standard deviation is 0.11‰ for $\delta^{18}O$ and 0.18‰ for $\delta^{13}C$. There is no general tendency of increasing or decreasing delta values with distance from the central axis. The Hendy test does not provide a clear indication of disequilibrium for vil-stm1, but it is not a sufficient condition for isotopic equilibrium (Dorale and Liu 2009).

We calculated theoretical temperatures of calcite precipitation based on different equations which relate temperature to the equilibrium isotopic fractionation between water and calcite (Kim and O'Neil 1997; Anderson and Arthur 1983; O'Neil et al. 1969; Craig 1965), using the drip water, fluid inclusion and calcite $\delta^{18}O$ data. Calculated and measured cave temperatures for modern samples differ by up to 6 °C (see also Genty 2008). This indicates that the calcite is not precipitated in isotopic equilibrium with the water, provided that the empirical equations adequately describe the temperature dependent equilibrium fractionation (on this issue see Coplen 2007). The temperatures calculated from oxygen isotope ratios in calcite and fluid inclusions from using the different equilibrium fractionation equations differ by up to 4 °C. For all equations, the amplitude of the reconstructed temperature variation from stalagmite vil-stm1 during the past 2300 years is about 7 °C, which is closer to glacial-interglacial temperature changes than to a likely temperature change during the past millennia. We conclude that isotopic equilibrium is not given for the stalagmite vil-stm1 from Villars cave, and that it is therefore not possible to calculate palaeo-temperatures from the $\delta^{18}O$ of calcite and fluid inclusion water.

10.5 Discussion

10.5.1 Fluid Inclusions in Modern Calcite Samples and Contemporaneous Drip Water

The understanding of present day precipitation–drip water–fluid inclusions relationships is crucial for the interpretation fluid inclusion $\delta^{18}O$ variability in the past. In Villars cave, the isotopic composition of drip water has been remarkably constant over the last 15 years and represents the average precipitation $\delta^{18}O$ of several years (Genty et al. 2014). Here, we measured fluid inclusions in modern calcite deposits to determine if the original drip water isotopic

composition is, in turn, preserved in the fluid inclusions. The fluid inclusion isotope ratios measured in the modern calcite samples vil-gal#1B and vil-stm#10B are in agreement with those of the feeding drip waters. The measurements are well replicated, and the small difference in the drip water isotopic composition between the upper and lower cave galleries is reflected in the fluid inclusion samples. This confirms that the isotopic composition of cave drip water is preserved in modern fluid inclusions. A post-depositional alteration of the fluid inclusions $\delta^{18}O$ through water–rock interactions is unlikely at time scales of several millennia and at Earth surface temperatures. Furthermore, the GMWL provides a control on such processes as there is no exchange of H atoms between trapped water and the enclosing calcite. The drip water isotopic composition should therefore also be preserved in older stalagmite samples.

The fluid inclusion samples of vil-plq#8, on the contrary, are offset from their corresponding drip water. For this sample only three drip water measurements taken in winter and spring are available, but the drip water isotope values are very similar to each other (standard deviation 0.02‰ for $\delta^{18}O$) and fall in the same range as the values from the long-term monitoring stations (Table 10.1). The principle difference with the other modern samples is that the calcite was deposited on a flat tile from a thick water film of approximately 1 mm, fed by three dripping stalactites, at a very high growth rate of 1.7 mm yr^{-1}. We do not have an explanation for the offset, but we consider that this sample is not representative of natural growth conditions of stalagmites, as their convex-shaped tip leads to a thinner water film. The water film thickness, together with the drip impact, influence the degassing of CO_2 and calcite growth kinetics. Furthermore, the drip water isotopic composition and its seasonal variability are not as well constrained as for the other samples, and the difference between replicate measurements was larger than the error.

10.5.2 Stalagmite vil-stm1: Variability of Fluid Inclusion $\delta^{18}O$ in the Last 2300 Years

The isotopic composition of fluid inclusions in stalagmite vil-stm1 shows a large amplitude compared to e.g. a flowstone from Villars cave, which changed by < 1‰ across glacial termination II (Wainer et al. 2011). This variability can have different causes linked to changes in (1) the average isotopic composition of precipitation; (2) the precipitation–drip water relationship; and (3) processes in the cave; or a combination of those. If we assume that the present-day relationship between precipitation and cave drip water (i.e. drip water corresponds to a weighted mean of pluri-annual precipitation which arrives in the cave unchanged) was also valid in the past, the fluid inclusion $\delta^{18}O$ variability would reflect changes in the average isotopic composition of precipitation at the site. These could be induced by changes in temperature, which controls the fractionation during condensation, by precipitation amount, by changes in the atmospheric circulation, which influence moisture sources and trajectories (Langebroek et al. 2011; Field 2010), or by changes in the seasonality of precipitation (Vachon et al. 2007). In some cases, surface and subsurface processes might modify the isotopic composition of the water before it arrives in the cave, and influence the precipitation–drip water relationship. Enhanced evaporation during dry periods enriches soil water in ^{18}O (Gazis and Feng 2004). Changes in the type and density of vegetation can lead to changes in interception (Pichon et al. 1996), the evaporation/transpiration ratio (Polissar and Freeman 2010; Hsieh et al. 1998), and the seasonality and depth distribution of water uptake by plants (Tang and Feng 2001; Hruska et al. 1999), all of which can change the soil water isotopic composition compared to average precipitation. Lastly, processes in the cave can influence the isotopic composition of fluid in-

clusions, e.g. the evaporation of water from the stalagmite surface, which is controlled by cave air humidity, ventilation and drip rate (Deininger et al. 2012).

In order to evaluate possible causes of the fluid inclusion $\delta^{18}O$ variability observed in stalagmite vil-stm1, we compare the fluid inclusion record to different proxies measured in the same stalagmite, as well as to other palaeoclimate records, which can give indications on e.g. past temperature changes. The causes of variability can be further constrained by theoretical considerations of the temperature, precipitation amount and seasonality effects on the isotopic composition of precipitation.

Temperature, Precipitation Amount and Seasonality

The present-day ratio between local annual precipitation $\delta^{18}O$ and annual surface temperature at Villars is 0.56‰ °C^{-1} (Genty et al. 2014), which is close to the average European $\delta^{18}O$-temperature ratio of 0.59‰ °C^{-1} (Rozanski et al. 1992). According to this relationship (but keeping in mind that the temperature–$\delta^{18}O$ correlation is only moderate, R^2=0.35), the temperature change associated with the 2‰ amplitude in the $\delta^{18}O$ of fluid inclusions, which represent 15–25 year averages, would be about 3.5 °C. This is overestimated compared to most northern hemisphere temperature reconstructions for the past two millennia (e.g. Masson-Delmotte et al. 2013), suggesting that temperature change cannot be the sole cause of fluid inclusion $\delta^{18}O$ variability. Modern precipitation $\delta^{18}O$ at Villars is not correlated with the amount of precipitation at an annual scale.

Changes in the seasonality of precipitation can cause variations in the average annual precipitation $\delta^{18}O$. At present, the average annual precipitation $\delta^{18}O$ is dominated by the winter $\delta^{18}O$, as most precipitation falls during the winter time. Modern meteorological data (Harris et al. 2013) indicate no significant trend in precipitation seasonality during the 20th century in the study area. However, Slonosky (2002) has shown that the seasonal distribution of precipitation has changed significantly during the past 300 years at the Paris Observatory: while summer (April–September) precipitation amounts have been relatively stable, winter (October–March) precipitation has significantly increased by 24 mm per century, leading to a relative decrease of summer precipitation from 60% to 50% of the yearly total. If we calculate the average annual precipitation $\delta^{18}O$ based on the present-day seasonal amplitude at Villars of –7.2 to –5.4‰ and consider a 10% increase in summer precipitation compared to the 20th century average, this change in seasonality would result in a 0.2‰ change of the amount-weighted annual precipitation $\delta^{18}O$. Seasonality changes might thus influence the fluid inclusion $\delta^{18}O$, but cannot provide an explanation for the amplitude of the observed variability.

A recent reconstruction of European temperature (PAGES 2k Network 2013) shows some common features with the Villars fluid inclusion record, especially during the most recent part (Figure 10.8). The fluid inclusion $\delta^{18}O$ decreases of $>$ 2‰ from 1400 to 1700 AD, possibly reflecting a temperature decrease during the Little Ice Age, followed by an increase of the same magnitude from the 18th century to today. A decreasing from 0–400 AD is also observed in both records. This link can be explained by the temperature effect on precipitation $\delta^{18}O$, and because high temperature might be associated with dry periods and enhanced evaporation. Evaporation from falling raindrops as well as from soil water during dry periods increases the $\delta^{18}O$ of the infiltrating water, so drought periods could influence fluid inclusions and, if associated with warmer conditions, explain the the large amplitude of the fluid inclusions compared to temperature. During Medieval times, on the other hand, which are characterized

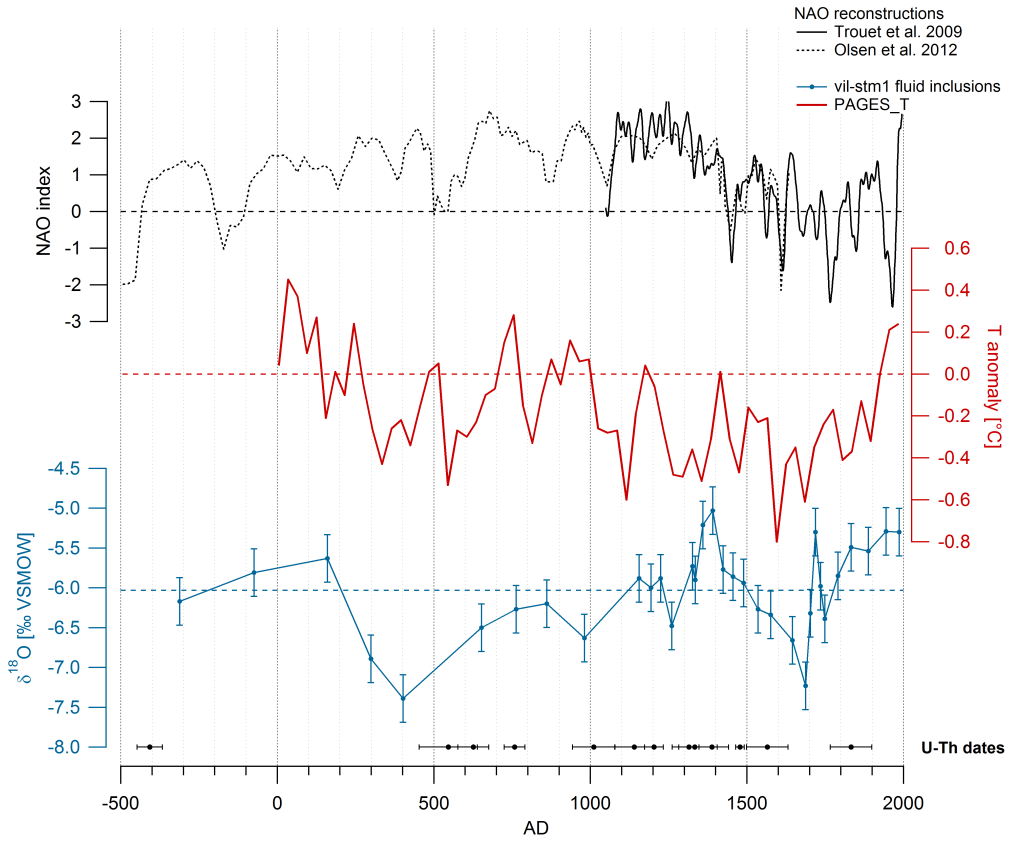

Figure 10.8: Vil-stm1 fluid inclusion $\delta^{18}O$ record compared to one of the most recent temperature reconstructions for Europe, based essentially on tree ring proxy data (PAGES 2k Network 2013). Temperature is given as anomalies relative to the reference period 1961–1990.

by a positive temperature anomaly, the fluid inclusion $\delta^{18}O$ values are on average 1‰ lower than at their peak around 1400 AD or during the 20th century. However, the resolution of the fluid inclusion record is much lower during this period, and consequently the $\delta^{18}O$ values are less well constrained.

Looking at this temperature reconstruction, there seems to be an influence of the long-term temperature variations on fluid inclusions $\delta^{18}O$, but temperature alone is not sufficient to explain the variability in the fluid inclusions. This is coherent with the modern temperature–precipitation $\delta^{18}O$ relationship discussed above. Precipitation $\delta^{18}O$ depends not only on local temperature, but also on the atmospheric circulation, which in Western Europe is controlled by the North Atlantic Oscillation (NAO) (Dietrich et al. 2013; Langebroek et al. 2011). Atmospheric circulation changes associated with warm or cold periods which could imply different source regions of the water vapour and different air mass trajectories. However, there is no evident link between reconstructed NAO patterns and the fluid inclusion isotope record (Figure 10.8).

Likewise, we found no link between the $\delta^{18}O$ of fluid inclusions and reconstructed precipitation amounts, but palaeo-records of hydro-climate are rare, and they might be spatially less coherent than temperature reconstructions. For these comparisons, it must be kept in mind that all proxy measurements and reconstructions are afflicted with their own uncertainties concerning dating, resolution, sensitivity, and spatial representativity. Furthermore, it is likely that the

isotopic composition of precipitation – assuming that it is what we see in the fluid inclusions – is influenced by a combination of vapour sources, temperature, and humidity, which are not represented together in other reconstructions.

Other Proxies from vil-stm1: Indicators of Vegetation and Aridity Changes

The other proxies from stalagmite vil-stm1 give evidence of local environmental changes. Most of the proxy records are correlated, which points to common causes of variability. As the amplitude of variability recorded in this late Holocene stalagmite is similar to the amplitude observed in other speleothems from Villars cave during major climate transitions, we suppose that other environmental changes besides climate must have had a substantial influence on the proxies. The large amplitude might partly be linked to the higher resolution compared to other Villars records (Bourdin 2012; Wainer et al. 2011; Genty et al. 2010, 2003), but the amplitude is mainly due to large shifts rather than high-frequency noise.

The variations in carbon isotope ratios indicate vegetation changes above the cave. A dense vegetation cover leads to an high soil CO_2 production through plant respiration and microbial activity. This raises the proportion of light carbon in the dissolution zone, and consequently lowers the $\delta^{13}C$ in speleothem calcite (Frisia et al. 2011; Baldini et al. 2005; Genty et al. 2003). The abrupt increase in $\delta^{13}C_{ct}$ at 700 AD is caused by a decrease in vegetation activity, probably due to anthropogenic deforestation, as a climate-induced vegetation change is unlikely. The increase in growth rate also coincides with the increase in $\delta^{13}C_{ct}$. This is somewhat counter-intuitive, as a reduced soil CO_2 production reduces the dissolution of calcium carbonate in the soil and epikarst, leading to lower Ca concentrations in the percolating water, which should reduce the growth rate. However, this effect is compensated by the fact that the cave air CO_2 concentration would also be reduced, leading to a rapid degassing of CO_2 from the solution and consequently rapid calcite precipitation, possibly accompanied by an increase in $\delta^{13}C_{ct}$ due to kinetic effects. Furthermore, a decrease in vegetation density might decrease the transpirational water loss, leading to increased infiltration, drip rates, and growth rates.

Kinetic effects could also lead to the observed co-variation in $\delta^{13}C$ and $\delta^{18}O$, although the shifts in $\delta^{18}O$ are less abrupt. The temperature calculation based on $\delta^{18}O$ in calcite and fluid inclusions also indicates dis-equilibrium conditions because of the largely overestimated amplitude in the reconstructed temperature. Nevertheless, the oxygen isotope composition of calcite seems to be dependent on the $\delta^{18}O$ of the drip water, as they display some common variance and a similar range of values. Forthcoming $\Delta 47$ measurements on this stalagmite might provide indications on equilibrium conditions during calcite precipitation and enable the reconstruction of palaeo-temperature.

The trace element concentrations in speleothem calcite are controlled by variations of the aeolian input, the intensity of soil leaching, the efficiency of transport in the seepage water, the degree of water-rock interaction in the karst through water residence time, and the extent of prior calcite precipitation (PCP), which denotes a removal of calcite from the percolating solution upflow of the studied speleothem (Fairchild et al. 2000). The partition coefficients (D) of these elements into calcite can depend on the speleothem growth rate (Ba, Sr), or on temperature (Mg) (Fairchild and Treble 2009; and references therein). D_{Na}, D_{Ba}, D_{Sr}, D_{Mg}, and D_U are proved to be lower than 1, while D_Y is higher than 1 (Curti 1999; Kitano and Oomori 1971). The co-variation of the concentration of different trace elements indicates that they have a common cause of variability. A single factor involving the partition coefficient

could explain a significant part of the variability in their concentrations. Increased levels of PCP due to degassing of CO_2 from the solution before it reaches the cave, associated with a longer water residence time in the karst, would cause an enrichment in the trace elements with a partition coefficient < 1 while lowering the concentrations in elements with a partition coefficient > 1 in a speleothem. The positive correlation between Sr, Mg and $\delta^{13}C$ strongly backs up a PCP control on these parameters (Griffiths et al. 2010a; Johnson et al. 2006).

Similarly large shifts in trace element concentrations and $\delta^{13}C$ have already been observed in a late Holocene stalagmite, and they were related to land use changes above the cave (Hartmann et al. 2013). Higher levels could be associated with periods when the forest cover above the cave had disappeared (e.g. around 1000 or 1800 AD), while lower $\delta^{13}C$ and trace element levels (before 700 AD) would correspond to forested vegetation cover. The period between 700 and 1000 AD could be associated to a partial removal of the vegetation while between 1400 and 1800 AD the natural vegetation may have returned partially. However, the connection between periods of high PCP and the presence of a deforested surface still has to be confirmed by modern observations.

The controls on the calcite stable isotopes and trace element proxies might have also influenced the isotopic composition of fluid inclusions. A sparser vegetation cover increases the evaporation-transpiration ratio compared to a forest canopy, which would lead to an enrichment of ^{18}O in the drip water, and consequently in the fluid inclusions. Secondly, if PCP indicates dry conditions, high temperatures and increased evaporation also lead to higher $\delta^{18}O$ values of the drip water. However, despite a certain degree of similarity between the fluid inclusion and other proxy time series, the isotopic composition of fluid inclusions seems to be unaffected by the large and abrupt changes in the vegetation.

10.6 Conclusions

The analysis of modern calcite samples has shown that fluid inclusions preserve the isotopic composition of the drip water. It is therefore possible to reconstruct drip water isotope variability from speleothem fluid inclusions. The isotope monitoring data from Villars cave confirm that the drip water represents the average precipitation at the site under present-day conditions.

This relationship is not well constrained in the past, however, as several interfering factors might have changed the cave drip water isotopic composition relative to the local precipitation. Vegetation changes, which are clearly evidenced by the calcite $\delta^{13}C$, might impact the hydrology and consequently the proxy records. It is therefore crucial to consider the specific cave environment when interpreting the isotopic composition of speleothem fluid inclusions. The co-variation of trace element concentrations, as indicators of prior calcite precipitation, and oxygen isotope ratios in fluid inclusions suggests that evaporation has possibly influenced the cave drip water isotopic composition relative to precipitation during dry periods.

Nevertheless, there is evidence that the fluid inclusion $\delta^{18}O$ provide a direct record of precipitation $\delta^{18}O$ in the past: (1) it is indicated by the modern calibration; (2) there is remarkably little scatter in the fluid inclusion data set; and (3) there is a good agreement with reconstructed temperature, at least for the last 1000 years, with low fluid inclusion $\delta^{18}O$ values during the Little Ice Age.

Despite the apparently complex influences on the functioning of the cave system, the multiple

proxies from this stalagmite provided insights the history of local climate and environmental changes. Further high-resolution records of palaeo-precipitation $\delta^{18}O$ from the same region will be necessary to confirm in how far the fluid inclusion record from Villars cave is representative of regional precipitation isotope patterns.

11 Climatic and Non-Climatic Influences on the $\delta^{18}O$ of Cellulose

The previous chapters have presented records of stable isotopes in precipitation and cave drip water from the southwest of France, which can provide estimates of the isotopic composition of soil water that is tapped by trees. This article investigates the respective influence of source water $\delta^{18}O$ and evaporative enrichment of leaf water on the isotopic composition of cellulose, as well as other climatic and non-climatic controlling factors at Angoulême and Le Mas. We identify two important non-climatic influences on cellulose $\delta^{18}O$ due to tree age and site effects: (1) an increasing trend during the juvenile phase of tree growth, likely due to height and canopy effects; and (2) an offset between the average level of cellulose $\delta^{18}O$ in two tree groups, which might be caused by different soil properties and differences in the fraction of the source water used by trees from different depths.

Cellulose $\delta^{18}O$ is strongly correlated to summer maximum temperature, relative humidity and evapotranspiration, and only moderately correlated to precipitation $\delta^{18}O$, indicating that leaf water enrichment has a stronger control on the inter-annual variability of cellulose $\delta^{18}O$ than the $\delta^{18}O$ of precipitation.

This is in agreement with the precipitation–drip water isotopic relationship in Villars cave (Chapter 9). The absence of a growing-season bias from plant transpiration in the isotopic composition of drip water suggests that the $\delta^{18}O$ of the source water which is taken up by trees represents a well-mixed soil water and not only the current growing season precipitation.

This study demonstrates the suitability of oak tree ring cellulose $\delta^{18}O$ for reconstructing past summer climate variability in southwest France, provided that the sampling and pooling strategy accounts for the fact that trees from different sites and of different age can introduce non-climatic signals. Supplementary material to this article is given in Appendix A.

Article published in Dendrochronologia

Tree Age, Site and Climate Controls on Tree Ring Cellulose $\delta^{18}O$: A Case Study on Oak Trees from South-Western France

Inga Labuhn[1], Valérie Daux[1], Monique Pierre[1], Michel Stievenard[1], Olivier Girardclos[2], Anaïs Féron[1], Dominique Genty[1], Valérie Masson-Delmotte[1], Olivier Mestre[3]

[1]Laboratoire des Sciences du Climat et de l'Environnement (LSCE/IPSL), laboratoire CEA/CNRS/UVSQ, CE Saclay, Orme des Merisiers, Gif-sur-Yvette, France
[2]Laboratoire Chrono-environnement, université de Franche-Comté, Besançon, France
[3]Météo-France, Direction de la Climatologie, Toulouse, France

11.1 Introduction

Tree rings are valuable climate archives. They have a seasonal resolution, are absolutely dated and available in a wide range of climate settings. Climatic and environmental conditions at the time of ring formation affect their width, density, and the isotopic composition of cellulose. The statistical relationships between these tree ring characteristics and local climate parameters form the basis for palaeoclimatic reconstructions using long time series of tree ring data. While tree ring width and maximum latewood density can be sensitive palaeoclimate indicators at sites where tree growth is strongly limited by a single climate variable (Cook et al. 1999; Büntgen et al. 2005; Esper et al. 2007; Grudd 2008), stable isotopes in cellulose potentially record a climate signal even when there is no dominant climatic control on growth, which is often the case in regions with temperate climate (e.g. Loader et al. 2008; Young et al. 2012). Oxygen isotope ratios in cellulose have successfully been employed in reconstructions of temperature (Etien et al. 2009; Daux et al. 2011; Coppola et al. 2013), precipitation amount (Treydte et al. 2006), drought stress (Masson-Delmotte et al. 2005), the $\delta^{18}O$ of precipitation (Saurer et al. 1997a; Robertson et al. 2001; Danis et al. 2006), or cloud cover (Shi et al. 2012). However, their suitability to reconstruct a certain climate parameter depends on the site and the specific climate response of the tree (Treydte et al. 2007).

The mechanisms which determine the isotopic composition of cellulose are fairly well understood, and attempts to model the $\delta^{18}O$ of cellulose exist (Roden et al. 2000; Barbour 2007; Ogée et al. 2009; Danis et al. 2012). The oxygen isotopic signal acquired by tree ring cellulose depends on the isotopic composition of the source water, on the evaporative enrichment in the leaves, and on biological fractionation during the formation of photosynthetic sugars (McCarroll and Loader 2004). The $\delta^{18}O$ of the soil water depends primarily on the $\delta^{18}O$ precipitation, which has various influences such as the water vapour source, air mass trajectories and rainout history, the condensation temperature and the precipitation amount (e.g. Darling et al. 2006). The soil water residence time determines the amount of mixing between rainfall events and precipitation from different seasons. Evaporation from the top soil layer leads to an enrichment, which is mixed into deeper soil horizons upon subsequent rainfall events. The rooting depth of a tree is important since the isotopic composition of soil water may change along the soil profile (Hsieh et al. 1998). There is no fractionation when tree roots take up water (White et al. 1985; Bariac et al. 1991). In the leaves, water is enriched in heavy isotopes due to evaporation. The extent of the enrichment is dominantly controlled by the isotopic

composition of atmospheric water vapour, and by relative humidity, which affects the vapour pressure difference between leaf air and ambient air, and is modulated by the Péclet effect (e.g. Barbour et al. 2004; Sternberg 2009; Gessler et al. 2013). Photosynthetic sugars are enriched in ^{18}O compared to the leaf water by 27‰. During the formation of cellulose in the tree ring, the sugars can exchange up to 50% of their oxygen atoms with the stem water. This proportion is variable and depends on the rate of cellulose synthesis and sugar import (Barbour and Farquhar 2000). The δ^{18}O of cellulose should therefore represent partly the isotopic signature of the source water, and partly the isotopic composition of leaf water.

In temperate forests, temperature and cellulose δ^{18}O are expected to be positively correlated since both the source water isotopic composition and the leaf water enrichment may be affected by temperature changes. However, contrary to the factors which influence leaf water evaporation (e.g. temperature and relative humidity), the variability of the source water signal is usually unknown. The source water isotopic signature can vary seasonally with the δ^{18}O of precipitation, or stay rather constant, depending on soil water residence time, mixing, and the water pool used by the trees (Tang and Feng 2001; Brooks et al. 2010). The depth distribution of the water uptake depends on the species and the age of the tree (Ehleringer and Dawson 1992; Phillips and Ehleringer 1995), and can change according to the soil moisture conditions (Bréda et al. 1995; Dara et al. 2013). Moreover, trees might use winter precipitation stored in the soil, which is not correlated with the current growing season temperature and thus adds a different signal.

While classical dendrochronology requires measurement of growth or density in a large number of samples in order to extract a common climate signal, the feasibility of the analytical protocol for stable isotope analysis is restricted to a few trees. It is therefore crucial to assess the validity of sampling and pooling strategies. This requires the investigation of tree-to-tree variability, age effects, and artefacts which can be introduced by pooling samples from different sites within a given area. The few studies investigating inter-tree variability (e.g. Raffalli-Delerce et al. 2004; Leavitt 2010; Daux et al. 2011; Roden et al. 2011) have highlighted a strong common signal which can be extracted from a few trees only, but also depicted offsets between individual trees. Detailed studies are required to investigate if outliers influence the pooled isotopic ratios, and to quantify the uncertainty associated with the mean signal.

It has long been known that tree ring width series must be corrected for age effects. Standardization methods have been developed and improved in order to remove non-climatic trends (Cook and Kairiukstis 1990; Hughes et al. 2011). So far, no such statistical treatment is applied to tree ring cellulose oxygen isotope records, and only a few studies acknowledge the possibility of age-related trends in δ^{18}O (Marshall and Monserud 2006; Treydte et al. 2006; Esper et al. 2010). No systematic study of the tree age effect on cellulose δ^{18}O has so far been conducted for oak trees in a temperate climate (but see Mayr et al. (2003) for an investigation of the age trend in δD of cellulose). If there is an age trend in the isotopic composition of cellulose, pooling together trees of different ages could introduce a shift or trend in the series, which might be falsely interpreted as a climatic signal.

This article examines the variability of oxygen isotope ratios in tree ring cellulose ($\delta^{18}O_{cell}$) and tree ring width (TRW) in *Quercus sp.* from karstic sites in the south-west of France, covering the period 1860 to 2010. The region is known for recurrent summer droughts, and the tree ring proxies have the potential to record the variability of summer climate in the past. Near our sites we have available long monitoring records of stable isotopes in precipitation and

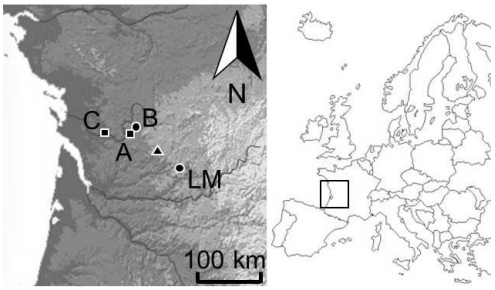

Figure 11.1: Location of the study area. Circles indicate the tree sampling sites Braconne forest (B) and Le Mas (LM), squares indicate the meteorological stations Angoulême (A) and Cognac (C), and the triangle indicates Villars cave.

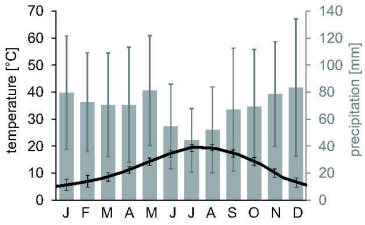

Figure 11.2: Mean monthly temperature and precipitation for Angoulême (1961–1990).

shallow cave drip water, which enable an estimation of the $\delta^{18}O$ of the source water taken up by the trees. With these estimates, we can attempt to decipher the respective contributions of source water $\delta^{18}O$ and the meteorological variables controlling leaf water enrichment to the isotopic composition of cellulose. Furthermore, we investigate the variability of $\delta^{18}O_{cell}$ among individual trees from the same site, between different age groups, and between closely located sites. The results allow a critical assessment of analysis strategies, possible constraints on the use of tree ring proxy data, and the suitability of tree ring $\delta^{18}O_{cell}$ in south-west France for palaeoclimatic reconstructions.

11.2 Material and Methods

The study area in south-western France (Figure 11.1) is characterized by a karstic limestone bedrock. The climate is temperate and oceanic, with mild winters and dry summers (Figure 11.2). In this area, climate is not a strongly limiting factor to tree growth, and consequently TRW is typically not well correlated with meteorological variables. Stable isotopes, however, have the potential to be a sensitive climate proxy.

11.2.1 Sites and Sampling

Our main sampling was conducted at Braconne forest (45°44'N, 0°18'E, 110 m a.s.l.) in 2000 and 2004, where oak trees of different ages were cored. It was complemented in 2010 by a sampling at Le Mas (45°08'N, 1°12'E, 191 m a.s.l.), 100 km to the south-east, where precipitation isotope monitoring data are available.

Braconne forest consists of 74% deciduous trees dominated by sessile oak (*Quercus petraea* (Matt.) Liebl.) and pedunculate oak (*Quercus robur* L.) (INPN 2013). Standardized coppice practices were implemented in this forest in the 17th century, and were still in use in the 19th century in some stands (Office National des Forêts, ONF, pers. comm.).

At Braconne forest, we sampled 6 "young" *Quercus sp.*, about 145 years old, from two adjacent stands, and 13 "old" *Quercus sp.*, between 310 and 405 years old, from a stand 1 km away (Figure 11.3). Some of the old trees were not cored to the pith, so the given ages are minimum ages. As karstic terrains are rather heterogeneous (White, 2002), the old and young tree sites may have different hydrological characteristics, despite their proximity. The old trees grow on a thin soil less than 30 cm deep, while the young trees grow on a thicker soil of at least 60 cm

depth. We could not obtain samples from old and young trees in the same stand. At Le Mas, four *Quercus petraea* were sampled. The trees were about 70 years old and grew in a sparse forest on a slope with a thin soil layer.

All trees were sampled either by coring with an increment borer of 5 mm diameter at breast height, or by cutting discs from felled trees at 2 m from the base of the stem. Three cores were taken from each living tree and three radii were cut from each disc at an angle of 120° to minimize the influence of TRW and $\delta^{18}O_{cell}$ variability within one ring (Fritts 1976; Helle and Schleser 2004b).

11.2.2 TRW and $\delta^{18}O_{cell}$ Measurements

For each tree, ring width was measured for the three cores and then averaged. Trees were cross-dated and the calendar year of each ring was determined. The dating was checked for errors using COFECHA (Holmes 1983; Grissino-Mayer 2001). TRW series were standardized with the programme ARSTAN (Cook 1985) using a 30-year spline to remove the age trend from the series and to create a tree ring index which emphasizes the inter-annual variability. A mean chronology was calculated for each site.

For the stable isotope analysis, the cross-dated cores were cut ring by ring under a binocular microscope using a scalpel. Earlywood and latewood were separated and only the latewood was analysed, because the earlywood is formed with photosynthates from the previous growing season, which do not depend on the meteorological conditions during the year of ring formation (Michelot et al. 2012). For each calendar year the rings of all three cores from a tree were pooled. As the $\delta^{18}O_{cell}$ varies within one ring (Helle and Schleser 2004b; Ogée et al. 2009), samples were homogenized using a centrifugal mill with a 0.08 mm sieve. This ensures that the small amount of cellulose which is measured is representative of the whole latewood. The isotopic analysis was performed on α-cellulose extracted from the wood powder according to the procedure developed by Green (1963) and modified by Leavitt and Danzer (1993). 0.2 mg of cellulose were weighed into silver capsules. The $\delta^{18}O_{cell}$ was measured using a thermal combustion elemental analyser (TC/EA) coupled with a Finnigan MAT252 mass spectrometer at LSCE in Gif-sur-Yvette, France. The measurements were corrected using the cellulose reference Whatman CC31. A sequence of 10 CC31 standards was measured before each sample run to ensure the stability of the mass spectrometer and check that the standard deviation was $< 0.20‰$. Additional standards were measured after every third sample. Each sample was measured at least twice and repeated up to four times when necessary. Outlier measurements were rejected. The analytical uncertainty was 0.20‰ based on the maximum accepted standard deviation. For the pooled sequences, a high analytical precision is crucial because no error can be calculated based on the inter-tree variability. Isotope ratios are reported with reference to VSMOW (Coplen 1994). Altogether, 730 samples have been measured for this study, excluding replicates.

11.2.3 Pooling of Trees

Figure 11.3 summarizes our pooling strategy. For Braconne, we measured $\delta^{18}O_{cell}$ in four of the old trees and all young trees. Trees were analysed individually for selected periods: 1758 to 1772 for the old trees, and 1860 to 1924 for the young trees. The corresponding rings of all trees were pooled prior to analysis for the remaining time spans. For Le Mas, tree by tree $\delta^{18}O_{cell}$ measurements were conducted, but only for the most recent period (1981–2010) which

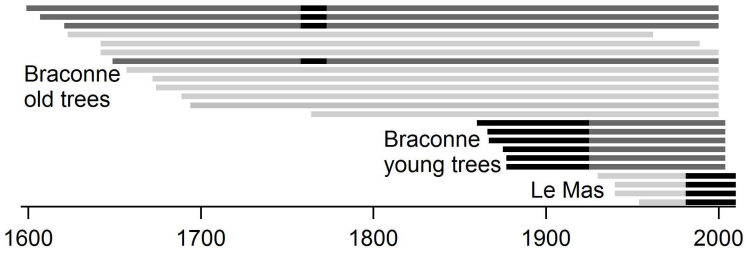

Figure 11.3: Sample time spans. Tree ring width was measured for all samples. Dark grey bars represent the samples which were selected for $\delta^{18}O_{cell}$ analysis. The black bars indicate the time spans where the trees were analysed individually; for the remaining time spans the $\delta^{18}O_{cell}$ analysis was performed on pooled samples.

overlaps with the precipitation isotope monitoring data and allows a 30-year comparison with the Braconne series.

The inter-tree variability of isotope ratios was determined first by analysing individual trees. To test whether an equal mass of wood should be weighed from each tree before pooling trees for the remaining time spans, the arithmetic mean $\delta^{18}O_{cell}$ value of all individually analysed trees was compared to a mean weighted by ring width (as an approximation of the mass of the ring). The first represents the value one would measure from pooled samples of equal mass; the latter represents the value one would measure if samples are pooled without weighing, where a tree with larger rings would have a stronger influence on the measured isotopic ratio of the pooled sample (Leavitt 2010). The difference between the weighted mean and the unweighted mean at each site is negligible (overall mean difference 0.04 ±0.05‰). Besides, further uncertainty might be introduced if the mass of wood, which is constrained by the narrowest ring, is very small and it is difficult to cut a piece of wood representative of the whole latewood. Therefore, rings were pooled without weighing.

11.2.4 Meteorological Data

We used homogenised monthly meteorological data (average and maximum temperature, precipitation, relative humidity and potential evapotranspiration) from the French national meteorological service, Météo-France, from Angoulême (20 km from Braconne) and Cognac (60 km from Braconne) (Figure 11.1). The Cognac station provides the longest records of relative humidity (RH) (since 1950) and potential evapotranspiration (PET) (since 1954) for the area, while Angoulême offers precipitation data back to 1930 and temperature data back to 1888. For their common period, records from these two stations are highly correlated: $r = 0.75$ ($P < 0.001$; number of observations $n = 27$) for average summer RH and $r = 0.90$ ($P < 0.001$; $n = 25$) for average summer PET. Mean annual temperature at Angoulême is 12.0°C; mean annual precipitation is 823 mm, with 18% of the precipitation falling during the summer months (June, July, August). Note that the average annual temperature at Le Mas is slightly colder (0.3°C), and average annual precipitation is slightly higher (47 mm) than at Angoulême. Correlation analyses were performed between the tree ring parameters (annual TRW and $\delta^{18}O_{cell}$) and monthly meteorological data from January of the previous year to October of the year of ring formation, for the time period covered by all target data (1954–2000).

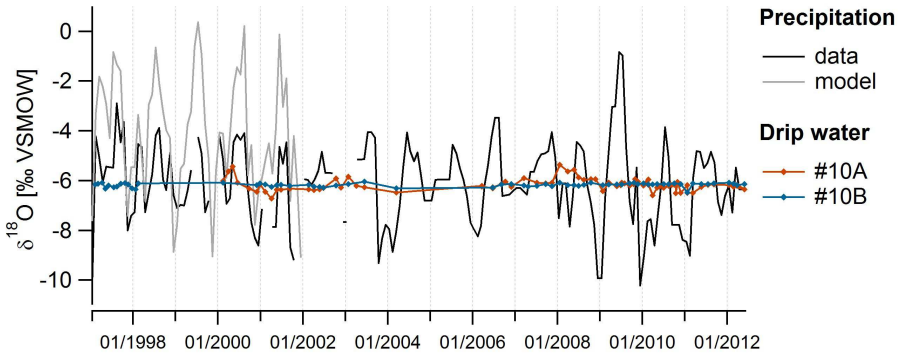

Figure 11.4: The oxygen isotopic composition of precipitation measured at Le Mas (black line; data from Genty et al. 2014), and simulated by the model REMOiso for the corresponding grid box (grey line; Sturm et al. 2005). The blue and orange lines represent measurements of drip water δ^{18}O from two dripping stalactites, #10A and #10B, in Villars cave at 10 m below the surface (data from Genty et al. 2014).

11.2.5 Precipitation and Infiltration Water δ^{18}O

The isotopic composition of precipitation has been recorded at Le Mas site since 1997 (Genty et al. 2014; Figure 11.4). While monthly $\delta^{18}O_{prec}$ shows a well-marked seasonal cycle with a mean amplitude of 4‰, parallel to the seasonal cycle of temperature, there is no inter-annual correlation between summer precipitation δ^{18}O and summer temperature.

Stable isotope measurements of precipitation and infiltration water are available from Villars cave (45°26'N, 0°47'E, 175 m a.s.l.) since 1997 (Figure 11.4). The isotopic composition of precipitation at Le Mas and Villars is very similar (Genty et al. 2014), so it is acceptable to compare results from these two sites. The cave data provide insight on the fate of water isotopes from precipitation to the shallow subsurface for a site with karstic limestone bedrock and forest vegetation, which is considered as representative of the tree sites. Infiltration water in Villars cave has been sampled regularly under two dripping stalactites at a depth of 10 m, where tree roots are visible on the cave ceiling. The drip water isotopic composition is constant throughout the monitoring period (–6.2‰), and is equal to the weighted mean δ^{18}O of several years of precipitation. There is no seasonal bias from plant transpiration and no evaporative enrichment before the water enters the cave (Genty et al. 2014).

In order to obtain a longer period of comparison between δ^{18}O in precipitation and cellulose, we also use monthly $\delta^{18}O_{prec}$ outputs from the model REMOiso (Sturm et al. 2005), available from 1960 to 2001. REMOiso is a regional model with a stable water isotope module, which uses physical parameterizations of the global circulation model ECHAM-4 (Roeckner et al. 1996), and is embedded in the global model (von Storch et al. 2000). REMOiso has a spatial resolution of 0.5°, 19 vertical layers and a time step of 5 minutes. The model simulations have been evaluated based on the data from Le Mas for the corresponding 0.5°grid cell (Genty et al. 2014). Although the model overestimates $\delta^{18}O_{prec}$ values and the amplitude of seasonal variation, it is able to capture the measured seasonal cycle and the inter-annual and intra-seasonal variability of $\delta^{18}O_{prec}$ at the site (Figure 11.4). In REMOiso, mean summer precipitation δ^{18}O and temperature are correlated with $r = 0.52$ ($P < 0.001$; $n = 42$).

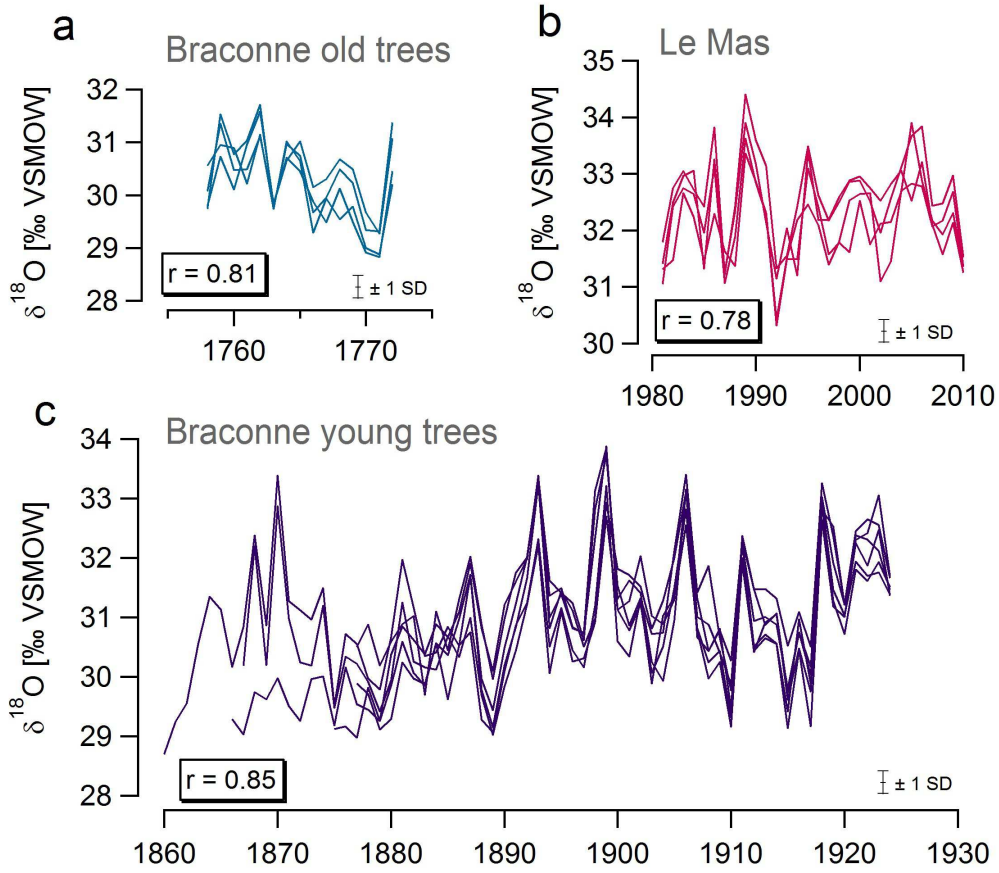

Figure 11.5: Cellulose δ^{18}O of individually analysed trees. (a) Braconne old trees, (b) Le Mas, and (c) Braconne young trees. The error bars indicate the analytical uncertainty (1 standard deviation). The average correlation between series (r) is given for each site.

Table 11.1: Average Pearson correlation coefficients and expressed population signal (EPS) between trees at a site for tree ring width and cellulose δ^{18}O. Correlations for tree ring width are first calculated for all available samples, then only for those samples and time spans which correspond to the δ^{18}O series.

	Number of samples	**Time span**	**Average correlation between series**	**EPS**
Braconne old trees				
Tree ring width	13	1599–2000	0.45	0.91
Tree ring width	4	1758–1772	0.67	0.89
Cellulose δ^{18}O	4	1758–1772	0.81	0.95
Braconne young trees				
Tree ring width	6	1860–2004	0.53	0.87
Tree ring width	6	1860–1924	0.61	0.90
Cellulose δ^{18}O	6	1860–1924	0.85	0.97
Le Mas				
Tree ring width	4	1930–2010	0.65	0.88
Tree ring width	4	1981–2010	0.72	0.91
Cellulose δ^{18}O	4	1981–2010	0.78	0.94

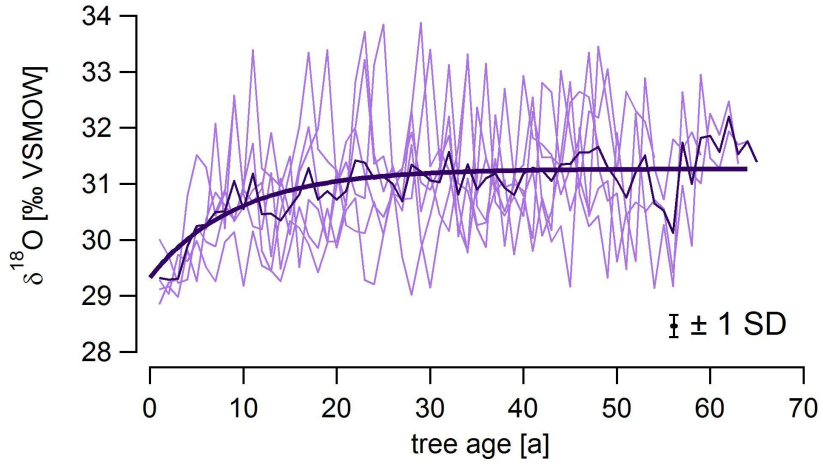

Figure 11.6: δ^{18}O of cellulose for Braconne young trees aligned by their cambial age and the mean value (dark purple line) with a fitted exponential curve (thick purple line).

11.3 Results

11.3.1 Variability Between Individually Analysed Trees

Non-standardized TRW curves in many of the samples at Le Mas and Braconne are characterized by long-term increasing and decreasing trends, which are likely the effect of changes in competition (possibly logging) in a closed stand with resulting suppression and release patterns. Although a common signal in TRW exists, which allows the samples to be crossdated, the absolute values differ significantly (Figure A.2).

Trees within a given stand show very similar inter-annual variations in oxygen isotope ratios (Figure 11.5), even if their growth patterns differ. The difference between two trees can be large in some exceptional years (e.g. $>$ 3‰ in the young trees in 1870), but it is generally small compared to the amplitude of inter-annual variability of the mean chronologies. The mean correlation coefficients between series (r $>$ 0.78) and the expressed population signal (EPS $>$ 0.94) (Wigley et al. 1984; Briffa and Jones 1990) confirm that 4 to 6 trees can be sufficient to capture a common $\delta^{18}O_{cell}$ signal, while this number of trees might not be sufficient to capture a representative growth signal (Table 11.1).

11.3.2 Cellulose δ^{18}O and Tree Age

When aligning the individual series of Braconne young trees according to their cambial age, the average $\delta^{18}O_{cell}$ shows an upward trend of about 2‰ over the first 30 years of growth, 1.2‰ increase being achieved in the first 10 years (Figure 11.6). The increasing trend is also visible in the mean young tree $\delta^{18}O_{cell}$ chronology, as they all started growing between 1860 and 1877. However, it is probably not a climatic trend, since it is not visible in the old trees during the same period (Figure 11.7). As the innermost part of the old tree cores is not available, the existence of a juvenile increasing trend in $\delta^{18}O_{cell}$ cannot be confirmed on this second set of samples. We applied the negative exponential fit from Figure 11.6 to correct the juvenile effect by removing the trend in the young trees before subsequent analyses.

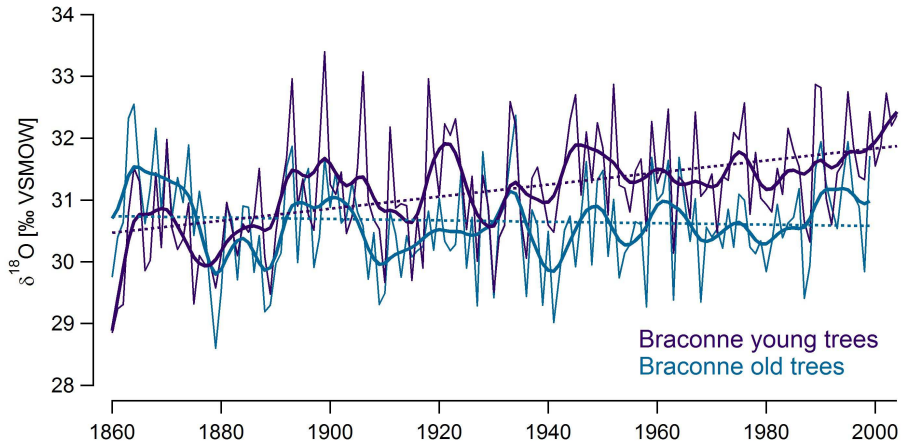

Figure 11.7: Comparison of δ^{18}O of cellulose for young (purple) and old (blue) trees from Braconne forest; annual values, 10-year smoothing splines (thick lines) and linear trends (dashed lines).

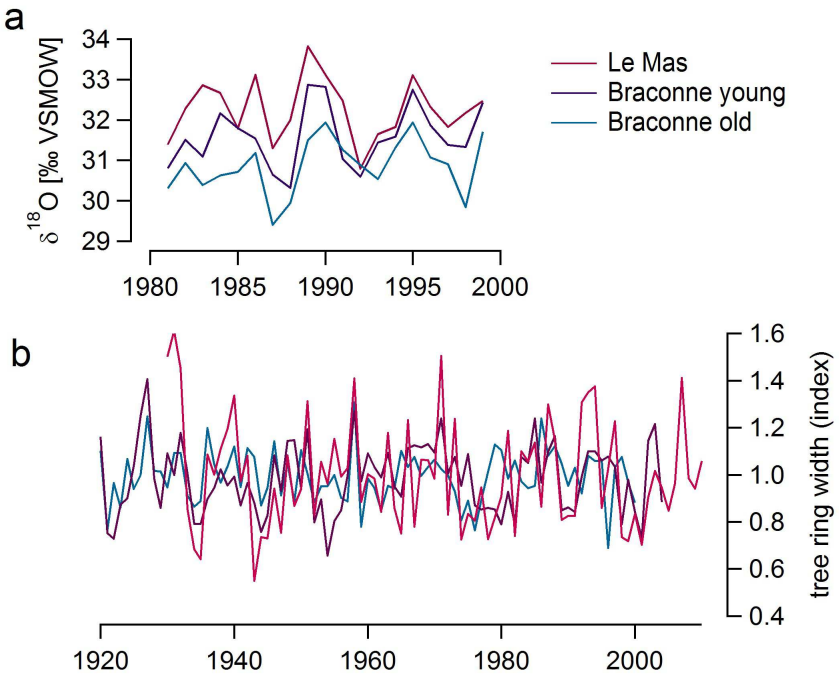

Figure 11.8: Mean chronologies of the three tree groups for their periods of overlap. (a) δ^{18}O of cellulose, and (b) a tree ring width index standardized using a 30-year spline.

Table 11.2: Pearson correlation coefficients between site chronologies for tree ring width and cellulose δ^{18}O. The common time periods of the respective proxy are given in Figure 11.2. The asterisks indicate the significance level: * < 0.05, ** < 0.01, *** < 0.001.

Sites	**Tree ring width**	**Cellulose δ^{18}O**
Le Mas – Braconne young	0.58**	0.64***
Le Mas – Braconne old	0.29	0.56*
Braconne young – Braconne old	0.23**	0.50***

11.3.3 Differences in $\delta^{18}O_{cell}$ Between Sites

The inter-site comparison shows large differences in absolute values of the non-standardized TRW chronologies of Le Mas and Braconne forest (Figure A.3), but crossdating is possible between the standardized TRW series (Figure 11.8). The strongest inter-site correlations are obtained for the $\delta^{18}O_{cell}$ series (Table 11.2). The inter-annual $\delta^{18}O_{cell}$ variability at Braconne and Le Mas is consistent (Figure 11.8a), but the data depict an offset between sites, with on average 0.60‰ higher mean values at Le Mas. Over their common period from 1860 to 2000, the $\delta^{18}O_{cell}$ of the young trees is on average 0.52‰ higher than that of the old trees (Figure 11.7). When leaving out the 30 first "juvenile" years, the $\delta^{18}O_{cell}$ is on average 0.76‰ higher in the young trees. Inter-annual variations and decadal trends between the two tree groups are similar, but the amplitude of $\delta^{18}O_{cell}$ variability is higher in the young trees between 1890 and 1920, with several extreme values around 1900.

The difference between old and young trees $\delta^{18}O_{cell}$ is large compared to the difference between individual trees. For the period 1860 to 1924, where $\delta^{18}O_{cell}$ has been measured individually for each tree, the correlations between each possible pair of young trees are higher (average $r = 0.85$; $P < 0.001$ for all pairs; $48 \leq n \leq 65$ depending on series length) than the correlation between the mean chronologies of young, corrected for the juvenile trend, and old trees ($r = 0.58$; $P < 0.001$; $n = 65$).

11.3.4 Correlations with Climate

Stronger correlations were obtained between $\delta^{18}O_{cell}$ and the different meteorological variables than between TRW and the same variables. Moreover, the strengths of the correlations are more coherent in the young and old trees for $\delta^{18}O_{cell}$ than for TRW (Figure 11.9). $\delta^{18}O_{cell}$ is negatively correlated to summer precipitation and relative humidity, and positively correlated to summer temperature and evapotranspiration. The strongest correlations were obtained with relative humidity (in June $r = -0.75$ for the young trees). Correlations were improved when using averages of several months (e.g. JJA maximum temperature), because the ring parameter integrates meteorological conditions throughout the growing season. There are no significant correlations with the monthly meteorological conditions of the previous year (not shown).

The linear regression between mean $\delta^{18}O_{cell}$ of all trees from Braconne forest and JJA maximum temperature leads to a slope of +1.47°C per 1‰ increase in $\delta^{18}O_{cell}$ (Figure 11.10). In a temperature reconstruction based on this model, a difference of 0.76‰ in $\delta^{18}O_{cell}$, as observed between old and young trees, would result in a 1.12 °C temperature difference.

Superimposing the time series plots of $\delta^{18}O_{cell}$ and summer maximum temperature (Figure 11.11) illustrates that the inter-annual variability as well as decadal trends are very similar in $\delta^{18}O_{cell}$ and temperature. The marked increase in temperature since 1980 is captured by the tree ring proxy records. However, the warmest summers ($> 2\sigma$ above the mean; 1928, 1947, 1976, and 2003), do not lead to the highest $\delta^{18}O_{cell}$ value in both tree groups. Extreme years are poorly represented in the isotope chronology, possibly because growth is reduced during hot and dry conditions. Consequently the proportion of the wood corresponding to this period is small.

11.3.5 $\delta^{18}O$ in Precipitation and Cellulose

Correlations between $\delta^{18}O_{prec}$ and $\delta^{18}O_{cell}$ at Le Mas (Figure 11.12), are not significant, possibly because the series have an overlap of only 13 years. The correlation between Braconne

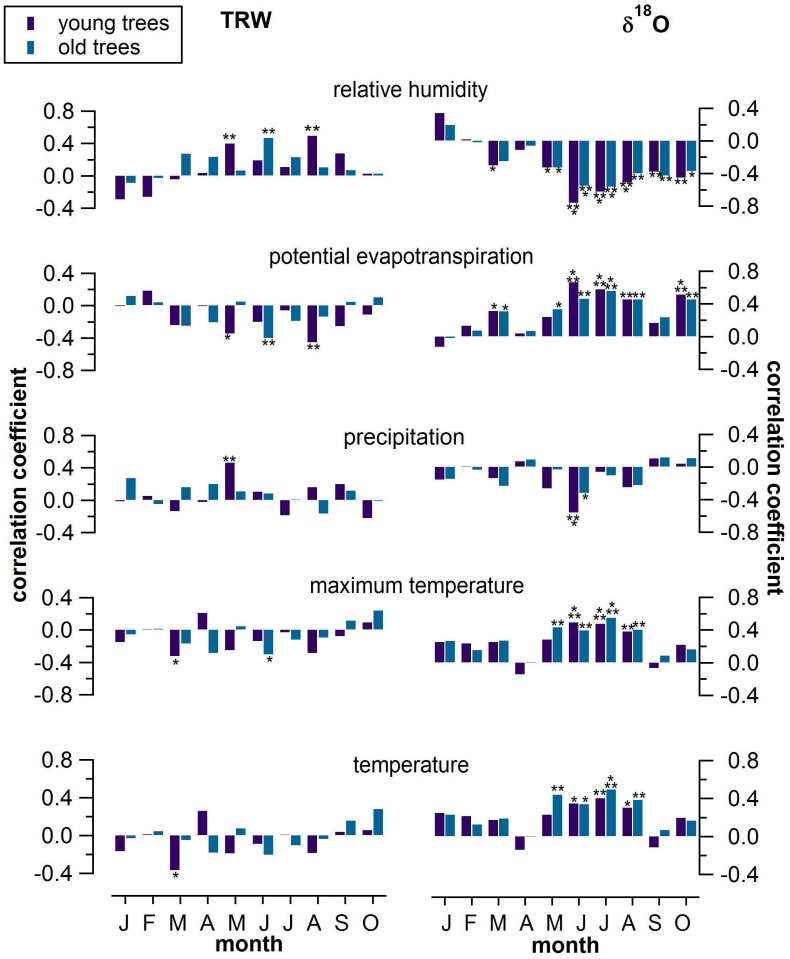

Figure 11.9: Pearson's correlation coefficients between monthly meteorological variables and tree ring parameters for the period 1954–2000. The panels of the left show correlations with the tree ring index (TRI), the panels on the right show correlations with the δ^{18}O of cellulose from young (purple bars) and old (blue bars) trees at Braconne forest. The asterisks indicate the significance level: * < 0.05, ** < 0.01, *** < 0.001.

$\delta^{18}O_{cell}$ and summer $\delta^{18}O_{prec}$ simulated by REMOiso (1960-2004) reaches r = 0.47 for the young trees and r = 0.35 for the old trees (Figure 11.12). There is no relationship between Braconne $\delta^{18}O_{cell}$ and winter or annual $\delta^{18}O_{prec}$.

In the REMOiso model simulation, the mean annual $\delta^{18}O_{prec}$ is dominated by the δ^{18}O of winter and spring precipitation, when most precipitation occurs (Figure 11.13, Figure 11.2). The inter-annual variability in $\delta^{18}O_{cell}$ resembles to some extent the variability of precipitation δ^{18}O during the summer, but there are no clear similarities in the inter-annual and decadal variability as can be seen between $\delta^{18}O_{cell}$ and maximum temperature.

11.4 Discussion

The oxygen isotopic composition of tree ring cellulose at our sites can be related to meteorological conditions at the time of ring formation, but there is an additional influence of non-climatic factors such as tree age and site hydrology.

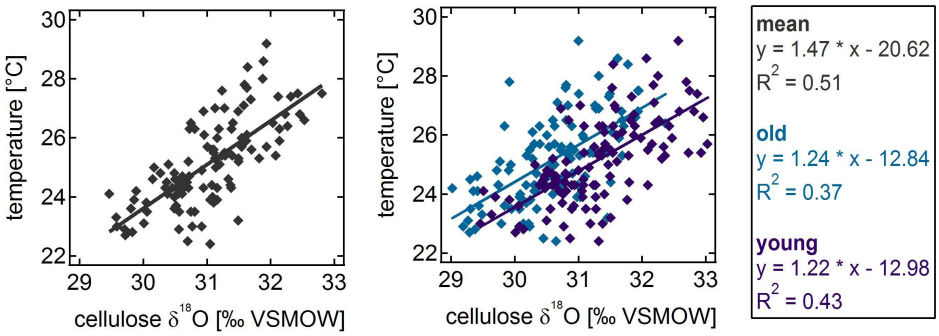

Figure 11.10: Scatter plots of pairs of cellulose δ^{18}O and maximum temperature averaged over June, July and August. Left panel: average δ^{18}O values for all trees from Braconne forest. Right panel: δ^{18}O values for young (purple) and old (blue) trees separately. The equations describe the respective least squares regression line.

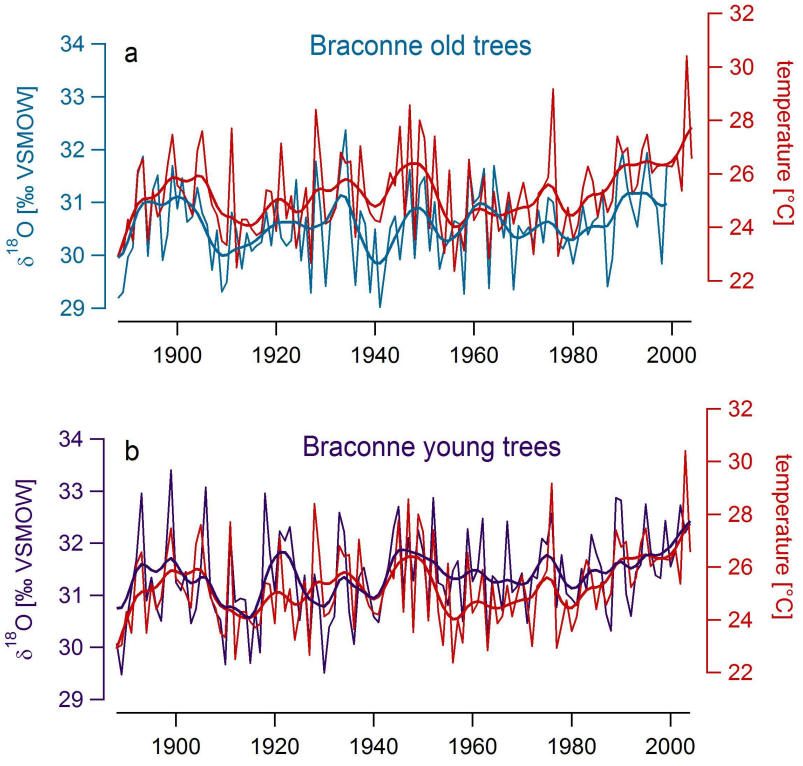

Figure 11.11: Inter-annual variability and decadal trends in the δ^{18}O of cellulose of (a) Braconne old trees and (b) Braconne young trees (corrected for juvenile effect), and maximum summer temperature averaged over June, July and August (red curves).

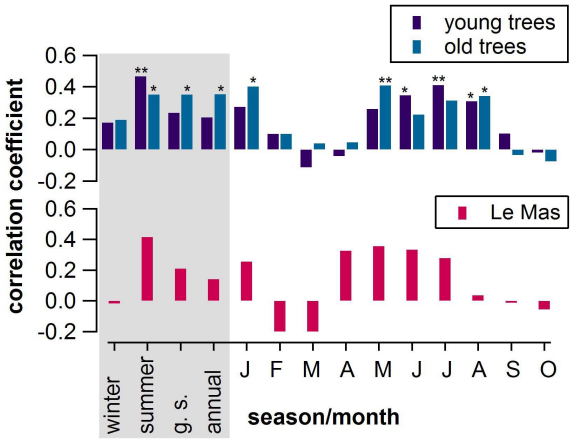

Figure 11.12: Pearson's correlation coefficients between the δ^{18}O of cellulose and monthly and seasonal δ^{18}O of precipitation. Top panel: correlations between the δ^{18}O of cellulose from young and old trees at Braconne forest, and the δ^{18}O of precipitation simulated by the model REMOiso (1960–2000; Sturm et al. 2005). Bottom panel: correlations between the δ^{18}O of cellulose at Le Mas with the measured δ^{18}O of precipitation (1997–2010; Genty et al. 2014). Correlation coefficients with seasonal means of precipitation δ^{18}O are in the grey shaded area: winter (DJF), summer (JJA), growing season ("g.s." AMJJAS), and the hydrological year ("annual", October to September). The asterisks indicate the significance level: * < 0.05, ** < 0.01.

11.4.1 Age Trends in $\delta^{18}O_{cell}$ Series

Our data depict a 30 year long age effect on $\delta^{18}O_{cell}$. Physiological changes with tree age are known to affect tree growth (TRW) and its sensitivity to climate variability (Voelker 2011). Oak trees have their highest growth rate during the first 40-45 years, when trees reach a height (H) of about 15 m, then at a reduced but still sustained rate during the following 60 years (H $\approx$ 25 m), and at a very low rate afterwards (H $\approx$ 30 m at an age of 200 years) (Duplat and Tran-Ha 1997). A height increase affects two parameters which have a potential influence on oxygen isotope ratios in cellulose: stomatal conductance, and the microclimate around the tree crown.

Stomatal conductance (G_s) decreases with tree height through a decrease of the hydraulic conductance. It has been shown that 30 m height difference in Fagus sylvatica resulted in a Gs difference of approximately 60% (Schäfer et al. 2000), and a 20 m difference between old and young Pinus ponderosa in almost 100% difference in G_s (Hubbard et al. 2001). The δ^{18}O in plant organic matter has been shown to be correlated to stomatal conductance (Scheidegger et al. 2000; Grams et al. 2007). However, it is still debated whether the effect of G_s on leaf water enrichment is direct or due to a common forcing, i.e. low relative humidity leads to reduced Gs and higher leaf water δ^{18}O (Sheshshayee et al. 2005; Farquhar et al. 2007). If the oxygen isotopic composition of tree cellulose is negatively correlated to stomatal conductance, a height increase during the juvenile phase of the trees is likely to lead to a $\delta^{18}O_{cell}$ increase. Theoretically, the enrichment should continue until height gain ceases. However, the total leaf area of a tree increases with age, leading to a larger net conductance which may counteract the decrease of leaf conductance (Schäfer et al. 2000). As the necessary data are not available in the literature, we cannot quantify the possible effect of oak tree growth on $\delta^{18}O_{cell}$ via G_s.

The microclimate around tree crowns changes during the first years of growth. As the coppice-

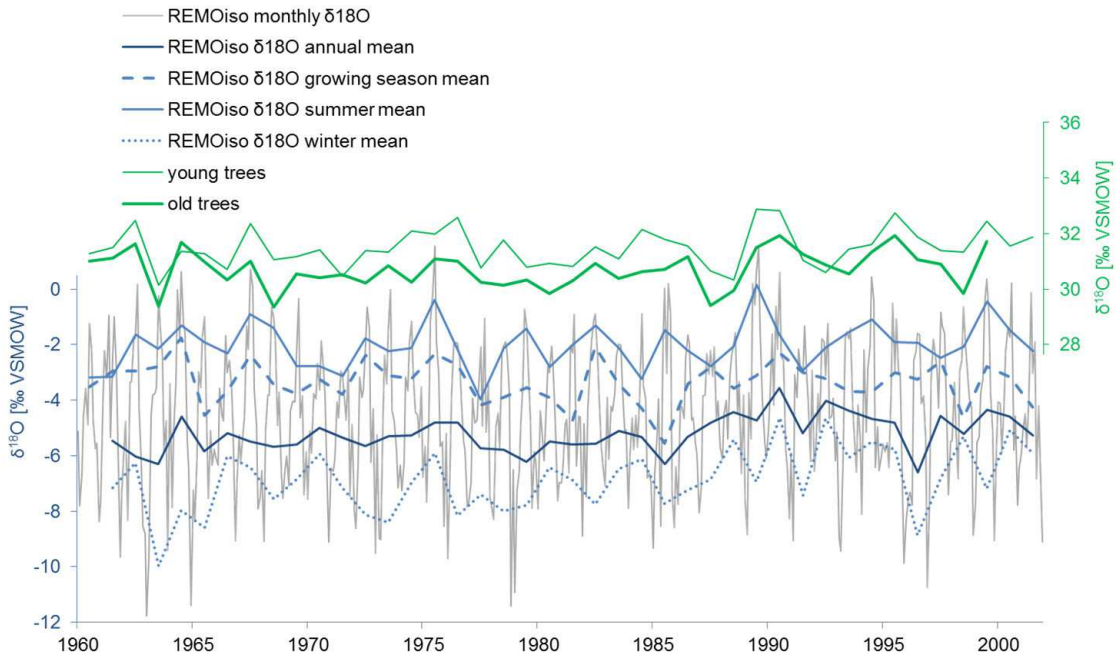

Figure 11.13: Inter-annual variability in δ^{18}O of cellulose compared to the inter-annual variability of δ^{18}O in precipitation for annual and seasonal means. The annual mean corresponds to the hydrological year October–September, the winter mean to December–February, the summer mean to June–August, and the growing season mean to April–September.

with-standards system was in use in the young oak stands, it is very likely that the trees have grown under a canopy. Gradients of temperature, relative humidity (RH), insolation, wind, and CO_2 are observed under a canopy. The crowns of small trees are situated in an environment which is cooler, more humid, less sunny and windy, and has a higher CO_2 partial pressure compared to the environment of taller tree crowns (Eliáš et al. 1989; Aussenac 2000). Among these parameters, RH is the one whose variations most strongly affect the oxygen isotope ratios. As reduced RH causes an increase of δ^{18}O in the leaf water and subsequently in cellulose (e.g. Barbour et al. 2004; Roden and Farquhar 2012; Roden and Siegwolf 2012), the $\delta^{18}O_{cell}$ increase with age recorded in the young trees may be related to an upward decrease of humidity. This phenomenon was thought to be responsible for the variation of the δ^{18}O of leaves in a tropical forest from the understory up to 9 m height in the canopy where the RH gradient was about 5% (Silveira et al. 1989). In temperate forests, the vertical RH gradients under canopies can be significant: 8% RH decrease was measured from the ground to 15 m height in oak (Eliáš et al. 1989)and Norway Spruce (Zweifel et al. 2002) forests. Above this height the gradient is small. Using the equations which describe the relationship between leaf water δ^{18}O and RH (Dongman et al. 1974), and the $\delta^{18}O_{cell}$ as a function of source water and leaf water δ^{18}O (Sternberg et al. 1986; Yakir and DeNiro 1990), we can define the difference in isotopic composition of the cellulose formed at the bottom and top of a humidity gradient by:

$$\Delta\delta^{18}O_{cell} = -\Delta RH * (\varepsilon^* + \varepsilon_k) \tag{11.1}$$

where ε^* and ε_k are the equilibrium and kinetic fractionation factors (see supplementary

material in the appendix for details). According to Equation 11.1, and using the fractionation factors at 20 °C given by Burk and Stuiver (1981) and Horita and Wesolowski (1994), an 8% increase in RH from ground to canopy results in a 2‰ increase in $\delta^{18}O_{cell}$. This value is of the same order as the juvenile isotopic trend observed for the young trees at Braconne. The above mentioned equations do not take into account the Péclet effect, which tends to reduce the leaf water enrichment (Barbour et al. 2004). Moreover, the effect of a humidity gradient on oxygen isotope fractionation can be different for individual trees due to competition. Nevertheless, it is a plausible process for explaining the juvenile $\delta^{18}O_{cell}$ increase in the first 20–30 years.

We conclude that the increase of $\delta^{18}O_{cell}$ during the juvenile phase of the Braconne oak trees may be due to a size-related decrease of the stomatal conductance, and to the isotopic enrichment of the leaf water in connection with a relative humidity decrease as trees gain height. The existence of a juvenile trend in $\delta^{18}O_{cell}$ series is very important for palaeoclimate reconstructions using $\delta^{18}O_{cell}$. Our results suggest that either detrending should be applied to individual tree series, or the earliest 20–30 years of each core should be omitted in pooled samples.

Another possible influence of tree age on $\delta^{18}O_{cell}$ besides the juvenile effect has been reported by Esper et al. (2010) and Treydte et al. (2006), who found decreasing trends over several centuries. The fact that young trees, after a short phase of rapid increase, have a higher $\delta^{18}O_{cell}$ than old trees is consistent with these findings. However, the results presented here do not provide any evidence for such a trend, and we cannot distinguish potential age trends which are superimposed upon the trends induced by climate variability. Instead, the offset between the age groups may be attributed to differences in site hydrology.

11.4.2 Impact of Soil Hydrology and Water Sources on $\delta^{18}O_{cell}$

The young trees average $\delta^{18}O_{cell}$ is 0.76‰ higher than that of the old trees at Braconne, and Le Mas has an average value which is 0.60‰ higher than the young trees. Slightly different meteorological conditions might account for the higher average isotope ratios for the 100 km distant site of Le Mas, e.g. the average summer $\delta^{18}O_{prec}$ is 0.40‰ higher at Le Mas. They cannot explain the offset between the young and old tree sites, which are 1 km apart. It cannot be ascribed to a tree height effect either, as the difference persists even when the young trees are more than 100 years old and have reached a height close to the final height of an oak tree (Duplat and Tran-Ha 1997).

A likely explanation for the difference in $\delta^{18}O_{cell}$ is a different access to water due to site-specific pedo-hydrological conditions (thickness of the soil layer and water holding capacity), and the rooting depth of the trees. These two parameters are linked because oak trees can develop a larger root system as an adaptation to dry site conditions (Hruska et al. 1999). Oaks form dense root mats in the upper 40 cm of the soil (Bréda et al. 1993; Thomas and Hartmann 1998), but also extend thick structural roots into the underlying fractured karst bedrock. Fine-root mats also fill the narrow crevices in the bedrock, suggesting the capacity of trees to take up water from rock layers below the soil (Bréda et al. 1993; Schwinning 2008; Heilman et al. 2009). Roots of oak trees have been observed in caves at depths of up to 10 m (Bréda et al. 1993; Genty 2008).

At Braconne, the soil layer at the young trees' site is twice as thick as at the old trees' site. It is likely that the old trees need to extract more water from deeper levels in the bedrock in order to maintain a sufficient water supply during dry periods, which leads to a difference

in their climate response. TRW is significantly correlated to spring precipitation only for the young trees. Considering that the old trees can access deeper water reserves, their growth may be less dependent on surface soil moisture in spring. Furthermore, the correlations confirm that they are less sensitive to summer $\delta^{18}O_{prec}$.

The larger contribution of deep water can explain the lower isotopic values in the old trees, because this water consists of annual or pluri-annual precipitation and has an isotopic signature which is lower than the average summer precipitation (cf. Figure 11.13). On the contrary, shallow soil water shows more seasonal variation and is enriched in 18O the growing season. Consequently, if the young trees have a shallower water reservoir, they access more water from the current growing season. This interpretation can be tested if we suppose a simple, two-layer soil model, where the water in the top layer has a $\delta^{18}O$ that corresponds to summer precipitation (–2‰), and the water in the bottom layer has a $\delta^{18}O$ that corresponds to mean annual precipitation (–5.2‰). A 25% difference in contribution from the top soil layer (e.g. the young trees take 35% and the old trees 10% of their water from the top layer) would lead to a difference in the $\delta^{18}O$ of the tree's source water of 0.8‰. This is in the same order of magnitude as the observed difference in $\delta^{18}O_{cell}$ between the two stands.

11.4.3 Influence of Source Water $\delta^{18}O$ vs. Leaf Evaporation on $\delta^{18}O_{cell}$

At our site, the statistical relationships demonstrate that $\delta^{18}O_{cell}$ and the factors which control evaporative enrichment in the leaves covary on an inter-annual time scale. The influence of the source water $\delta^{18}O$ signal, however, is not as obvious on this time scale. If the $\delta^{18}O_{cell}$ were correlated with winter precipitation $\delta^{18}O$, it would be possible to distinguish the influence of winter precipitation $\delta^{18}O$ (source water), and the independent climatic influence on leaf water evaporation during the growing season. However, the highest correlations of $\delta^{18}O_{cell}$ with $\delta^{18}O_{prec}$ and with temperature occur during the same months (May/June to August). This could mean two things. First, the trees take a proportion of their water from the top soil layers, whose isotopic composition is close to that of the current precipitation. Both leaf water enrichment and $\delta^{18}O_{prec}$ – the two main controls on $\delta^{18}O_{cell}$ – depend partly on temperature and influence the isotopic composition of cellulose in the same direction: higher temperature leads to a higher $\delta^{18}O_{prec}$, and a further enrichment of the heavy isotope in the leaf water. Together, this would result in strong correlations between $\delta^{18}O_{cell}$ and temperature and make the isotopic composition of cellulose a good temperature proxy.

Alternatively, summer $\delta^{18}O_{prec}$ and $\delta^{18}O_{cell}$ are correlated because they both depend on temperature, but there is no direct link between the two. Soil water has an attenuated $\delta^{18}O$ variability compared to precipitation because it consists of a mixture of different rainfall events and different seasons, and its residence time can be several months (Hesterberg and Siegenthaler 1991; Gazis and Feng 2004). The $\delta^{18}O$ variability of soil water decreases towards deeper soil layers. The decrease is site dependent, but several studies found constant $\delta^{18}O$ values below 50 cm (Hsieh et al. 1998; Tang and Feng 2001; Gazis and Feng 2004). The water that trees take from deeper layers could therefore have a relatively constant isotopic composition which does not reflect the seasonal variability of $\delta^{18}O$ in precipitation. However, there may still be relevant inter-annual variability in source water, depending on the water residence time in the soil.

The drip water isotopic composition at Villars cave corresponds to the average precipitation of several years without any evaporative enrichment (cf. Section 11). The ratio of evaporation

and transpiration determines the proportion of water lost with or without fractionation (Hsieh et al. 1998). There is little direct evaporation since there is no bare soil at the site. The water lost from the soil to the atmosphere in canopied forests is lost dominantly through the transpiring vegetation (Polissar and Freeman 2010). Transpirational water loss can influence the isotopic composition of the infiltration water if plants take up a large part of the summer precipitation and only winter precipitation arrives in the cave. At Villars cave, however, plants must dominantly obtain their water supply from a mixed water in the soil and not directly from the growing season precipitation. It could be argued that the amount of water taken by trees is small compared to total precipitation so that the effect of a seasonal bias would not be visible in the drip water. But this is unlikely because at this site the water excess is negative (PET > precipitation) during several months each year (Genty 2008), which means that the water quantity lost from the soil to the atmosphere is not negligible.

Almost half of the isotopic signal in cellulose originates from the source water $\delta^{18}O$. Since there is no strong $\delta^{18}O_{prec}$ signal in cellulose, the predominant source water does not carry a seasonal precipitation signal, but has the isotopic signature of several years of rainfall mixed together. On the contrary, the different climate parameters which control the enrichment of ^{18}O in the leaf influence the inter-annual variability of $\delta^{18}O_{cell}$. If the source water isotopic composition does not vary on an inter-annual time scale, it means that there is no "disturbance" of the leaf water enrichment signal. The cellulose signal is also undisturbed by possibly contrasting influences like the isotopic composition of winter precipitation. This makes $\delta^{18}O_{cell}$ at the studied site a good indicator of the parameters which control the evaporative enrichment in the leaves.

11.4.4 Potential and Constraints of $\delta^{18}O_{cell}$ and TRW as Climate Proxies

As the inter-annual variations and mean values of $\delta^{18}O_{cell}$ of the trees at each of our sites were similar, the pooling of rings from different trees was acceptable. The inter-annual variations were also consistent between sites 100 km away from each other, pointing to a common climatic forcing. The climate signal is thus not only local but representative of a larger region. However, sizable differences of the mean isotopic compositions were observed from one site to another. Therefore multi-site pooling could introduce non-climatic trends or breaks in the final isotope chronology. To deal with such offsets, an adjustment to the mean value for each site could be applied. The "Join-point" method (Gagen et al. 2012) could constitute an efficient alternative for producing robust reconstructions.

The $\delta^{18}O_{cell}$ at our site is positively correlated with summer temperature and potential evapotranspiration, and negatively correlated with relative humidity. Studies conducted on $\delta^{18}O_{cell}$ of oak trees in Europe have evidenced similar links with temperature and moisture parameters (Reynolds-Henne et al. 2009; Treydte et al. 2007; Loader et al. 2008; Saurer et al. 2008; Haupt et al. 2011). On the contrary, tree growth in the study area, expressed by TRW, does not display a strong climate sensitivity, in agreement with previous studies on oaks from northern France (Mérian et al. 2011), and elsewhere in Europe (Szczepanek et al. 2006; Hilasvuori and Berninger 2010; and references therein). The coppicing practice employed in Braconne forest might obscure the climate signal in this proxy in the past, as it has an influence on the growth of trees (Altman et al. 2013). Our study demonstrates that $\delta^{18}O_{cell}$ from oak trees is an adequate proxy for reconstructing the regional summer climate variations in south western France, provided that different cohorts of samples are not simply pooled.

11.5 Conclusions

A reliable palaeoclimate reconstruction based on tree ring proxies requires a comprehension of the influencing factors and possible uncertainties due to inter-tree and inter-site variability, which can have implications for sampling and analysis strategy.

Here we have demonstrated age and site effects on oak $\delta^{18}O_{cell}$, which could introduce biases in average chronologies. At Braconne forest, where a coppice-with-standards system had been applied, a trend in $\delta^{18}O_{cell}$ during the juvenile phase is likely due to height and canopy effects. It might not be as pronounced with other types of forest management. For climate reconstruction, the trend can be corrected if trees are analysed individually, or the respective part of the tree cores is omitted from the analysis. A varied age distribution and a sufficiently large number of trees help reduce biases, when for any given year trees of different cambial ages are averaged to form a representative mean chronology.

The significant differences we found in $\delta^{18}O_{cell}$ of tree cohorts from closely located sites makes pooling problematic. Pooling of several trees eliminates the possibility to distinguish individual tree or site effects. When analysing timber wood, the problem of spatial variability is even more critical as the exact location of the tree site is generally unknown. Inter-tree and inter-site variability should be tested and corrections of offsets applied when possible. In a long chronology, any shift or trend must be critically evaluated if it is attributed to individual trees or if it is climatic.

The trees at our site display a strong common signal due to common climatic influence, the isotopic composition of cellulose being a more sensitive climate proxy than tree ring width. Since the trees' source water originates to a large extent from deep soil layers, with an isotopic composition that is rather constant and does not vary seasonally with the δ^{18}O of precipitation, the site is not suited for the reconstruction of inter-annual precipitation δ^{18}O variability. On the contrary, inter-annual variations in the oxygen isotope ratios in cellulose are largely controlled by leaf water enrichment, with a resulting strong link with summer temperature.

12 Reconstruction of Summer Droughts Based on Tree Rings

The site-specific calibration presented in the previous chapter provides the basis for a climate reconstruction. Here, we extend our annually resolved tree ring cellulose δ^{18}O chronology back to 1360 AD using living-tree and timber material from Angoulême. We have demonstrated in Chapter 11 the suitability of south-west France tree rings to reconstruct summer climate, as well as the preponderant effect of isotopic fractionation in leaves on the inter-annual variability of cellulose δ^{18}O. Moreover, this study has evidenced a juvenile effect in cellulose δ^{18}O during the first 20 years of tree growth, and offsets in average δ^{18}O values between tree cohorts, both of which must be taken into account when interpreting cellulose δ^{18}O chronologies in terms of climate. These results had implications for the subsequent pooling and analysis strategy of the timber samples. First, the innermost 20 rings of each core were omitted from the analysis to avoid the influence of a juvenile effect during the first years of growth. Second, the difference between sites proved the necessity to perform an inter-tree comparison for the timber samples, for which the site conditions were unknown, and to correct offsets in the average δ^{18}O values between sites in the final chronology.

Using the corrected δ^{18}O chronology, we developed a model based on linear regression to reconstruct the drought index SPEI (Beguería et al. 2010; Vicente-Serrano et al. 2010). The high correlation between drought index and cellulose δ^{18}O, as well as the verification of the model by independent data support the validity of this reconstruction. Moreover, there is a good agreement of the drought reconstruction with grape harvest dates from the regions, which provide another proxies of summer climate.

The δ^{18}O chronology from Angoulême is further compared to another long tree ring δ^{18}O chronology from Fontainebleau in the north of France, to test the regional coherency of the oxygen isotope signal. While the two sites are highly correlated during the 20$^{\text{th}}$ century, there is a significant decrease in the correlation coefficient between 1550 and 1800 AD, which indicates either a weaker climate sensitivity of the tree ring proxies during this period, or a more heterogeneous climate in the north and the south of France. Supplementary material to this article is given in Appendix A.

Article in preparation

Reconstruction of summer droughts in southwest France since 1360 AD based on tree ring cellulose $\delta^{18}O$

Inga Labuhn[1], Valérie Daux[1], Olivier Girardclos[2], Michel Stievenard[1], Monique Pierre[1], Adrien Deroubaix[3], Dominique Genty[1], Valérie Masson-Delmotte[1]

[1]*Laboratoire des Sciences du Climat et de l'Environnement (LSCE/IPSL), laboratoire CEA/CNRS/UVSQ, CE Saclay, Orme des Merisiers, Gif-sur-Yvette, France*
[2]*Laboratoire Chrono-environnement, université de Franche-Comté, Besançon, France*
[3]*Laboratoire Inter-universitaire des Systèmes Atmosphériques (LISA/IPSL), Créteil, France*

12.1 Introduction

Droughts can have severe impacts on ecosystems and on human activity (Diaz and Trouet 2014; Büntgen et al. 2010). The southwest of France is characterized by recurrent drought periods, and future climate change might increase the risk of droughts, augmenting the pressure on water resources and impacting the sustainability of the current agricultural system (Levrault et al. 2010; Itier 2008). This region has experienced a rise in temperature during the 20th century which is larger than the French or the global average (Moisselin et al. 2002). Little is known about the past intensity, return period and spatial extent of drought events, and the question arises whether these droughts can be attributed to the ongoing warming trend. A reconstruction of drought periods and precipitation patterns in the past would constitute a valuable basis to address the issue.

In semi-arid regions, tree ring width chronologies can provide records of past drought periods (e.g. Yadav 2013; Linares et al. 2012; Li et al. 2006). The climate signal in tree ring width and density proxies is strongest when trees grow at their climatic distribution limit. Drought, however, can also occur in high-rainfall areas and is a recurrent feature of the European climate (European Environment Agency 2001). A great amount of high-resolution proxy data from Europe exists, but many tree-ring based reconstructions focus on high-altitude or high-latitude sites, where tree ring width and density show a strong sensitivity to temperature. Stable isotopes in tree ring cellulose have proven to be the more reliable proxy in areas where tree growth is not strongly dependent on climate, typically at low elevation, mid-latitude sites (e.g. Young et al. 2012; Loader et al. 2008; Saurer et al. 2008), and can therefore help extend climate reconstructions into regions which are not yet well covered (Leavitt et al. 2010).

A complete understanding of past climate variability must include the whole frequency spectrum from inter-annual to multi-centennial scales. A challenge of tree ring based climate reconstructions is the preservation of low-frequency variability in the proxy records. Tree ring width chronologies necessitate the standardization of individual ring width series (Cook et al. 1990a; Cook 1985), remove non-climatic growth trends due to tree age, but also internal and external disturbances, such as fires, insect outbreaks, or competition effects which result in increasing and decreasing ring width trends. However, standardization eliminates also part of the low-frequency climatic trends in the series. Esper et al. (2004) identified the standardization method which is applied to tree ring width and density data as the most important cause of differences in low-frequency trends between different hemispheric scale temperature reconstructions of the past millennium. If appropriate data and methods are used, multi-centennial

variability can be preserved in ring width (Briffa et al. 2002; Esper et al. 2002), but large numbers of samples are required.

There are two important advantages of using tree ring isotopes in this context. First, a strong common signal between trees at a site is usually found, which means that only a few trees (4–6) are necessary to obtain a robust climate signal (Daux et al. 2011; Shi et al. 2011; Leavitt 2010). This is especially beneficial if the number of available samples is limited, e.g. when subfossil wood or ancient building material is used. Second, stable isotope series have a greater potential to retain long-term climatic trends (Gagen et al. 2011). However, a problem can arise when combining different trees or tree cohorts into an isotope chronology, as there might be offsets in average isotope values between individual trees or sub-series. This issue has not always been addressed in the past, but recent studies propose methods to deal with offsets (Gagen et al. 2012; Hangartner et al. 2012; Esper et al. 2010). When using building material or subfossil wood, it is not always possible to determine whether climate or the local site conditions where trees grew are responsible for offsets between overlapping series.

In order to eliminate possible juvenile trends in isotope chronologies, the innermost rings of each tree can simply be left out (Labuhn et al. 2014; Gagen et al. 2007). Few studies have observed or suspected long-term, age-related trends in oxygen isotope chronologies (Esper et al. 2010; Treydte et al. 2006)but δ^{18}O chronologies are usually not standardized. Even without standardization, isotope chronologies cannot retain low-frequency climate variability which exceeds the length of individual series, as it is the case for tree ring width (Cook et al. 1995), if site related factors lead to offsets between individual trees or cohorts. A correction of such offsets might therefore be necessary. However, it induces not only a partial loss of low-frequency climate information, but also makes it difficult to relate differences in absolute isotope values between distant sites to climatic gradients, because the effects of these gradients can be superimposed by the influence of the local environment.

In this article, we present annually resolved chronologies of oxygen isotope ratios in latewood cellulose (δ^{18}O) and tree ring width (TRW) constructed from *Quercus spp.* living trees and timbers at two sites in France: (1) an extension of the previously published series from Fontainebleau (1596–2000) (Etien et al. 2009, 2008) to 1326; and (2) an extension of the previously published series from Angoulême (1860–2004) (Labuhn et al. 2014) to 1360. These chronologies now constitute the longest continuous cellulose δ^{18}O time series in France, covering more than six centuries. The previous studies have investigated correlations between tree ring parameters and meteorological variables at each site. They have shown that TRW does not strongly depend on a single variable, while δ^{18}O responds to summer temperature and moisture availability. Etien et al. (2008) have combined cellulose δ^{18}Oand grape harvest dated from Burgundy to reconstruct the growing season temperature for Fontainebleau. Here, we present a new reconstruction of summer droughts for Angoulême based on cellulose δ^{18}O. Furthermore, we investigate the δ^{18}O variability between trees and between sites: (1) We assess the absolute and relative variability between individual trees and between tree cohorts from the same site. Offsets in average δ^{18}O values between trees and cohorts introduce an uncertainty in tree-ring based climate reconstructions and has implications for the potential to keep a low-frequency signal in tree-ring isotope series. (2) We compare δ^{18}O and TRW between Fontainebleau and Angoulême at different time scales (inter-annual and decadal) to test if they are coherent, and if their relationship is stable over time. As meteorological data are only available for the 20$^{\text{th}}$ century, this comparison can give indications on the temporal stability of the common climatic forcing which influences tree growth and isotope ratios in tree ring cellulose at these sites.

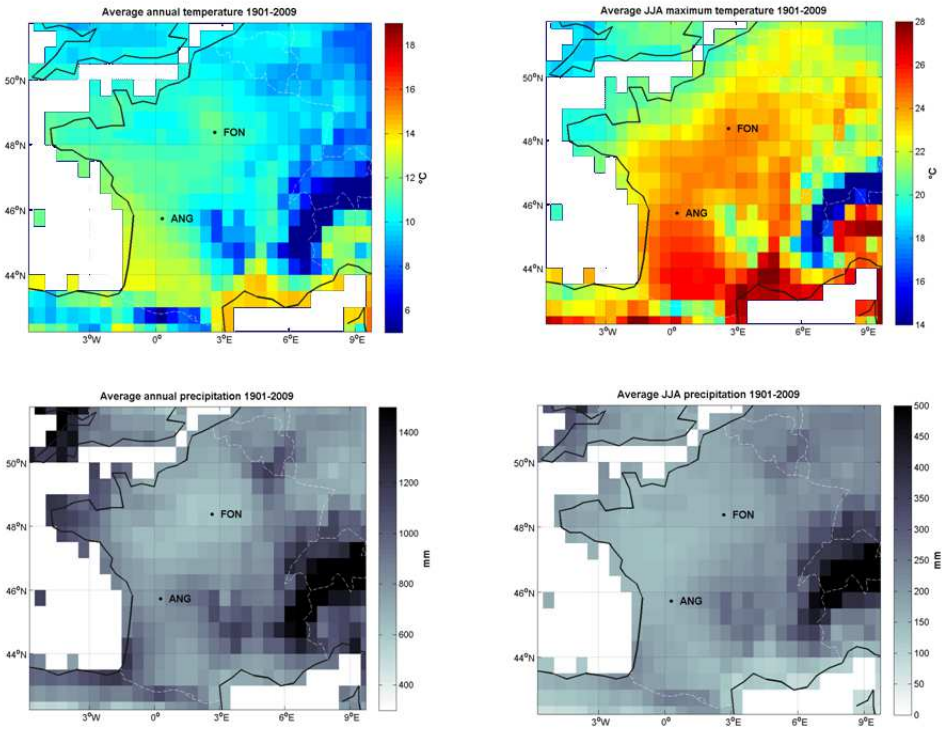

Figure 12.1: Maps of France showing 1901 to 2009 averages of annual temperature, June–August maximum temperature, annual precipitation, and June–August precipitation. Data were obtained from the CRU TW3.10 data set (Harris et al. 2013). The locations of the tree ring chronologies from Fontainebleau (FON) and Angoulême (ANG) are indicated.

12.2 Study Sites

The two studied sites, Fontainebleau (FON; 48°23' N, 2°40' E) and Angoulême (ANG; 45°44'N, 0°18'E; Figure 12.1) are about 300 km away from each other and lie at a similar low altitude: FON 144 m a.s.l., and ANG 110 m a.s.l. The soil at FON is 1.5 m deep and the texture is dominated by sand mixed with loam and clay. ANG is located in a hilly karstic landscape with a cambisol layer of 0.3 to 0.6 m depth.

Both sites are characterized by a temperate oceanic climate. The average annual temperature is between 11.5 °C (FON) and 11.9 °C (ANG), the average summer (JJA) temperature is 18.8 °C at both sites. Average annual precipitation sums range from 600 mm (FON) to 770 mm (ANG), while average summer precipitation at both sites is about 160 mm. FON has remarkably drier winters compared to the ANG.

The interannual variability of summer temperature, precipitation and cloud cover, is very similar at both sites throughout the 20th century, and there is no marked climatic gradient between the sites (Figure 12.2). The same holds true for different drought indices. Furthermore, the drought indices, whether they include only precipitation, or also temperature and soil properties (see Section 12.3.2), identify similar patterns of drought intensity and frequency, e.g. the extremely dry year 1976 which is followed by a period of wetter years. If summer droughts influence the tree ring proxies, we can therefore expect similar interannual variability of the proxies from both sites.

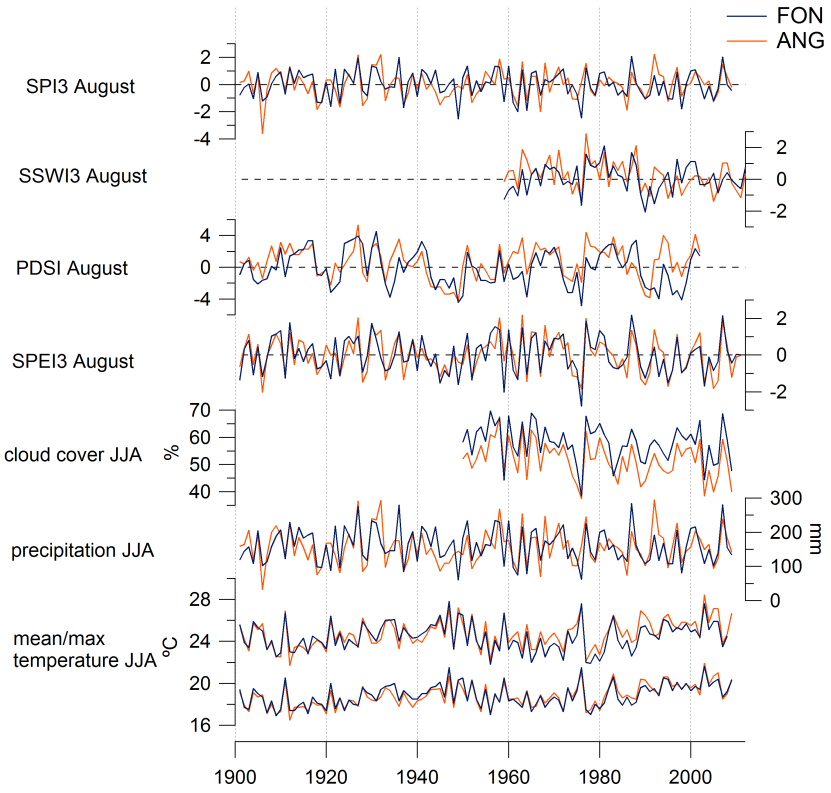

Figure 12.2: Time series of drought indices and meteorological data (June–August averages) for the Fontainebleau (FON) and Angoulême (ANG). See text for data sources.

12.3 Data and Methods

12.3.1 Tree Samples

The previously published FON $\delta^{18}O$ and TRW chronologies (1596–2000; Etien et al. 2009, 2008), constructed from living oak trees from Fontainebleau forest and oak timbers from Fontainebleau castle, were extended using 27 oak timber cores from three buildings of Fontainebleau castle, which constitute different construction periods: Porte Dorée (PD), Chapelle (CH), Petites Ecuries 1 (PE1), and Petites Ecuries 2 (PE2). One core was taken per timber beam. The building wood likely originates from the neighbouring forest (Etien et al. 2008). 14 cores were selected for isotope analysis, resulting in a sample depth of 2 to 9 trees.

The previously published ANG $\delta^{18}O$ and TRW chronologies from Braconne forest (1860–2004; Labuhn et al. 2014) consist of two age groups with an average age difference of 210 years: Braconne young trees (ANG-B), and Braconne old trees (ANG-GR). The chronologies were extended using the older part of the ANG-GR samples (1626–1859) and samples from oak timbers in historic buildings in and around the city of Angoulême (ANG-T), 15 km from the forest. A total of 70 cores was taken from 6 different buildings (one core per timber beam): Angoulême Hôtel de Ville (AHDV), Angoulême Musée (AMUS), Angoulême Maison du Comte (AMDC), Poullignac church (POUL), La Couronne Oisellerie (OISEL), and La Rochefoucauld castle and its stable (LRF). According to the shape and length of the beams, a beam likely corresponds to one tree. The provenance of the timbers is not documented, but a local origin of the wood can be assumed. The possibility to crossdate timber cores and living

trees demonstrates a common climatic influence on interannual ring width variability. A subset of cores was selected for isotope analysis to obtain a sample depth of 4 to 6 trees for each year with sufficient overlap between samples; only between 1556 and 1591 is the number of trees < 4.

The living trees at FON are *Q. petraea*. At ANG, the species has not been determined in the field, but *Q. petraea* and *Q. robur* are the dominant species in the forest. For all timber wood, the oak species is unknown. Although methodologies to determine the species based on wood anatomy exist (for a review see Feuillat et al. 1997), an unambiguous discrimination between *Q. petraea* and *Q. robur* is not possible (Schoch et al. 2004). To our knowledge, there has been no study which compares the $\delta^{18}O$ between oak species, but it is possible that there is an influence of the species on the isotopic composition of cellulose. Even if there is no direct species effect, different species have different site preferences (Lévy et al. 1992), and the site hydrology can influence the $\delta^{18}O$. However, site effects can also influence the $\delta^{18}O$ of trees within a species. We therefore consider that the uncertainty due to unknown site is more important that the uncertainty due to unknown species.

TRW Measurements, Crossdating and Standardization

Tree ring width (TRW) was measured under a binocular microscope using a measurement stage with a precision of 0.01 mm, and cores were crossdated. The crossdating was verified visually and statistically with the programme COFECHA (Grissino-Mayer 2001; Holmes 1983). The cores from the same tree were averaged to form a single TRW series for each tree (1–2 cores from timber samples and 3–4 cores from living trees). The TRW series were standardised with the programme ARSTAN (Cook 1985) to remove non-climatic trends from the series and preserve the inter-annual variability, using a cubic smoothing spline with a 50% variance cutoff at a period of 30 years. This data-adaptive method was chosen because the series differ in length and there is no common growth pattern in all of them, e.g. an exponential decline in TRW with increasing tree age. The low-frequency ring width variability is likely influenced by stand dynamics, e.g. due to felling. Standardization methods like regional curve standardization (RCS; Esper 2003; Briffa et al. 1992) are not useful here because of the small number of samples, and an average biological growth curve cannot be determined if TRW is influenced by competition effects. A chronology was calculated for each site (FON and ANG) as the average of the standardized tree series.

$\delta^{18}O$ – Measurements

For isotope analysis, the selected cores were cut ring by ring with a scalpel and earlywood was separated from latewood. Only the latewood was analysed. Corresponding rings of multiple cores taken from the same tree were pooled. The wood samples were homogenized and cellulose was extracted according to Green (1963) and Leavitt and Danzer (1993). The $\delta^{18}O$ of cellulose was measured using a thermal combustion elemental analyser (Finnigan Thermo TC-EA) coupled with a Finnigan MAT252 mass spectrometer at LSCE in Gif-sur-Yvette, France. The measurements were corrected using the cellulose reference Whatman CC31. Each sample was measured at least twice. The analytical uncertainty was 0.20‰. $\delta^{18}O$ values are reported with reference to VSMOW (Coplen 1994). A total of 1371 samples (787 ANG, 584 FON) was measured for this study, excluding replicates.

δ^{18}O – Pooling of Samples

Due to the time-consuming and costly isotope analysis, the rings of several trees are often pooled prior to analysis. However, pooling masks the inter-tree variability and it is not possible to calculate an error around the mean. For the previously published FON δ^{18}O chronologies, wood from all living tree and timber cores had been pooled for each year. In this study, the new FON samples were pooled by building, thereby grouping together tree cohorts of approximately the same age.

Although the inter-tree variability of cellulose δ^{18}O at a site is generally low, a systematic offset was observed between the old (ANG-GR) and the young (ANG-B) trees at Braconne forest, which is likely due to differences in the site hydrology (Labuhn et al. 2014). We therefore performed an inter-tree comparison for the timber wood, since the sites where the trees grew are unknown, and hydrological differences could induce a different climate response of the trees. We selected the rings of every 5^{th} year of each core for the inter-tree analysis. For the remaining years, the rings of all timber cores were pooled prior to cellulose extraction.

δ^{18}O – Juvenile Effect

A juvenile effect of increasing δ^{18}O during the first 20 years of a tree's life was observed in the trees from site ANG-B (Labuhn et al. 2014). In the ANG data and the new FON data (1326–1595), the juvenile effect was taken into account by omitting the first 20 years of each tree core from the analysis. For the previously published series from FON, several trees had been pooled and a correction is not possible. Furthermore, for most samples, only the calendar year of each ring is known but not their cambial age. It was not possible to verify for the previously measured samples whether the trees had been cored to the pith, and we do not know whether the innermost rings of a core actually correspond to a period of juvenile growth.

δ^{18}O – Cohort Offset Correction

Offsets in the average isotope ratios required a treatment of the raw δ^{18}O values to make them comparable between sites and between tree cohorts. Both the FON and ANG chronologies are composed of several sub-series, which have been analysed separately. The sub-series showed differences in the mean isotope values for their periods of overlap of up to 1‰ (see Section 12.4.2). These offsets are likely due to the local site conditions (competition, microclimate, rooting depth, soil hydrology), because all trees were exposed to the same climatic conditions. ANG-GR and ANG-B sites for example, only 1 km apart, show an average offset of 0.76‰, despite a low inter-tree variability within each site, which can be explained by different water sources (Labuhn et al. 2014). For timber samples, site conditions are unknown.

We tested different methods to merge the overlapping series (see Hangartner et al. 2012) in order to investigate the effects of such offsets on the final chronology: (1) no correction was applied; (2) the mean δ^{18}O values of the older cohorts were adjusted to match the mean of the corresponding younger cohorts in their period of overlap; (3) all cohorts were normalised to have the same mean ($\mu = 0$) before merging them. In all cases, the averages of two cohorts were calculated weighting each cohort by the number of trees.

12.3.2 Meteorological Data and Drought Indices

Monthly meteorological data (average temperature, maximum temperature, precipitation, and cloud cover; 1901–2009) were obtained from the CRU TS3.10 data set (Harris et al. 2013),

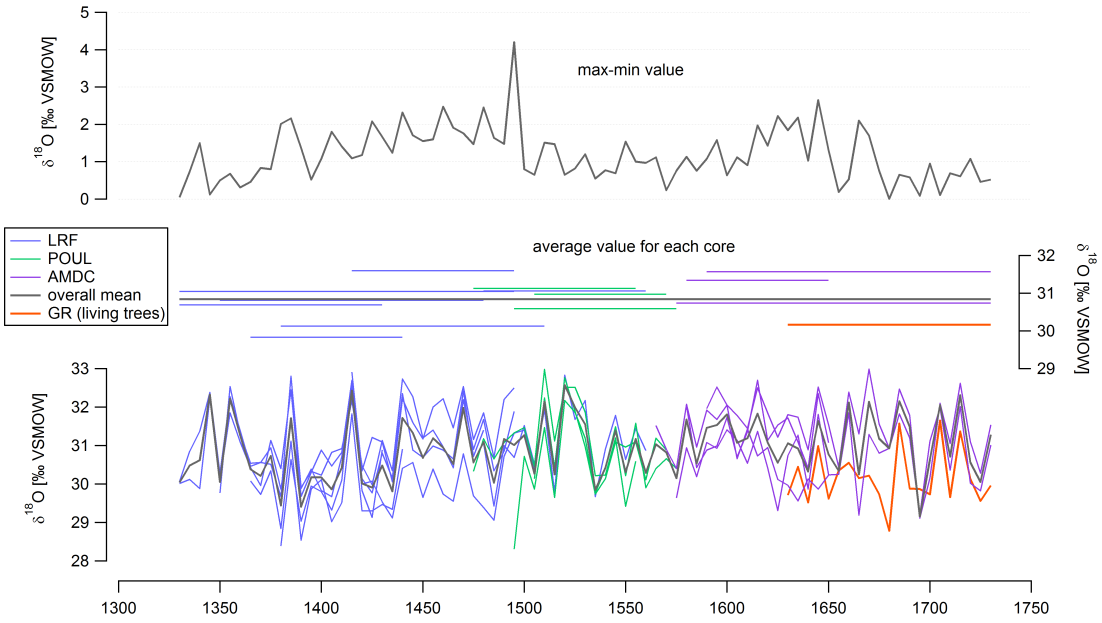

Figure 12.3: Bottom: Cellulose δ^{18}O measured every 5th year for individual timber cores from different buildings in Angoulême (LRF, POUL, and AMDC). The orange line shows the δ^{18}O of living trees (GR). Middle: Time spans and average δ^{18}O values for the respective cores. The thick grey line is the mean δ^{18}O of all timber cores over the whole period. Top: Range of measured values for each year (maximum minus minimum value).

and time series were extracted for the grid cells containing the study sites.

Four different drought indices are employed in this study. (1) The Standardized Precipitation Index (SPI; 1901–2009; McKee et al. 1993). The SPI was calculated for the site grid cells at time steps of 3, 6, 12 and 24 months from CRU TS3.10 precipitation data using the program SPI SL6 (available at http://drought.unl.edu). (2) The Standardized Precipitation Evapotranspiration Index (SPEI; 1901–2001; Beguería et al. 2010; Vicente-Serrano et al. 2010). SPEI data for the site grid cells were obtained from http://sac.csic.es/spei/database.html at a resolution of 3, 6, 12, and 24 months. Their calculation is also based on CRU data. (3) A monthly self-calibrating Palmer Drought Severity index (scPDSI; 1901–2002; van der Schrier et al. 2006). The scPDSI is based on CRU temperature and precipitation data and soil water holding capacities from Webb and Rosenzweig (1993). The calculation of the index is described in Wells et al. (2004). (4) The Standardized Soil Wetness Index (SSWI; 1959–2008; Vidal et al. 2010). The SSWI is a measure of agricultural drought and represents hydrological conditions which are relevant for tree growth. It was calculated for grid boxes over France at a spatial resolution of 8 km. We obtained SSWI data for the grid cells containing our sample site at two different time scales, summer (3-month index June to August, SSWI3-Aug) and growing season (6-month index April to September, SSWI6-Sep).

12.3.3 Statistical Analyses

Statistical analyses were performed using the R software (R Development Core Team 2011). The site chronologies were decomposed to high-pass and low-pass filtered data using a cubic smoothing spline with a 50% variance cutoff at a period of 10 years, which enables a comparison of the inter-annual and decadal variability between series. Running correlations were calculated

between sites, and between the TRW and $\delta^{18}O$ chronologies from a site using a window of 51 years. Pearson's product moment correlation coefficients were calculated between annual tree ring data (TRW and $\delta^{18}O$) and the meteorological variables and drought indices at a monthly and seasonal time scale, in order to investigate the climate response of the trees and to identify the climate parameters which can be reconstructed from the tree ring proxies.

A model for reconstruction of the drought index was developed based on a linear regression between the drought index and cellulose $\delta^{18}O$. The validity of the model was tested by dividing the drought index data into a calibration (2/3 of the values) and a verification data set (1/3 of the values). This enables a quantitative comparison of the reconstructed drought index with independent data which was not used in the calibration. The subsets of data were selected randomly and the procedure was repeated 1000 times. For each iteration, several statistics were calculated, including the standard deviation of all iterations, to evaluate the skill of the model in estimating the drought index: the Pearson correlation coefficient (r), the reduction of error statistic (RE), and the coefficient of efficiency (CE) (National Research Council 2006; Briffa et al. 1988).

RE is a verification test which compares the values estimated by the model with estimates made by presuming that all values of the verification period are equal to the mean of the calibration period:

$$RE = 1 - \frac{\sum_{i=1}^{n}(y_i - \hat{y}_i)^2}{\sum_{i=1}^{n}(y_i - \overline{y})^2} \tag{12.1}$$

where y_i is the observed data, $\hat{y}_i$ denotes the reconstructed values for the verification period, and $\overline{y}$ is the mean of the dependent data set used for calibration. If the reconstructed values are closer to the observed independent data than the average value of the calibration period, RE is greater than zero. In this case, the reconstruction has a predictive value.

To calculate the CE, the mean of the dependent data set ($\overline{y}$) is replaced by the mean of the verification data in Equation 12.1. The CE is measure of the common variance between the observed and the estimated data over the verification period.

Splitting the period of measurements into a calibration and verification period is necessary in order to verify reconstruction results. After the model for reconstruction was verified using the split data set, a new model was calibrated using the entire period of the observed drought index. Based on the final model, the drought index was reconstructed for the full length of the $\delta^{18}O$ chronology. The confidence interval around the reconstruction was determined based on the differences between the measured and the reconstructed drought index values (± 2 standard deviations of the differences).

12.4 Results

12.4.1 Inter-tree Comparison for ANG Timber Samples

The difference in the average cellulose $\delta^{18}O$ values of ANG timber cores which were measured individually every 5th year is up to 1.8‰ (Figure 12.3). It is highest for the LRF cores (1.77‰), low for POUL cores (0.53‰), and intermediate (0.83‰) for AMDC cores. The difference between cores which do not cover exactly the same time period can also be due to

changing climatic influence. However, the offset in δ^{18}O for cores which largely overlap illustrates that possible individual tree or site effects influence the mean δ^{18}O. The difference between the maximum and minimum values of a single year ranges from 0.01‰ to 4.20‰, the mean difference being 1.18‰.

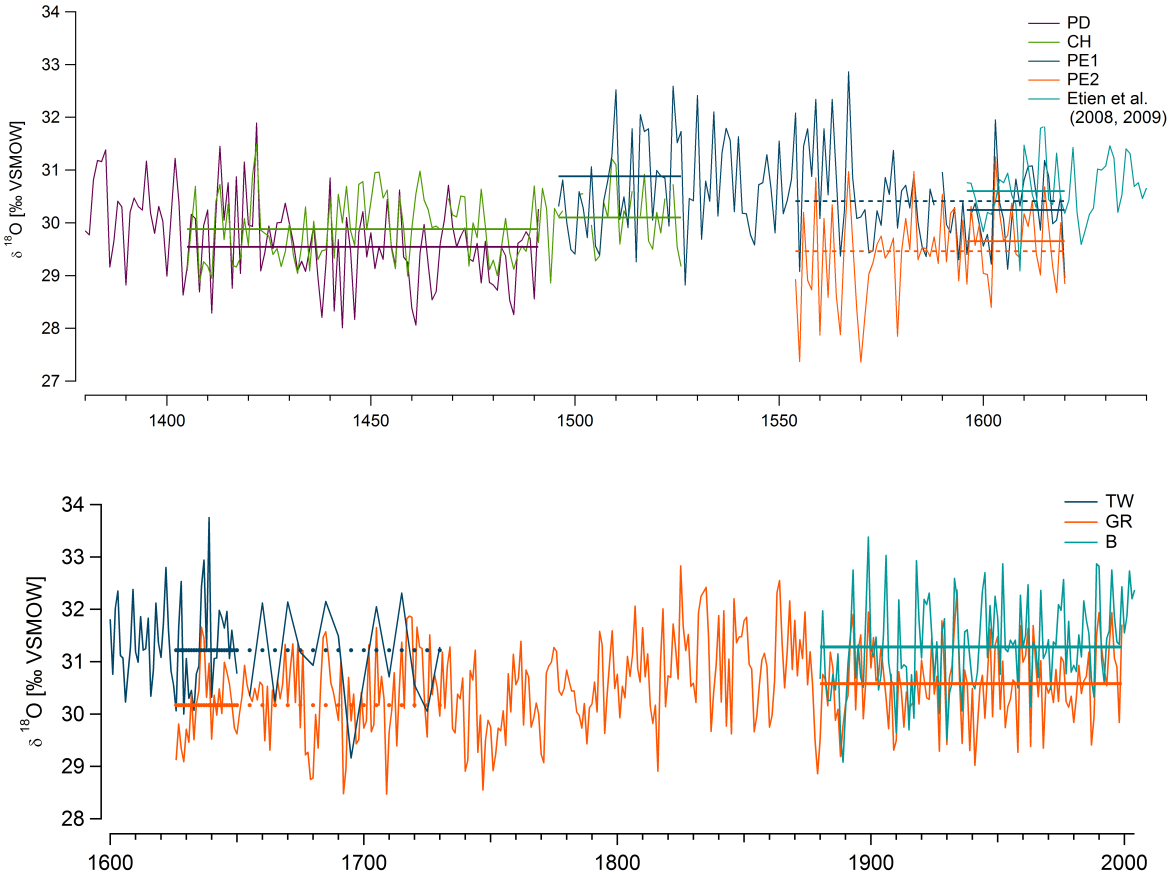

Figure 12.4: Top: The cellulose δ^{18}O series for different tree cohorts from Fontainebleau (FON). Bottom: The cellulose δ^{18}O series for living tree cohorts (B and GR), and timber wood (TW) from Angoulême (ANG). Horizontal lines indicate the mean of each series for the period of overlap. TW samples have been measured every 5$^{\text{th}}$ year only in the period covered by the dotted line.

Table 12.1: Offsets in average cellulose δ^{18}O values and correlations between tree cohorts for their periods of overlap.

Site	Cohorts	Offset [‰]	Correlation	Years of overlap
FON	PD–CH	0.34	0.38	87
	CH–PE1	0.78	0.50	31
	PE1–PE2	0.96	0.53	66
	PE1–Etien et al. (2008)	0.36	0.19	24
	PE2–Etien et al. (2008)	0.95	0.22	24
ANG	B–GR	0.76	0.6	120
	GR–T	1.05	0.63	41

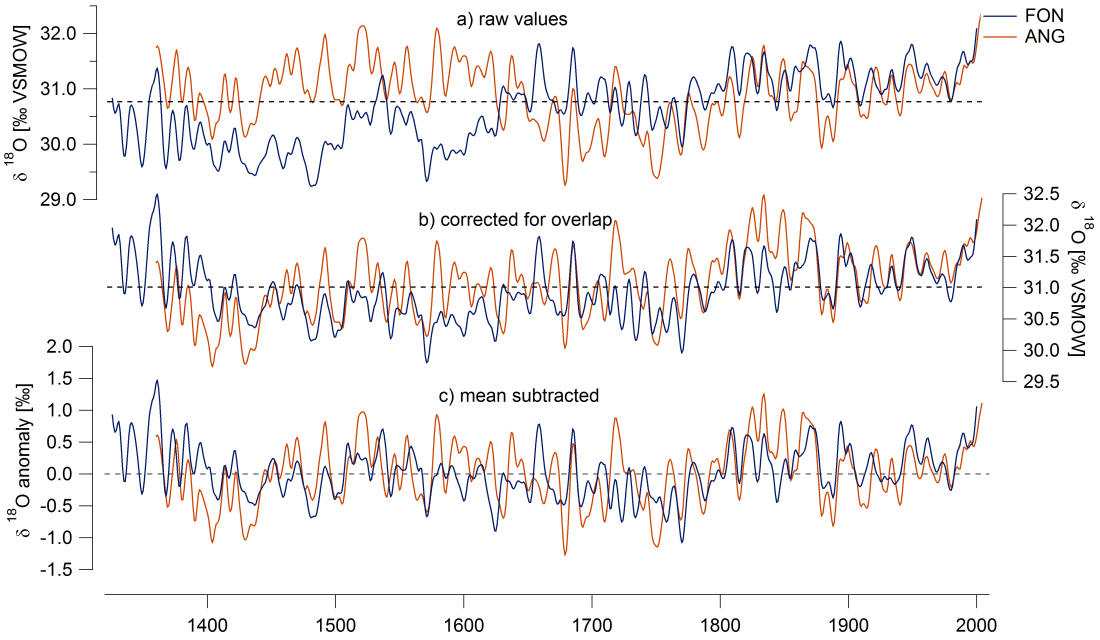

Figure 12.5: δ^{18}O chronologies from Fontainebleau (FON) and Angoulême (ANG), low-pass filtered data. Different methods were used in order to combine overlapping tree cohorts to a site chronology: (a) the original measured values; (b) the chronologies were corrected for the offset between cohorts (see Figure 12.4), by adjusting the mean of the older cohorts to the mean of the respective younger cohort; (c) all cohorts were normalised by subtracting the mean of each cohort from the respective δ^{18}O values before combining them. In each case, an average weighted by the number of trees was then calculated for overlap periods between cohorts.

Despite the differences in average values, these series display a coherent year-to-year variability. The average correlation coefficient between cores is $r = 0.72$, the average Gleichläufigkeit (Schweingruber 1988) is 76%, and the expressed population signal (EPS; Wigley et al. 1984) is 0.97. There is no relationship between average cellulose δ^{18}O and average ring width or mean sensitivity (Fritts 1976) of the cores.

12.4.2 Offsets Between Tree Cohorts

At both FON and ANG sites, separately analysed tree cohorts show offsets in the average δ^{18}O during their overlap periods (Table 12.1; Figure 12.4). Despite significant correlations between cohorts, there are differences in the absolute δ^{18}O values of up to ~ 1‰. The method to join the cohorts in order to form a long chronology significantly influences the long-term trends in this chronologies (Figure 12.5). For FON, a correction of the offset leads to values which are on average > 1‰ higher than the uncorrected values before 1600. For ANG, the corrected values are lower on average than the raw values before 1640, and higher on average after this year.

The corrected series of FON and ANG (with the mean of the older cohort adjusted to the mean of the younger cohort for the period of overlap, or centred to a mean of zero), show a good agreement for the centennial trends (Figure 12.5). The uncorrected series, on the contrary, differ in long-term trends and display large differences in the δ^{18}O values before 1620, although the

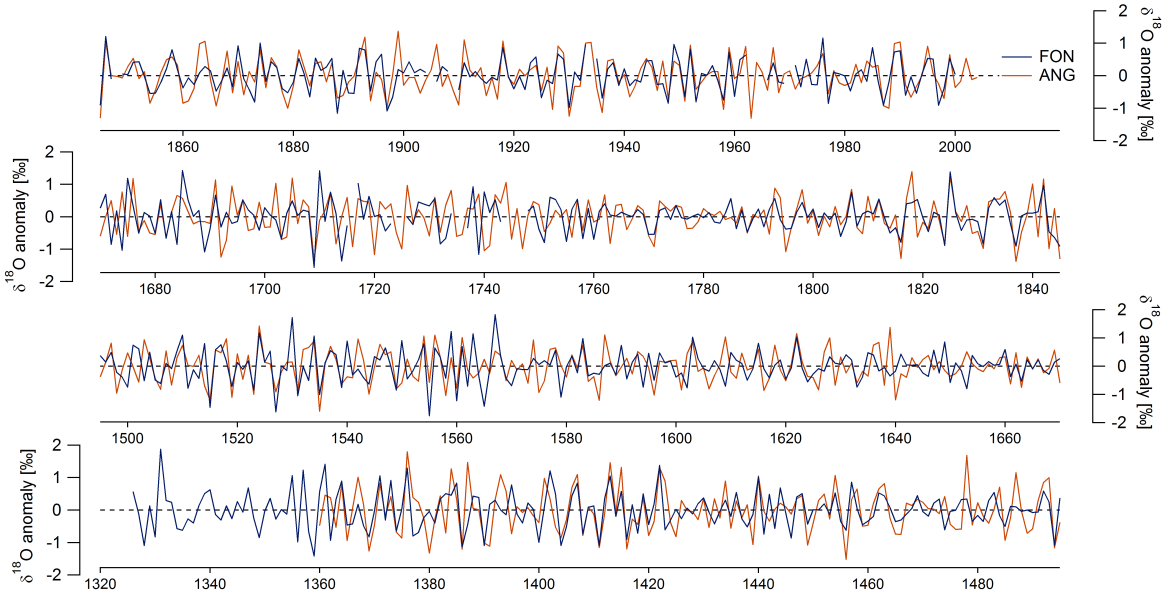

Figure 12.6: Inter-annual variability in δ^{18}O chronologies from Fontainebleau (FON) and Angoulême (ANG), high-pass filtered data.

decadal trends are largely synchronous. The subsequent analyses are based on the chronologies which are corrected by subtracting the mean from each cohort before merging them.

12.4.3 δ^{18}O and TRW Site Chronologies

The δ^{18}O chronologies from FON and ANG are highly correlated during the 20th century. The correlation shows a marked decrease between 1550 and 1800. These patterns are similar for the inter-annual variability and the decadally smoothed chronologies (Figure 12.6; Figure 12.7). The standard deviation calculated for a 51-year moving window illustrates common periods of low inter-annual variability at FON and ANG around 1470, 1620 and 1800.

The TRW chronologies are also characterised by periods of stronger and weaker correlations between sites, but these periods differ from the ones observed in the δ^{18}O chronologies. Changes in running standard deviation of TRW are less coherent between sites compared to δ^{18}O, and could be linked to changes in sample depth (Figure A.4; Figure A.5). Correlations show that TRW is less sensitive to climate variations than cellulose δ^{18}O (see following section), and possibly more prone to react to non-climatic influences such as changes in competition. The comparison of sites should be interpreted with more caution with respect to climate.

12.4.4 Correlations with Drought Indices and Meteorological Variables

The strength and direction of the correlations between cellulose δ^{18}O and different meteorological variables and drought indices is very similar for FON and ANG (Table A.1). Cellulose δ^{18}O is positively correlated to temperature during the summer months, with stronger correlations for maximum temperature than for average temperature. The strongest correlations are obtained with maximum temperature averaged over June, July and August. Negative correlations are obtained with cloud cover, precipitation, and the different drought indices during

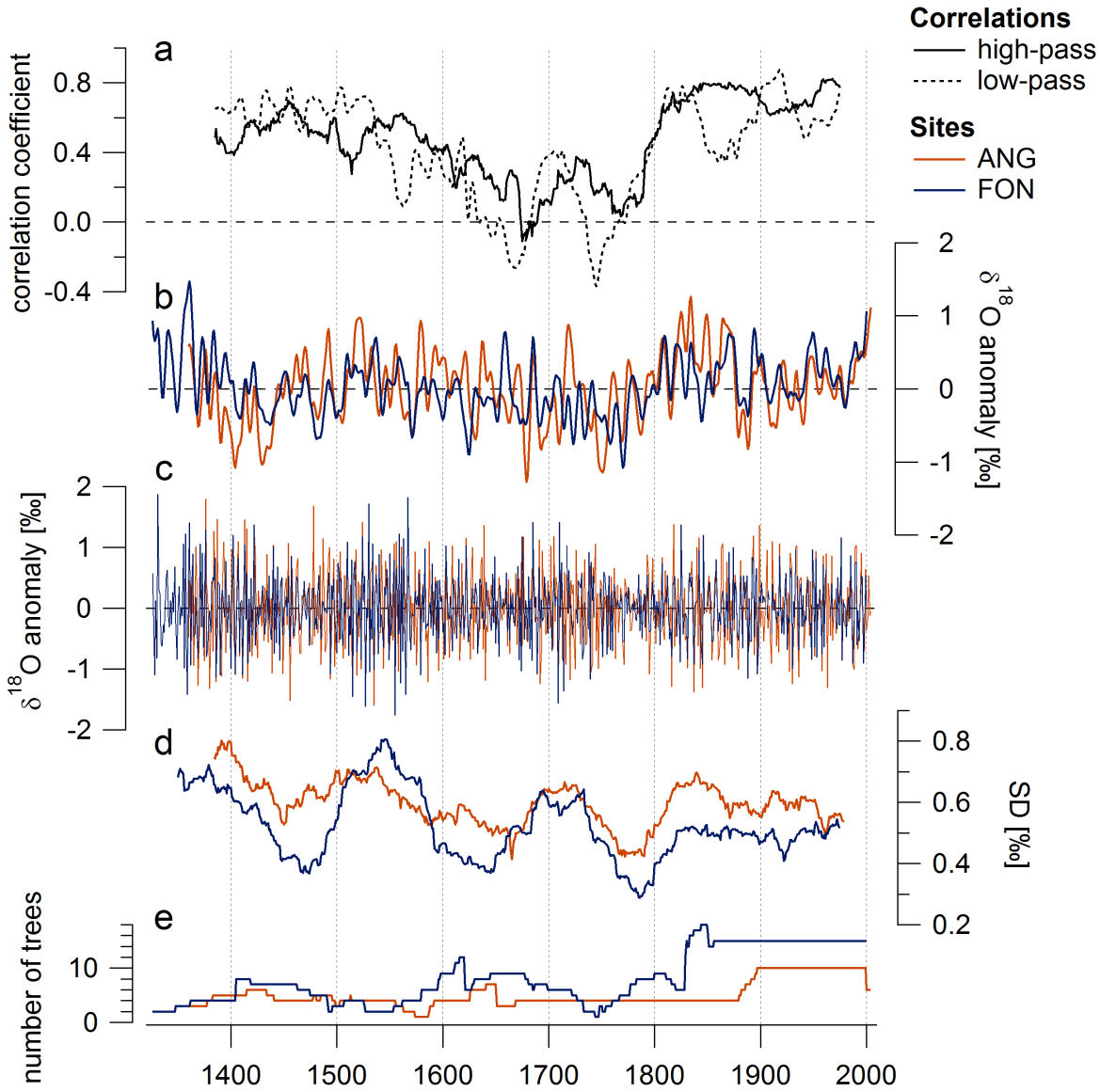

Figure 12.7: Comparison of δ^{18}O chronologies from Fontainebleau (FON) and Angoulême (ANG). (a) 51-year running correlation between FON and ANG; (b) low-pass filtered data; (c) high-pass filtered data; (d) standard deviation of the high-pass filtered data calculated for 51-year running windows; (e) number of trees.

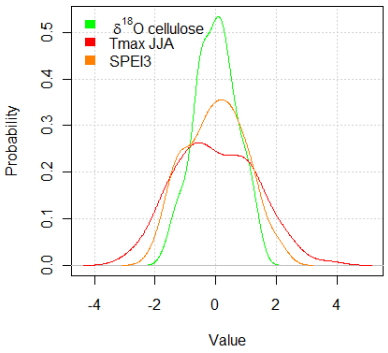

Figure 12.8: Probability distribution of cellulose δ^{18}O, summer (JJA) maximum temperature and SPEI values, all centred at a mean of zero.

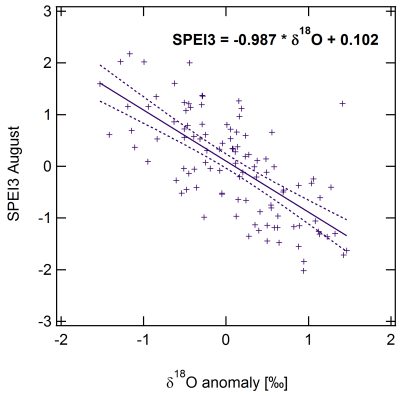

Figure 12.9: Linear regression between the SPEI3 and cellulose δ^{18}O. The equation describing the regression line provide the model for drought reconstruction.

Table 12.2: Comparison of reconstructed and observed climate variables: correlation coefficient (r), reduction of error statistic (RE) and coefficient of efficiency (CE). To calculate these statistics, the data were divided into randomly selected calibration (2/3) and verification (1/3) data sets. The given values are the averages and standard deviations of 1000 iterations of this validation.

Climate Variable	Statistic	Average	Standard Deviation
Temperature	r	0.71	0.06
	RE	0.48	0.09
	CE	0.45	0.11
SPEI3	r	0.69	0.09
	RE	0.45	0.14
	CE	0.42	0.15

the summer months. Again, correlations are improved when considering the summer months together (precipitation sums for June to August, and the multi-scale drought indices at a 3-month resolution which integrate June to August). The strongest correlations are obtained with the SPEI3 drought index. The probability distribution of δ^{18}O, JJA maximum temperature, and SPEI3 values indicate that extreme meteorological conditions might be less well represented in the δ^{18}O chronology, and that the distribution of δ^{18}O values is closer to the drought index than to temperature (Figure 12.8). The relationship between δ^{18}O and maximum JJA temperature/SPEI3 is relatively stable throughout the 20$^{\text{th}}$ century, as correlation coefficients (r) calculated for a 31-year moving window vary only slightly (standard deviation of r is 0.05 for temperature and 0.04 for SPEI3).

TRW is negatively correlated to temperature, and positively correlated to precipitation, cloud cover, and the drought indices (Table A.1). However, the correlations are generally weaker, and the climate response of TRW is less coherent between FON and ANG than to cellulose δ^{18}O. FON displays significant correlations with precipitation and drought indices, which may be related to the low water holding capacity of the soil.

12.4.5 Drought Reconstruction

Considering the low climate sensitivity of the TRW proxy compared to cellulose $\delta^{18}O$ in the temperate climate of France, and the fact that relatively few trees are used in this study, this reconstruction will be based only on $\delta^{18}O$. We selected the August SPEI drought index at a 3-month resolution (SPEI3) for the reconstruction. This index integrates drought conditions during the summer months (JJA). It has higher correlations with $\delta^{18}O$ than the other indices and provides a longer time series for calibration than the SSWI (104 vs. 46 years). The correlation between SPEI3 and $\delta^{18}O$ is $r = -0.69$ ($p < 0.001$, $N = 104$). The equation describing the linear regression line between the two variables is used to estimate the drought index SPEI3 from cellulose $\delta^{18}O$ (Figure 12.9). The r, RE and CE statistics give satisfying results and confirm the validity of the model (high r, positive RE and CE; see Briffa et al. 1988; Table 12.2). The squared correlation is $R^2 = 48$, which means that 48% of the variability in the drought index is accounted for by the model. The standard deviation of the differences between modelled and observed SPEI3 is 0.7, which defines the confidence interval for the reconstruction (Figure 12.10).

The oldest part of the reconstruction is characterised by a prolonged period of relatively wet conditions (1360–1450), followed by a period of drier conditions until 1600 (Figure 12.11). Another wet period until 1760 follows, with a short increase to relatively drier conditions around 1720. The most marked trend in the reconstruction is the shift to dry conditions from 1760 to 1850. The late 20th century is characterized by increasingly dry summer, but these SPEI values are not unprecedented in the record.

12.5 Discussion

12.5.1 Variability Between Trees and Cohorts

Despite the relative coherence in the inter-annual variability, there are absolute differences between individual trees and between tree cohorts of up to more than 1‰. Although the local origin of the timber samples cannot be ascertained, it is likely that the construction wood has not been transported very far. When the overlap between cohorts is short, we cannot exclude that the shifts are – at least partly – climatic because changes of this magnitude in the average $\delta^{18}O$ exist within one cohort, e.g. the increase from 1750 to 1815 in ANG-GR. It might be possible to verify this by comparison with other proxies. However, an influence of local site conditions (soil hydrology, competition, microclimate) is likely for the cohorts which largely overlap but still differ in average $\delta^{18}O$ values, and these site conditions cannot be verified for timbers or subfossil wood. $\delta^{18}O$ can also vary around the circumference of a tree (see e.g. Szymczak et al. 2012 and references in Leavitt 2010), which could contribute to the inter-tree variability in the timber wood, where only one core per beam was taken (compared to 3–4 cores from the living trees).

Standardisation therefore seems necessary when combining different trees or cohorts in order to avoid artificial trends in the final chronology, even if this implies a partial loss of the low-frequency variability. A solution to this problem would be to increase the sample size and to measure trees individually, possibly at the expense of the temporal resolution. This would allow to identify outliers and to calculate a confidence interval around the mean $\delta^{18}O$ value. However, it could be problematic to find appropriate samples for the older periods where no living tree material is available.

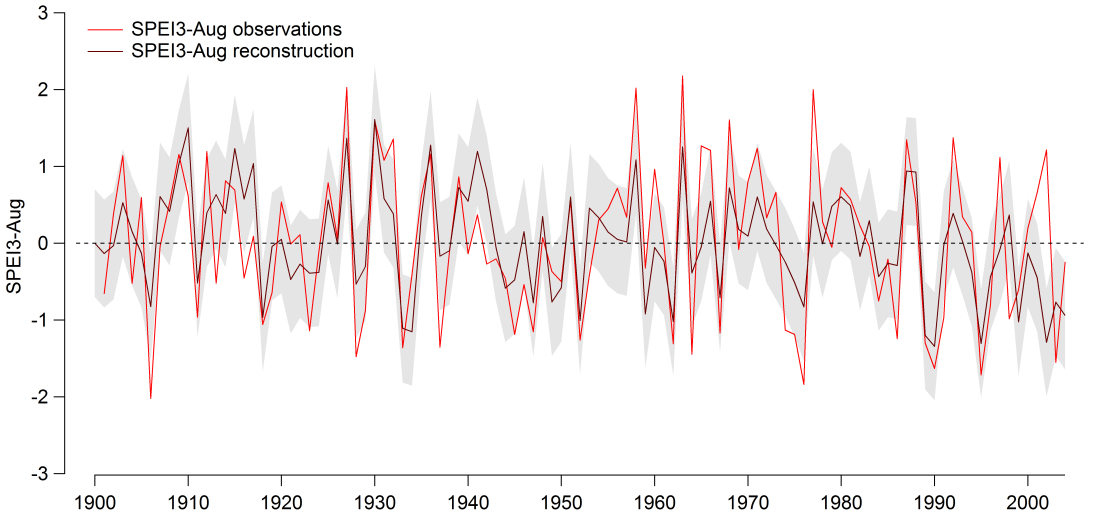

Figure 12.10: Observed and reconstructed drought index SPEI for August (3-month resolution). Negative values indicate dry conditions. The shaded are marks the confidence interval of the reconstruction.

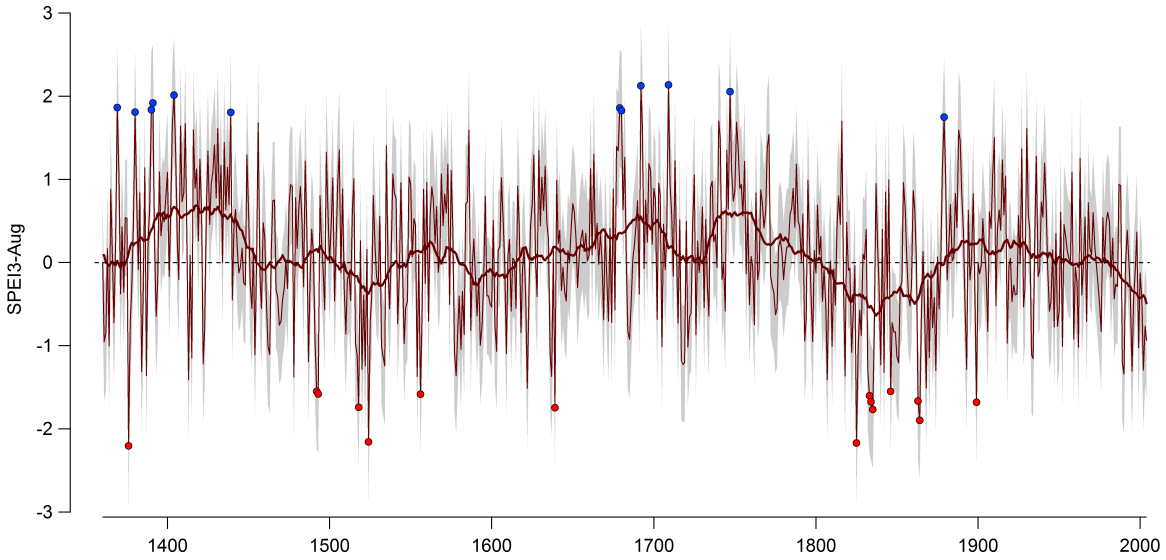

Figure 12.11: Reconstruction of summer droughts at Angoulême, expressed by the SPEI drought index at a 3-month resolution, based on tree ring cellulose $\delta^{18}O$. The thick line is the 31-year running mean. The shaded are marks the confidence interval of the reconstruction. Blue and red circles indicate the wettest and driest years respectively (more than ±2 standard deviations from the mean).

It might not be appropriate to compare absolute isotope values at different sites, and there is a risk of introducing artificial shifts or trends in the series which are not climatic when averaging uncorrected series. By applying a normalization, low-frequency climate variability which exceed the length of the cohorts may not be preserved.

12.5.2 Coherence Between Site Chronologies and Temporal Stability

The δ^{18}O chronologies from FON and ANG reveal common patterns of variability on different time scales, but their relationship is not stable over time. High correlations between the two isotope chronologies, e.g. during the 19th and 20th century, indicate a common forcing factor on cellulose δ^{18}O variability. The only possible forcing which is coherent on this spatial scale is climate. We propose two hypotheses to explain the decline in the correlation between sites prior to 1800 AD: (1) a changing climate sensitivity of the trees; and (2) changing climate patterns over France.

Proxies often show a non-linear response to climate Schleser et al. (1999). The climate sensitivity of trees is known to change with time, with tree age, and also between individual trees (e.g. Rozas and Olano 2013; Linares et al. 2012; Dorado Liñán et al. 2011a; Voelker 2011; Reynolds-Henne et al. 2007). The periods of low correlation between sites could be explained by a weaker climate sensitivity of the proxy, i.e. the δ^{18}O is not strongly influenced by variations in temperature or drought variability. This hypothesis is supported by the fact that the amplitude of inter-annual variability at both sites (illustrated by the running standard deviation; Figure 12.7) also declines when correlation are low, except in the 15th century, where a high correlation coincides with a low standard deviation.

If the climate response of the tree changes, this has implications for our climate reconstruction, which is based on the climate-proxy relationship during the 20th century, where instrumental measurements of meteorological variables are available.

A second explanation for the temporal instability of the correlations between the FON and ANG oxygen isotope chronologies could be a change in the regional homogeneity of the climate. The 20th century is characterized by coherent patterns in all available meteorological variables at FON and ANG (Figure 12.2), and during this period we observe high correlation between the δ^{18}O chronologies. However, the climate in France might have been more heterogeneous in the past. Yiou et al. (2012) have identified a shift in the North–South temperature gradient in France during the Little Ice Age based on historical records of grape harvest dates. The authors relate this shift to changes in the prevailing atmospheric circulation over the North Atlantic. Although the temperature difference does not impact the the relationship between cellulose δ^{18}O records at distant sites, the study illustrates that atmospheric circulation changes can have different impacts on the local climate on spatial scales which correspond to the distance between our sites.

While temperature variations are likely to be coherent between the sites at a time scale which is relevant for the proxy, i.e. the growing season, precipitation patterns are generally more variable in space. There are two effects of precipitation on the δ^{18}O of cellulose. First, moisture availability and relative humidity during the growing season influence transpiration and therefore the isotopic composition of the leaf water. Second, the isotopic composition of precipitation determines the isotopic composition of the source water. The season of the trees water supply (e.g. winter or growing season precipitation), is likely to vary over time and between sites. Therefore, changes in the spatial and seasonal distribution of precipitation could be re-

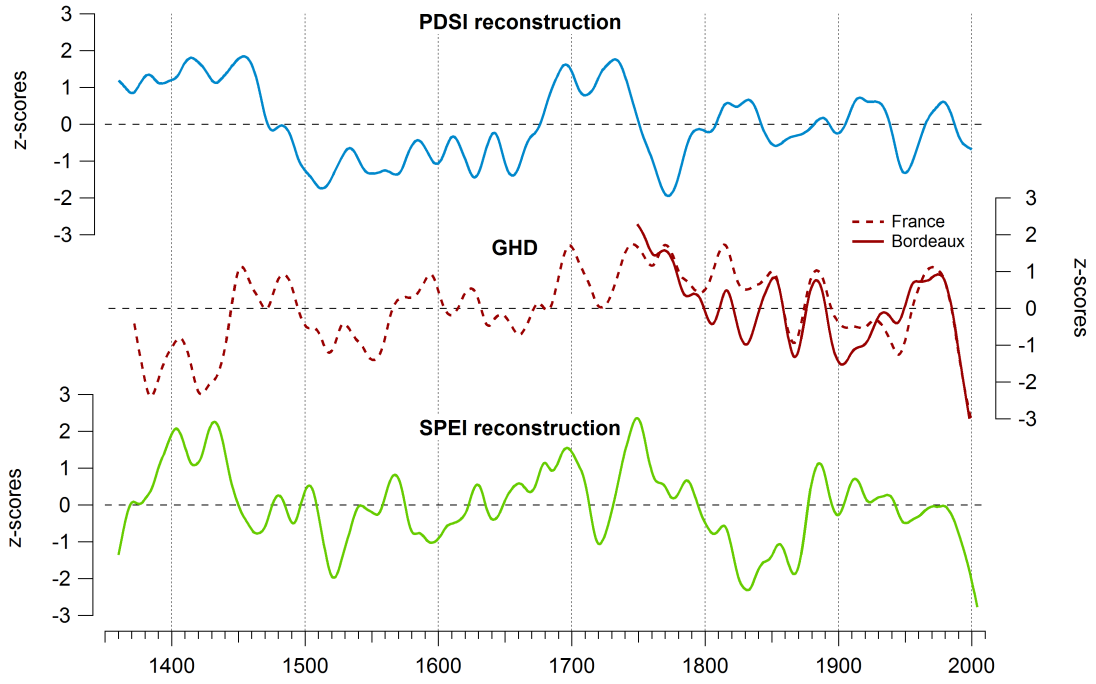

Figure 12.12: Reconstruction of the SPEI drought index for Angoulême comared to other climate records: grape harvest dates (GHD) in Bordeaux and a composite GHD record for France (Daux et al. 2012); a PDSI reconstruction based on Mediterranean tree ring proxies (Nicault et al. 2008).

sponsible for the temporal instability of the relationship between the FON and ANG δ^{18}O chronologies.

12.5.3 Drought Reconstruction and Comparison with Other Records

The relationship between the tree ring proxies and climate observed at our sites match the results of previous studies in temperate regions (e.g. Haupt et al. 2011; Mérian et al. 2011; Hilasvuori and Berninger 2010; Treydte et al. 2007; Szczepanek et al. 2006). As the climatic and non-climatic influences of TRW are complex, this reconstruction is based on oxygen isotope ratios in cellulose. The cellulose δ^{18}O is related to drought conditions because they influence the δ^{18}O of the source water and the physiological processes in a tree. High temperature and low relative humidity increases the evaporation of leaf water, which leads to higher cellulose δ^{18}O values (e.g. Gessler et al. 2013; Sternberg 2009; Barbour et al. 2004). Furthermore, a higher condensation temperature of the rain water and evaporation from falling drops and from soil water increases the δ^{18}O of the source water (e.g. Gat 1996).

We selected the drought index SPEI for reconstruction because it yielded the highest correlations with cellulose δ^{18}O. This index includes the potential evapotranspiration, and it might therefore be more representative of the influence on tree physiological processes than e.g. the SPI, which is based on precipitation alone. Drought indices which incorporate soil moisture, like the PDSI or the SSWI, should reflect the hydric state of the trees. However, the soil water holding capacity is derived from coarse gridded data sets of soil properties, which might not be representative of the sites.

The validity of the local drought reconstruction from Angoulême is supported by the high correlation between drought index and cellulose $\delta^{18}O$, as well as the verification of the model by independent data. Moreover, a comparison with other proxy records of summer climate shows a relatively good agreement with our reconstruction (Figure 12.12).

Tree ring cellulose $\delta^{18}O$ is significantly correlated ($r = –0.50$) with grape harvest dates (GHD) from the Bordeaux region (Daux et al. 2012). The correlation with a French composite GHD record is only moderate ($r = –0.27$) at the inter-annual scale, but the long-term variability in both records displays common trends, e.g. an increase from 1500 to 1750 AD, followed by a decrease in the mid-18th and 19th century. GHD are influenced by agricultural practices, but they also depend on summer temperature. Warm and dry summers therefore lead to high cellulose $\delta^{18}O$ values, and early grape harvest.

Records of the regional hydroclimate are rare, but Nicault et al. (2008) provide a gridded data set of April–September PDSI reconstruction. This record, extracted for the grid box which contains the ANG site, shows a different long-term variability of drought, and is not correlated to the ANG $\delta^{18}O$ time series. However, the reconstruction is based on interpolations of tree ring records from the Mediterranean region, and our study site is at the limits of this interpolation.

12.6 Conclusions

This study has demonstrated that oxygen isotope ratios in tree ring cellulose can provide records of summer droughts in the past. The observed offsets in absolute $\delta^{18}O$ values between trees and between cohorts highlights the importance of isotope measurements on individual trees in order to detect such characteristic in the isotope series. If corrections need to be applied to account for these offsets, however, a part of the low-frequency variability in the chronology might be lost. Moreover, the effect of non-climatic factors on the average $\delta^{18}O$ value makes it difficult to use tree ring isotope networks to reconstruct spatial gradients in climate.

Nevertheless, the trees studied here display a very good agreement in the inter-annual variability, and highly significant correlations with climate variables. This has enabled a reconstruction of summer droughts in the southwest of France during the last 650 years. However, the comparison between distant sites indicates that response of the proxy to climate might be non-linear, or that the spatial patterns of climate in France have changed. A detailed comparison of other proxy records will be necessary to confirm this hypothesis.

13 A Multi-Proxy Approach to Drought Reconstruction

Tree rings have been the principal source of information for hemispheric-scale temperature reconstructions of the past millennium (D'Arrigo et al. 2006; Briffa et al. 2004; Esper et al. 2002; Mann et al. 1999). Their advantage lies in the annual resolution and the precise dating. Tree ring proxies can be well replicated and quantified by comparing them directly to meteorological variables from the year of ring formation. Their calibration is based on the statistical relationships with climate. Models for climate reconstruction based on these relationships can be verified using independent meteorological data, i.e. data which has not been used in the calibration, and the variance explained by the model can be quantified (e.g. Briffa et al. 1992). However, tree ring proxies can be biased towards climate conditions during the growing season, and a reconstructed summer temperature, for example, might not be representative of the evolution of the annual temperature (Jones et al. 2003). Furthermore, tree rings, in particular tree ring widths, are limited for reconstructing low-frequency climate variability because of the standardization process and the limited length of individual tree series (Moberg et al. 2005; Esper et al. 2004; Cook et al. 1995).

Speleothems have the potential to provide a low-frequency signal. However, the dating of speleothems is less precise. Despite the high analytical precision which can be achieved for U-Th dating (Cheng et al. 2013; Hoffmann et al. 2009), and the possibility to count annual growth layers in some speleothem samples (Shen et al. 2013; Baker et al. 2008; Tan et al. 2006), slight changes in the growth rate, or even short hiatuses increase the error in the chronology, making it difficult to compare a stalagmite record to instrumental data or to high-resolution proxy data from tree rings. While adequate samples, which have a high growth rate and a precisely dated lamination, enable a direct calibration by comparison with meteorological data (e.g. Proctor et al. 2000; Genty and Quinif 1996), in many cases the calibration relies on an understanding of the cave processes, based on cave monitoring data, laboratory experiments, and modelling exercises (e.g. Treble et al. 2013; Wackerbarth et al. 2012; Tremaine et al. 2011; Genty 2008; Spötl et al. 2005). Lastly, an environmental signal can be lagged and/or attenuated before it is transmitted to the cave interior (Fairchild and Baker 2012), whereas tree ring proxies often reflect the environmental signal directly, i.e. during the current growing season.

13.1 Combining Tree Ring and Speleothem Proxies

Few studies have attempted to directly compare tree rings and speleothems. Berkelhammer et al. (2013) and Trouet et al. (2009) used tree ring and speleothem proxy records from remote regions to study teleconnections and atmospheric circulation indices. Betancourt et al. (2002) compared annual band widths in tree rings and a stalagmite from the same site and found no correspondence, but their approach has been criticized because even if the banding in both archives is annual, the band width in each proxy might not depend on the same

influences (Baker and Genty 2003). However, if tree ring and speleothem proxies from the same region respond to the same dominant factors, e.g. droughts, they can show similar patterns (Wassenburg et al. 2013; Sinha et al. 2011).

Managave (2014) used a model to investigate to what extent the oxygen isotopic composition of tree ring cellulose and speleothem calcite can be correlated if they have the same source water. The author determined that a correspondence between these proxies is likely when the variation in the $\delta^{18}O$ of precipitation is high compared to the variation induced by the influences on each single proxy (i.e. the cave temperature and equilibrium disequilibrium conditions during precipitation for calcite $\delta^{18}O$, and relative humidity, leaf temperature and the isotopic composition of atmospheric water vapour for cellulose $\delta^{18}O$).

The specificity of this thesis is that both isotope proxies are compared directly, and not the reconstructed climate variables. The previous chapters have shown the calibration of speleothem and tree ring proxies from the southwest of France, and have identified climatic and non-climatic influences on these proxies. The fluid inclusion $\delta^{18}O$ measurements from Villars cave potentially provide a record of palaeo-precipitation $\delta^{18}O$, and the cellulose $\delta^{18}O$ series from Angoulême enables the reconstruction of summer droughts. However, each of the proxies is afflicted with its own uncertainties. We will now explore the potential and limits of a multi-proxy climate reconstruction based on oxygen isotope records from speleothem fluid inclusions and from tree ring cellulose. Their combination might enable a reconstruction of both high- and low frequency climate variability.

We can assume that the closely located sites of Villars and Angoulême, at approximately the same altitude and distance from the coast, experience similar variations in temperature, moisture conditions, and in the isotopic composition of the precipitation feeding the soil water reservoir which is tapped by the trees, and which infiltrates into the cave. We therefore hypothesise that it is possible to use the fluid inclusion $\delta^{18}O$ as an independent estimation of the source water $\delta^{18}O$ for the trees. In a first step, we investigate the co-variation of the two time series, the fluid inclusions and the cellulose $\delta^{18}O$. In a second step, we assume that the fluid inclusion $\delta^{18}O$ represents the tree source water $\delta^{18}O$, and, using the cellulose $\delta^{18}O$, we calculate the isotopic enrichment of the leaf water above the source water, as well as relative humidity, which is the dominant controlling factor of this enrichment. Then, we compare this reconstruction of relative humidity with the drought reconstruction based only on tree rings.

13.2 Speleothem Fluid Inclusions vs. Tree Ring Cellulose $\delta^{18}O$

For this comparison, the cellulose $\delta^{18}O$ time series was smoothed by a 25-year running mean, which was chosen because it corresponds to the time period represented in a fluid inclusion sample, which can be approximated from sample size, growth rate and infiltration time (Chapter 10). The $\delta^{18}O$ records in tree-ring cellulose from Angoulême and in speleothem fluid inclusions from Villars cave display some common trends: a decrease from 1500 to 1700, an increase from 1750 to present, and a marked peak around 1720 is seen in both records (Figure 13.1). However, there is also a period where the two series show opposing trends, between 1360 and 1500. Furthermore, even if the general increasing trend in the most recent period is apparent in both records, the large increase in the cellulose time series from 1750 to 1850 and the subsequent rapid decrease are not seen in the fluid inclusions. The range of absolute $\delta^{18}O$ values in both the fluid inclusions and the smoothed cellulose $\delta^{18}O$ time series is about 2‰. However, the common peak at 1720 AD is about twice as large in the fluid inclusions.

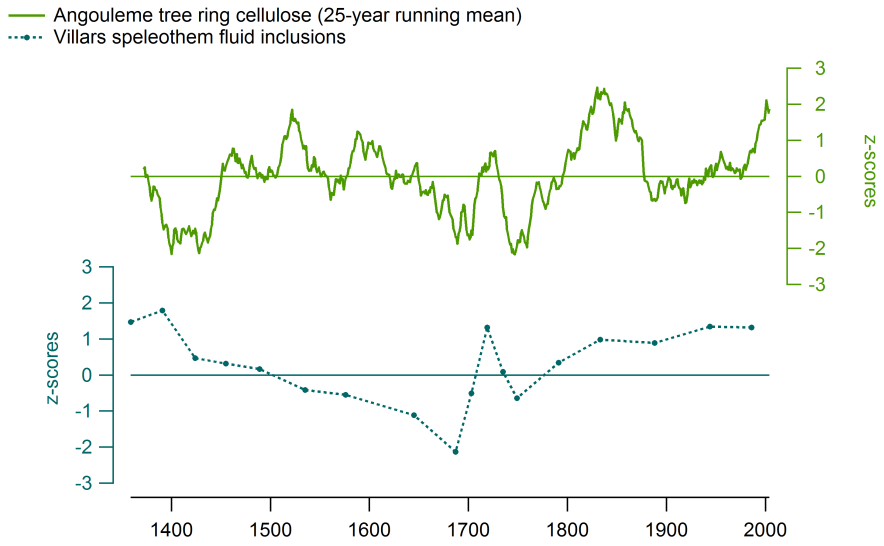

Figure 13.1: Comparison of the speleothem fluid inclusion and tree ring cellulose δ^{18}O time series (z-scores).

The co-variation in both can be ascribed to a common source water δ^{18}O, which is controlled by the average δ^{18}O of precipitation in the region. Furthermore, enhanced evaporation and transpiration during dry periods might cause an increase of δ^{18}O in both proxies. Although the cellulose δ^{18}O is strongly influenced by leaf water enrichment on an inter-annual scale, the underlying low-frequency variability can be considered as the variability of the source water. Several factors can explain the disagreement between cellulose and fluid inclusions:

- The isotopic composition of the source water can be modified before it becomes preserved in the proxy. The modern calibration indicates that speleothem fluid inclusions correspond to a weighted mean of pluri-annual precipitation, without any significant modification (Chapter 10). The δ^{18}O of cellulose, on the other hand, reflects partly the isotopic composition of the source water, and partly the isotopic composition of enriched leaf water (Equation 5.2). Their relative contribution to the δ^{18}O of cellulose has been estimated (Cernusak et al. 2005; Roden et al. 2000), but is likely to vary over the growing season, as well as over longer time periods (Offermann et al. 2011; Gessler et al. 2009).
- The cellulose δ^{18}O time series might not capture well the low frequency variability in precipitation/source water δ^{18}O. The source water δ^{18}O can be different for the individual trees which are combined in this time series, due to local soil hydrology or rooting depth (Chapter 11). Moreover, the correction we have applied for offsets in average δ^{18}O values between tree cohorts removes some of the low-frequency trends (Chapter 12).
- The resolution of the fluid inclusion record is much lower, which could explain why the peaks in the smoothed cellulose time series are not all seen in the fluid inclusions, e.g. around 1540 or 1850 AD.
- The dating of the stalagmite is less precise than the dating of the tree rings. Although there is generally a good agreement between layer counting, ^{14}C and U-Th dates for the stalagmite vil-stm1, the error of the age model is up to 100 years (Chapter 10).

- The seasonality of the proxies is different. The speleothem fluid inclusions represent the mean annual precipitation δ^{18}O, which is dominated by the δ^{18}O of winter precipitation because most precipitation falls during the winter months. Tree ring cellulose δ^{18}O could be biased towards growing season precipitation. However, it is possible that trees use water stored in the soil from the previous winter, especially during dry summers (e.g. Daux et al. 2011; Phillips and Ehleringer 1995). Although the inter-annual variability of cellulose δ^{18}O is dominated by leaf water enrichment during the summer months (Chapter 11), the source water δ^{18}O may still reflect annual precipitation.

13.3 Calculation of Leaf Water Enrichment and Relative Humidity

In order to combine the speleothem and tree ring isotope proxies, we suppose that the fluid inclusion δ^{18}O represents the tree source water. This assumption is supported by the fact that at Villars cave there is no seasonal bias in the isotopic composition of the drip water, indicating that plants take up a mixed water, and not only growing season water, which consequently must have the same δ^{18}O as the drip water.

First, the fluid inclusion δ^{18}O values were linearly interpolated between measurements to obtain a time series of annual resolution. Then, this new time series was smoothed using a 25-year running mean. The average cellulose δ^{18}O time series, which had been corrected for site offsets by centring all tree cohorts at a mean of 0 (Chapter 12), was adjusted to the mean δ^{18}O value of recent cellulose ($\mu = 31‰$). The interpolated and smoothed fluid inclusion δ^{18}O values were supposed to be the source water δ^{18}O for the trees each year. Then, the equations in Appendix A were used to calculate the δ^{18}O of leaf water from cellulose and fluid inclusions, and consequently, the relative humidity, which is the principal controlling factor of leaf water enrichment above source water.

The calculated leaf water is enriched compared to the source water by 13 to 23‰. This enrichment is in the same order of magnitude as found in studies on trees (Gessler et al. 2013; Saurer et al. 1998a,b) and other plants (Ferrio et al. 2012; Sheshshayee et al. 2005).

13.3.1 Observed vs. Reconstructed Relative Humidity

We compare the reconstructed RH to the observed summer RH (JJA), as these are the months which give the highest significant correlations between RH cellulose δ^{18}O (Chapter 11). The inter-annual variability of RH is well captured by the reconstruction, but the average values are too low (Figure 13.2). This calculation likely too simplistic for several reasons:

It assumes the kinetic isotope fractionation as water diffuses through stomata and through the boundary layer (ε_k in Equation A.1) to be constant; but ε_k varies with the boundary layer conditions, which depend on wind speed (Burk and Stuiver 1981; Dongman et al. 1974). The fractionation factor significantly influences the reconstructed RH. Applying the values given by Burk and Stuiver (1981) ($\varepsilon_k = 32$, for static, $\varepsilon_k = 21$ for laminar, or $\varepsilon_k = 16$ for turbulent boundary conditions) yields an average RH of 36%, 46%, and 60% respectively for the period 1961–2004. The average of the observed RH during this period is 71%. Supposing static leaf boundary layer conditions therefore gives the best estimate. However, turbulent conditions are more realistic in nature (Gonfiantini 1986).

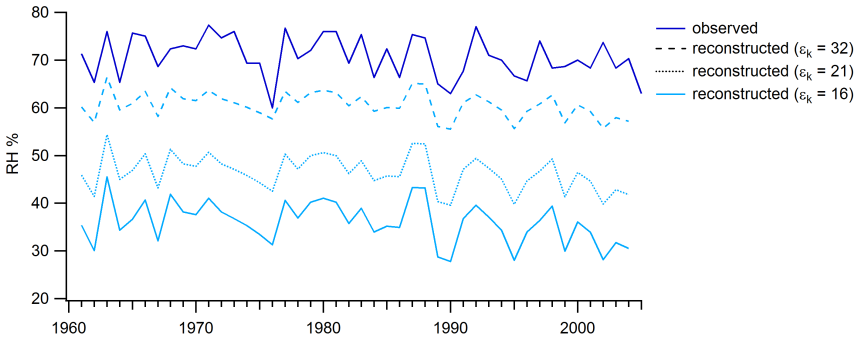

Figure 13.2: Observed vs. reconstructed relative humidity (RH). The reconstructions are based on different fractionation factors (ε_k) for static (32‰), laminar (21‰), and turbulent (16‰) leaf boundary layer condtitions. The values are given by Burk and Stuiver (1981).

As we do not have an independent temperature reconstruction, we also suppose that the temperature, and consequently the temperature-dependent equilibrium isotope fractionation (ε^* in Equation A.1) is constant. However, according to the fractionation factors given by Barbour et al. (2004) for 20 °C and 25 °C, this temperature difference changes the reconstructed RH by only 1%.

Furthermore, our calculation ignores the influence of a Péclet effect, which leads to a leaf water that is less enriched than predicted by the equations. If the calculated leaf water enrichment is too high, the reconstructed RH is too low. The Péclet effect could lower the leaf water δ^{18}O by 2‰ (Barbour et al. 2004). This would correspond to a 7% increase in RH.

Likewise, the calculation neglects that trees can take water from different soil depths (Bréda et al. 1995). Superficial soil water is more enriched than deeper soil water, and its isotopic composition is more variable as it is influenced by evaporation and rainfall events (Tang and Feng 2001). The average summer precipitation δ^{18}O is 3‰ higher than average annual precipitation in the study area (section 6.1). This difference in the δ^{18}O of the source water results in a 10% change in the reconstructed RH.

Lastly, it is also supposed that the atmospheric water vapour is in isotopic equilibrium with the soil water. Although this might be a good approximation for a growing-season average (Förstel and Hutzen 1982), the isotopic composition of the vapour varies significantly on shorter time scales (Berkelhammer et al. 2013).

The average reconstructed RH is significantly underestimated, and none of the factors discussed here are sufficient to explain the differences with the observations, unless we suppose unrealistic boundary layer conditions. A more complex model would be needed to adequately represent RH values, e.g. by taking into account variations in the depth of the water supply, the δ^{18}O of atmospheric water vapour, or temperature, as well as the Péclet effect. However, even if some of these parameters could be adjusted to present-day observations, they are unknown in the past and are likely to vary.

Nevertheless, the inter-annual variability in RH is well represented by the reconstruction. Despite the offset, we can compare relative variations in reconstructed SPEI (based on cellulose δ^{18}O) and reconstructed RH (based on a combination of cellulose and fluid inclusion δ^{18}O) using the z-scores of both.

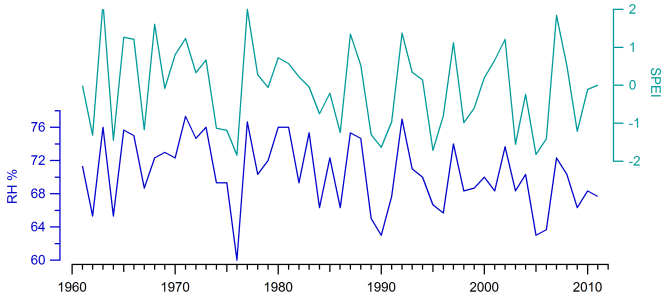

Figure 13.3: Comparison of summer (JJA) relative humidity (RH) at Cognac, which is the longest available RH record from the study area, and the drought index SPEI at a 3-month resolution for August. The correlation between RH and SPEI is $r = 0.85$.

13.3.2 Drought Reconstruction With and Without a Source Water $\delta^{18}O$ Estimate

The observed drought index SPEI (for August, at a 3-month resolution) and summer RH (JJA) are highly correlated during the period of observations (1961–2011) and should be comparable to represent summer moisture conditions in the study area (Figure 13.3). The inter-annual variability in the RH reconstruction based on fluid inclusion and cellulose $\delta^{18}O$ and the SPEI reconstruction based only on cellulose $\delta^{18}O$ (Chapter 12) is the same as they both depend linearly on the inter-annual variability in the cellulose $\delta^{18}O$ time series (not shown). However, the two reconstructions give a different picture of the long-term moisture changes in the past: The marked $\delta^{18}O$ peak at 1720 AD, for example, disappears in the RH reconstruction, because it is ascribed to changes in the source water isotopic composition, and not to increased drought. Moreover, the RH reconstruction indicates drier conditions during the 16^{th} and 17^{th} century, and wetter conditions during the 19^{th} and 20^{th} century than the SPEI reconstruction.

The model for the tree-ring based drought reconstruction is well-verified with independent data, and correlations between the proxy and the reconstructed drought index are highly significant and stable throughout the 20^{th} century, all of which gives strong indications for the validity of this reconstruction. However, the low-frequency drought variability may not be well represented in this record. The RH reconstruction supposedly captures better the low frequency. However, it must be interpreted with caution because of the age uncertainties in the stalagmite and the low resolution of fluid inclusion measurements compared to the tree rings. Most importantly, a replication of the fluid inclusion record is needed to determine whether it represents average regional precipitation $\delta^{18}O$, and therefore can serve as an estimation of the trees' source water.

To conclude, these investigations confirm that there is a great potential in combining speleothem fluid inclusions and tree ring cellulose to reconstruct moisture conditions, and the theoretical approach is demonstrated. This combination of proxies might provide an estimate of past drought conditions that comprises both the low- and high-frequency variability, combining the strengths of the two climate archives while compensating there weaknesses when used alone. However, more measurements are needed to confirm the observed low frequency trends in moisture conditions.

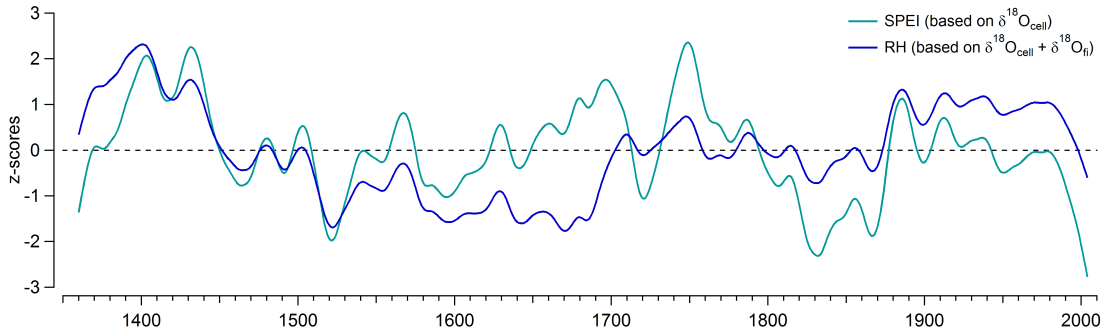

Figure 13.4: The drought index (SPEI), reconstructed using tree ring cellulose δ^{18}O, and relative humidity (RH), reconstructed using the calculation of leaf water enrichment from cellulose δ^{18}O and speleothem fluid inclusion δ^{18}O (as an estimate of the source water isotopic composition). Both curves have been smoothed using a 30-year spline and their z-scores have been calculated. Positive values indicate wet conditions, negative values indicate dry conditions.

Part IV

CONCLUSIONS

This thesis has produced new proxy records from speleothems and tree rings for the southwest of France, a region where high-resolution reconstructions of climate and environmental changes during the last millennia were lacking. The exceptionally long monitoring data of precipitation and drip water isotopes, together with meteorological data, provided the basis for proxy calibration: an investigation of the statistical relationships between climate and the proxies, as well as an improved understanding of the processes linking the isotopic composition of precipitation with the proxy source water, and its possible modifications during the formation of the archive.

The fluid inclusion record from a stalagmite from Villars cave presented here evidenced a variable isotopic composition of cave drip water in the past. It is potentially the first direct record of stable isotopes in palaeo-precipitation measured at a high resolution for the last 2000 years. Even if its interpretation proved to be complex due to a possible influence of vegetation and hydrology changes, and even if the reconstructed amplitude of precipitation δ^{18}O appears to be large (2‰), the modern calibration gives strong evidence that the δ^{18}O of precipitation is preserved in the fluid inclusions.

The second important accomplishment of this thesis is a precisely dated, annually resolved reconstruction of summer droughts during the last 650 years based on oxygen isotope ratios in tree ring cellulose from living trees and timber wood from Angoulême. 1500 cellulose samples have been analysed. Comparison of δ^{18}O between trees and between sites revealed significant offsets in absolute values, and also evidenced a juvenile effect, highlighting the importance individual-tree measurements. Nevertheless, the highly coherent interannual patterns, and the strong correlation with summer maximum temperature and drought indices enabled this reconstruction, which is coherent with other French climate records.

A direct comparison of the speleothem and tree ring proxies is difficult because they differ in resolution, and possibly in their seasonal representation. Nevertheless, the resemblance between the oxygen isotope records in fluid inclusion and cellulose points to a common influence, the isotopic composition of their source water, which is controlled by the isotopic composition of precipitation and by evaporation during dry periods. If we consider the fluid inclusions as representative of the tree source water δ^{18}O signal, we can further attempt to reconstruct relative humidity, the principal influence on leaf water enrichment, based on the isotopic composition of cellulose and the source water.

Outlook on Future Speleothem Work

Monitoring at Villars cave continues, and will eventually provide the data to investigate long-term changes in the functioning of the cave system, such as a possible influence of the currently observed warming trend on the isotopic composition of precipitation, cave drip water and calcite. Measurements of clumped isotopes (Δ47) on the fluid inclusion samples from vil-stm1 which have been analysed in this thesis are in progress. The Δ47, together with the δ^{18}O of calcite and of fluid inclusions, can be used to quantify kinetic fractionation effects and could eventually enable a temperature reconstruction.

Most importantly, a replication of the fluid inclusion record from another stalagmite from Villars or another cave in western Europe, at a similar resolution, will be necessary to confirm that the fluid inclusions represent a regional precipitation δ^{18}O signal, or that they are modified by local cave processes. Since the δ^{18}O of precipitation can serve as a tracer of the atmospheric circulation (Sturm et al. 2010; Schmidt et al. 2007; Hoffmann et al. 2005), a comparison of the

fluid inclusion record with general circulation models which include the water isotopes (e.g. LMDZ-iso, Risi et al. 2010) can provide a means to test whether the atmospheric circulation and the water cycle adequately represented in the models. Inversely, the models can help identify the circulation patterns which lead to a certain isotopic composition of the local precipitation, if model and reconstruction agree.

Outlook on Future Tree Ring Work

A perspective of future tree ring work would be to measure the carbon isotopic composition of cellulose. A combination of the carbon and oxygen isotope ratios can help distinguish the different influences on each individual proxy: the isotopic composition of the source water (for $\delta^{18}O$), the photosynthetic rate (for $\delta^{13}C$), and stomatal conductance (for both) (Roden and Farquhar 2012; Danis et al. 2006; Saurer et al. 1997a). The isotopic composition of cellulose can also be simulated by ecophysiological models (e.g. MAIDENiso, Danis et al. 2012; ORCHIDEE-iso, Krinner et al. 2005). Instead of relying on statistical relationships between the proxy and instrumental data for climate reconstruction, such models can explore how specific combinations of meteorological and hydrological parameters lead to certain tree ring proxy values (Boucher et al. 2013). Using the data presented in this thesis, an estimation of the source water $\delta^{18}O$ can be obtained from the speleothem fluid inclusions.

Moreover, the tree ring records from the southwest of France could be continued further back in time. In the villages around Angoulême, Romanesque churches from the 11^{th} to 12^{th} century can be found. Although wood beams in their roof structure have often been replaced in later periods, there is a potential to extend the local chronology and investigate moisture variability in the context of the Medieval Climate Anomaly.

Despite the commonly found good coherence in the inter-annual variability between tree-ring isotope time series of individual trees, the differences in absolute values can have a significant influence on reconstructed low-frequency climate variability. More individual-tree isotope measurements are therefore desirable, so that the uncertainty can be estimated (Loader et al. 2013; Woodley et al. 2012), in the same rigorous manner which is common practice in tree ring width studies (Cook and Kairiukstis 1990).

Lastly, the increasing number of records will also promote the development of tree-ring isotope networks to investigate spatial patterns of climate change (Leavitt et al. 2010; Saurer et al. 2008; Liu et al. 2007; Treydte et al. 2007).

Concluding Remarks

Both speleothems and tree rings have significantly contributed to our knowledge of past climate and environmental changes. The valuable information which can be obtained from stable isotope records in these archives requires an understanding of the processes in the system atmosphere–soil–plant and atmosphere–soil–bedrock–cave–stalagmite. A multi-proxy approach to climate reconstruction can help to gain a better understanding of climate variability in the past on different temporal and spatial scales, and ultimately improve our predictions for future climate change.

References

Affek, H. P., Bar-Matthews, M., Ayalon, A., Matthews, A., and Eiler, J. M. (2008). Glacial/interglacial temperature variations in Soreq cave speleothems as recorded by 'clumped isotope' thermometry. *Geochimica et Cosmochimica Acta*, 72(22):5351–5360.

Aggarwal, P. K., Alduchov, O. A., Froehlich, K. O., Araguas-Araguas, L. J., Sturchio, N. C., and Kurita, N. (2012). Stable isotopes in global precipitation: A unified interpretation based on atmospheric moisture residence time. *Geophysical Research Letters*, 39(11):L11705.

Alley, R. B. and Cuffey, K. M. (2001). Oxygen- and Hydrogen-Isotopic Ratios of Water in Precipitation: Beyond Paleothermometry. *Reviews in Mineralogy and Geochemistry*, 43:527–553.

Allison, G. (1998). Stable isotopes in soil and water studies. *Colloques et séminaires - Institut français de recherche scientifique pour le développement en coopération*, pages 23–38.

Altman, J., Hédl, R., Szabó, P., MazÅŕrek, P., Riedl, V., Müllerová, J., Kopecký, M., and Doležal, J. (2013). Tree-Rings Mirror Management Legacy: Dramatic Response of Standard Oaks to Past Coppicing in Central Europe. *PLoS ONE*, 8(2):e55770.

Anderson, T. F. and Arthur, M. A. (1983). Stable isotopes of oxygen and carbon and their application to sedimentologic and paleoenvironmental problems. In Arthur, M. A., Anderson, T. F., Kaplan, I. R., Veizer, J., and Land, L. S., editors, *Stable Isotopes in Sedimentary Geology*, SEPM Short Course No. 10. SEPM, Dallas.

Anderson, W. T., Bernasconi, S. M., McKenzie, J. A., Saurer, M., and Schweingruber, F. (2002). Model evaluation for reconstructing the oxygen isotopic composition in precipitation from tree ring cellulose over the last century. *Chemical Geology*, 182:121–137.

Appelo, C. A. J. and Postma, D. (2005). *Geochemistry, Groundwater and Pollution*. A. A. Balkema Publishers, Leiden.

Asrat, A., Baker, A., Mohammed, M. U., Leng, M. J., Calsteren, P. V., and Smith, C. (2007). A high-resolution multi-proxy stalagmite record from Mechara, Southeastern Ethiopia: palaeohydrological implications for speleothem palaeoclimate reconstruction. *Journal of Quaternary Science*, 22(1):53–63.

Aussenac, G. (2000). Interactions between forest stands and microclimate: Ecophysiological aspects and consequences for silviculture. *Annals of Forest Science*, 57(3):287–301.

Baker, A., Asrat, A., Fairchild, I. J., Leng, M. J., Thomas, L., Widmann, M., Jex, C. N., van Calsteren, P., and Bryant, C. (2010). Decadal-scale rainfall variability in Ethiopia recorded in an annually laminated, Holocene-age, stalagmite. *The Holocene*, 20(6):827–836.

Baker, A. and Genty, D. (2003). Comment on "a test of annual resolution in stalagmites using tree rings". *Quaternary Research*, 59(3):476–478.

Baker, A., Genty, D., Dreybrodt, W., Barnes, W. L., Mockler, N. J., and Grapes, J. (1998). Testing Theoretically Predicted Stalagmite Growth Rate with Recent Annually Laminated Samples: Implications for Past Stalagmite Deposition. *Geochimica et Cosmochimica Acta*, 62(3):393–404.

Baker, A., Smith, C., Jex, C., Fairchild, I. J., Genty, D., and Fuller, L. (2008). Annually laminated speleothems: a review. *International Journal of Speleology*, 37(3):193–206.

Baldini, J., Mcdermott, F., Baker, a., Baldini, L., Mattey, D., and Railsback, L. (2005). Biomass effects on stalagmite growth and isotope ratios: A 20th century analogue from Wiltshire, England. *Earth and Planetary Science Letters*, 240(2):486–494.

Baldini, L. M., McDermott, F., Foley, A. M., and Baldini, J. U. L. (2008). Spatial variability in the European winter precipitation δ18O-NAO relationship: Implications for reconstructing NAO-mode climate variability in the Holocene. *Geophysical Research Letters*, 35(4):1–6.

Bar-Matthews, M., Ayalon, A., Matthews, A., Sass, E., and Halicz, L. (1996). Carbon and oxygen isotope study of the active water-carbonate system in a karstic Mediterranean cave: Implications for paleoclimate research in semiarid regions. *Geochimica et Cosmochimica Acta*, 60(2):337–347.

Barbaroux, C. and Bréda, N. (2002). Contrasting distribution and seasonal dynamics of carbohydrate reserves in stem wood of adult ring-porous sessile oak and diffuse-porous beech trees. *Tree Physiology*, 22(17):1201–10.

Barbour, M. M. (2007). Stable oxygen isotope composition of plant tissue: a review. *Functional Plant Biology*, 34:83–94.

Barbour, M. M., Cernusak, L. A., and Farguhar, G. D. (2005). Factors affecting the oxygen isotope ratio of plant organic material. In Flanagan, L. B., Ehleringer, J. R., and Pataki, D. E., editors, *Stable Isotopes and Biosphere-Atmosphere Interactions: Processes and Biological Controls*, pages 9–28. Elsevier, Amsterdam.

Barbour, M. M. and Farquhar, G. D. (2000). Relative humidity- and ABA-induced variation in carbon and oxygen isotope ratios of cotton leaves. *Plant, Cell & Environment*, 23:473–485.

Barbour, M. M., Roden, J. S., Farquhar, G. D., and Ehleringer, J. R. (2004). Expressing leaf water and cellulose oxygen isotope ratios as enrichment above source water reveals evidence of a Péclet effect. *Oecologia*, 138(3):426–35.

Barbour, M. M., Walcroft, A. S., and Farquhar, G. D. (2002). Seasonal variation in delta13C and delta18O of cellulose from growth rings of Pinus radiata. *Plant, Cell & Environment*, 25(11):1483–1499.

Bard, E., Raisbeck, G., Yiou, F., and Jouzel, J. (2000). Solar irradiance during the last 1200 years based on cosmogenic nuclides. *Tellus B*, 52(3):985–992.

Bariac, T., Deleens, E., Gerbaud, A., Andre, M., and Mariotti, A. (1991). La composition isotopique (18O,2H) de la vapeur d'eau transpirée: Étude en conditions asservies. *Geochimica et Cosmochimica Acta*, 55(11):3391–3402.

Barnes, C. and Allison, G. (1988). Tracing of water movement in the unsaturated zone using stable isotopes of hydrogen and oxygen. *Journal of Hydrology*, 100(1-3):143–176.

Beguería, S., Vicente-Serrano, S. M., and Angulo-Martínez, M. (2010). A Multiscalar Global Drought Dataset: The SPEIbase: A New Gridded Product for the Analysis of Drought Variability and Impacts. *Bulletin of the American Meteorological Society*, 91:1351–1356.

Berger, A. and Loutre, M. (1991). Insolation values for the climate of the last 10 million years. *Quaternary Science Reviews*, 10(4):297–317.

Berkelhammer, M., Sinha, A., Mudelsee, M., Cheng, H., Yoshimura, K., and Biswas, J. (2013). On the low frequency component of the ENSO-Indian Monsoon relationship; a paired proxy perspective. *Climate of the Past Discussions*, 9(3):3103–3123.

Betancourt, J. L., Grissino-Mayer, H. D., Salzer, M. W., and Swetnam, T. W. (2002). A Test of "Annual Resolution" in Stalagmites Using Tree Rings. *Quaternary Research*, 58(2):197–199.

Bigeleisen, J. (1965). Chemistry of isotopes. *Science*, 147:463–471.

Björklund, J. a., Gunnarson, B. E., Krusic, P. J., Grudd, H. k., Josefsson, T., Östlund, L., and Linderholm, H. W. (2012). Advances towards improved low-frequency tree-ring reconstructions, using an updated Pinus sylvestris L. MXD network from the Scandinavian Mountains. *Theoretical and Applied Climatology*, 113(3-4):697–710.

Boch, R., Spötl, C., and Frisia, S. (2011). Origin and palaeoenvironmental significance of lamination in stalagmites from Katerloch Cave, Austria. *Sedimentology*, 58(2):508–531.

Boettger, T., Haupt, M., Knöller, K., Weise, S. M., Waterhouse, J. S., Rinne, K. T., Loader, N. J., Sonninen, E., Jungner, H., Masson-Delmotte, V., Stievenard, M., Guillemin, M.-T., Pierre, M., Pazdur, A., Leuenberger, M., Filot, M., Saurer, M., Reynolds, C. E., Helle, G., and Schleser, G. H. (2007). Wood cellulose preparation methods and mass spectrometric analyses of δ13C, δ18O, and nonexchangeable δ2H values in cellulose, sugar, and starch: An interlaboratory comparison. *Analytical Chemistry*, 79:4603–4612.

Bond, B. J. (2000). Age-related changes in photosynthesis of woody plants. *Trends in Plant Science*, 5(8):349–353.

Borella, S., Leuenberger, M., Saurer, M., and Siegwolf, R. (1998). Reducing uncertainties in δ13 analysis of tree rings: Pooling, milling, and cellulose extraction. *Journal of Geophysical Research*, 103(D16):19519.

Bottrell, S. H. and Atkinson, T. C. (1992). Tracer study of flow and storage in the unsaturated zone of a karstic limestone aquifer. In Hotzl, H. and Werner, A., editors, *Tracer Hydrology*, pages 207–211. A. A. Balkema, Rotterdam.

Boucher, E., Guiot, J., Hatté, C., Daux, V., Danis, P.-A., and Dussouillez, P. (2013). An inverse modeling approach for tree-ring-based climate reconstructions under changing atmospheric CO2 concentrations. *Biogeosciences Discussions*, 10(11):18479–18514.

Bourdin, C. (2012). *Enregistrement des variations climatiques par les éléments traces dans les stalagmites*. PhD thesis, Université Paris Sud.

Bourdin, C., Douville, E., and Genty, D. (2011). Alkaline-earth metal and rare-earth element incorporation control by ionic radius and growth rate on a stalagmite from the Chauvet Cave, Southeastern France. *Chemical Geology*, 290(1-2):1–11.

Bowen, G. and Wilkinson, B. (2002). Spatial distribution of δ18O in meteoric precipitation. *Geology*, 30(4):315–318.

Braconnot, P., Harrison, S. P., Kageyama, M., Bartlein, P. J., Masson-Delmotte, V., Abe-Ouchi, A., Otto-Bliesner, B., and Zhao, Y. (2012). Evaluation of climate models using palaeoclimatic data. *Nature Climate Change*, 2(6):417–424.

Bradley, C., Baker, A., Jex, C. N., and Leng, M. J. (2010). Hydrological uncertainties in the modelling of cave drip-water δ18O and the implications for stalagmite palaeoclimate reconstructions. *Quaternary Science Reviews*, 29(17-18):2201–2214.

Braud, I., Bariac, T., Vauclin, M., Boujamlaoui, Z., Gaudet, J., Biron, P., and Richard, P. (2005). SiSPAT-Isotope, a coupled heat, water and stable isotope (HDO and H218O) transport model for bare soil. Part II. Evaluation and sensitivity tests using two laboratory data sets. *Journal of Hydrology*, 309(1):301–320.

Bréda, N., Cochard, H., Dreyer, E., and Granier, A. (1993). Field comparison of transpiration, stomatal conductance and vulnerability to cavitation of Quercus petraea and Quercus robur under water stress. *Annals of Forest Science*, 50(6):571–582.

Bréda, N. and Granier, A. (1996). Intra- and interannual variations of transpiration, leaf area index and radial growth of a sessile oak stand (Quercus petraea). *Annals of Forest Science*, 53:521–536.

Bréda, N., Granier, A., Barataud, F., and Moyne, C. (1995). Soil water dynamics in an oak stand. I. Soil moisture, water potentials and water uptake by roots. *Plant and Soil*, 172:17–27.

Breitenbach, S. F. M., Rehfeld, K., Goswami, B., Baldini, J. U. L., Ridley, H. E., Kennett, D. J., Prufer, K. M., Aquino, V. V., Asmerom, Y., Polyak, V. J., Cheng, H., Kurths, J., and Marwan, N. (2012). COnstructing Proxy Records from Age models (COPRA). *Climate of the Past*, 8(5):1765–1779.

Brienen, R. J. W., Helle, G., Pons, T. L., Guyot, J.-L., and Gloor, M. (2012). Oxygen isotopes in tree rings are a good proxy for Amazon precipitation and El Nino-Southern Oscillation variability. *Proceedings of the National Academy of Sciences of the United States of America*, 109(42):16957–62.

Briffa, K., Osborn, T., and Schweingruber, F. (2004). Large-scale temperature inferences from tree rings: a review. *Global and Planetary Change*, 40(1-2):11–26.

Briffa, K. R. (2000). Annual climate variability in the Holocene: Interpreting the message of ancient trees. *Quaternary Science Reviews*, 19(1-5):87–105.

Briffa, K. R. and Jones, P. D. (1990). Basic Chronology Statistics and Assessment. In Cook, E. R. and Kairiukstis, L. A., editors, *Methods of Dendrochronology - Applications in the Environmental Sciences*, pages 137–152. Kluwer Academic Publishers, Dordrecht.

Briffa, K. R., Jones, P. D., Bartholin, T. S., Eckstein, D., Schweingruber, F. H., Karlén, W., Zetterberg, P., and Eronen, M. (1992). Fennoscandian summers from AD 500: temperature changes on short and long timescales. *Climate Dynamics*, 7(3):111–119.

Briffa, K. R., Jones, P. D., Pilcher, J. R., and Hughes, M. K. (1988). Reconstructing summer temperatures in northern Fennoscandinavia back to AD 1700 using tree-ring data from Scots pine. *Arctic and Alpine Research*, 20(4):385–394.

Briffa, K. R., Osborn, T. J., Schweingruber, F. H., Harris, I. C., Jones, P. D., Shiyatov, S. G., and Vaganov, E. A. (2001). Low-frequency temperature variations from a northern tree ring density network. *Journal of Geophysical Research*, 106(D3):2929.

Briffa, K. R., Schweingruber, F. H., Jones, P. D., Osborn, T. J., Harris, I. C., Shiyatov, S. G., Vaganov, E. A., and Grudd, H. (1998). Trees tell of past climates: But are they speaking less clearly today? *Philosophical Transactions of the Royal Society B*, 353:65–73.

Briffa, K. R. K., Osborn, T. T. J., Schweingruber, F. H., Jones, P. D., Shiyatov, S. G., and Vaganov, E. A. (2002). Tree-ring width and density data around the Northern Hemisphere: Part 2, spatio-temporal variability and associated climate patterns. *The Holocene*, 12(6):759–789.

Brochet, P. (1977). La sécheresse 1976 en France: aspects climatologiques et conséquences/The 1976 drought in France: climatological aspects and consequences. *Hydrological Sciences Bulletin*, 22(3):393–411.

Brooks, R. J., Barnard, H. R., Coulombe, R., and McDonnell, J. J. (2010). Ecohydrologic separation of water between trees and streams in a Mediterranean climate. *Nature Geoscience*, 3(2):100–104.

Büntgen, U., Esper, J., Frank, D. C., Nicolussi, K., and Schmidhalter, M. (2005). A 1052-year tree-ring proxy for Alpine summer temperatures. *Climate Dynamics*, 25(2-3):141–153.

Büntgen, U., Trouet, V., Frank, D., Leuschner, H. H., Friedrichs, D., Luterbacher, J., and Esper, J. (2010). Tree-ring indicators of German summer drought over the last millennium. *Quaternary Science Reviews*, 29(7):1005–1016.

Burk, R. L. and Stuiver, M. (1981). Oxygen Isotope Ratios in Trees Reflect Mean Annual Temperature and Humidity. *Science*, 211(4489):1417–1419.

Caballero, E., Jiménez De Cisneros, C., and Reyes, E. (1996). A stable isotope study of cave seepage waters. *Applied Geochemistry*, 11(4):583–587.

Carrasco, F., Andreo, B., Liñán, C., and Mudry, J. (2006). Contribution of stable isotopes to the understanding of the unsaturated zone of a carbonate aquifer (Nerja Cave, southern Spain). *Comptes Rendus Geoscience*, 338(16):1203–1212.

Celle, H., Daniel, M., Mudry, J., and Blavoux, B. (2000). Signal pluie et traçage par les isotopes stables en Méditerranée occidentale. Exemple de la région avignonnaise (Sud-Est de la France). *Comptes Rendus de l'Académie des Sciences - Series IIA - Earth and Planetary Science*, 331(10):647–650.

Celle-Jeanton, H., Gonfiantini, R., Travi, Y., and Sol, B. (2004). Oxygen-18 variations of rainwater during precipitation: application of the Rayleigh model to selected rainfalls in Southern France. *Journal of Hydrology*, 289:165–177.

Celle-Jeanton, H., Travi, Y., and Blavoux, B. (2001). Isotopic typology of the precipitation in the Western Mediterranean Region at three different time scales. *Geophysical Research Letters*, 28(7):1215–1218.

Cernusak, L. A., Farquhar, G. D., and Pate, J. S. (2005). Environmental and physiological controls over oxygen and carbon isotope composition of Tasmanian blue gum, Eucalyptus globulus. *Tree Physiology*, 25(2):129–146.

Chapman, J. B., Ingraham, N. L., and Hess, J. W. (1992). Isotopic investigation of infiltration and unsaturated zone flow processes at Carlsbad Cavern, New Mexico. *Journal of Hydrology*, 133(3-4):343–363.

Cheng, H., Lawrence Edwards, R., Shen, C.-C., Polyak, V. J., Asmerom, Y., Woodhead, J., Hellstrom, J., Wang, Y., Kong, X., Spötl, C., Wang, X., and Calvin Alexander, E. (2013). Improvements in 230Th dating, 230Th and 234U half-life values, and U–Th isotopic measurements by multi-collector inductively coupled plasma mass spectrometry. *Earth and Planetary Science Letters*, 371-372:82–91.

Christensen, J., Hewitson, B., Busuioc, A., Chen, A., Gao, X., Held, I., Jones, R., Kolli, R., Kwon, W.-T., Laprise, R., Rueda, V. M. n., Mearns, L., Menéndez, C., Räisänen, J., Rinke, A., Sarr, A., and Whetton, P. (2007). Regional Climate Projections. In Solomon, S., Qin, D., Manning, M., Chen, Z., Marquis, M., Averyt, K., Tignor, M., and Miller, H., editors, *Climate Change 2007: The Physical Science Basis. Contribution of Working Group I to the Fourth Assessment Report of the Intergovernmental Panel on Climate Change*, pages 847–940. Cambridge University Press, Cambridge, UK and New York, USA.

Clark, I. D. and Fritz, P. (1997). *Environmental Isotopes in Hydrogeology*. Lewis Publishers, Boca Raton, London, New York.

Clark, R. T., Brown, S. J., and Murphy, J. M. (2010). Modeling Northern Hemisphere Summer Heat Extreme Changes and Their Uncertainties Using a Physics Ensemble of Climate Sensitivity Experiments. *Journal of Climate*, 19:4418–4435.

Cook, E. R. (1985). *A Time Series Analysis Approach to Tree Ring Standardization*. PhD thesis, University of Arizona.

Cook, E. R., Briffa, K. R., Meko, D. M., Graybill, D. A., and Funkhouser, G. (1995). The 'segment length curse' in long tree-ring chronology development for palaeoclimatic studies. *The Holocene*, 5(2):229–237.

Cook, E. R., Briffa, K. R., Shiyatov, S., and Mazepa, V. (1990a). Tree-Ring Standardization and Growth-Trend Estimation. In Cook, E. R. and Kairiukstis, L. A., editors, *Methods of Dendrochronology – Applications in the Environmental Sciences*, pages 104–123. Kluwer Academic Publishers, Dordrecht.

Cook, E. R. and Kairiukstis, L. A. (1990). *Methods of Dendrochronology - Applications in the Environmental Sciences*. Kluwer Academic Publishers, Dordrecht.

Cook, E. R. and Krusic, P. J. (2005). Program ARSTAN: A tree-ring standardization program based on detrending and autoregressive time series modeling, with interactive graphics.

Cook, E. R., Meko, D. M., Stahle, D. W., and Cleaveland, M. K. (1999). Drought reconstructions for the continental United States. *Journal of Climate*, 12(4):1145–1162.

Cook, E. R., Shiyatov, S., and Mazepa, V. (1990b). Estimation of the Mean Chronology. In Cook, E. R. and Kairiukstis, L. A., editors, *Methods of Dendrochronology - Applications in the Environmental Sciences*, pages 123–132. Kluwer Academic Publishers, Dordrecht.

Coplen, T. B. (1994). Reporting of stable hydrogen, carbon, and oxygen isotopic abundances. *Pure and Applied Chemistry*, 66(2):273–276.

Coplen, T. B. (2007). Calibration of the calcite–water oxygen-isotope geothermometer at Devils Hole, Nevada, a natural laboratory. *Geochimica et Cosmochimica Acta*, 71(16):3948–3957.

Coppola, A., Leonelli, G., Salvatore, M. C., Pelfini, M., and Baroni, C. (2013). Tree-ring–based summer mean temperature variations in the Adamello–Presanella Group (Italian Central Alps), 1610-2008 AD. *Climate of the Past*, 9(1):211–221.

Corcho Alvarado, J., Leuenberger, M., Kipfer, R., Paces, T., and Purtschert, R. (2011). Reconstruction of past climate conditions over central Europe from groundwater data. *Quaternary Science Reviews*, 30(23):3423–3429.

Craig, H. (1961). Isotopic variations in meteoric waters. *Science*, 133(3465):1702–1703.

Craig, H. (1965). The measurement of oxygen isotope paleotemperatures. In Tongiorgi, E., editor, *Stable Isotopes in Oceanographic Studies and Paleotemperatures*, pages 161–182. Consiglio Nazionale delle Ricerche, Pisa.

Criss, R. E. and Farquhar, J. (2008). Abundance, notation, and fractionation of light stable isotopes. *Reviews in Mineralogy & Geochemistry*, 68:15–30.

Cruz, F. W., Karmann, I., Viana, O., Burns, S. J., Ferrari, J. a., Vuille, M., Sial, A. N., and Moreira, M. Z. (2005). Stable isotope study of cave percolation waters in subtropical Brazil: Implications for paleoclimate inferences from speleothems. *Chemical Geology*, 220(3-4):245–262.

Cullen, L. E. and Grierson, P. F. (2006). Is cellulose extraction necessary for developing stable carbon and oxygen isotopes chronologies from Callitris glaucophylla? *Palaeogeography, Palaeoclimatology, Palaeoecology*, 236(3-4):206–216.

Curti, E. (1999). Coprecipitation of radionuclides with calcite: estimation of partition coefficients based on a review of laboratory investigations and geochemical data. *Applied Geochemistry*, 14(4):433–445.

Daëron, M., Guo, W., Eiler, J., Genty, D., Blamart, D., Boch, R., Drysdale, R., Maire, R., Wainer, K., and Zanchetta, G. (2011). 13C18O clumping in speleothems: Observations from natural caves and precipitation experiments. *Geochimica et Cosmochimica Acta*, 75(12):3303–3317.

Danis, P.-A., Hatté, C., Misson, L., and Guiot, J. (2012). MAIDENiso: a multiproxy biophysical model of tree-ring width and oxygen and carbon isotopes. *Canadian Journal of Forest Research*, 42:1697–1713.

Danis, P. A., Masson-Delmotte, V., Stievenard, M., Guillemin, M. T., Daux, V., Naveau, P., and von Grafenstein, U. (2006). Reconstruction of past precipitation δ18O using tree-ring cellulose δ18O and δ13C: A calibration study near Lac d'Annecy, France. *Earth and Planetary Science Letters*, 243:439–448.

Dansgaard, W. (1964). Stable isotopes in precipitation. *Tellus*, 16:436–468.

Dara, A., Moradi, A. B., and Oswald, S. (2013). Spatiotemporal Pattern of Root Water Uptake for Locally Differing Soil Water Availability. *Geophysical Research Abstracts*, 15:13123.

Darling, G. W., Bath, A. H., Gibson, J. J., and Rozanski, K. (2006). Isotopes in Water. In Leng, M. J., editor, *Isotopes in Palaeoenvironmental Research*, pages 1–66. Springer, Dordrecht.

Darling, W. G. (2004). Hydrological factors in the interpretation of stable isotopic proxy data present and past: a European perspective. *Quaternary Science Reviews*, 23:743–770.

D'Arrigo, R., Wilson, R., and Jacoby, G. (2006). On the long-term context for late twentieth century warming. *Journal of Geophysical Research*, 111(D3):1–12.

Daux, V., Edouard, J., Masson-Delmotte, V., Stievenard, M., Hoffmann, G., Pierre, M., Mestre, O., Danis, P., and Guibal, F. (2011). Can climate variations be inferred from tree-ring parameters and stable isotopes from Larix decidua? Juvenile effects, budmoth outbreaks, and divergence issue. *Earth and Planetary Science Letters*, 309(3-4):221–233.

Daux, V., Garcia de Cortazar-Atauri, I., Yiou, P., Chuine, I., Garnier, E., Le Roy Ladurie, E., Mestre, O., and Tardaguila, J. (2012). An open-access database of grape harvest dates for climate research: data description and quality assessment. *Climate of the Past*, 8(5):1403–1418.

Daux, V., Lécuyer, C., Adam, F., Martineau, F., and Vimeux, F. (2005). Oxygen Isotope Composition Of Human Teeth And The Record Of Climate Changes In France (Lorraine) During The Last 1700 Years. *Climatic Change*, 70(3):445–464.

de Cisneros, C. J., Caballero, E., Vera, J. A., and Andreo, B. (2011). An optimized thermal extraction system for preparation of water from fluid inclusions in speleothems. *Geologica Acta*, 9(2):149–158.

Dearing, J. A. (2006). Climate-human-environment interactions: resolving our past. *Climate of the Past*, 2(4):563–604.

Deininger, M., Fohlmeister, J., Scholz, D., and Mangini, A. (2012). Isotope disequilibrium effects: The influence of evaporation and ventilation effects on the carbon and oxygen isotope composition of speleothems – A model approach. *Geochimica et Cosmochimica Acta*, 96:57–79.

Delluc, B. and Delluc, G. (1974). La grotte ornée de Villars. *Gallia Préhistoire*, 17(1):1–67.

DeNiro, M. J. and Epstein, S. (1979). Relationship between the oxygen isotope ratios of terrestrial plant cellulose, carbon dioxide, and water. *Science*, 204(4388):51–3.

Dennis, P. F., Rowe, P. J., and Atkinson, T. C. (2001). The recovery and isotopic measurement of water from fluid inclusions in speleothems. *Geochimica et Cosmochimica Acta*, 65(6):871–884.

Denniston, R., González, L., Baker, R., Reagan, M., Asmerom, Y., Edwards, R., and Alexander, E. (1999). Speleothem evidence for Holocene fluctuations of the prairie-forest ecotone, north-central USA. *The Holocene*, 9(6):671–676.

DeSoto, L., De la Cruz, M., and Fonti, P. (2011). Intra-annual patterns of tracheid size in the Mediterranean tree Juniperus thurifera as an indicator of seasonal water stress. *Canadian Journal of Forest Research*, 41(6):1280–1294.

Dewalle, D. R. and Swistock, B. R. (1994). Differences in oxygen-18 content of throughfall and rainfall in hardwood and coniferous forests. *Hydrological Processes*, 8(1):75–82.

Diaz, H. and Trouet, V. (2014). Some Perspectives on Societal Impacts of Past Climatic Changes. *History Compass*, 12(2):160–177.

Dietrich, S., Werner, M., Spangehl, T., and Lohmann, G. (2013). Influence of orbital forcing and solar activity on water isotopes in precipitation during the mid- and late Holocene. *Climate of the Past*, 9(1):13–26.

Dongman, G., Nürnberg, H. W., Förstel, H., and Wagener, K. (1974). On the enrichment of H218O in the leaves of transpiring plants. *Radiation and Environmental Biophysics*, 11:41–52.

Donohoe, A. and Battisti, D. S. (2011). Atmospheric and Surface Contributions to Planetary Albedo. *Journal of Climate*, 24(16):4402–4418.

Dorado Liñán, I., Gutiérrez, E., Heinrich, I., Andreu-Hayles, L., Muntán, E., Campelo, F., and Helle, G. (2011a). Age effects and climate response in trees: a multi-proxy tree-ring test in old-growth life stages. *European Journal of Forest Research*, 131(4):933–944.

Dorado Liñán, I., Gutiérrez, E., Helle, G., Heinrich, I., Andreu-Hayles, L., Planells, O., Leuenberger, M., Bürger, C., and Schleser, G. (2011b). Pooled versus separate measurements of tree-ring stable isotopes. *The Science of the Total Environment*, 409(11):2244–51.

Dorale, J. and Liu, Z. (2009). Limitations of Hendy test criteria in judging the paleoclimatic suitability of speleothems and the need for replication. *Journal of Cave and Karst Studies*, 71(1):73–80.

Dreybrodt, W. (1988). *Processes in Karst Systems. Physics, Chemistry, and Geology*. Springer, New York.

Dreybrodt, W. (2008). Evolution of the isotopic composition of carbon and oxygen in a calcite precipitating H2O–CO2–CaCO3 solution and the related isotopic composition of calcite in stalagmites. *Geochimica et Cosmochimica Acta*, 72(19):4712–4724.

Dreybrodt, W. (2011). Letter: Comments on processes contributing to the isotope composition of 13C and 18O in calcite deposited to speleothems. *Acta Carsologica*, 40:233–238.

Dreybrodt, W. and Scholz, D. (2011). Climatic dependence of stable carbon and oxygen isotope signals recorded in speleothems: From soil water to speleothem calcite. *Geochimica et Cosmochimica Acta*, 75(3):734–752.

Dublyansky, Y. V. and Spötl, C. (2009). Hydrogen and oxygen isotopes of water from inclusions in minerals: design of a new crushing system and on-line continuous-flow isotope ratio mass spectrometric analysis. *Rapid Communications in Mass Spectrometry*, 23:2605–2613.

Dubreuil, V. (1997). La sécheresse dans la France de l'Ouest : une contrainte climatique trop souvent oubliée (Drought in western France: a common but often ignored climatic constraint). In French. *Sécheresse*, 8(1):47–55.

Dubreuil, V., Lejeune, C., and Mounier, J. (1997). Changements climatiques régionaux dans la France de l'Ouest (Regional climate changes in the west of France). In French. *Publications de l'Association Internationale de Climatologie*, 9:437–445.

Duplat, P. and Tran-Ha, M. (1997). Modélisation de la croissance en hauteur dominante du chêne sessile (Quercus petraea Liebl) en France. Variabilité inter-régionale et effet de la période récente (1959-1993). *Annals of Forest Sciences*, 54(7):611–634.

Easterling, D. R. (2000). Climate Extremes: Observations, Modeling, and Impacts. *Science*, 289(5487):2068–2074.

Eckstein, D. (2013). 'A new star' – but why just parenchyma for dendroclimatology? *New Phytologist*, 198:328–330.

Edwards, T. L., Crucifix, M., and Harrison, S. P. (2007). Using the past to constrain the future: how the palaeorecord can improve estimates of global warming. *Progress in Physical Geography*, 31(5):481–500.

Ehleringer, J. R. and Dawson, T. E. (1992). Water uptake by plants: perspectives from stable isotope composition. *Plant, Cell & Environment*, 15(9):1073–1082.

Eliáš, P., Kratochvílová, I., Janouš, D., Marek, M., and Masarovičová, E. (1989). Stand microclimate and physiological activity of tree leaves in an oak-hornbeam forest. *Trees*, 3(4):227–233.

Epstein, S., Thompson, P., and Yapp, C. J. (1977). Oxygen and hydrogen isotopic ratios in plant cellulose. *Science*, 198(4323):1209–1215.

Esper, J., Cook, E. R., and Schweingruber, F. H. (2002). Low-frequency signals in long tree-ring chronologies for reconstructing past temperature variability. *Science*, 295(5563):2250–2253.

Esper, J., Frank, D., Büntgen, U., Verstege, A., Luterbacher, J., and Xoplaki, E. (2007). Long-term drought severity variations in Morocco. *Geophysical Research Letters*, 34:1–5.

Esper, J., Frank, D., and Wilson, R. (2004). Climate reconstructions: Low-frequency ambition and high-frequency ratification. *Eos*, 85(12):113–120.

Esper, J., Frank, D. C., Battipaglia, G., Buntgen, U., Holert, C., Treydte, K., Siegwolf, R., and Saurer, M. (2010). Low-frequency noise in delta C-13 and delta O-18 tree ring data: A case study of Pinus uncinata in the Spanish Pyrenees. *Global Biogeochemical Cycles*, 24:1–11.

Esper, J. A. N. (2003). Tests of the RCS method for preserving low-frequency variabiliy in long tree-ring chronologies. *Tree-Ring Research*, 59(2):81–98.

Etien, N. (2008). *Variabilité climatique récente en France: L'apport des isotopes de la cellulose du bois final des chênes de Fontainebleau*. PhD thesis, Université Paris 6.

Etien, N., Daux, V., Masson-Delmotte, V., Mestre, O., Stievenard, M., Guillemin, M. T., Boettger, T., Bréda, N., Haupt, M., and Perraud, P. P. (2009). Summer maximum temperature in northern France over the past century: instrumental data versus multiple proxies (tree-ring isotopes, grape harvest dates and forest fires). *Climatic Change*, 94:429–456.

Etien, N., Daux, V., Masson-Delmotte, V., Stievenard, M., Bernard, V., Durost, S., Guillemin, M. T., Mestre, O., and Pierre, M. (2008). A bi-proxy reconstruction of Fontainebleau (France) growing season temperature from A.D. 1596 to 2000. *Climate of the Past*, 4:1–16.

European Environment Agency (2001). Sustainable Water Use in Europe, Part 3: Extreme Hydrological Events: Floods and Droughts. Environmental issue report No 21.

Fairchild, I., Baker, A., Fuller, L., Borsato, A., Miorandi, R., Frisia, S., Mattey, D., McMillan, E., Spötl, C., Andreo, B., Vadillo, I., and Carrasco, F. (2006a). Speleophysiology: a key to understanding high-resolution information in speleothem. In Onac, B., Tamas, T., Constantin, S. and Persoiu, A., editor, *Archives of Climate Change in Karst, Proceedings of the symposium Climate Change: The Karst Record (IV), (Baile Herculane, Romania) 26-29 May 2006*, pages 4–5, Leesburg, Virginia. Karst Water Institute.

Fairchild, I. I. J., Borsato, A., Tooth, A. F. A., Frisia, S., Hawkesworth, C. J., Huang, Y., McDermott, F., and Spiro, B. (2000). Controls on trace element (Sr–Mg) compositions of carbonate cave waters: implications for speleothem climatic records. *Chemical Geology*, 166(3-4):255–269.

Fairchild, I. J. and Baker, A. (2012). *Speleothem Science – From Process to Past Environments*. Wiley Blackwell, Chichester.

Fairchild, I. J., Smith, C. L., Baker, A., Fuller, L., Spötl, C., Mattey, D., McDermott, F., and E.I.M.F (2006b). Modification and preservation of environmental signals in speleothems. *Earth-Science Reviews*, 75:105–153.

Fairchild, I. J., Spötl, C., Frisia, S., Borsato, A., Susini, J., Wynn, P. M., and Cauzid, J. (2010). Petrology and geochemistry of annually laminated stalagmites from an Alpine cave (Obir, Austria): seasonal cave physiology. *Geological Society, London, Special Publications*, 336(1):295–321.

Fairchild, I. J. and Treble, P. C. (2009). Trace elements in speleothems as recorders of environmental change. *Quaternary Science Reviews*, 28(5-6):449–468.

Farquhar, G. D., Cernusak, L. a., and Barnes, B. (2007). Heavy water fractionation during transpiration. *Plant Physiology*, 143(1):11–8.

Farquhar, G. D., Ehleringer, J. R., and Hubick, K. T. (1989). Carbon isotope discrimintation and photosynthesis. *Annu. Rev. Plant Physiol. Plant Mol. Biol.*, 40:503–537.

Farquhar, G. D., Henry, B. K., and Styles, J. M. (1997). A rapid on-line technique for determination of oxygen isotope composition of nitrogen-containing organic matter and water. *Rapid Communications in Mass Spectrometry*, 11(14):1554–1560.

Farquhar, G. D. and Lloyd, J. (1993). Carbon and Oxygen Isotope Effects in the Exchange of Carbon Dioxide between Terrestrial Plants and the Atmosphere. In Ehleringer, J. R., Hall, A. E., and Farquhar, G. D., editors, *Stable Isotopes and Plant Carbon-water Relations*, pages 47–70. Academic Press, San Diego.

Fernández-Donado, L., González-Rouco, J. F., Raible, C. C., Ammann, C. M., Barriopedro, D., García-Bustamante, E., Jungclaus, J. H., Lorenz, S. J., Luterbacher, J., Phipps, S. J., Servonnat, J., Swingedouw, D., Tett, S. F. B., Wagner, S., Yiou, P., and Zorita, E. (2013). Large-scale temperature response to external forcing in simulations and reconstructions of the last millennium. *Climate of the Past*, 9(1):393–421.

Ferrio, J. P., Pou, A., Florez-Sarasa, I., Gessler, A., Kodama, N., Flexas, J., and Ribas-Carbó, M. (2012). The Péclet effect on leaf water enrichment correlates with leaf hydraulic conductance and mesophyll conductance for CO(2). *Plant, Cell & Environment*, 35(3):611–25.

Feuillat, F., Dupouey, J.-L., Sciama, D., and Keller, R. (1997). A new attempt at discrimination between Quercus petraea and Quercus robur based on wood anatomy. *Canadian Journal of Forest Research*, 27:343–351.

Field, R. D. (2010). Observed and modeled controls on precipitation δ18O over Europe: From local temperature to the Northern Annular Mode. *Journal of Geophysical Research*, 115(D12101):1–14.

Flatley, W. T., Lafon, C. W., Grissino-Mayer, H. D., and LaForest, L. B. (2013). Fire history and its relation to climate and land use in three Southern Appalachian landscapes in the Eastern U.S. *Ecological Applications*, 23:1250–1266.

Fleitmann, D., Burns, S. J., Neff, U., Mangini, A., and Matter, A. (2003). Changing moisture sources over the last 330,000 years in Northern Oman from fluid-inclusion evidence in speleothems. *Quaternary Research*, 60(2):223–232.

Fohlmeister, J., Scholz, D., Kromer, B., and Mangini, A. (2011). Modelling carbon isotopes of carbonates in cave drip water. *Geochimica et Cosmochimica Acta*, 75(18):5219–5228.

Fohlmeister, J., Vollweiler, N., Spötl, C., and Mangini, A. (2012). COMNISPA II: Update of a mid-European isotope climate record, 11 ka to present. *The Holocene*, 23(5):749–754.

Fontugne, M., Shao, Q., Frank, N., Thil, F., Guidon, N., and Boeda, E. (2013). Cross-dating (Th/U-14C) of calcite covering prehistoric paintings at Serra da Capivara National Park, Piaui, Brazil. *Radiocarbon*, 55(3-4):1191–1198.

Ford, D. and Williams, P. (2007). *Karst Hydrology and Geomorphology*. Wiley, Chichester.

Förstel, H. and Hutzen, H. (1982). Use of water with different 18O content to study transport processes in plants. In Schmidt, H. L., Förstel, H., and Heinzinger, K., editors, *Stable Isotopes. Proceedings of the 4th International Conference, Jülich, March 23-26, 1981*, pages 511–516. Elsevier, Amsterdam.

Fricke, H. C. and O'Neil, J. R. (1999). The correlation between O-18/O-16 ratios of meteoric water and surface temperature: its use in investigating terrestrial climate change over geologic time. *Earth and Planetary Science Letters*, 170:181–196.

Friedrich, H. and Smart, P. L. (1981). Dye tracer studies of the unsaturated zone: recharge of the carboniferous limestone aquifer of the Mendip Hills, England. In *Proceedings of the 8th International Congress of Speleology*, pages 283–286, Kentucky.

Friedrich, M., Remmele, S., Kromer, B., Hofmann, J., Spurk, M., Kaiser, K. F., Orcel, C., and Küppers, M. (2004). The 12,460-year Hohenheim oak and pine tree-ring chronology from central Europe – A unique annual record for radiocarbon calibration and paleoenvironment reconstructions. *Radiocarbon*, 46(3):1111–1122.

Frisia, S., Fairchild, I. J., Fohlmeister, J., Miorandi, R., Spötl, C., and Borsato, A. (2011). Carbon mass-balance modelling and carbon isotope exchange processes in dynamic caves. *Geochimica et Cosmochimica Acta*, 75(2):380–400.

Fritts, H. C. (1976). *Tree Rings and Climate*. Academic Press, London.

Fritts, H. C. and Guiot, J. (1990). Methods of Calibration, Verification, and Reconstruction. In Cook, E. R. and Kairiukstis, L. A., editors, *Methods of Dendrochronology – Applications in the Environmental Sciences*, pages 163–217. Kluwer Academic Publishers, Dordrecht.

Gagen, M., McCarroll, D., Jalkanen, R., Loader, N., Robertson, I., and Young, G. (2012). A rapid method for the production of robust millennial length stable isotope tree ring series for climate reconstruction. *Global and Planetary Change*, 82-83:96–103.

Gagen, M., McCarroll, D., Loader, N. J., and Robertson, I. (2011). Stable Isotopes in Dendroclimatology: Moving Beyond 'Potential'. In Hughes, M. K., Swetnam, T. W., and Diaz, H. F., editors, *Dendroclimatology: Progress and Prospects*, pages 147–172. Springer, Dordrecht.

Gagen, M., McCarroll, D., Loader, N. J., Robertson, I., Jalkanen, R., and Anchukaitis, K. J. (2007). Exorcising the 'segment length curse': summer temperature reconstruction since AD 1640 using non-detrended stable carbon isotope ratios from pine trees in northern Finland. *The Holocene*, 17(4):435–446.

Gat, J. R. (1996). Oxygen and hydrogen isotopes in the hydrologic cycle. *Annual Review of Earth and Planetary Sciences*, 24:225–262.

Gat, J. R. (2000). Atmospheric water balance: the isotopic perspective. *Hydrological Processes*, 14(8):1357–1369.

Gazis, C. and Feng, X. (2004). A stable isotope study of soil water: evidence for mixing and preferential flow paths. *Geoderma*, 119(1-2):97–111.

Gehrels, J. and Peeters, J. (1998). The mechanism of soil water movement as inferred from 18O stable isotope studies. *Hydrological Sciences*, 43(4):579–594.

Genty, D. (1993). Mise en évidence d'alternances saisonnières dans la structure interne des stalagmites. Intérêt pour la reconstitution des paléoenvironnements continentaux. *Comptes rendus de l'Académie des sciences. Série 2, Mécanique, Physique, Chimie, Sciences de l'univers, Sciences de la Terre*, 317(9):1229–1236.

Genty, D. (2008). Palaeoclimate Research in Villars Cave (Dordogne, SW-France). *International Journal of Speleology*, 37:173–191.

Genty, D., Baker, A., Massault, M., Proctor, C., Gilmour, M., Pons-Branchu, E., and Hamelin, B. (2001a). Dead carbon in stalagmites: carbonate bedrock paleodissolution vs. ageing of soil organic matter. Implications for 13C variations in speleothems. *Geochimica et Cosmochimica Acta*, 65(20):3443–3457.

Genty, D., Baker, A., and Vokal, B. (2001b). Intra- and inter-annual growth rate of modern stalagmites. *Chemical Geology*, 176(1–4):191–212.

Genty, D., Blamart, D., Ouahdi, R., Gilmour, M., Baker, A., Jouzel, J., and Van-Exter, S. (2003). Precise dating of Dansgaard-Oeschger climate oscillations in western Europe from stalagmite data. *Nature*, 421(6925):833–837.

Genty, D., Combourieu-Nebout, N., Peyron, O., Blamart, D., Wainer, K., Mansuri, F., Ghaleb, B., Isabello, L., Dormoy, I., von Grafenstein, U., Bonelli, S., Landais, A., and Brauer, A. (2010). Isotopic characterization of rapid climatic events during OIS3 and OIS4 in Villars Cave stalagmites (SW-France) and correlation with Atlantic and Mediterranean pollen records. *Quaternary Science Reviews*, 25(19-20):2799–2820.

Genty, D. and Deflandre, G. (1998). Drip flow variations under a stalactite of the Père Noël cave (Belgium). Evidence of seasonal variations and air pressure constraints. *Journal of Hydrology*, 211(1-4):208–232.

Genty, D., Konik, S., Valladas, H., Blamart, D., Hellstrom, J., Touma, M., Moreau, C., Dumoulin, J.-P., Nouet, J., Dauphin, Y., and Weil, R. (2011). Dating the Lascaux Cave Gour Formation. *Radiocarbon*, 53(3):479–500.

Genty, D., Labuhn, I., Hoffmann, G., Danis, P. A., Mestre, O., Bourges, F., Wainer, K., Massault, M., Regnier, E., Orengo, P., Falourd, S., and Minster, B. (2014). Rainfall and cave water isotopic relationships in two South-France sites. *Geochimica et Cosmochimica Acta*, 131:323–343.

Genty, D. and Massault, M. (1997). Bomb 14C Recorded in Laminated Speleothems: Calculation of Dead Carbon Proportion. *Radiocarbon*, 39(1):33–48.

Genty, D. and Massault, M. (1999). Carbon transfer dynamics from bomb-14C and 13C time series of a laminated stalagmite from SW France-modelling and comparison with other stalagmite records. *Geochimica et Cosmochimica Acta*, 63(10):12.

Genty, D., Massault, M., Gilmour, M., Baker, A., Verheyden, S., and Keppens, E. (1999). Calculation of past dead carbon proportion and variability by the comparison of AMS 14C and TIMS U/Th ages on two Holocene stalagmites. *Radiocarbon*, 41(3):251–270.

Genty, D., Plagnes, V., Causse, C., Cattani, O., Stievenard, M., Falourd, S., Blamart, D., Ouahdi, R., and Van-Exter, S. (2002). Fossil water in large stalagmite voids as a tool for paleoprecipitation stable isotope composition reconstitution and paleotemperature calculation. *Chemical Geology*, 184:83–95.

Genty, D. and Quinif, Y. (1996). Annually Laminated Sequences in the Internal Structure of Some Belgian Stalagmites–Importance for Paleoclimatology. *SEPM Journal of Sedimentary Research*, Vol. 66(1):275–288.

Genty, D., Vokal, B., Obelic, B., and Massault, M. (1998). Bomb 14C time history recorded in two modern stalagmites – importance for soil organic matter dynamics and bomb 14C distribution over continents. *Earth and Planetary Science Letters*, 160(3–4):795–809.

Gessler, A., Brandes, E., Buchmann, N., Helle, G., Rennenberg, H., and Barnard, R. L. (2009). Tracing carbon and oxygen isotope signals from newly assimilated sugars in the leaves to the tree-ring archive. *Plant, cell & environment*, 32(7):780–95.

Gessler, A., Brandes, E., Keitel, C., Boda, S., Kayler, Z. E., Granier, A., Barbour, M., Farquhar, G. D., and Treydte, K. (2013). The oxygen isotope enrichment of leaf-exported assimilates - does it always reflect lamina leaf water enrichment? *The New Phytologist*, 200:144–157.

Gindl, W. (2001). Cell-wall lignin content related to tracheid dimensions in drought-sensitive Austrian pone (pinus nigra). *IAWA Journal*, 22(2):113–120.

Gonfiantini, R. (1986). Environmental isotopes in lake studies. In Fritz, P. and Fontes, J. C., editors, *Handbook of Environmental Isotope Geochemistry, The Terrestrial Environment*, pages 113–168. Elsevier, Amsterdam.

Goosse, H., Crespin, E., Dubinkina, S., Loutre, M.-F., Mann, M. E., Renssen, H., Sallaz-Damaz, Y., and Shindell, D. (2012). The role of forcing and internal dynamics in explaining the "Medieval Climate Anomaly". *Climate Dynamics*, 39(12):2847–2866.

Grams, T. E. E., Kozovits, A. R., Haberle, K. H., Matyssek, R., Dawson, T. E., and Häberle, K.-H. (2007). Combining delta 13C and delta 18O analyses to unravel competition, CO2 and O3 effects on the physiological performance of different-aged trees. *Plant, Cell & Environment*, 30(8):1023–1034.

Green, J. W. (1963). Wood Cellulose. In Whistler, R. L., editor, *Methods of Carbohydrate Chemistry*, pages 9–21. Academic Press, New York.

Griffiths, M. L., Drysdale, R. N., Gagan, M. K., Frisia, S., Zhao, J.-x., Ayliffe, L. K., Hantoro, W. S., Hellstrom, J. C., Fischer, M. J., and Feng, Y.-X. (2010a). Evidence for Holocene changes in Australian–Indonesian monsoon rainfall from stalagmite trace element and stable isotope ratios. *Earth and Planetary Science Letters*, 292(1–2):27–38.

Griffiths, M. L., Drysdale, R. N., Vonhof, H. B., Gagan, M. K., Zhao, J.-x., Ayliffe, L. K., Hantoro, W. S., Hellstrom, J. C., Cartwright, I., Frisia, S., and Suwargadi, B. W. (2010b). Younger Dryas-Holocene temperature and rainfall history of southern Indonesia from delta-18O in speleothem calcite and fluid inclusions. *Earth and Planetary Science Letters*, 295:30–36.

Grissino-Mayer, H. D. (2001). Evaluating crossdating accuracy: A manual and tutorial for the computer program COFECHA. *Tree-Ring Research*, 57(2):205–221.

Grootes, P. M., Stuiver, M., White, J. W. C., Johnsen, S., and Jouzel, J. (1993). Comparison of oxygen isotope records from the GISP2 and GRIP Greenland ice cores. *Nature*, 366(6455):552–554.

Grudd, H. (2008). Torneträsk tree-ring width and density AD 500–2004: A test of climatic sensitivity and a new 1500-year reconstruction of north Fennoscandian summers. *Climate Dynamics*, 31(7):843–857.

Hangartner, S., Kress, A., Saurer, M., Frank, D., and Leuenberger, M. (2012). Methods to merge overlapping tree-ring isotope series to generate multi-centennial chronologies. *Chemical Geology*, 294:127–134.

Hardenbroek, M., Gröcke, D. R., Sauer, P. E., and Elias, S. A. (2012). North American transect of stable hydrogen and oxygen isotopes in water beetles from a museum collection. *Journal of Paleolimnology*, 48(2):461–470.

Harding, D. J., Arden, J. W., and Rickaby, R. E. M. (2006). A method for precise analysis of trace element/calcium ratios in carbonate samples using quadrupole inductively coupled plasma mass spectrometry. *Geochemistry, Geophysics, Geosystems*, 7(6):Q06003.

Harlow, B. A., Marshall, J. D., and Robinson, A. P. (2006). A multi-species comparison of delta13C from whole wood, extractive-free wood and holocellulose. *Tree Physiology*, 26(6):767–74.

Harris, I., Jones, P., Osborn, T., and Lister, D. (2013). Updated high-resolution grids of monthly climatic observations – the CRU TS3.10 Dataset. *International Journal of Climatology*, 34(3):623–642.

Hartmann, A., Eiche, E., Neumann, T., Fohlmeister, J., Schröder-Ritzrau, A., Mangini, A., and Haryono, E. (2013). Multi-proxy evidence for human-induced deforestation and cultivation from a late-Holocene stalagmite from middle Java, Indonesia. *Chemical Geology*, 357:8–17.

Harwood, K., Gillon, J., Roberts, A., and Griffiths, H. (1999). Determinants of isotopic coupling of CO2 and water vapour within a Quercus petraea forest canopy. *Oecologia*, 119:109–119.

Haupt, M., Weigl, M., Grabner, M., and Boettger, T. (2011). A 400-year reonstruction of July relative air humidity for the Vienna region (eastern Austria) based on carbon and oxygen stable isotope ratios in tree-ring latewood cellulose of oaks (Quercus petraea Matt. Liebl.). *Climatic Change*, 105:243–262.

Hayes, J. M. (2001). Fractionation of Carbon and Hydrogen Isotopes in Biosynthetic Processes. *Reviews in Mineralogy and Geochemistry*, 43(1):225–277.

Hays, J. D., Imbrie, J., and Shackleton, N. J. (1976). Variations in the Earth's Orbit: Pacemaker of the Ice Ages. *Science*, 194(4270):1121–32.

Heilman, J., McInnes, K., Kjelgaard, J., Keith Owens, M., and Schwinning, S. (2009). Energy balance and water use in a subtropical karst woodland on the Edwards Plateau, Texas. *Journal of Hydrology*, 373(3-4):426–435.

Heinrich, I., Weidner, K., Helle, G., Vos, H., Lindesay, J., and Banks, J. C. G. (2009). Interdecadal modulation of the relationship between ENSO, IPO and precipitation: insights from tree rings in Australia. *Climate Dynamics*, 33(1):63–73.

Helle, G. and Schleser, G. H. (2004a). Beyond CO2-fixation by Rubisco – an interpretation of 13C/12C variations in tree rings from novel intra-seasonal studies on broad-leaf trees. *Plant, Cell & Environment*, 27(3):367–380.

Helle, G. and Schleser, G. H. (2004b). Interpreting Climate Proxies from Tree-rings. In Fischer, H., Kumke, T., Lohmann, G., Flöser, G., Miller, H., von Storch, H., and Negendank, J. F. W., editors, *The Climate in Historical Times. Towards a Synthesis of Holocene Proxy Data and Climate Models*, pages 129–148. Springer, Berlin.

Hellstrom, J. and McCulloch, M. (2000). Multi-proxy constraints on the climatic significance of trace element records from a New Zealand speleothem. *Earth and Planetary Science Letters*, 179(2):287–297.

Hendy, C. H. (1971). The isotopic geochemistry of speleothems–I. The calculation of the effects of different modes of formation on the isotopic composition of speleothems and their applicability as palaeoclimatic indicators. *Geochimica et Cosmochimica Acta*, 35(8):801–824.

Hesterberg, R. and Siegenthaler, U. (1991). Production and stable isotopic composition of CO2 in a soil near Bern, Switzerland. *Tellus*, 43B:197–205.

Hilasvuori, E. and Berninger, F. (2010). Dependence of tree ring stable isotope abundances and ring width on climate in Finnish oak. *Tree Physiology*, 30(5):636–47.

Hill, S. A., Waterhouse, J. S., Field, E. M., Switsur, V. R., and Ap Rees, T. (1995). Rapid recycling of triose phosphates in oak stem tissue. *Plant, Cell & Environment*, 18(8):931–936.

Hoefs, J. (2009). *Stable Isotope Geochemistry*. Springer, Berlin.

Hoffmann, D. L., Spötl, C., and Mangini, A. (2009). Micromill and in situ laser ablation sampling techniques for high spatial resolution MC-ICPMS U-Th dating of carbonates. *Chemical Geology*, 259(3–4):253–261.

Hoffmann, G., Cuntz, M., Jouzel, J., and Werner, M. (2005). How much climate information do water isotopes contain? A systematic comparison between the IAEA/GNIP isotope network and the ECHAM4 atmospheric general circulation model. In Aggarwal, P. K., Gat, J. R., and Froehlich, K. F. O., editors, *Isotopes in the Water Cycle: Past, Present and Future of a Developing Science*, pages 303–320. Springer, Dordrecht.

Hoffmann, G., Jouzel, J., and Masson, V. (2000). Stable water isotopes in atmospheric general circulation models. *Hydrological Processes*, 14(8):1385–1406.

Hoffmann, G., Werner, M., and Heimann, M. (1998). Water isotope module of the ECHAM atmospheric general circulation model: A study on timescales from days to several years. *Journal of Geophysical Research*, 103(D14):16871.

Holmes, R. L. (1983). Computer-assisted quality control in tree-ring dating and measurement. *Tree-Ring Bulletin*, 43:69–78.

Horita, J. and Wesolowski, D. J. (1994). Liquid-vapor fractionation of oxygen and hydrogen isotopes of water from the freezing to the critical temperature. *Geochimica et Cosmochimica Acta*, 58(16):3425–3437.

Hruska, J., Cermák, J., and Sustek, S. (1999). Mapping tree root systems with ground-penetrating radar. *Tree Physiology*, 19(2):125–130.

Hsieh, J. C. C., Chadwick, O. A., Kelly, E. F., and Savin, S. M. (1998). Oxygen isotopic composition of soil water: Quantifying evaporation and transpiration. *Geoderma*, 82(1-3):269–293.

Hu, C., Henderson, G., Huang, J., Chen, Z., and Johnson, K. (2008). Report of a three-year monitoring programme at Heshang Cave, Central China. *International Journal of Speleology*, 37(3):143–151.

Hua, Q. (2009). Radiocarbon: A chronological tool for the recent past. *Quaternary Geochronology*, 4(5):378–390.

Hua, Q., McDonald, J., Redwood, D., Drysdale, R., Lee, S., Fallon, S., and Hellstrom, J. (2012). Robust chronological reconstruction for young speleothems using radiocarbon. *Quaternary Geochronology*, 14:67–80.

Hubbard, R. M., Ryan, M. G., Stiller, V., and Sperry, J. S. (2001). Stomatal conductance and photosynthesis vary linearly with plant hydraulic conductance in ponderosa pine. *Plant, Cell & Environment*, 24(1):113–121.

Hughes, M. K., Swetnam, T. W., and Diaz, H. F., editors (2011). *Dendroclimatology - Progress and Prospects*. Springer, Dordrecht.

IAEA (1997). Technical Procedure for cumulative monthly sampling of precipitation for isotopic analyses. Available at http://www-naweb.iaea.org/NAALIHL/docs/tech_info/Precipitation%20Sampling97.pdf. Technical report, IAEA.

IAEA/WMO (2006). Global Network of Isotopes in Precipitation. The GNIP Database. Accessible at: http://www.iaea.org/water.

INPN (2013). FR5400406 - Forêts de la Braconne et de Bois Blanc. Inventaire Nationale du Patrimoine Naturel. Natura 2000. Available at http://inpn.mnhn.fr/docs/natura2000/fsdpdf/FR5400406.pdf.

IPCC (2013). *Climate Change 2013: The Physical Science Basis. Contribution of Working Group I to the Fifth Assessment Report of the Intergovernmental Panel on Climate Change*. Cambridge University Press, Cambridge, UK and New York, USA.

Itier, B. (2008). Agriculture et sécheresse: le contexte et les enjeux (Agriculture and drought: context and challenges). In French. *Innovations Agronomiques*, 2:1–8.

Jacob, D. (2001). A note to the simulation of the annual and inter-annual variability of the water budget over the Baltic Sea drainage basin. *Meteorology and Atmospheric Physics*, 77(1-4):61–73.

Jacob, D. and Podzun, R. (1997). Sensitivity studies with the regional climate model REMO. *Meteorology and Atmospheric Physics*, 63(1-2):119–129.

Jacoby, G. C. and D'Arrigo, R. (1989). Reconstructed Northern Hemisphere annual temperature since 1671 based on high-latitude tree-ring data from North America. *Climatic Change*, 14(1):39–59.

Jasechko, S., Sharp, Z. D., Gibson, J. J., Birks, S. J., Yi, Y., and Fawcett, P. J. (2013). Terrestrial water fluxes dominated by transpiration. *Nature*, 496(7445):347–350.

Johnsen, S. J., Dahl-Jensen, D., Gundestrup, N., Steffensen, J. P., Clausen, H. B., Miller, H., Masson-Delmotte, V., Sveinbjörnsdottir, A. E., and White, J. (2001). Oxygen isotope and palaeotemperature records from six Greenland ice-core stations: Camp Century, Dye-3, GRIP, GISP2, Renland and NorthGRIP. *Journal of Quaternary Science*, 16(4):299–307.

Johnson, K., Hu, C., Belshaw, N., and Henderson, G. (2006). Seasonal trace-element and stable-isotope variations in a Chinese speleothem: The potential for high-resolution paleomonsoon reconstruction. *Earth and Planetary Science Letters*, 244(1-2):394–407.

Jones, P. D., Briffa, K. R., and Osborn, T. J. (2003). Changes in the Northern Hemisphere annual cycle: Implications for paleoclimatology? *Journal of Geophysical Research*, 108(D18):4588.

Jones, P. D., Briffa, K. R., Osborn, T. J., Lough, J. M., van Ommen, T. D., Vinther, B. M., Luterbacher, J., Wahl, E. R., Zwiers, F. W., Mann, M. E., Schmidt, G. A., Ammann, C. M., Buckley, B. M., Cobb, K. M., Esper, J., Goosse, H., Graham, N., Jansen, E., Kiefer, T., Kull, C., Kuttel, M., Mosley-Thompson, E., Overpeck, J. T., Riedwyl, N., Schulz, M., Tudhope, A. W., Villalba, R., Wanner, H., Wolff, E., and Xoplaki, E. (2009). High-resolution palaeoclimatology of the last millennium: a review of current status and future prospects. *Holocene*, 19:3–49.

Jones, P. D. and Mann, M. E. (2004). Climate over past millennia. *Reviews of Geophysics*, 42(2):RG2002.

Jönsson, K. and Nilsson, C. (2009). Scots Pine (Pinus sylvestris L.) on shingle fields: A dendrochronologic reconstruction of early summer precipitation in mid-east Sweden. *Journal of Climate*, 22(17):4710–4722.

Joussaume, S., Sadourny, R., and Jouzel, J. (1984). A general circulation model of water isotope cycles in the atmosphere. *Nature*, 311(5981):24–29.

Jouzel, J., Alley, R. B., Cuffey, K. M., Dansgaard, W., Grootes, P., Hoffmann, G., Johnsen, S. J., Koster, R. D., Peel, D., Shuman, C. A., Stievenard, M., Stuiver, M., and White, J. (1997). Validity of the temperature reconstruction from water isotopes in ice cores. *Journal of Geophysical Research*, 102(C12):26471.

Jouzel, J., Delaygue, G., Landais, A., Masson-Delmotte, V., Risi, C., and Vimeux, F. (2013). Water isotopes as tools to document oceanic sources of precipitation. *Water Resources Research*, 49(11):7469–7486.

Jouzel, J., Lorius, C., Petit, J. R., Genthon, C., Barkov, N. I., Kotlyakov, V. M., and Petrov, V. M. (1987). Vostok ice core: a continuous isotope temperature record over the last climatic cycle (160,000 years). *Nature*, 329(6138):403–408.

Katz, R. W. and Brown, B. G. (1992). Extreme events in a changing climate: Variability is more important than averages. *Climatic Change*, 21(3):289–302.

Kaufman, A., Bar-Matthews, M., Ayalon, A., and Carmi, I. (2003). The vadose flow above Soreq Cave, Israel: a tritium study of the cave waters. *Journal of Hydrology*, 273(1-4):155–163.

Keeling, C. D., Piper, S. C., Bacastow, R. B., Wahlen, M., Whorf, T. P., Heimann, M., and Meijer, H. A. (2005). Atmospheric CO2 and 13CO2 Exchange with the Terrestrial Biosphere and Oceans from 1978 to 2000: Observations and Carbon Cycle Implications. In Baldwin, I., Caldwell, M., Heldmaier, G., Jackson, R. B., Lange, O., Mooney, H., Schulze, E.-D., Sommer, U., Ehleringer, J. R., Denise Dearing, M., and Cerling, T. E., editors, *A History of Atmospheric CO2 and Its Effects on Plants, Animals, and Ecosystems*, volume 177 of *Ecological Studies*, pages 83–113. Springer, New York.

Kern, Z., Kohán, B., and Leuenberger, M. (2013). Monthly resolved biannual precipitation oxygen isoscape for Switzerland. *Atmospheric Chemistry and Physics Discussions*, 13(4):9895–9916.

Kim, S.-T. and O'Neil, J. R. (1997). Equilibrium and nonequilibrium oxygen isotope effects in synthetic carbonates. *Geochimica et Cosmochimica Acta*, 61(16):3461–3475.

Kitano, Y. and Oomori, T. (1971). The coprecipitation of uranium with calcium carbonate. *Journal of the Oceanographical Society of Japan*, 27(1):34–42.

Klemm, D., Heublein, B., Fink, H.-P., and Bohn, A. (2005). Cellulose: fascinating biopolymer and sustainable raw material. *Angewandte Chemie (International ed. in English)*, 44(22):3358–93.

Kluge, T. (2008). *Fluid inclusions in speleothems as a new archive for the noble gas palaeothermometer*. PhD thesis, University of Heidelberg.

Kluge, T. and Affek, H. P. (2012). Quantifying kinetic fractionation in Bunker Cave speleothems using $\Delta 47$. *Quaternary Science Reviews*, 49:82–94.

Kluge, T., Affek, H. P., Marx, T., Aeschbach-Hertig, W., Riechelmann, D. F. C., Scholz, D., Riechelmann, S., Immenhauser, A., Richter, D. K., Fohlmeister, J., Wackerbarth, A., Mangini, A., and Spötl, C. (2013). Reconstruction of drip-water δ18O based on calcite oxygen and clumped isotopes of speleothems from Bunker Cave (Germany). *Climate of the Past*, 9(1):377–391.

Kluge, T., Riechelmann, D., Wieser, M., Spötl, C., Sültenfuß, J., Schröder-Ritzrau, a., Niggemann, S., and Aeschbach-Hertig, W. (2010). Dating cave drip water by tritium. *Journal of Hydrology*, 394(3-4):396–406.

Kohn, M. J. and Welker, J. M. (2005). On the temperature correlation of δ18O in modern precipitation. *Earth and Planetary Science Letters*, 231(1-2):87–96.

Koster, R. D., de Valpine, D. P., and Jouzel, J. (1993). Continental water recycling and H218 O concentrations. *Geophysical Research Letters*, 20(20):2215–2218.

Koziet, J. (1997). Isotope ratio mass spectrometric method for the on-line determination of oxygen-18 in organic matter. *Journal of Mass Spectrometry*, 32(1):103–8.

Kress, A., Hangartner, S., Bugmann, H., Büntgen, U., Frank, D. C., Leuenberger, M., Siegwolf, R. T., and Saurer, M. (2014). Swiss tree-rings reveal warm and wet summers during medieval times. *Geophysical Research Letters. In press.*

Krinner, G., Viovy, N., de Noblet-Ducoudré, N., Ogée, J., Polcher, J., Friedlingstein, P., Ciais, P., Sitch, S., and Prentice, I. C. (2005). A dynamic global vegetation model for studies of the coupled atmosphere-biosphere system. *Global Biogeochemical Cycles*, 19:GB1015.

Kromer, B., Friedrich, M., and Spurk, M. (2001). Natürliche Klimaschwankungen im Spätglazial und Holozän im Spiegel von Baumringen. *Nova Acta Leopoldina*, 88(331):151–159.

Krüger, Y., Marti, D., Staub, R. H., Fleitmann, D., and Frenz, M. (2011). Liquid–vapour homogenisation of fluid inclusions in stalagmites: Evaluation of a new thermometer for palaeoclimate research. *Chemical Geology*, 289(1-2):39–47.

Labuhn, I., Daux, V., Pierre, M., Stievenard, M., Girardclos, O., Féron, A., Genty, D., Masson-Delmotte, V., and Mestre, O. (2014). Tree age, site and climate controls on tree ring cellulose δ18O: A case study on oak trees from south-western France. *Dendrochronologia*, 32:78–89.

Lacelle, D., Lauriol, B., and Clark, I. D. (2004). Seasonal isotopic imprint in moonmilk from Caverne de l'Ours (Quebec, Canada): implications for climatic reconstruction. *Canadian Journal of Earth Sciences*, 41(12):1411–1423.

Lachniet, M. S. (2009). Climatic and environmental controls on speleothem oxygen-isotope values. *Quaternary Science Reviews*, 28:412–432.

Lang, N. and Wolff, E. W. (2011). Interglacial and glacial variability from the last 800 ka in marine, ice and terrestrial archives. *Climate of the Past*, 7(2):361–380.

Langebroek, P., Werner, M., and Lohmann, G. (2011). Climate information imprinted in oxygen-isotopic composition of precipitation in Europe. *Earth and Planetary Science Letters*, 311(1-2):144–154.

Larson, E. R., Kipfmueller, K. F., Hale, C. M., Frelich, L. E., and Reich, P. B. (2009). Tree rings detect earthworm invasions and their effects in northern Hardwood forests. *Biological Invasions*, 12(5):1053–1066.

Laumer, W., Andreu, L., Helle, G., Schleser, G. H., Wieloch, T., and Wissel, H. (2009). A novel approach for the homogenization of cellulose to use micro-amounts for stable isotope analyses. *Rapid Communications in Mass Spectrometry*, 23:1934–1940.

Lawrence, J. R. and White, J. W. C. (1991). The elusive climate signal in the isotopic composition of precipitation. In Taylor, H. P., O'Neil, J. R., and Kaplan, I. R., editors, *Stable Isotope Geochemistry*, pages 169–185. Geochemical Society, St. Louis, Missouri.

Leavitt, S. W. (2008). Tree-ring isotopic pooling without regard to mass: No difference from averaging δ13C values of each tree. *Chemical Geology*, 252(1-2):52–55.

Leavitt, S. W. (2010). Tree-ring C-H-O isotope variability and sampling. *The Science of the total environment*, 408(22):5244–53.

Leavitt, S. W. and Danzer, S. R. (1993). Method for batch processing small wood samples to holocellulose for stable-carbon isotope analysis. *Analytical Chemistry*, 65(1):87–89.

Leavitt, S. W., Treydte, K., and Yu, L. (2010). Environment in Time and Space: Opportunities from Tree-Ring Isotope Networks. In West, J. B., Bowen, G. J., Dawson, T. E., and Tu, K. P., editors, *Isoscapes*, pages 113–135. Springer, Dordrecht.

Lécolle, P. (1985). The oxygen isotope composition of landsnail shells as a climatic indicator: Applications to hydrogeology and paleoclimatology. *Chemical Geology: Isotope Geoscience section*, 58(1-2):157–181.

Lemaire, J., Lacouture, Y., Soleau, M., Weben, C., Mounier, M., and Guyon, A. (2010). Les chênaies atlantiques face aux changements climatiques globaux : comprendre et agir (Atlantic oak forests in the light of global changes: understanding and acting). In French. *Forêt – entreprise*, 191:50–53.

Levrault, F., Brisson, N., Pieri, P., and Bosc, A. (2010). Climate change in the South-West zone: the main agricultural and forest impacts. In Brisson, N. and Levrault, F., editors, *Climate Change, Agriculture and Forests in France: Simulations of the Impacts on the Mail Species. The Green Book of the CLIMATOR project (2007-2010)*, pages 287–296. ADEME.

Lévy, G., Becker, M., and Duhamel, D. (1992). A comparison of the ecology of pedunculate and sessile oaks: Radial growth in the centre and northwest of France. *Forest Ecology and Management*, 55(1-4):51–63.

Li, B., Nychka, D. W., and Ammann, C. M. (2010). The Value of Multiproxy Reconstruction of Past Climate. *Journal of the American Statistical Association*, 105(491):883–895.

Li, J., Gou, X., Cook, E. R., and Chen, F. (2006). Tree-ring based drought reconstruction for the central Tien Shan area in northwest China. *Geophysical Research Letters*, 33:1–5.

Linares, J. C., Taïqui, L., Sangüesa-Barreda, G., Seco, J. I., and Camarero, J. J. (2012). Age-related drought sensitivity of Atlas cedar (Cedrus atlantica) in the Moroccan Middle Atlas forests. *Dendrochronologia*, 31(2):88–96.

Liu, X., Shao, X., Zhao, L., Qin, D., Chen, T., and Ren, J. (2007). Dendroclimatic Temperature Record Derived from Tree-Ring Width and Stable Carbon Isotope Chronologies in the Middle Qilian Mountains, China. *Arctic, Antarctic, and Alpine Research*, 39(4):651–657.

Loader, N., Robertson, I., and McCarroll, D. (2003). Comparison of stable carbon isotope ratios in the whole wood, cellulose and lignin of oak tree-rings. *Palaeogeography, Palaeoclimatology, Palaeoecology*, 196(3-4):395–407.

Loader, N., Santillo, P., Woodman-Ralph, J., Rolfe, J., Hall, M., Gagen, M., Robertson, I., Wilson, R., Froyd, C., and McCarroll, D. (2008). Multiple stable isotopes from oak trees in southwestern Scotland and the potential for stable isotope dendroclimatology in maritime climatic regions. *Chemical Geology*, 252(1-2):62–71.

Loader, N., Switsur, V., and Field, E. (1995). High-resolution stable isotope analysis of tree rings: implications of 'microdendroclimatology' for palaeoenvironmental research. *The Holocene*, 5(4):457–460.

Loader, N. J., Young, G. H., McCarroll, D., and Wilson, R. J. (2013). Quantifying uncertainty in isotope dendroclimatology. *The Holocene*, 23(9):1221–1226.

Managave, S. R. (2014). Model evaluation of the coherence of a common source water oxygen isotopic signal recorded by tree-ring cellulose and speleothem calcite. *Geochemistry, Geophysics, Geosystems. In press.*

Mann, M. E. (2002). Climate reconstruction. The value of multiple proxies. *Science*, 297(5586):1481–1482.

Mann, M. E., Bradley, R. S., and Hughes, M. K. (1999). Northern hemisphere temperatures during the past millennium: Inferences, uncertainties, and limitations. *Geophysical Research Letters*, 26(6):759–762.

Marlin, C., Dever, L., Vachier, P., and Courty, M.-A. (1993). Variations chimiques et isotopiques de l'eau du sol lors de la reprise en gel d'une couche active sur pergélisol continu (Presqu'île de Brögger, Svalbard). *Canadian Journal of Earth Sciences*, 30(4):806–813.

Marshall, J. D. and Monserud, R. A. (2006). Co-occurring species differ in tree-ring delta O-18 trends. *Tree Physiology*, 26(8):1055–1066.

Masson-Delmotte, V., Raffalli-Delerce, G., Danis, P. A., Yiou, P., Stievenard, M., Guibal, F., Mestre, O., Bernard, V., Goosse, H., Hoffmann, G., and Jouzel, J. (2005). Changes in European precipitation seasonality and in drought frequencies revealed by a four-century-long tree-ring isotopic record from Brittany, western France. *Climate Dynamics*, 24:57–69.

Masson-Delmotte, V., Schulz, M., Abe-Ouchi, A., Beer, J., Ganopolski, A., González Rouco, J., Jansen, E., Lambeck, K., Luterbacher, J., Naish, T., Osborn, T., Otto-Bliesner, B., Quinn, T., Ramesh, R., Rojas, M., Shao, X., and Timmermann, A. (2013). Information from Paleoclimate Archives. In Stocker, T., Qin, D., Plattner, G.-K., Tignor, M., Allen, S., Boschung, J., Nauels, A., Xia, Y., Bex, V., and Midgley, P., editors, *Climate Change 2013: The Physical Science Basis. Contribution of Working Group I to the Fifth Assessment Report of the Intergovernmental Panel on Climate Change*, pages 383–464. Cambridge University Press, Cambridge, UK and New York, USA.

Mattey, D., Lowry, D., Duffet, J., Fisher, R., Hodge, E., and Frisia, S. (2008). A 53 year seasonally resolved oxygen and carbon isotope record from a modern Gibraltar speleothem: Reconstructed drip water and relationship to local precipitation. *Earth and Planetary Science Letters*, 269(1-2):80–95.

Matthews, A., Ayalon, A., and Bar-Matthews, M. (2000). D/H ratios of fluid inclusions of Soreq cave (Israel) speleothems as a guide to the Eastern Mediterranean Meteoric Line relationships in the last 120 ky. *Chemical Geology*, 166(3-4):183–191.

Mayr, C., Frenzel, B., Friedrich, M., Spurk, M., Stichler, W., and Trimborn, P. (2003). Stable carbon- and hydrogen-isotope ratios of subfossil oaks in southern Germany: methodology and application to a composite record for the Holocene. *The Holocene*, 13(3):393–402.

McCarroll, D. and Loader, N. J. (2004). Stable isotopes in tree rings. *Quaternary Science Reviews*, 23:771–801.

McDermott, F. (2004). Palaeo-climate reconstruction from stable isotope variations in speleothems: a review. *Quaternary Science Reviews*, 23(7–8):901–918.

McDermott, F., Atkinson, T., Fairchild, I., Baldini, L., and Mattey, D. (2011). A first evaluation of the spatial gradients in δ18O recorded by European Holocene speleothems. *Global and Planetary Change*, 79(3-4):275–287.

McDermott, F., Schwarcz, H. P., and Rowe, P. J. (2006). Isotopes in Speleothems. In Leng, M. J., editor, *Isotopes in Palaeoenvironmental Research*, pages 185–226. Springer, Dordrecht.

McGarry, S., Bar-Matthews, M., Matthews, A., Vaks, A., Schilman, B., and Ayalon, A. (2004). Constraints on hydrological and paleotemperature variations in the Eastern Mediterranean region in the last 140ka given by the δD values of speleothem fluid inclusions. *Quaternary Science Reviews*, 23(7-8):919–934.

McKee, T. B., Doesken, N. J., and Kleist, J. (1993). The relationship of drought frequency and duration to time scales.

McKinney, C. R., McCrea, J. M., Epstein, S., Allen, H. A., and Urey, H. C. (1950). Improvements in mass spectrometers for the measurement of small differences in isotope abundance ratios. *Review of Scientific Instruments*, 21:724–730.

Melayah, A., Bruckler, L., and Bariac, T. (1996). Modeling the transport of water stable isotopes in unsaturated soils under natural conditions: 2. Comparison with field experiments. *Water Resources Research*, 32(7):2055–2065.

Mérian, P., Bontemps, J.-D., Bergès, L., and Lebourgeois, F. (2011). Spatial variation and temporal instability in climate-growth relationships of sessile oak (Quercus petraea [Matt.] Liebl.) under temperate conditions. *Plant Ecology*, 212(11):1855–1871.

Merlivat, L. and Jouzel, J. (1979). Global climatic interpretation of the deuterium-oxygen 18 relationship for precipitation. *Journal of Geophysical Research*, 84(C8):5029.

Michelot, A., Simard, S., Rathgeber, C., Dufrêne, E., and Damesin, C. (2012). Comparing the intra-annual wood formation of three European species (Fagus sylvatica, Quercus petraea and Pinus sylvestris) as related to leaf phenology and non-structural carbohydrate dynamics. *Tree Physiology*, 32(8):1033–45.

Mickler, P. J., Banner, J. L., Stern, L., Asmerom, Y., Edwards, R. L., and Ito, E. (2004). Stable isotope variations in modern tropical speleothems: Evaluating equilibrium vs. kinetic isotope effects. *Geochimica et Cosmochimica Acta*, 68(21):4381–4393.

Mickler, P. J., Stern, L. a., and Banner, J. L. (2006). Large kinetic isotope effects in modern speleothems. *Geological Society of America Bulletin*, 118(1–2):65–81.

Mitchell, J. F. B. (1989). The "Greenhouse" effect and climate change. *Reviews of Geophysics*, 27(1):115.

Moberg, A., Sonechkin, D. M., Holmgren, K., Datsenko, N. M., Karlén, W., and Lauritzen, S.-E. (2005). Highly variable Northern Hemisphere temperatures reconstructed from low- and high-resolution proxy data. *Nature*, 433(7026):613–7.

Moisselin, J.-m., Schneider, M., and Canellas, C. (2002). Les changements climatiques en France au XXe siècle: Étude des longues séries homogénéisées de données de température et de précipitations (Climatic changes in France in the XXth century. A study of long, homogenized temperature and precipitation series). *La Météorologie*, 38:45–56.

Mook, W. G. (2000). Volume I Introduction. Theory Methods Review. In Mook, W. G., editor, *Environmental isotopes in the hydrological cycle. Principles and applications*. UNESCO/IAEA, Paris.

Mook, W. G. and van der Plicht, J. (1999). Reporting 14C activities and concentrations. *Radiocarbon*, 41(3):227–239.

Moore, G. (1952). Speleothem – a new cave term. *National Speleological Society News*, 10(6):2.

Moreira, M. Z., Sternberg, L., Martinelli, L., Victoria, R., Barbosa, E., Bonates, L., and Nepstad, D. (1997). Contribution of transpiration to forest ambient vapour based on isotopic measurements. *Global Change Biology*, 3(5):439–450.

National Research Council (2006). *Surface Temperature Reconstructions for the Last 2,000 Years*. The National Academies Press, Washington, D.C.

Nicault, A., Alleaume, S., Brewer, S., Carrer, M., Nola, P., and Guiot, J. (2008). Mediterranean drought fluctuation during the last 500 years based on tree ring data. *Climate Dynamics*, 31(2–3):227–245.

Obrist, D., Yakir, D., and Arnone III, J. a. (2004). Temporal and spatial patterns of soil water following wildfire-induced changes in plant communities in the Great Basin in Nevada, USA. *Plant and Soil*, 262(1/2):1–12.

Offermann, C., Ferrio, J. P., Holst, J., Grote, R., Siegwolf, R., Kayler, Z., and Gessler, A. (2011). The long way down–are carbon and oxygen isotope signals in the tree ring uncoupled from canopy physiological processes? *Tree Physiology*, 31(10):1088–1102.

Ogée, J., Barbour, M. M., Wingate, L., Bert, D., Bosc, A., Stievenard, M., Lambrot, C., Pierre, M., Bariac, T., Loustau, D., and Dewar, R. C. (2009). A single-substrate model to interpret intra-annual stable isotope signals in tree-ring cellulose. *Plant, Cell & Environment*, 32(8):1071–90.

Olano, J. M., Arzac, A., García-Cervigón, A. I., von Arx, G., and Rozas, V. (2013). New star on the stage: amount of ray parenchyma in tree rings shows a link to climate. *The New Phytologist*, 198(2):486–95.

O'Neil, J. R., Clayton, R. N., and Mayeda, T. K. (1969). Oxygen Isotope Fractionation in Divalent Metal Carbonates. *The Journal of Chemical Physics*, 51:5547–5558.

Oster, J. L., Montañez, I. P., and Kelley, N. P. (2012). Response of a modern cave system to large seasonal precipitation variability. *Geochimica et Cosmochimica Acta*, 91:92–108.

PAGES 2k Network (2013). Continental-scale temperature variability during the past two millennia. *Nature Geoscience*, 6:339–346.

Paillard, D., Labeyrie, L., and Yiou, P. (1996). Macintosh Program performs time-series analysis. *Eos, Transactions American Geophysical Union*, 77(39):379–379.

Palmer, W. C. (1965). Meteorological Drought. US Weather Bureau. Washington, D.C.

Parham, R. A. and Gray, R. L. (1984). Formation and Structure of Wood. In Rowell, R., editor, *The Chemistry of Soild Wood*, pages 3–56. American Chemical Society, Washington, D.C.

Paritsis, J. and Veblen, T. T. (2011). Dendroecological analysis of defoliator outbreaks on Nothofagus pumilio and their relation to climate variability in the Patagonian Andes. *Global Change Biology*, 17(1):239–253.

Peñuelas, J. (2005). Plant physiology: a big issue for trees. *Nature*, 437(7061):965–966.

Pettersen, R. C. (1984). The Chemical Composition of Wood. In Rowell, R., editor, *The Chemistry of Solid Wood*, volume 207 of *Advances in Chemistry*, pages 57–126. American Chemical Society, Washington, DC.

Phillips, S. L. and Ehleringer, J. R. (1995). Limited uptake of summer precipitation by bigtooth maple. *Trees*, 9:214–219.

Pichon, A., Travi, Y., and Marc, V. (1996). Chemical and isotopic variations in throughfall in a Mediterranean context. *Geophysical Research Letters*, 23(5):531–534.

Polag, D., Scholz, D., Mühlinghaus, C., Spötl, C., Schröder-Ritzrau, A., Segl, M., and Mangini, A. (2010). Stable isotope fractionation in speleothems: Laboratory experiments. *Chemical Geology*, 279(1-2):31–39.

Polissar, P. J. and Freeman, K. H. (2010). Effects of aridity and vegetation on plant-wax δD in modern lake sediments. *Geochimica et Cosmochimica Acta*, 74(20):5785–5797.

Poulos, H., Villanueva Díaz, J., Cerano Paredes, J., Camp, A., and Gatewood, R. (2013). Human influences on fire regimes and forest structure in the Chihuahuan Desert Borderlands. *Forest Ecology and Management*, 298:1–11.

Proctor, C. J., Baker, A., and Barnes, W. L. (2002). A three thousand year record of North Atlantic climate. *Climate Dynamics*, 19(5-6):449–454.

Proctor, C. J., Baker, A., Barnes, W. L., and Gilmour, M. A. (2000). A thousand year speleothem proxy record of North Atlantic climate from Scotland. *Climate Dynamics*, 16(10-11):815–820.

R Development Core Team (2011). R: A Language and Environment for Statistical Computing. http://www.r-project.org.

Raffalli-Delerce, G., Masson-Delmotte, V., Dupouey, J. L., Stievenard, M., Bréda, N., Moisselin, J. M., and Munksgaard, B. (2004). Reconstruction of summer droughts using tree-ring cellulose isotopes: a calibration study with living oaks from Brittany (western France). *Tellus*, 56B:160–174.

Reece, J. B., Taylor, M. R., Simon, E. J., and Dickey, J. L. (2011). *Campbell Biology: Concepts & Connections*. Benjamin Cummings, San Francisco, 7th edition.

Reimer, P., Bard, E., and Bayliss, A. (2013). IntCal13 and Marine13 radiocarbon age calibration curves 0–50,000 years cal BP. *Radiocarbon*, 55(4):1869–1887.

Reynolds-Henne, C. E., Saurer, M., and Siegwolf, R. T. W. (2009). Temperature versus species-specific influences on the stable oxygen isotope ratio of tree rings. *Trees*, 23(4):801–811.

Reynolds-Henne, C. E., Siegwolf, R. T. W., Treydte, K. S., Esper, J., Henne, S., and Saurer, M. (2007). Temporal stability of climate-isotope relationships in tree rings of oak and pine (Ticino, Switzerland). *Global Biogeochemical Cycles*, 21(4):1–12.

Rinne, K., Boettger, T., Loader, N., Robertson, I., Switsur, V., and Waterhouse, J. (2005). On the purification of α-cellulose from resinous wood for stable isotope (H, C and O) analysis. *Chemical Geology*, 222(1-2):75–82.

Risi, C., Bony, S., Vimeux, F., and Jouzel, J. (2010). Water-stable isotopes in the LMDZ4 general circulation model: Model evaluation for present-day and past climates and applications to climatic interpretations of tropical isotopic records. *Journal of Geophysical Research*, 115(D12):1–27.

Robertson, I., Waterhouse, J. S., Barker, A. C., Carter, A. H. C., and Switsur, V. R. (2001). Oxygen isotope ratios of oak in east England: implications for reconstructing the isotopic composition of precipitation. *Earth and Planetary Science Letters*, 191(1-2):21–31.

Roden, J. and Siegwolf, R. (2012). Is the dual-isotope conceptual model fully operational? *Tree Physiology*, 32(10):1179–1182.

Roden, J. S. and Farquhar, G. D. (2012). A controlled test of the dual-isotope approach for the interpretation of stable carbon and oxygen isotope ratio variation in tree rings. *Tree Physiology*, 32(4):490–503.

Roden, J. S., Johnstone, J. A., and Dawson, T. E. (2009). Intra-annual variation in the stable oxygen and carbon isotope ratios of cellulose in tree rings of coast redwood (Sequoia sempervirens). *The Holocene*, 19(2):189–197.

Roden, J. S., Johnstone, J. A., and Dawson, T. E. (2011). Regional And Watershed-Scale Coherence In the Stable-Oxygen and Carbon Isotope Ratio Time Series In Tree Rings Of Coast Redwood (Sequoia sempervirens). *Tree-Ring Research*, 67(2):71–86.

Roden, J. S., Lin, G., and Ehleringer, J. R. (2000). A mechanistic model for interpretation of hydrogen and oxygen isotope ratios in tree-ring cellulose. *Geochimica et Cosmochimica Acta*, 64:21–35.

Roeckner, E., Arpe, K., Bengtsson, L., Christoph, M., Claussen, M., Dümenil, L., Esch, M., Giorgetta, M., Schlese, U., and Schulzweida, U. (1996). The atmospheric general circulation model ECHAM-4: Model description and simulation of present-day climate. Technical report, MPI, Max Planck Insitut für Meteorologie. Report No. 218.

Romanov, D., Kaufmann, G., and Dreybrodt, W. (2008). δ13C profiles along growth layers of stalagmites: Comparing theoretical and experimental results. *Geochimica et Cosmochimica Acta*, 72(2):438–448.

Rosenthal, Y., Field, M. P., and Sherrell, R. M. (1999). Precise determination of element/-calcium ratios in calcareous samples using sector field inductively coupled plasma mass spectrometry. *Analytical chemistry*, 71(15):3248–53.

Rozanski, K., Araguás-Araguás, L., and Gonfiantini, R. (1992). Relation between long-term trends of oxygen-18 isotope composition of precipitation and climate. *Science*, 258(5084):981–985.

Rozanski, K., Sonntag, C., and Münnich, K. O. (1982). Factors controlling stable isotope composition of European precipitation. *Tellus*, 34:142–150.

Rozas, V. and Olano, J. M. (2013). Environmental heterogeneity and neighbourhood interference modulate the individual response of Juniperus thurifera tree-ring growth to climate. *Dendrochronologia*, pages 1–9.

Rudzka, D., McDermott, F., Baldini, L., Fleitmann, D., Moreno, a., and Stoll, H. (2011). The coupled δ13C-radiocarbon systematics of three Late Glacial/early Holocene speleothems; insights into soil and cave processes at climatic transitions. *Geochimica et Cosmochimica Acta*, 75(15):4321–4339.

Saurer, M., Aellen, K., and Siegwolf, R. (1997a). Correlating delta13C and delta18O in cellulose of trees. *Plant, Cell & Environment*, 20(12):1543–1550.

Saurer, M., Borella, S., and Leuenberger, M. (1997b). δ18O of tree rings of beech (Fagus silvatica) as a record of δ18O of the growing season precipitation. *Tellus*, 49B:80–92.

Saurer, M., Cherubini, P., Reynolds-Henne, C. E., Treydte, K. S., Anderson, W. T., and Siegwolf, R. T. W. (2008). An investigation of the common signal in tree ring stable isotope chronologies at temperate sites. *Journal of Geophysical Research*, 113:G04035.

Saurer, M., Robertson, I., Siegwolf, R., and Leuenberger, M. (1998a). Oxygen Isotope Analysis of Cellulose: An Interlaboratory Comparison. *Analytical Chemistry*, 70(10):2074–2080.

Saurer, M., Siegwolf, R., Borella, S., and Schweingruber, F. (1998b). Environmental information from stable isotopes in tree rings of Fagus sylvatica. In Beniston, M. and Innes, J. L., editors, *The Impacts of Climate Variability on Forests*, volume 74 of *Lecture Notes in Earth Sciences*, pages 241–253. Springer, Berlin/Heidelberg.

Savard, M. M., Bégin, C., Marion, J., Arseneault, D., and Bégin, Y. (2012). Evaluating the integrity of C and O isotopes in sub-fossil wood from boreal lakes. *Palaeogeography, Palaeoclimatology, Palaeoecology*, 348–349:21–31.

Saxena, R. K. (1986). Estimation of canopy reservoir capacity and oxygen-18 fractionation in throughfall in a pine forest. *Nordic Hydrology*, 17(4-5):251–260.

Schäfer, K. V. R., Oren, R., and Tenhunen, J. D. (2000). The effect of tree height on crown level stomatal conductance. *Plant, Cell & Environment*, 23:365–375.

Scheidegger, Y., Baur, H., Brennwald, M. S., Fleitmann, D., Wieler, R., and Kipfer, R. (2010). Accurate analysis of noble gas concentrations in small water samples and its application to fluid inclusions in stalagmites. *Chemical Geology*, 272(1-4):31–39.

Scheidegger, Y., Brennwald, M. S., Fleitmann, D., Jeannin, P.-Y., Wieler, R., and Kipfer, R. (2011). Determination of Holocene cave temperatures from Kr and Xe concentrations in stalagmite fluid inclusions. *Chemical Geology*, 288(1-2):61–66.

Scheidegger, Y., Saurer, M., Bahn, M., and Siegwolf, R. (2000). Linking stable oxygen and carbon isotopes with stomatal conductance and photosynthetic capacity: a conceptual model. *Oecologia*, 125(3):350–357.

Schleser, G. G. H., Helle, G., Lucke, A., Vos, H., and Lücke, A. (1999). Isotope signals as climate proxies: the role of transfer functions in the study of terrestrial archives. *Quaternary Science Reviews*, 18(7):927–943.

Schmidt, G. A., Annan, J. D., Bartlein, P. J., Cook, B. I., Guilyardi, E., Hargreaves, J. C., Geoscientific, S. P., Kageyama, M., Legrande, A. N., Development, M., Konecky, B., Model, S., Mann, M. E., Risi, C., Thompson, D., Timmermann, A., and Yiou, P. (2013). Using paleo-climate comparisons to constrain future projections in CMIP5. *Climate of the Past Discussions*, 9:755–835.

Schmidt, G. A., LeGrande, A. N., and Hoffmann, G. (2007). Water isotope expressions of intrinsic and forced variability in a coupled ocean-atmosphere model. *Journal of Geophysical Research*, 112(D10):D10103.

Schoch, W., Heller, I., Schweingruber, F., and Kienast, F. (2004). Wood anatomy of central European Species. Online version: www.woodanatomy.ch.

Scholz, D. and Hoffmann, D. L. (2011). StalAge – An algorithm designed for construction of speleothem age models. *Quaternary Geochronology*, 6(3–4):369–382.

Scholz, D., Hoffmann, D. L., Hellstrom, J., and Bronk Ramsey, C. (2012). A comparison of different methods for speleothem age modelling. *Quaternary Geochronology*, 14:94–104.

Schurer, A. P., Hegerl, G. C., Mann, M. E., Tett, S. F. B., and Phipps, S. J. (2013). Separating Forced from Chaotic Climate Variability over the Past Millennium. *Journal of Climate*, 26(18):6954–6973.

Schwarcz, H. P., Harmon, R. S., Thompson, P., and Ford, D. C. (1976). Stable isotope studies of fluid inclusions in speleothems and their paleoclimatic significance. *Geochimica et Cosmochimica Acta*, 40(6):657–665.

Schweingruber, F. H. (1988). *Tree Rings: Basics and Applications of Dendrochronology.* Kluwer, Dordrecht.

Schweingruber, F. H. (1996). *Tree Rings and Environment Dendrochronology.* Haupt, Bern.

Schwinning, S. (2008). The water relations of two evergreen tree species in a karst savanna. *Oecologia*, 158(3):373–83.

Shen, C.-C., Lawrence Edwards, R., Cheng, H., Dorale, J. A., Thomas, R. B., Bradley Moran, S., Weinstein, S. E., and Edmonds, H. N. (2002). Uranium and thorium isotopic and concentration measurements by magnetic sector inductively coupled plasma mass spectrometry. *Chemical Geology*, 185(3-4):165–178.

Shen, C.-C., Lin, K., Duan, W., Jiang, X., Partin, J. W., Edwards, R. L., Cheng, H., and Tan, M. (2013). Testing the annual nature of speleothem banding. *Scientific Reports*, 3(2633):1–5.

Sheshshayee, M. S., Bindumadhava, H., Ramesh, R., Prasad, T. G., Lakshminarayana, M. R., and Udayakumar, M. (2005). Oxygen isotope enrichment (delta18O) as a measure of time-averaged transpiration rate. *Journal of Experimental Botany*, 56(422):3033–9.

Shi, C., Daux, V., Zhang, Q.-B., Risi, C., Hou, S.-G., Stievenard, M., Pierre, M., Li, Z., and Masson-Delmotte, V. (2012). Reconstruction of southeast Tibetan Plateau summer climate using tree ring δ18O: moisture variability over the past two centuries. *Climate of the Past*, 8(1):205–213.

Shi, C. M., Masson-Delmotte, V., Risi, C., Eglin, T., Stievenard, M., Pierre, M., Wang, X. C., Gao, J., Breon, F. M., Zhang, Q. B., and Daux, V. (2011). Sampling strategy and climatic implications of tree-ring stable isotopes on the southeast Tibetan Plateau. *Earth and Planetary Science Letters*, 301:307–316.

Sigg, L. and Stumm, W. (2011). *Aquatische Chemie. Eine Einführung in die Chemie natürlicher Gewässer (Aquatic Chemistry. An Introduction to the Chemistry of Natural Waters). In German.* UTB, Stuttgart.

Silveira, L., Sternberg, L., Mulkey, S. S., and Joseph Wright, S. (1989). Oxygen isotope ratio stratification in a tropical moist forest. *Oecologia*, 81(1):51–56.

Singh, J. and Yadav, R. R. (2013). Tree-ring-based seven century long flow records of Satluj River, western Himalaya, India. *Quaternary International*, 304:156–162.

Sinha, A., Stott, L., Berkelhammer, M., Cheng, H., Edwards, R. L., Buckley, B., Aldenderfer, M., and Mudelsee, M. (2011). A global context for megadroughts in monsoon Asia during the past millennium. *Quaternary Science Reviews*, 30(1-2):47–62.

Sjolte, J., Hoffmann, G., Johnsen, S. J., Vinther, B. M., Masson-Delmotte, V., and Sturm, C. (2011). Modeling the water isotopes in Greenland precipitation 1959–2001 with the meso-scale model REMO-iso. *Journal of Geophysical Research*, 116(D18):D18105.

Slonosky, V. C. (2002). Wet winters, dry summers? Three centuries of precipitation data from Paris. *Geophysical Research Letters*, 29(19):10–13.

Snyder, C. W. (2010). The value of paleoclimate research in our changing climate. *Climatic Change*, 100(3-4):407–418.

Speer, J. H. (2012). *Fundamentals of Tree Ring Research*. University of Arizona Press.

Spiker, E. C. and Hatcher, P. G. (1987). The effects of early diagenesis on the chemical and stable carbon isotopic composition of wood. *Geochimica et Cosmochimica Acta*, 51(6):1385–1391.

Spötl, C., Fairchild, I. J., and Tooth, A. F. (2005). Cave air control on dripwater geochemistry, Obir Caves (Austria): Implications for speleothem deposition in dynamically ventilated caves. *Geochimica et Cosmochimica Acta*, 69(10):2451–2468.

Spötl, C. and Mangini, A. (2002). Stalagmite from the Austrian Alps reveals Dansgaard–Oeschger events during isotope stage 3: Implications for the absolute chronology of Greenland ice cores. *Earth and Planetary Science Letters*, 203(1):507–518.

Spötl, C., Mangini, A., Frank, N., Eichstadter, R., and Burns, S. J. (2002). Start of the last interglacial period at 135 ka: Evidence from a high Alpine speleothem. *Geology*, 30(9):815–818.

Stahle, D. W., Fye, F. K., Cook, E. R., and Griffin, R. D. (2007). Tree-ring reconstructed megadroughts over North America since AD 1300. *Climatic Change*, 83(1-2):133–149.

Sternberg, L. D. S. L., DeNiro, M. J., and Savidge, R. A. (1986). Oxygen Isotope Exchange between Metabolites and Water during Biochemical Reactions Leading to Cellulose Synthesis. *Plant Physiology*, 82(2):423–427.

Sternberg, L. d. S. L. O. (2009). Oxygen stable isotope ratios of tree-ring cellulose: the next phase of understanding. *The New Phytologist*, 181(3):553–62.

Stocker, T. F. (2011). *Introduction to Climate Modelling*. Springer, Berlin.

Sturm, C., Hoffmann, G., and Langmann, B. (2007). Simulation of the Stable Water Isotopes in Precipitation over South America: Comparing Regional to Global Circulation Models. *Journal of Climate*, 20(15):3730–3750.

Sturm, C., Zhang, Q., and Noone, D. (2010). An introduction to stable water isotopes in climate models: benefits of forward proxy modelling for paleoclimatology. *Climate of the Past*, 6(1):115–129.

Sturm, K., Hoffmann, G., Langmann, B., and Stichler, W. (2005). Simulation of delta O-18 in precipitation by the regional circulation model REMOiso. *Hydrological Processes*, 19:3425–3444.

Szczepanek, M., Pazdur, A., Pawelczyk, S., Böttger, T., Haupt, M., Halas, S., Bednarz, Z., Krapiec, M., and Szychowska-Krapiec, E. (2006). Hydrogen, carbon and oxygen isotopes in pine and oak tree rings from Southern Poland as climatic indicators in years 1900-2003. *Geochronometria*, 25:67–76.

Szymczak, S., Joachimski, M., Bräuning, A., Hetzer, T., and Kuhlemann, J. (2012). Are pooled tree ring δ13C and δ18O series reliable climate archives? – A case study of Pinus nigra spp. laricio (Corsica/France). *Chemical Geology*, 308-309:40–49.

Tan, M., Baker, A., Genty, D., Smith, C., Esper, J., and Cai, B. G. (2006). Applications of stalagmite laminae to paleoclimate reconstructions: Comparison with dendrochronology/climatology. *Quaternary Science Reviews*, 25(17–18):2103–2117.

Tang, K. and Feng, X. (2001). The effect of soil hydrology on the oxygen and hydrogen isotopic compositions of plants' source water. *Earth and Planetary Science Letters*, 185(3-4):355–367.

Tardif, J., Conciatori, F., and Leavitt, S. (2008). Tree rings, δ13C and climate in Picea glauca growing near Churchill, subarctic Manitoba, Canada. *Chemical Geology*, 252(1-2):88–101.

Tebaldi, C., Hayhoe, K., Arblaster, J. M., and Meehl, G. A. (2006). Going to the Extremes. *Climatic Change*, 79(3-4):185–211.

Thomas, F. M. and Hartmann, G. (1998). Tree rooting patterns and soil water relations of healthy and damaged stands of mature oak (Quercus robur L. and Quercus petraea [Matt.] Liebl.). *Plant and Soil*, 203(1):145–158.

Thompson, L. G., Mosley-Thompson, E., Davis, M. E., Lin, P.-N., Henderson, K., and Mashiotta, T. A. (2003). Tropical Glacier and Ice Core Evidence of Climate Change on Annual to Millennial Time Scales. In Diaz, H. F., editor, *Climate Variability and Change in High Elevation Regions: Past, Present & Future*, volume 15 of *Advances in Global Change Research*, pages 137–155. Springer Netherlands, Dordrecht.

Tooth, A. F. and Fairchild, I. J. (2003). Soil and karst aquifer hydrological controls on the geochemical evolution of speleothem-forming drip waters, Crag Cave, southwest Ireland. *Journal of Hydrology*, 273(1-4):51–68.

Travis, D. T. and Meentemeyer, V. (1990). Stressed trees produce a better climatic signal than healthy trees. *Tree-Ring Bulletin*, 50:29–32.

Treble, P., Budd, W., Hope, P., and Rustomji, P. (2005). Synoptic-scale climate patterns associated with rainfall δ18O in southern Australia. *Journal of Hydrology*, 302(1-4):270–282.

Treble, P., Shelley, J., and Chappell, J. (2003). Comparison of high resolution sub-annual records of trace elements in a modern (1911–1992) speleothem with instrumental climate data from southwest Australia. *Earth and Planetary Science Letters*, 216(1):141–153.

Treble, P. C., Bradley, C., Wood, A., Baker, A., Jex, C. N., Fairchild, I. J., Gagan, M. K., Cowley, J., and Azcurra, C. (2013). An isotopic and modelling study of flow paths and storage in Quaternary calcarenite, SW Australia: implications for speleothem paleoclimate records. *Quaternary Science Reviews*, 64:90–103.

Tremaine, D. M., Froelich, P. N., and Wang, Y. (2011). Speleothem calcite farmed in situ: Modern calibration of δ18O and δ13C paleoclimate proxies in a continuously-monitored natural cave system. *Geochimica et Cosmochimica Acta*, 75(17):4929–4950.

Treydte, K., Frank, D., Esper, J., Andreu, L., Bednarz, Z., Berninger, F., Boettger, T., D'Alessandro, C. M., Etien, N., Filot, M., Grabner, M., Guillemin, M. T., Gutierrez, E., Haupt, M., Helle, G., Hilasvuori, E., Jungner, H., Kalela-Brundin, M., Krapiec, M., Leuenberger, M., Loader, N. J., Masson-Delmotte, V., Pazdur, A., Pawelczyk, S., Pierre, M., Planells, O., Pukiene, R., Reynolds-Henne, C. E., Rinne, K. T., Saracino, A., Saurer, M., Sonninen, E., Stievenard, M., Switsur, V. R., Szczepanek, M., Szychowska-Krapiec, E., Todaro, L., Waterhouse, J. S., Weigl, M., and Schleser, G. H. (2007). Signal strength and climate calibration of a European tree-ring isotope network. *Geophysical Research Letters*, 34:L24302.

Treydte, K., Schleser, G. H., Schweingruber, F. H., and Winiger, M. (2001). The climatic significance of δ13C in subalpine spruces (Lötschental, Swiss Alps). *Tellus B*, 53(5):593–611.

Treydte, K. S., Schleser, G. H., Helle, G., Frank, D. C., Winiger, M., Haug, G. H., and Esper, J. (2006). The twentieth century was the wettest period in northern Pakistan over the past millennium. *Nature*, 440:1179–1182.

Trouet, V., Esper, J., Graham, N., Baker, A., Scourse, J. D., and Frank, D. C. (2009). Persistent positive North Atlantic Oscillation mode dominated the medieval climate anomaly. *Science*, 324:78–80.

Uppala, S. M., Kallberg, P. W., Simmons, A. J., Andrae, U., Bechtold, V. D. C., Fiorino, M., Gibson, J. K., Haseler, J., Hernandez, A., Kelly, G. A., Li, X., Onogi, K., Saarinen, S., Sokka, N., Allan, R. P., Andersson, E., Arpe, K., Balmaseda, M. A., Beljaars, A. C. M., Berg, L. V. D., Bidlot, J., Bormann, N., Caires, S., Chevallier, F., Dethof, A., Dragosavac, M., Fisher, M., Fuentes, M., Hagemann, S., Hólm, E., Hoskins, B. J., Isaksen, L., Janssen, P. A. E. M., Jenne, R., Mcnally, A. P., Mahfouf, J.-F., Morcrette, J.-J., Rayner, N. A., Saunders, R. W., Simon, P., Sterl, A., Trenberth, K. E., Untch, A., Vasiljevic, D., Viterbo, P., and Woollen, J. (2005). The ERA-40 re-analysis. *Quarterly Journal of the Royal Meteorological Society*, 131(612):2961–3012.

Vachon, R. W., White, J. W. C., Gutman, E., and Welker, J. M. (2007). Amount-weighted annual isotopic (δ18O) values are affected by the seasonality of precipitation: A sensitivity study. *Geophysical Research Letters*, 34(11):L21707.

van Aalst, M. K. (2006). The impacts of climate change on the risk of natural disasters. *Disasters*, 30(1):5–18.

van Breukelen, M. R., Vonhof, H. B., Hellstrom, J. C., Wester, W. C. G., and Kroon, D. (2008). Fossil dripwater in stalagmites reveals Holocene temperature and rainfall variation in Amazonia. *Earth and Planetary Science Letters*, 275:54–60.

van der Schrier, G., Briffa, K. R., Jones, P. D., and Osborne, T. J. (2006). Summer moisture variability across Europe. *Journal of Climate*, 19(12):2818–2834.

Van Rampelbergh, M., Fleitmann, D., Verheyden, S., Cheng, H., Edwards, L., De Geest, P., De Vleeschouwer, D., Burns, S. J., Matter, A., Claeys, P., and Keppens, E. (2013). Mid- to late Holocene Indian Ocean Monsoon variability recorded in four speleothems from Socotra Island, Yemen. *Quaternary Science Reviews*, 65(null):129–142.

Vicente-Serrano, S. M., Beguería, S., López-Moreno, J. I., Angulo, M., and El Kenawy, A. (2010). A new global 0.5 degree gridded dataset (1901–2006) of a multiscalar drought index: comparison with current drought index datasets based on the Palmer Drought Severity Index. *Journal of Hydrometeorology*, 11(4):1033–1043.

Vidal, J.-P., Martin, E., Franchistéguy, L., Habets, F., Soubeyroux, J.-M., Blanchard, M., and Baillon, M. (2010). Multilevel and multiscale drought reanalysis over France with the Safran-Isba-Modcou hydrometeorological suite. *Hydrology and Earth System Sciences*, 14:459–478.

Voelker, S. L. (2011). Age-Dependent Changes in Environmental Influences on Tree Growth and Their Implications for Forest Responses to Climate Change. In Meinzer, F. C., Lachenbruch, B., and Dawson, T. E., editors, *Size- and Age-Related Changes in Tree Structure and Function*, pages 455–479. Springer, Dordrecht.

Vogel, N., Scheidegger, Y., Brennwald, M. S., Fleitmann, D., Figura, S., Wieler, R., and Kipfer, R. (2013). Stalagmite water content as a proxy for drip water supply in tropical and subtropical areas. *Climate of the Past*, 9(1):1–12.

von Grafenstein, U., Erlenkeuser, H., Brauer, A., Jouzel, J., and Johnsen, S. (1999). A Mid-European Decadal Isotope-Climate Record from 15,500 to 5000 Years B.P. *Science*, 284(5420):1654–1657.

von Grafenstein, U., Erlenkeuser, H., Müller, J., Trimborn, P., and Alefs, J. (1996). A 200 year mid-European air temperature record preserved in lake sediments: An extension of the δ18Op-air temperature relation into the past. *Geochimica et Cosmochimica Acta*, 60(21):4025–4036.

von Storch, H., Langenberg, H., and Feser, F. (2000). A Spectral Nudging Technique for Dynamical Downscaling Purposes. *Monthly Weather Review*, 128(10):3664–3673.

Vonhof, H. B., Atkinson, T. C., van Breukelen, M. R., and Postma, O. (2007). Fluid inclusion hydrogen and oxygen isotope analysis using the "Amsterdam Device": a progress report. *Geophysical Research Abstracts*, 9:5702.

Vonhof, H. B., van Breukelen, M. R., Postma, O., Rowe, P. J., Atkinson, T. C., and Kroon, D. (2006). A continuous-flow crushing device for on-line delta2H analysis of fluid inclusion water in speleothems. *Rapid communications in mass spectrometry*, 20(17):2553–2558.

Wackerbarth, A., Langebroek, P. M., Werner, M., Lohmann, G., Riechelmann, S., Borsato, A., and Mangini, A. (2012). Simulated oxygen isotopes in cave drip water and speleothem calcite in European caves. *Climate of the Past*, 8(6):1781–1799.

Wainer, K., Genty, D., Blamart, D., Daëron, M., Bar-Matthews, M., Vonhof, H., Dublyansky, Y., Pons-Branchu, E., Thomas, L., van Calsteren, P., Quinif, Y., and Caillon, N. (2011). Speleothem record of the last 180 ka in Villars cave (SW France): Investigation of a large δ18O shift between MIS6 and MIS5. *Quaternary Science Reviews*, 30(1-2):130–146.

Wang, Y., Cheng, H., Edwards, R. L., Kong, X., Shao, X., Chen, S., Wu, J., Jiang, X., Wang, X., and An, Z. (2008). Millennial- and orbital-scale changes in the East Asian monsoon over the past 224,000 years. *Nature*, 451(7182):1090–3.

Wang, Y. J., Cheng, H., Edwards, R. L., An, Z. S., Wu, J. Y., Shen, C. C., and Dorale, J. A. (2001). A high-resolution absolute-dated late Pleistocene Monsoon record from Hulu Cave, China. *Science*, 294(5550):2345–8.

Wassenburg, J., Immenhauser, A., Richter, D., Niedermayr, A., Riechelmann, S., Fietzke, J., Scholz, D., Jochum, K., Fohlmeister, J., Schröder-Ritzrau, A., Sabaoui, A., Riechelmann, D., Schneider, L., and Esper, J. (2013). Moroccan speleothem and tree ring records suggest a variable positive state of the North Atlantic Oscillation during the Medieval Warm Period. *Earth and Planetary Science Letters*, 375:291–302.

Watkins, J. M., Nielsen, L. C., Ryerson, F. J., and DePaolo, D. J. (2013). The influence of kinetics on the oxygen isotope composition of calcium carbonate. *Earth and Planetary Science Letters*, 375:349–360.

Webb, R. S. and Rosenzweig, C. E. (1993). Specifying land surface characteristics in general circulation models: Soil profile data set and derived water-holding capacities. *Global Biogeochemical Cycles*, 7(1):97–108.

Wells, N., Goddard, S., and Hayes, M. J. (2004). A self-calibrating Palmer Drought Severity Index. *Journal of Climate*, 17(12):2335–2351.

Werner, R. A., Kornexl, B. E., Rossmann, A., and Schmidt, H. L. (1996). On-line determination of delta O-18 values of organic substances. *Analytica Chimica Acta*, 319(1–2):159–164.

White, J. W., Cook, E. R., Lawrence, J. R., and Wallace S., B. (1985). The D/H ratios of sap in trees: Implications for water sources and tree ring D/H ratios. *Geochimica et Cosmochimica Acta*, 49(1):237–246.

White, W. B. (2002). Karst hydrology: recent developments and open questions. *Engineering Geology*, 65(2-3):85–105.

Wiedner, E., Scholz, D., Mangini, A., Polag, D., Mühlinghaus, C., and Segl, M. (2008). Investigation of the stable isotope fractionation in speleothems with laboratory experiments. *Quaternary International*, 187(1):15–24.

Wigley, T. M. L., Briffa, K. R., and Jones, P. D. (1984). On the average value of correlated time series, with applications in dendroclimatology and hydrometeorology. *Journal of Applied Meteorology*, 23(2):201–213.

Williams, P. W. and Fowler, A. (2002). Relationship between oxygen isotopes in rainfall, cave percolation waters and speleothem calcite at Waitomo, New Zealand. *Journal of Hydrology (NZ)*, 41:53–70.

Wilson, A. T. and Grinsted, M. J. (1977). 12C/13C in cellulose and lignin as palaeothermometers. *Nature*, 265(5590):133–135.

Woodley, E., Loader, N., McCarroll, D., Young, G., Robertson, I., Heaton, T., and Gagen, M. (2012). Estimating uncertainty in pooled stable isotope time-series from tree-rings. *Chemical Geology*, 294-295:243–248.

Xia, Q., Zhao, J.-x., and Collerson, K. (2001). Early–Mid Holocene climatic variations in Tasmania, Australia: multi-proxy records in a stalagmite from Lynds Cave. *Earth and Planetary Science Letters*, 194(1-2):177–187.

Yadav, R. (2013). Tree ring–based seven-century drought records for the Western Himalaya, India. *Journal of Geophysical Research: Atmospheres*, 118(10):4318–4325.

Yakir, D. and DeNiro, M. J. (1990). Oxygen and Hydrogen Isotope Fractionation during Cellulose Metabolism in Lemna gibba L. *Plant Physiology*, 93(1):325–332.

Yiou, P., García de Cortázar-Atauri, I., Chuine, I., Daux, V., Garnier, E., Viovy, N., van Leeuwen, C., Parker, a. K., and Boursiquot, J.-M. (2012). Continental atmospheric circulation over Europe during the Little Ice Age inferred from grape harvest dates. *Climate of the Past*, 8(2):577–588.

Yoder, B. J., Ryan, M. G., Waring, R. H., Schoettle, A. W., and Kaufmann, M. R. (1994). Evidence of Reduced Photosynthetic Rates in Old Trees. *Forest Science*, 40(3):513–527.

Yonge, C., Ford, D., Gray, J., and Schwarcz, H. (1985). Stable isotope studies of cave seepage water. *Chemical Geology*, 58(1–2):97–105.

Young, G. H. F., Bale, R. J., Loader, N. J., Mccarroll, D., Nayling, N., and Vousden, N. (2012). Central England temperature since AD 1850: the potential of stable carbon isotopes in British oak trees to reconstruct past summer temperatures. *Journal of Quaternary Science*, 27(6):606–614.

Young, G. H. F., Demmler, J. C., Gunnarson, B. E., Kirchhefer, A. J., Loader, N. J., and McCarroll, D. (2011). Age trends in tree ring growth and isotopic archives: A case study of Pinus sylvestris L. from northwestern Norway. *Global Biogeochemical Cycles*, 25(GB2020):1–6.

Zhang, M., Yuan, D., Lin, Y., Qin, J., Bin, L., Cheng, H., and Edwards, R. L. (2004). A 6000-year high-resolution climatic record from a stalagmite in Xiangshui Cave, Guilin, China. *The Holocene*, 14(5):697–702.

Zhang, R., Schwarcz, H. P., Ford, D. C., Schroeder, F. S., and Beddows, P. a. (2008). An absolute paleotemperature record from 10 to 6Ka inferred from fluid inclusion D/H ratios of a stalagmite from Vancouver Island, British Columbia, Canada. *Geochimica et Cosmochimica Acta*, 72(4):1014–1026.

Zweifel, R., Böhm, J. P., and Häsler, R. (2002). Midday stomatal closure in Norway spruce-reactions in the upper and lower crown. *Tree Physiology*, 22(15-16):1125–36.

List of Symbols and Abbreviations

Symbols

α	fractionation factor
δ	isotope ratio
$\delta^{18}O_{cell}$	oxygen isotopic composition of cellulose
$\delta^{18}O_{lw}$	oxygen isotopic composition of leaf water
$\delta^{18}O_{prec}$	oxygen isotopic composition of precipitation
$\delta^{18}O_{s}$	oxygen isotopic composition of source water
$\delta^{18}O_{v}$	oxygen isotopic composition of water vapour
ε^{*}	equilibrium fractionation factor between liquid water and vapour
ε_k	kinetic fractionation factor as water diffuses through leaf stomata and through the boundary layer
ε_{wc}	fractionation factor between carbonyl oxygen and water
A	photosynthetic rate
d	deuterium excess
c_a	atmospheric CO_2 concentration
c_i	leaf internal CO_2 concentration
e_a	atmospheric vapour pressure
e_i	intercellular vapour pressure in a leaf
g	stomatal conductance
$p\mathrm{CO}_2$	CO_2 partial pressure

Abbreviations

AMS	accelerator mass spectrometry
dcp	dead carbon percentage
DIC	dissolved inorganic carbon
GC	gas chromatography
GHD	grape harvest dates
GMWL	global meteoric water line
GNIP	Global Network of Isotopes in Precipitation
IPCC	Intergovernmental Panel on Climate Change
IRMS	isotope ratio mass spectrometry
LMWL	local meteoric water line
m a.s.l.	meters above sea level
MC-ICP-MS	multicollector inductively coupled plasma mass spectrometry
MXD	maximum latewood density
NAO	North Atlantic Oscillation
PCP	prior calcite precipitation
RH	relative humidity
pMC	percent modern carbon
TIMS	thermal ionization mass spectrometry

TRI	tree ring index
TRW	tree ring width
VPDB	Vienna PeeDee Belemnite
VSMOW	Vienna Sandard Mean Ocean Water
WUE	water use efficiency

Concentrations are given in square brackets, e.g. $[HCO_3^-]$.

SI units are not explained.

Appendix

Supplementary material to Chapter 10

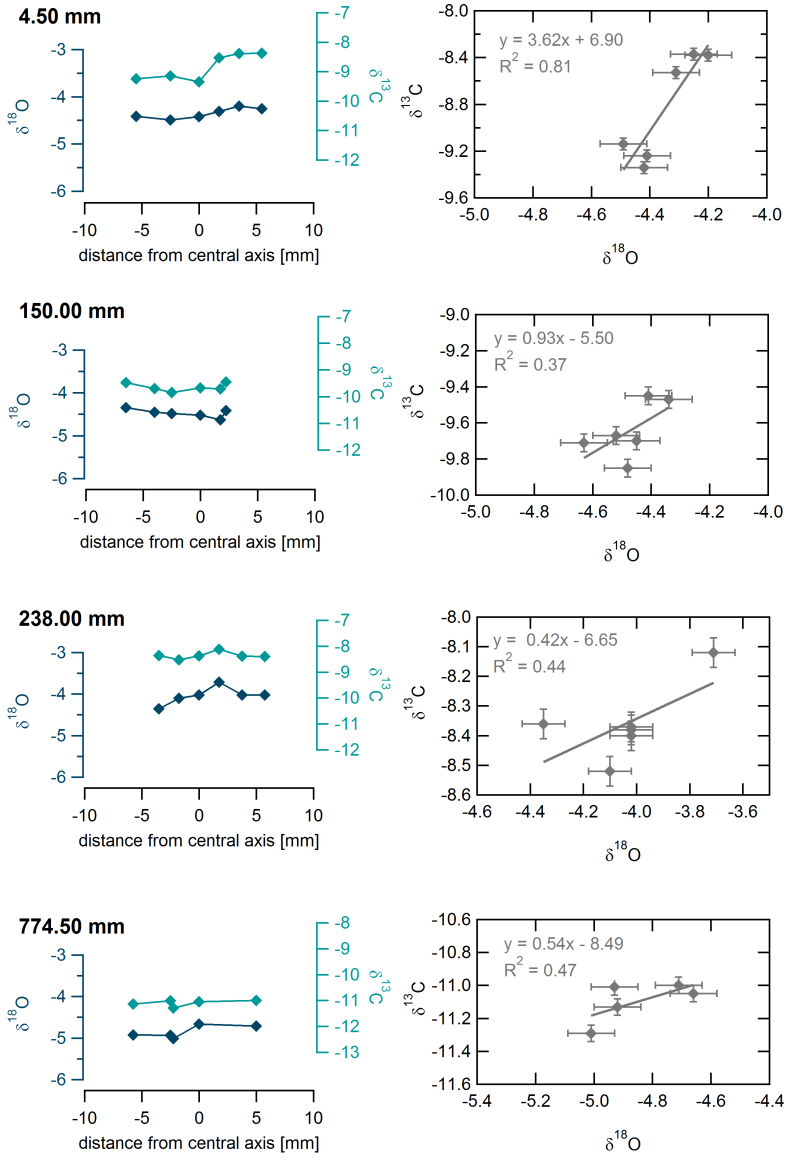

Figure A.1: "Hendy test" results for four growth layers of the stalagmite vil-stm1 at 4.5, 150, 238 and 774.5 mm from the top. Left panels: variability of calcite δ^{18}O (blue) and δ^{13}C (green) along single growth layers with distance from the central axis. Right panels: Correlation between δ^{18}O and δ^{13}C for the respective growth layers. The equations describe the regression lines.

Supplementary material to Chapter 11

The following equations describe the relationship between relative humidity and cellulose δ^{18}O. The oxygen isotope composition of leaf water ($\delta^{18}O_{lw}$) is related to relative humidity (RH) as follows (Dongman et al. 1974):

$$\delta^{18}O_{lw} = \delta^{18}O_s * (1 - RH) + \delta^{18}O_v * RH + \varepsilon^* + \varepsilon_k * (1 - RH) \tag{A.1}$$

where $\delta^{18}O_s$ and $\delta^{18}O_v$ are the oxygen isotopic composition of the source water and of the vapour, RH is the relative humidity, ε^* and ε_k are the equilibrium and kinetic fractionation factors. ε_k is equal to 16‰ (Burk and Stuiver 1981). At 20 °C, ε^* is equal to 9.7‰ (Horita and Wesolowski 1994). Under normal European summer conditions, the water vapour is, on average, approximately in isotopic equilibrium with soil water (Förstel and Hutzen 1982). Thus,

$$\delta^{18}O_v = \delta^{18}O_s - \varepsilon^* \tag{A.2}$$

Combining Equation A.1 and A.2 gives

$$\delta^{18}O_{lw} = \delta^{18}O_s + (1 - RH) * (\varepsilon^* + \varepsilon_k) \tag{A.3}$$

The oxygen isotopic composition of cellulose can be related to the isotopic composition of leaf water and source water (Sternberg et al. 1986; Yakir and DeNiro 1990):

$$\delta^{18}O_{cell} = 0.42 * (\delta^{18}O_s + \varepsilon_{wc}) + 0.58 * (\delta^{18}O_{lw} + \varepsilon_{wc}) \tag{A.4}$$

where ε_{wc}, the fractionation factor between carbonyl oxygen and water, is approximately equal to 27‰. The difference between the isotopic composition of the cellulose formed at the bottom and op of the gradient is given by:

$$\delta^{18}O_{cell} = -RH * (\varepsilon^* + \varepsilon_k) \tag{A.5}$$

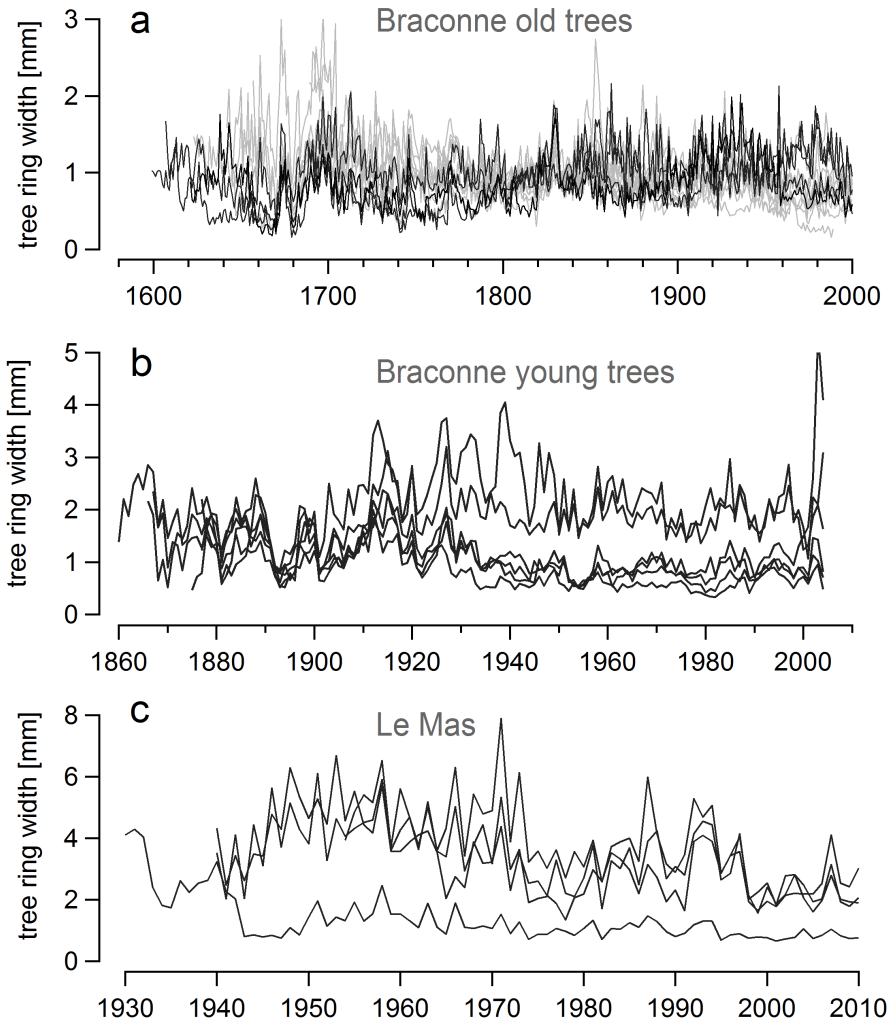

Figure A.2: Non-standardized tree ring width curves for individual trees. (a) Braconne old trees (black lines represent the samples selected for isotope analysis), (b) Braconne young trees, and (c) Le Mas. The long-term increasing and decreasing trends in ring width are likely the effects of changes in competition in a closed stand with resulting suppression and release patterns, probably due to logging. Before 1870 the forest was managed as a standardized coppice system with logging every 20 to 30 years. From 1870 onward, logging was carried out more frequently, on a 10 to 12 year basis (ONF, pers. comm.). A common signal in TRW allows the samples to be crossdated. Absolute values, however, differ significantly by up to 3.5 mm. Note the strong divergence in TRW of Braconne young trees after 1920.

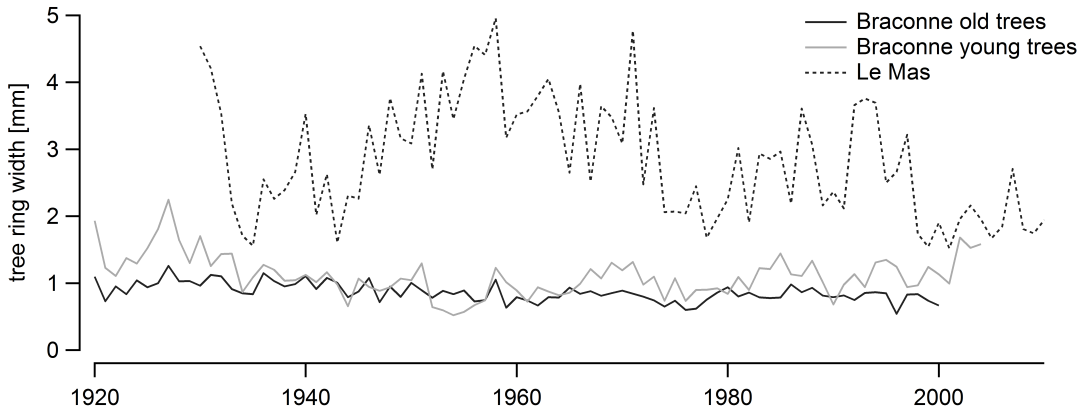

Figure A.3: Average non-standardized ring width curves of the three tree groups for their period of overlap.

Supplementary material to Chapter 12

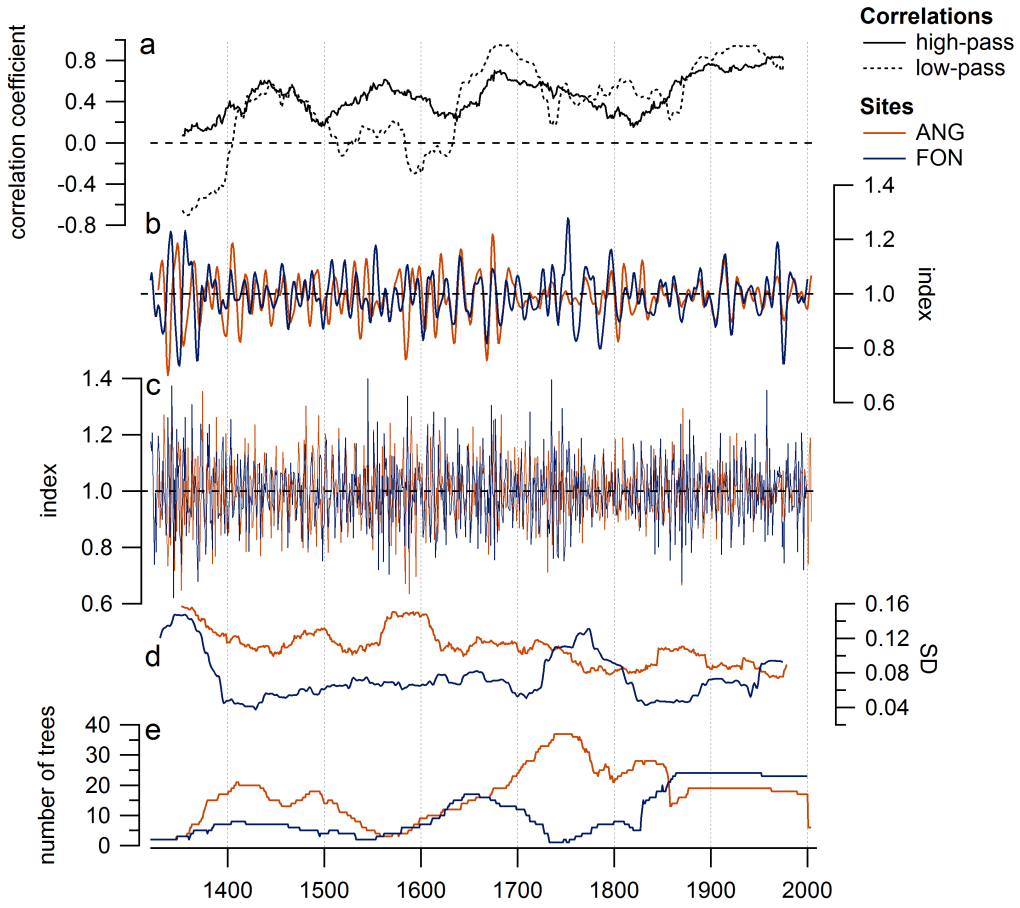

Figure A.4: Comparison of TRW chronologies from Fontainebleau (FON) and Angoulême (ANG). (a) 51-year running correlation between FON and ANG; (b) low-pass filtered data; (c) high-pass filtered data; (d) standard deviation of the high-pass filtered data calculated for 51-year running windows; (e) number of trees.

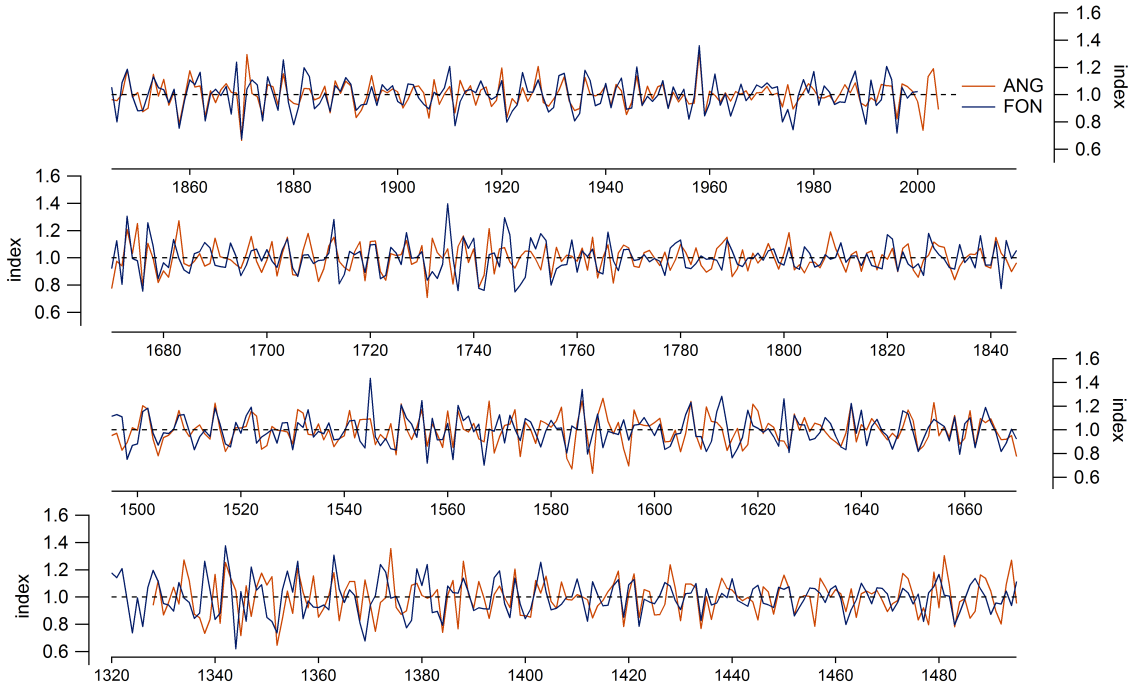

Figure A.5: Inter-annual variability in TRW chronologies from Fontainebleau (FON) and Angoulême (ANG), high-pass filtered data.

Table A.1: Pearson correlation coefficients (r) between cellulose δ^{18}O, tree ring width (TRW) and monthly meteorological variables. 1–12 denote the months January to December, 6–8 and 4–9 denote summer and growing season averages respectively (see text for data sources and time spans).

Variable		FON δ^{18}O	ANG δ^{18}O	FON TRW	ANG TRW
Cloud cover	cld01	–0.04	0.07	–0.06	–0.15
	cld02	–0.12	–0.11	0.26	0.15
	cld03	–0.19	–0.15	0.05	–0.05
	cld04	0.06	–0.09	0.19	0.11
	cld05	–0.20	–0.14	0.24	0.14
	cld06	–0.53	–0.56	0.31	0.29
	cld07	–0.50	–0.39	0.14	0.02
	cld08	–0.28	–0.31	0.31	0.18
	cld09	–0.01	–0.08	–0.12	–0.02
	cld10	–0.18	–0.23	–0.16	0.05
	cld11	–0.10	0.04	0.00	–0.02
	cld12	0.04	0.04	–0.01	0.19
	cld6–8	–0.59	–0.60	0.34	0.23
	cld4–9	–0.49	–0.51	0.35	0.23
Precipitation	pre01	–0.19	–0.09	0.26	0.13
	pre02	–0.18	–0.11	0.24	0.03
	pre03	–0.13	–0.24	0.05	0.15
	pre04	0.03	0.06	0.14	–0.06
	pre05	–0.25	–0.25	0.39	0.37
	pre06	–0.48	–0.47	0.30	0.28
	pre07	–0.39	–0.40	0.38	0.17
	pre08	–0.30	–0.14	0.13	0.07
	pre09	0.15	0.12	–0.08	0.02
	pre10	–0.08	0.09	–0.04	–0.04
	pre11	–0.03	0.04	–0.12	–0.02
	pre12	0.08	0.12	0.01	–0.03
	pre6–8	–0.60	–0.53	0.42	0.28
	pre4–9	–0.49	–0.40	0.49	0.33
Average temperature	tmp01	–0.04	0.12	–0.01	0.00
	tmp02	0.03	0.15	0.11	0.13
	tmp03	0.05	0.23	–0.07	0.03
	tmp04	0.17	0.15	0.02	0.05
	tmp05	0.26	0.32	–0.06	–0.03
	tmp06	0.18	0.41	–0.24	–0.15
	tmp07	0.53	0.55	–0.28	–0.23
	tmp08	0.34	0.45	–0.17	–0.16
	tmp09	0.19	0.17	0.05	0.00
	tmp10	0.19	0.25	0.08	–0.03
	tmp11	–0.03	0.04	0.08	0.21
	tmp12	–0.02	0.03	–0.01	0.00
	tmp6–8	0.49	0.62	–0.32	–0.24
	tmp4–9	0.48	0.57	–0.20	–0.15
Maximum temperature	tmx01	–0.03	0.15	0.00	0.00
	tmx02	0.06	0.17	0.07	0.14
	tmx03	0.08	0.27	–0.09	–0.01
	tmx04	0.15	0.17	–0.03	0.00
	tmx05	0.28	0.34	–0.12	–0.10
	tmx06	0.25	0.48	–0.27	–0.24
	tmx07	0.57	0.60	–0.30	–0.28
	tmx08	0.36	0.48	–0.23	–0.24
	tmx09	0.20	0.19	0.01	–0.05
	tmx10	0.20	0.22	0.09	0.00
	tmx11	–0.03	0.03	0.07	0.23
	tmx12	–0.03	0.03	–0.01	0.00
	tmx6–8	0.54	0.70	–0.36	–0.34
	tmx4–9	0.51	0.65	–0.26	–0.26
sc–PDSI	pdsi01	–0.08	–0.08	0.42	0.18
	pdsi02	–0.12	–0.12	0.47	0.19
	pdsi03	–0.15	–0.14	0.46	0.20
	pdsi04	–0.18	–0.14	0.45	0.19
	pdsi05	–0.26	–0.18	0.53	0.23
	pdsi06	–0.34	–0.34	0.59	0.27
	pdsi07	–0.45	–0.42	0.64	0.31
	pdsi08	–0.44	–0.44	0.64	0.34
	pdsi09	–0.40	–0.33	0.55	0.32
	pdsi10	–0.36	–0.29	0.47	0.27
	pdsi11	–0.36	–0.27	0.43	0.23
	pdsi12	–0.33	–0.22	0.41	0.20
SSWI	sswi3	–0.63	–0.62	0.47	0.18
	sswi6	–0.52	–0.62	0.37	0.14
SPI	SPI3aug	–0.60	–0.52	0.44	0.28
	SPI6sep	–0.49	–0.40	0.51	0.33
	SPI12sep	–0.48	–0.39	0.53	0.29
	SPI24sep	–0.23	–0.16	0.56	0.25
SPEI	SPEI3aug	–0.69	–0.68	0.41	0.33
	SPEI6sep	–0.62	–0.57	0.44	0.36
	SPEI12sep	–0.57	–0.48	0.50	0.32
	SPEI24sep	–0.31	–0.24	0.54	0.26

Acknowledgments

First of all, I would like to thank my advisors Valérie Daux and Dominique Genty for their kindness, their confidence and their support throughout the thesis.

I also want to thank Gerd Helle and Christoph Spötl, who reviewed the thesis manuscript, as well as the other jury members Christelle Marlin, Valérie Masson-Delmotte and Hubert Vonhof for having accepted this task, and for the interesting discussions at my defence.

The compilation of the enormous amount of data presented here was only possible with the help of my colleagues during field work, sampling and measurements: I am grateful to Monique Pierre, Michel Stievenard, Edouard Régnier, Dominique Blamart, Jiaoyang Ruan, Anaïs Féron, Bénédicte Minster, Richard Maire, Gregory Dandurand, and Thierry Baritaud. I would especially like to thank Hubert Vonhof for hosting me at his lab in Amsterdam and for his help with the fluid inclusion measurements. Lastly, thanks to Henning Labuhn and Felix Vogel for proof-reading the manuscript.

And of course, a number of people have contributed to the success by helping me keep in shape (running and swimming), and keep up the spirit when the mass spec was down or the RER B was late. A big thanks to everyone who made the thesis time more enjoyable with our picnics, coffee breaks, happy hours, ...

Paris, May 2014
Inga Labuhn